Engineering Design of a Fission Converter-Based Epithermal Beam for Neutron Capture Therapy

by

Balendra Sutharshan

B.A.Sc., University of Toronto, Toronto (1991)
M.A.Sc., University of Toronto (1993)

Submitted to the Department of Nuclear Engineering
in partial fulfillment of the requirements for the degrees of

DOCTOR OF PHILOSOPHY

at the

MASSACHUSETTS INSTITUTE OF TECHNOLOGY

February 1998

Signature of Author: _____
Department of Nuclear Engineering
January 29, 1996

Certified by: _____
Prof. Otto K. Harling
Thesis Supervisor

_____
Prof. Neil Todreas
Thesis Supervisor

Accepted by: _____
Prof. Lawrence M. Lidsky
Chairman, Department Committee on Graduate Students

Engineering Design of a Fission Converter-Based Epithermal Beam for Neutron Capture Therapy

by

Balendra Sutharshan

Submitted to the Department of Nuclear Engineering on January 29, 1998
in partial fulfillment of the requirements for the degree of

Doctor of Philosophy in Nuclear Engineering

Abstract

There is a need for high intensity and low contamination epithermal neutron beams, for boron neutron capture therapy research and for routine treatment if this becomes a successful modality for treating cancers. A fission converter based design for high performance epithermal neutron beam was developed at the Nuclear Reactor Laboratory of the Massachusetts Institute of Technology. This epithermal beam has the capability of delivering a treatment within minutes with negligible background contamination. This thesis deals with the engineering design of this facility. This fission converter based epithermal facility will be installed in the present thermal column and hohlraum of the MITR-II.

The fission converter tank, which contains eleven MITR-II fuel elements, was designed with minimum front plate thickness to minimize

neutron absorption. The converter tank structural analysis was performed analytically, and numerically with the finite element code ADINA.

Three heat removal designs, natural convection, forced convection with bypass channel and simple forced convection, were considered to remove heat from eleven fuel elements in the fission converter tank. For all three designs, steady state and transient analyses were performed. The transient analysis includes loss of flow, loss of flow with shutter failure (converter scram) and loss of coolant. Most of these steady state and transient analyses were performed by both analytically and numerically. The results show that the fuel disruption will not occur during credible and incredible accident scenarios.

Three shutters, cadmium shutter, water shutter and mechanical fast acting shutter were designed to control the beam at the patient position. The shutters were designed using the Monte Carlo radiation transport code MCNP. A medical irradiation room was designed for patient irradiation. The shielding computations for the medical room were also carried out with the MCNP.

Fuel handling was investigated and proposed two options for refueling, which are similar to the MITR-II refueling.

Acknowledgments

I would like to express my sincere appreciation to my thesis advisors, Prof. O. Harling and Prof. N. Todreas, for all of their patience, assistance and providing me with opportunity to work on this exciting project.

The students and faculty staffs have given me support and assistance on this project. In particular, I would like to thank:

Prof. M. Driscoll

Prof. P. Griffith

Prof. M. Kazimi

Prof. Lanning

Dr. Lin-Wen Hu

W.S. Kiger III

K. Riley

S.Sakamoto

The Nuclear Reactor Laboratory staffs have been very helpful in providing data and assistance. E.Block, T. Newton, T.Date and F. McWilliams have been especially helpful. G. Koshe and Y. Ostrovsky have been very helpful during this project.

Although I cannot list them all, there are many others who have contributed to my overall experience at MIT.

I would like to thank my family and friends for their support and their encouragements.

This research was supported by the U.S. Department of Energy under contract No. DE-FG02-87ER 60600.

Table of Contents

List of Figures

List of Tables

CHAPTER ONE

INTRODUCTION

1. Objective

The objective is the design an overall fission converter based epithermal neutron beam facility for boron neutron capture therapy. This includes the following tasks:

1. Incorporating the neutronic design performed by W.S. Kiger[20] and S.Sakamoto[21],
2. Designing a heat removal system,
3. Performing a safety analysis, and
4. Designing shutters to control the beam and a medical room for patient irradiation.

2. Boron Neutron Capture Therapy

An ideal cancer treatment would be the one which could selectively destroy tumor cells without damaging normal cells and prevent the reoccurrence of tumor cells. The existing standard treatment facilities such as surgery, radiation therapy, and chemotherapy have failed not only to meet the ideal requirements but also have showed many treatment failures especially for highly malignant brain cancers such as glioblastoma multiform and intercranial melanoma. The potential advantages of the experimental cancer therapy called boron neutron capture therapy (BNCT) has led many scientists around the world to perform further studies and trials with animals and humans.

BNCT is a binary radiation therapy that brings together two components. These two components, ^{10}B and low energy neutrons, have minor effects on the cells when they are kept separate. When a ^{10}B containing compound is administered orally or intra-venously to a patient, it is preferentially attracted by tumor cells. After the administration of a ^{10}B containing compound, tumor cells are irradiated externally with an epithermal neutron beam, which has the energy of 1 keV to 10 keV. These epithermal neutrons scatter in the tissues at and near the surface of the body and lose their energy to become thermal neutrons. The thermalized neutrons are captured by ^{10}B atoms, which become ^{11}B atoms in an excited state for a very short period of time

(about 10^{-12} seconds). The excited ^{11}B atom returns to the ground energy state by emitting energetic alpha particles and ^{7}Li recoil nuclei. The emitted alpha particles and ^{7}Li recoil nuclei have a combined range (about 13 microns) smaller than a cell diameter in a cell medium. Therefore, both of these particles lose their energy primarily within a tumor cell and kill the tumor cell while sparing adjacent healthy tissues.

The concept of neutron capture therapy was first introduced by G.L. Locher of the Franklin Institute at Pennsylvania in 1936[1]. In 1951, Sweet[2] first used neutron capture therapy to treat brain tumors. He also suggested that neutron capture therapy can be useful to treat the most highly malignant and therapeutically persistent of all brain tumors, such as glioblastoma multiform (GBM). Sweet and his colleges[3] showed that certain ^{10}B compounds selectively concentrate in a tumor cell rather than in a normal cell. They chose sodium tetraborate as the capture agent. Clinical trials were performed at Brookhaven National Laboratory (BNL)[4,5] from 1951 to 1952 and at Massachusetts Institute of Technology[6] from 1961 to 1962. These trials did not show any therapeutic efficacy. One of the reasons for their lack of success is that thermal neutrons were attenuated by the tissues at or near the surface of the body. Therefore the thermal neutrons useful penetration depth was 3-4 cm. In addition, the boron compounds, which were used, were freely diffusable and low molecular weight substance. These boron compounds

did not achieve the necessary selective localization in the tumor. For these reasons the trials were terminated.

BNCT trials gained momentum again after reports by Hatanaka[7] of successful brain cancer treatments and reports by Mishima[8] of melanoma treatments. In the USA, the current series of trials were initiated on September 1994 at MIT in collaboration with the New England Medical Center, and a few days later at BNL. Epithermal neutron beam and *p*-Boronophenylalanine (BPA) are used in the current USA trials.

This section only provided a very brief and basic introduction to BNCT. However, there are number of references available with more specific and detailed information about BNCT[17,18,19].

3. Current Epithermal Neutron Beam Facilities for BNCT

Currently, there are three epithermal neutron beam facilities available. Two of them, the Massachusetts Institute of Technology Research Reactor (MITR-II) and the Brookhaven Medical Research Reactor (BMRR) at Brookhaven National Laboratory, are already being used in clinical trials. The first clinical trial with epithermal neutron beam and BPA boron compound was carried out on September 6, 1994

at MIT with the collaboration of medical staff from the New England Medical Center. The clinical trials at BMRR were initiated a few days after those at MIT. The third epithermal neutron beam facility is available at the High Flux Reactor (HFR) at Petten in The Netherlands. The HFR facility is being used by the European Collaboration on Neutron Capture Therapy to perform clinical trials. The first clinical trial at Petten was carried out in November 1997.

The MIT medical irradiation room is located below the MTR-II core and the medical beam's orientation is vertical. The MIT medical beam[9] is filtered by D_2O, aluminum, cadmium, sulfur, and bismuth. The BMRR[10] medical beam's orientation is horizontal and it is filtered by bismuth, aluminum, Al_2O_3, and cadmium. Further design studies have been carried out at BNL to improve the beam intensity and to reduce the fast and gamma dose level at the patient position. The HFR medical beam's[11] orientation is horizontal and the beam is filtered by liquid argon. The three measured medical beam performance data in the air for these three facilities are tabulated in table 1.1.

If a complete BNCT treatment requires 1000 RBE cGy healthy tissue dose, the required treatment time is about an hour at BMRR and 2.5 hours at MITR-II. It is uncomfortable for a patient to be in an immobilized position for 2.5 hours. Many clinical trial subjects have complained about the discomfort. In some cases, irradiations had to be interrupted to allow for breaks. If it is a bilateral irradiation, then the

required time is double what is mentioned above. The current MIT facility is only adequate for early clinical trials. However, if the BNCT is to progress then a high intensity beam is required for advanced clinical trials and to meet the demand for eventual nontrial therapy.

Table 1.1: Measured in air beam performance for existing epithermal neutron beams. (D_{fn} and D_{γ} are fast and gamma dose rates (cGy/s) respectively)

Beam	**Reactor Power** **MW**	Φ_{epi} **n/cm²s**	D_{fn}/Φ_{epi} **cGy cm2/n**	D_{γ}/Φ_{epi} **CGy cm²/n**
MIT[9]	5	2.1E+08	8.7E-11	1.3E-10
BMRR[10]	3	1.8E+09	4.3E-11	1.3E-11
Petten[11]	45	3.3E+08	1.04E-10	8.4E-11

The current fast neutron and gamma dose contaminations have a non-negligible effect on in-phantom profile measurements. The fast neutron and gamma dose components to healthy tissue are comparable to the boron related background dose when current boron compounds such as BPA and the existing epithermal neutron beam are used for a treatment. The dose to healthy tissues limits the dose that can be delivered to a tumor. By decreasing the contamination dose components,

one can deliver more dose to the tumor. Therefore, it is desirable to have a less contaminated epithermal neutron beam to increase the therapeutic advantage.

In recent years, many design studies have been reported in the literature to obtain high intensity epithermal beam and to reduce the contamination in the beam. Some of these design studies of beam performance are summarized in table 1.2.

Table 1.2: Summarized in air beam performances of recent design studies

	Φ_{epi} **n/cm²s**	$D_{fn}/\Phi epi$ **cGy cm²/s**	D_{γ}/Φ_{epi} **cGy cm²/s**	**Remarks**
Musashi Institute of Technology[12]	3.8E+08			Reactor core is redesigned, Filter Al/Al_2O_3
Tsing Hua Open Pool Reactor[13]	1.7E+07	3.58E-11	1.74E-11	Current reactor power of 1MW with a potential to be upgraded to 3MW, Filter Al/Al_2O_3
Brookhaven Medical Research Reactor[14]	1.2E+10	2.8E-11	<1.0E-11	Fission plate converter design, Filter Al/Al_2O_3
George Institute of Technology Research Reactor[15]	2.5E+09	1.3E-11	1.8E-11	Reactor power 5MW, Filter D_20-Al- Lithiated aluminum plates
Massachusetts Institute of Technology Research Reactor[20,21]	2.0E+10	1.3E-11	1.2E-11	Converter Design, Filter Al/AlF_3
Research Reactor Institute Kyoto University[16]	2.4E+08	2.3E7 n/cm2.s		Reactor power 5MW, Filter Al-D_2O

4. Design Goal

On average, the existing epithermal neutron beam facilities can irradiate about 2 to 3 patients a day. There are 7000 new primary brain tumor patients per year in the USA alone and several other numerous cancers, which potentially can be treated by BNCT. If BNCT becomes a successful treatment modality for certain cancers, there will be a need for high intensity and low contamination epithermal neutron beams. The first goal is to design an epithermal neutron beam facility, which can treat a patient rapidly e.g. within 1 to 5 minutes. This is comparable to the conventional radiation therapy and allows high throughput to meet the potential demand. A fission converter based design for high performance epithermal neutron beam has been developed at MIT. This thesis deals with engineering design of this facility.

The existing facilities use neutrons from a research reactor after filtering with suitable filter materials. These research reactors are either solely used for BNCT purpose or experience some type of interference during trials. For example, MITR-II power level has to be brought down before accessing the medical room. This introduces interference to other projects at MITR-II. The second goal is to design a fission converter facility with minimal interference to reactor operation.

Fission converter facility will be accessed by professionals such as clinicians, medical physicists, patients, and patients' relatives and others

who accompany the patient. It is also not an isolated from the general experimental area in the reactor's containment building. Therefore, it is very important to design a system which is safe. The design includes adequate heat removal, protecting integrity of fuel during any conceivable accidents and controlling the radiation dose to the public during normal operation.

In addition to the above design goals, the overall system should satisfy a number of other requirements. The overall fission converter facility will be housed in the thermal column area of the MITR-II. This includes adapting some of the existing systems and materials and requirements for minimal modification of the thermal column area of MITR. The new system should be economically feasible to build and to operate. The system should be simple, easy to maintain, and flexible to modify any part of the fission converter facility. Finally, decommissioning of the existing thermal column area and installation of the new facility should be economically feasible and easy to perform.

5. Description of the MITR-II and Thermal Column Area

Since the MITR-II reactor is the source for the fission converter facility and the fission converter facility will be built in the thermal

column area, it is important to describe the MITR-II and especially the thermal column area. A brief introduction to the MITR-II reactor, experimental facilities at the MITR-II and the thermal column area are provided in this section. The most attention is given to the systems, materials and equipment of MITR-II which are part of the fission converter design study.

5.1 MITR-II Reactor

The MITR-II reactor is a 5 MW research reactor that is cooled and moderated by light water. Heavy water is used as a reflector. Currently a study is being conducted to increase the power to 10 MW. Figure 1.1 is an artist's isometric view of the MITR-II. The reactor has two concentric tanks; an inner tank holds the reactor core and light water, and an outer tank holds the heavy water reflector. The outer tank has an inner diameter of 1.22 meters (4 feet) and contains a blister tank welded at the bottom. This blister tank contains heavy water and the energy spectrum of neutron flux to the current medical room can be controlled by changing the heavy water level in the blister tank. The outer tank is surrounded by a graphite reflector, thermal shield, and dense concrete biological shield. The annular graphite reflector region is 0.61 meters (2 feet) thick.

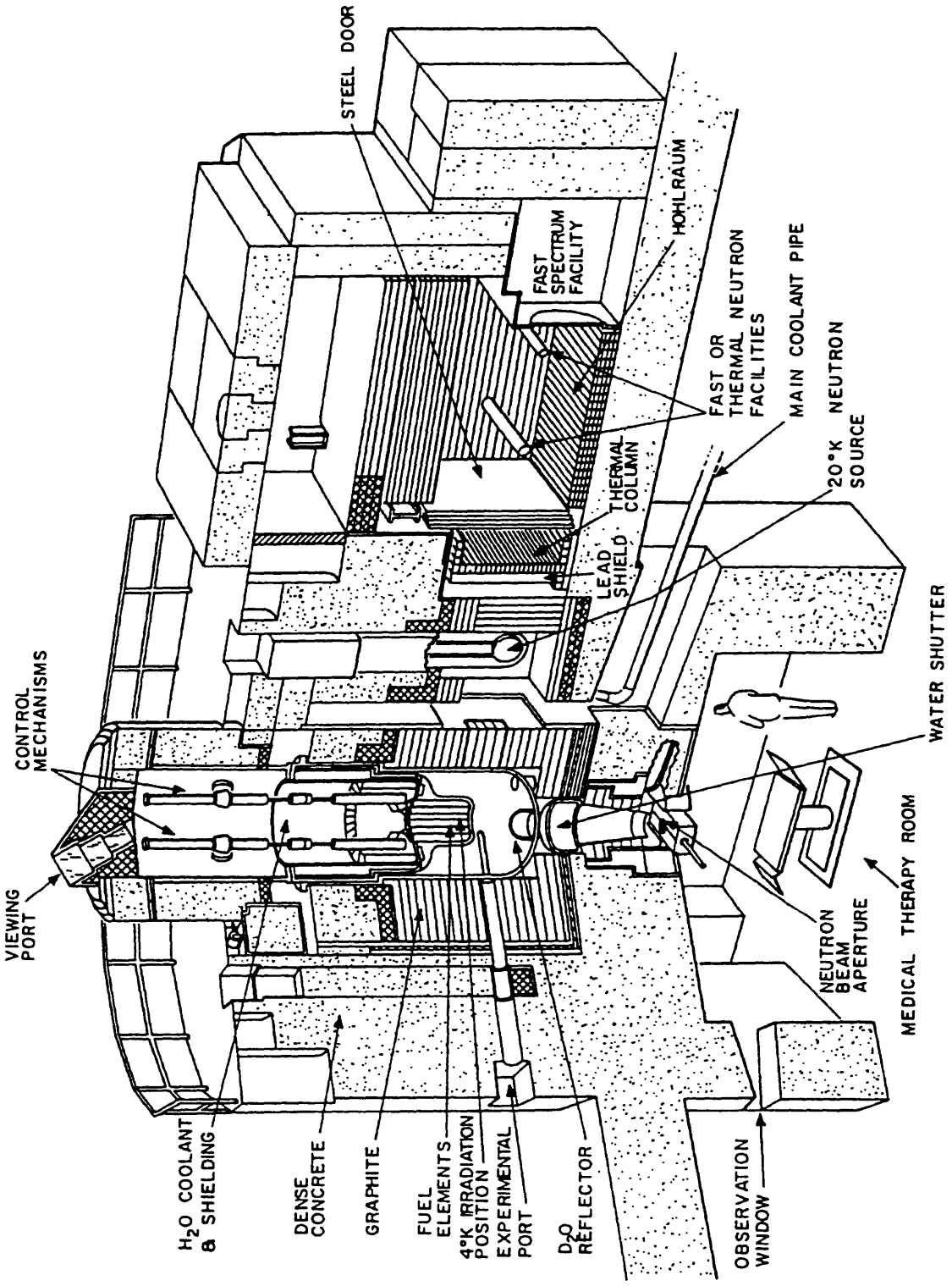

Figure 1.1: Artist's Isometric View of the Entire MITR-II

The thermal shield consists of two cylinders of 5.08 cm (2 inch) of steel each surrounding an annulus of 3.81 cm (1.5 inches) of lead and is followed by the dense concrete biological shield 1.68 meters (5.5 feet) thickness.

The reactor core is a hexagon. It consists of three concentric hexagonal rings of fuel with 15 fuel elements in the outer hexagon, 9 elements in the next hexagon and 3 elements in the center. The MITR-II fuel elements are a rhomboidal shape to facilitate the hexagonal core arrangement. Each fuel element contains 15 finned fuel plates that are held in place 0.381 cm (0.15 in) apart by two grooved aluminum 6061 side plates. Each fuel element contains 93% enriched UAl_x cermet clad in aluminum 6061. Nozzles are welded to the side plates at the top and the bottom of each fuel element to be secured in the core by a lower grid plate and an upper lock down plate. Each fuel element is 66.67 cm (26.25 in) long and has active fuel length of 56.83 cm (22.375 in). The fuel loading of each fresh fuel element is 510 g ^{235}U. A side and a cross-sectional view of MITR-II fuel element are shown in figure 1.2.

The reactor is controlled by 6 shim control blades and one regulator rod. The shims are flat blades suspended from a magnet on a translating screw drive system. Blades position is measured by two servomotors and the in and out limits are controlled by switches. Shim blades are made of stainless steel containing 1% boron.

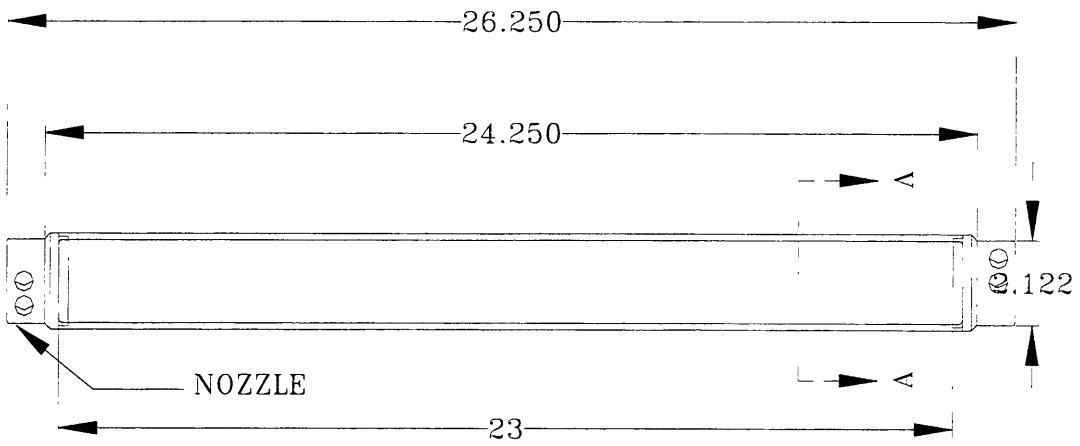

Section A-A (fins are not shown)

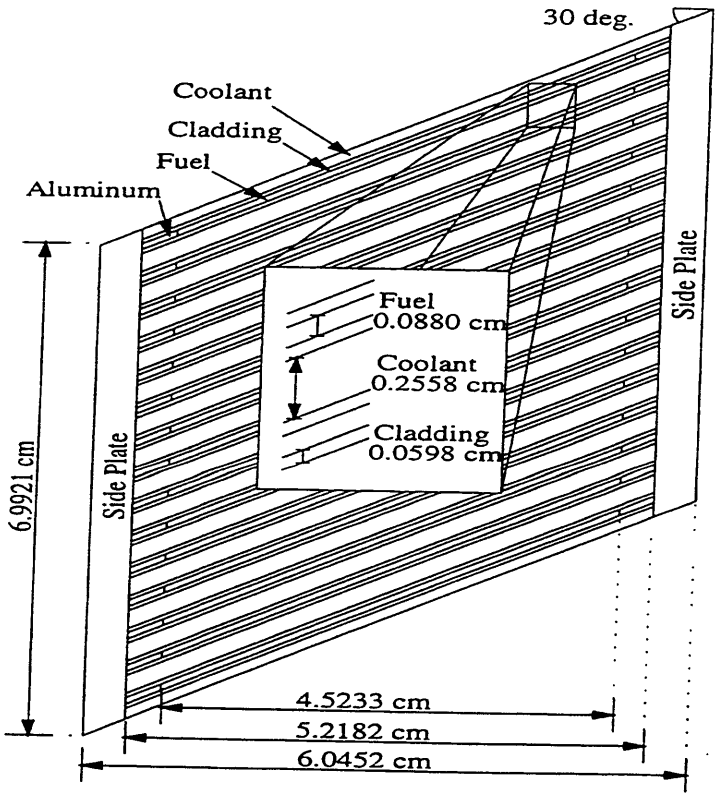

Figure 1.2: MITR-II Fuel Element Side and Cross Sectional Views are Shown (Top figure dimensions are given in inches)

On a scram signal the magnets holding the shim blades are deactivated and the armature rod-absorber unit falls by gravity into the core. The safety channel response and blade drop time is less than 1 second. A single large pipe in the heavy water reflector tank permits rapid emptying of the heavy water reflector, providing a secondary safety mechanism for shutdown.

A block diagram of the major components in the MITR-II heat removal system is shown in figure 1.3. During normal operating conditions the heat generated in the core is transferred to primary coolant by forced convection. The direction of primary coolant flow in the core is upward. In the main heat exchangers, the primary coolant transfers its heat to the secondary coolant. The secondary coolant flows to the cooling towers where the heat is ultimately rejected to the atmosphere. The primary flow rate is about 2000 gpm and primary coolant core inlet and outlet temperatures are about 40 ^{0}C and 56 ^{0}C respectively. The secondary flow rate is about 1550 gpm and cooling tower inlet and outlet temperatures are about 35 ^{0}C and 25 ^{0}C respectively.

The MITR-II reactor building has three levels; the basement, the first floor and the second floor or the reactor top floor. These floors are described below.

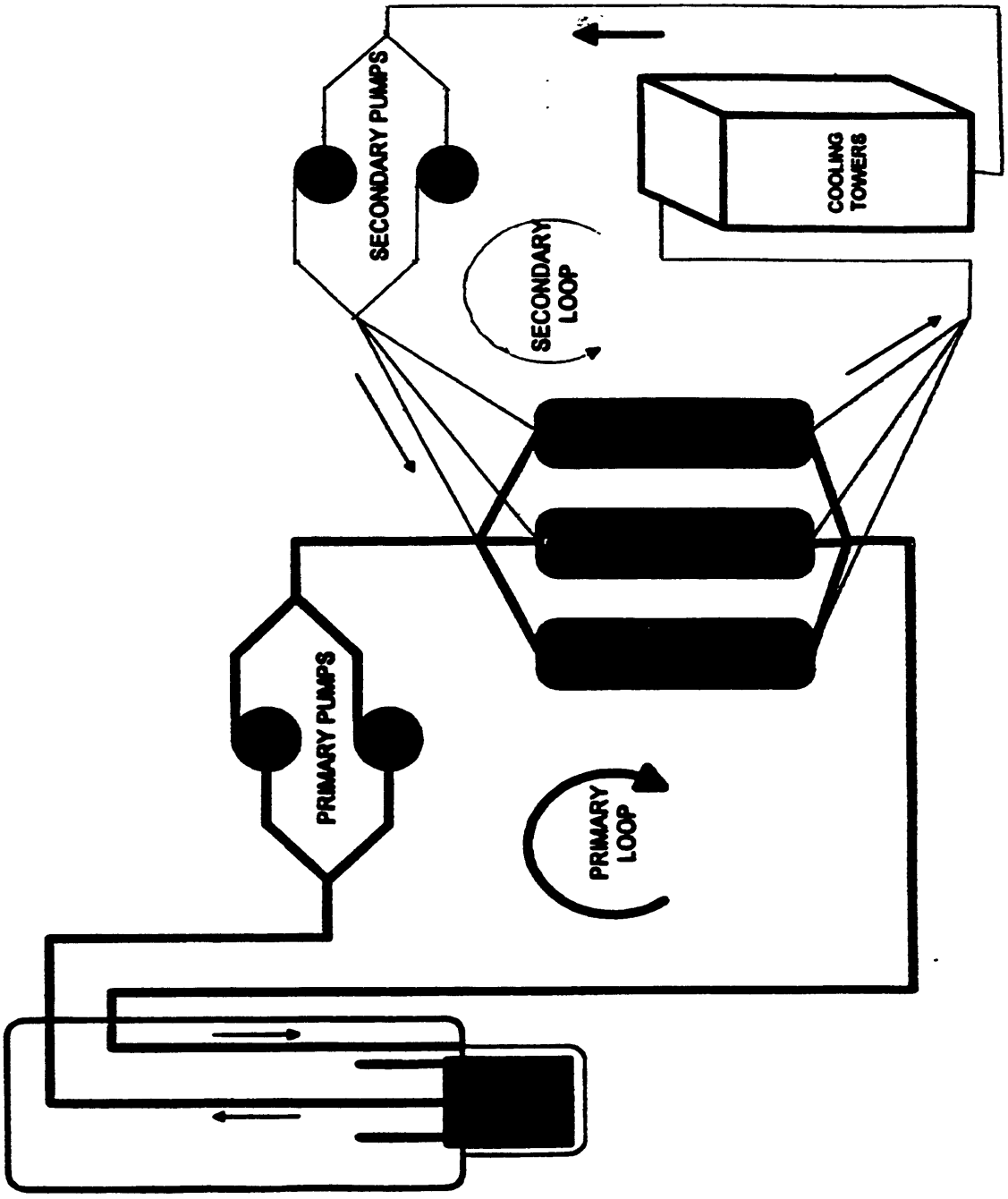

Figure 1.3: Schematic of MITR-II heat removal system showing major components of primary and secondary loops. (Courtesy of M. McGwire)

The basement floor contains the reactor control room, current medical therapy room, current medical therapy control area, spent fuel storage facility, mechanical room and hot storage room. A plan view of the basement floor level is shown in figure 1.4. The control room contains the control console and process instrumentation for the reactor. The medical therapy room is primarily used to irradiate human subjects and animals. Subjects are positioned under the neutron beam aperture in the medical room ceiling. The medical control area is directly outside of the medical therapy room. A transparent shielded window allows observation of a subject from the medical therapy area. The beam monitoring system is also located in the medical control area. The spent fuel storage facility consists of a room containing a 6.1 meters (20 feet) deep well of water. A steel structure is placed on the top of this well, and the fuel transfer cask (nessy) is set on this steel structure before spent fuel is transferred into the well. There is a grid structure at the bottom of the well to position the spent fuel elements. There is enough cadmium to prevent accidental assembly of a critical array. Hot storage consists of holes in the concrete floor for temporary storage of relatively low activity equipment and waste.

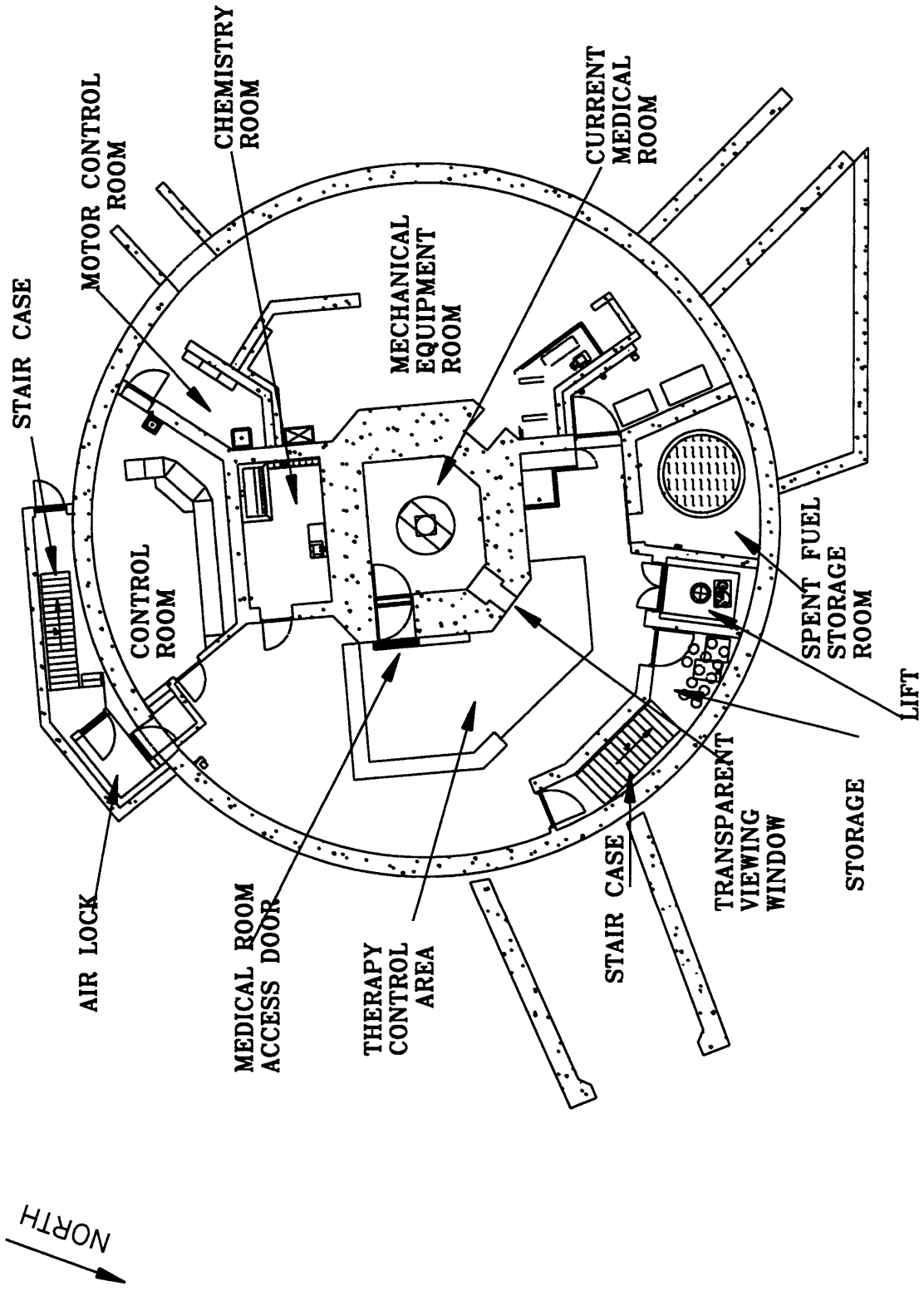

Figure 1.4: MITR-II Reactor Basement Plan View (Courtesy of T. Date)

The first floor serves as the main reactor room floor. A plan view of the first floor is shown in figure 1.5. A personnel air lock and a truck air lock provide access to this floor. The first floor is adequate to support a load of 3000 pounds per square foot within 8 ft. of the reactor base and 2000 pounds per square foot elsewhere. The hot plug storage in the wall of the reactor room consists of mild steel pipes welded into the gas-tight enclosure and extending outward into a shield vault. The thermal column area is on the right side of the MITR-II reactor.

The second floor includes the reactor top, a movable bridge, a circular platform around the building, various equipment platforms and a polar crane with a 20 ton capacity. Access to the reactor top from the first floor is provided by a stairway. The plan view of the reactor top is shown in figure 1.6.

5.2 MITR-II Thermal Column Area

The thermal column area includes the thermal column vertical duct, and hohlraum. A cross-sectional view of the MITR-II reactor and the thermal column area is depicted in figure 1.7. Thermal columns are found in many research reactors. They are characterized by a high degree of neutron thermalization and usually provide large area thermal neutron beams.

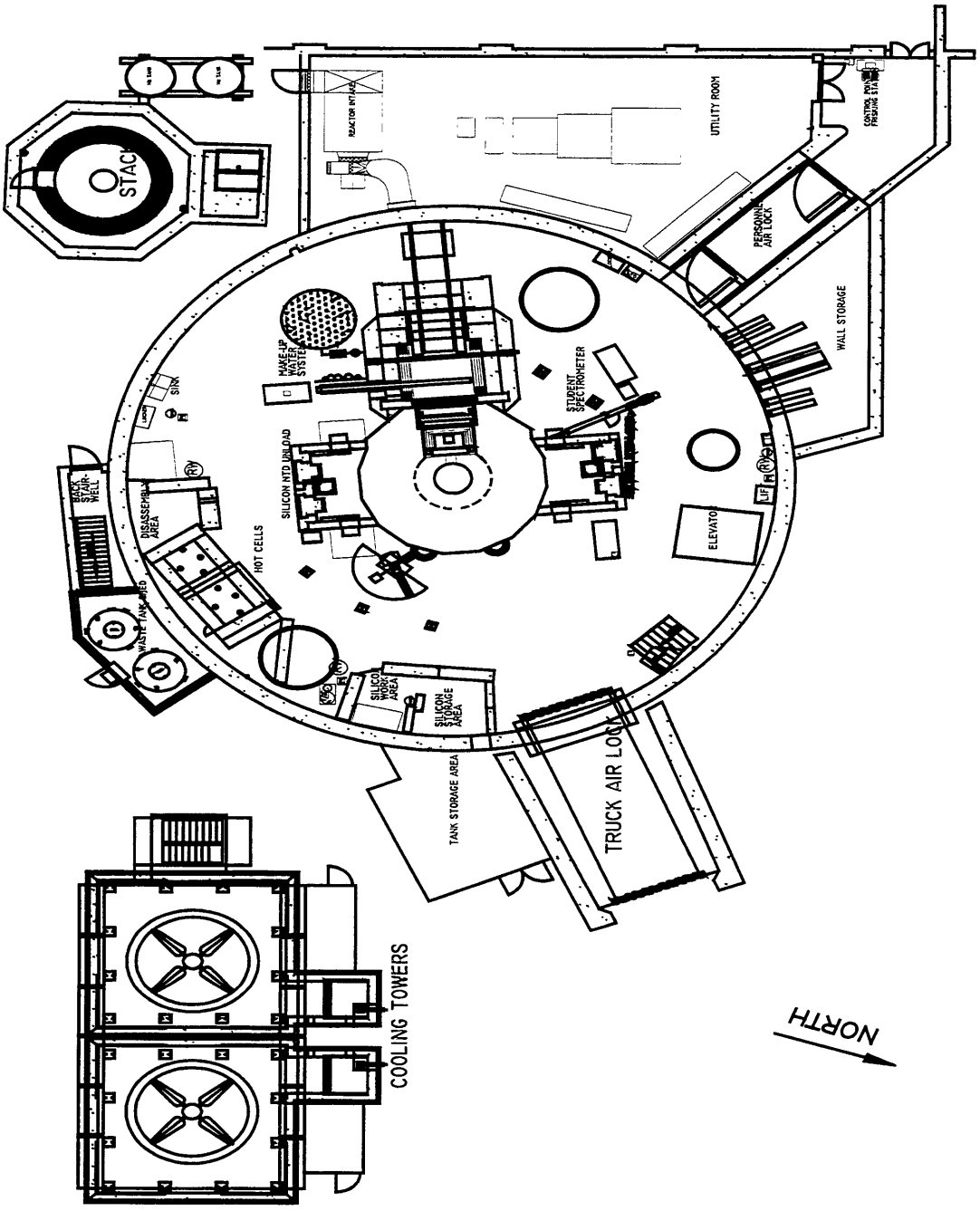

Figure 1.5: MITR-II Reactor First Floor Plan View (Courtesy of T. Date)

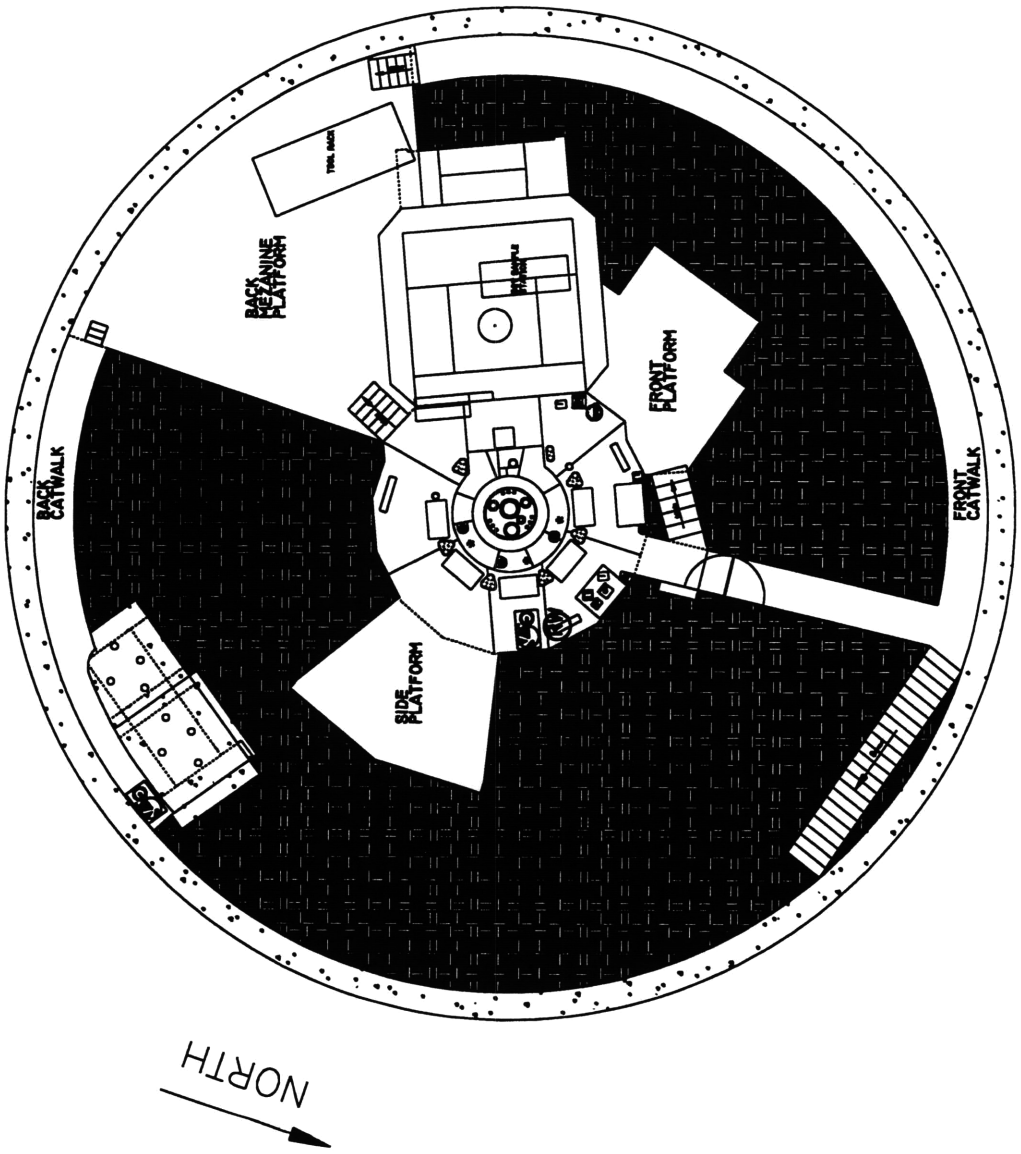

Figure 1.6: Reactor Top Floor Plan View (Courtesy of T. Date)

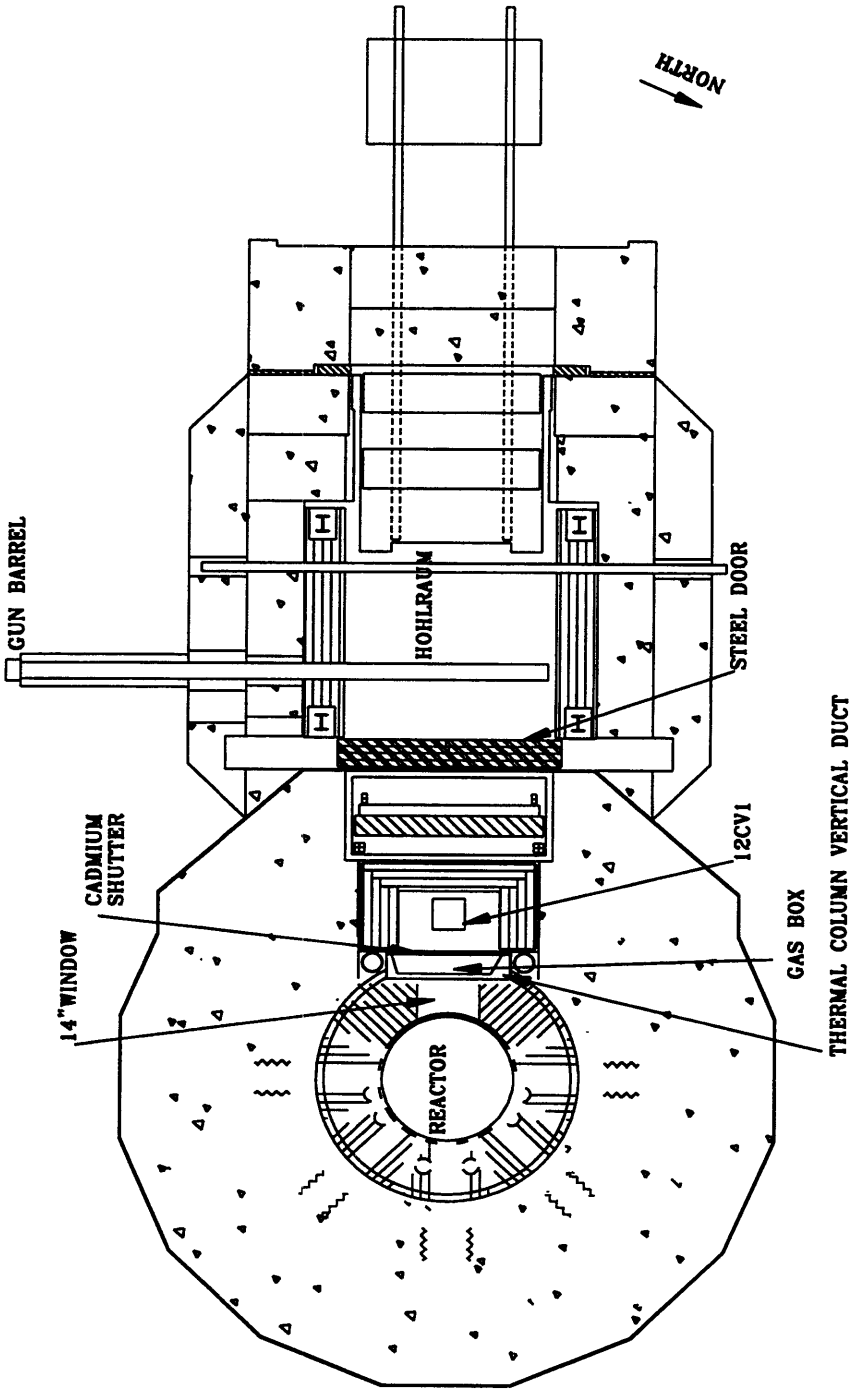

Figure 1.7: Horizontal cross section view of reactor and thermal column area, showing current setup in the thermal column area (Courtesy of T.Date)

The thermal column vertical duct is the space between the graphite reflector and the thermal column. This thermal column vertical duct contains the two reactor primary coolant pipes, a trapezoidal aluminum gas box filled with CO_2 and a cadmium shutter which controls thermal neutron flux in the thermal column. The gas box and the cadmium shutter hang on the same frame. This frame is attached on the rear edge of the vertical duct. Two shield blocks, the upper shield block and lower shield block, are placed in the top part of the thermal column vertical duct to minimize the radiation dose in the upward direction. The cadmium shutter motor and shaft, and control rod motor are placed on the top of the upper shield block. Figure 1.8 depicts the plan view of the thermal column vertical duct.

The cadmium shutter and the frame are shown in figure 1.9. The cadmium shutter has three parts; two permanently fixed cadmium-aluminum sandwiches (item 1 and item 2 in figure 1.9) and a movable cadmium-aluminum sandwich. The movable part of the cadmium shutter slides up and down in the shutter frame. Six bumpers, three on each side of the movable cadmium shutter, allow minimal contact between the shutter and the frame, and reduce friction between the shutter and the frame during the movement. The cadmium shutter movement is controlled by the gear motor assembly, which is shown in figure 1.10. The gear motor is attached to the chain sprocket by a chain. When the motor is on, the gear motor rotates the chain sprocket and the

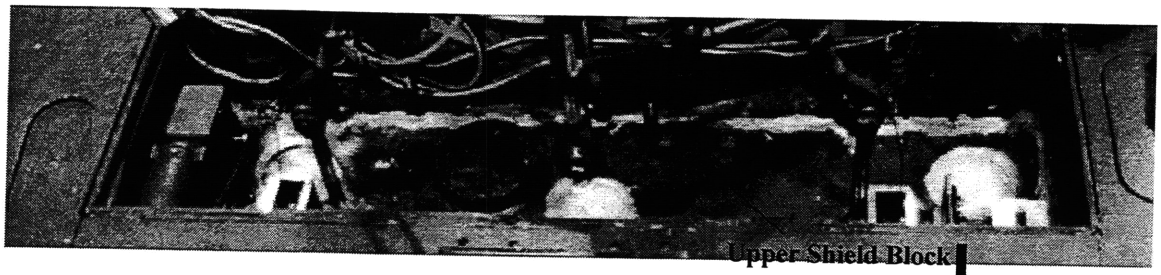

Plan view of the thermal column cavity showing the upper shield block

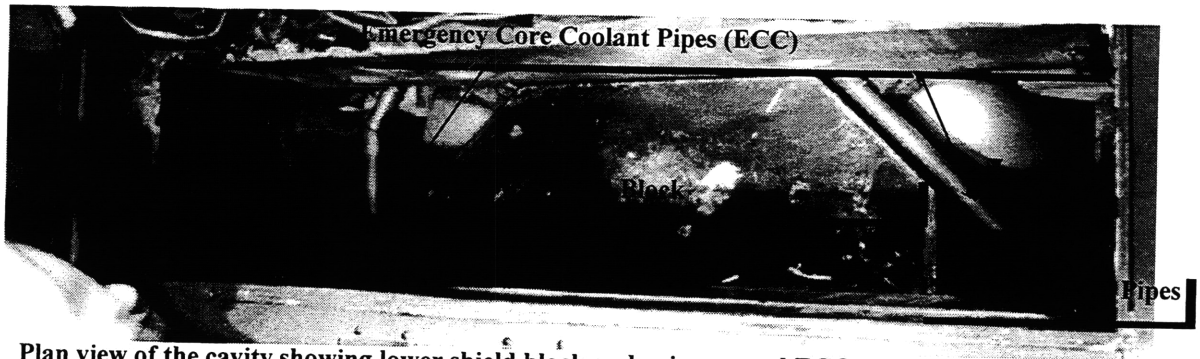

Plan view of the cavity showing lower shield block and primary and ECC pipes after removing the upper shield block

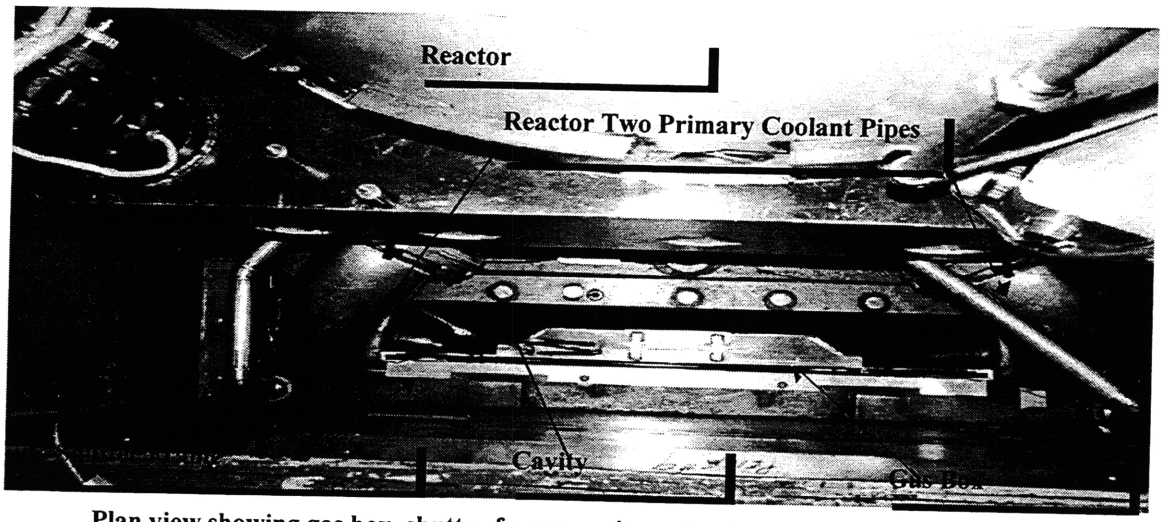

Plan view showing gas box, shutter frame, cavity and primary coolant and ECC pipes

Figure 1.8: Plan View Pictures of Thermal Column Cavity Showing Upper and Lower Shield Blocks

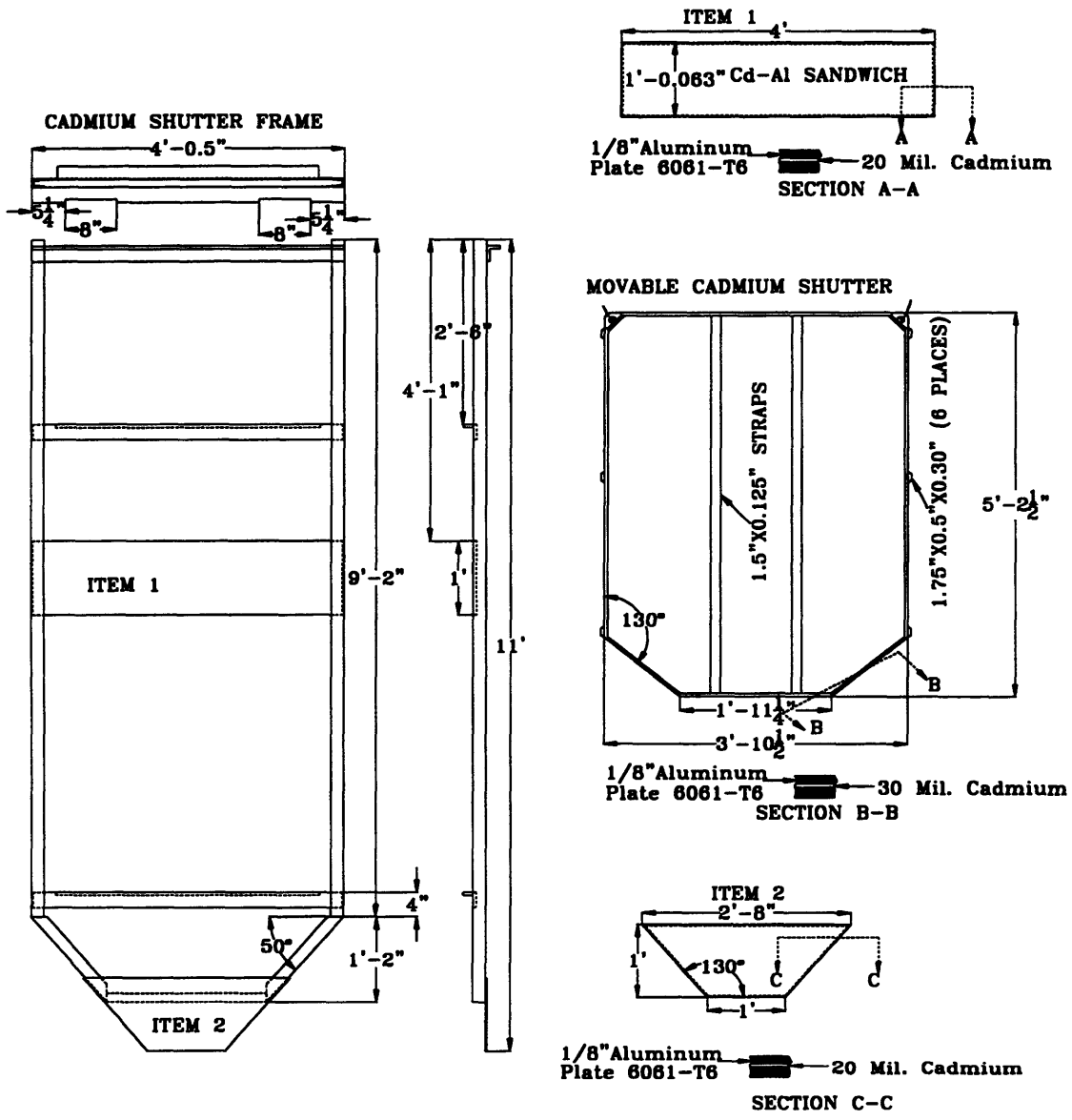

Figure 1.9: Current Cadmium Shutter and Shutter Frame (Dimensions are taken from blue prints)

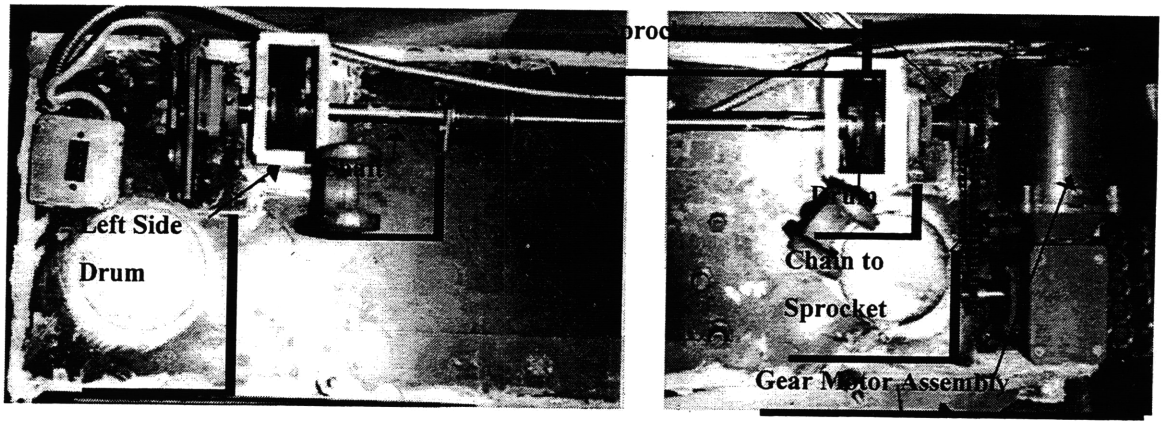

Figure 1:10: Cadmium Shutter Gear Motor Assembly for Raising and Lowering Shutter

shaft which is connected to the chain sprocket. Two drums, one on the right side and the other one on the left side are attached to the shaft.

The rolled wire cables on the drums will move the shutter up or down depending on the direction the drums rotates. These two cables are attached to each side of the movable cadmium shutter. The torque limiter stops the motor after the shutter is fully closed or opened. There is also a trip switch at the top of the shutter to indicate a fully opened position.

Two irradiation ports are located in a graphite lined cavity (called the hohlraum, see figure 1.7) beyond the steel door which open side-ways. 6CH1 is composed of a 7 inch diameter horizontal tube, which penetrates the hohlraum shield wall. The hohlraum was originally used in MITR-I to feed thermal neutrons into heavy water exponential tank.

During the reactor renovation, the heavy water tank was removed and the hohlraum area was converted to a fast reactor blanket test facility. The top shielding is a removable block. The hohlraum is about 2.7 m wide to 2.6 m long. The future medical room will be located in the hohlraum. The hohlraum area is shown in figures 1.11 and 1.12.

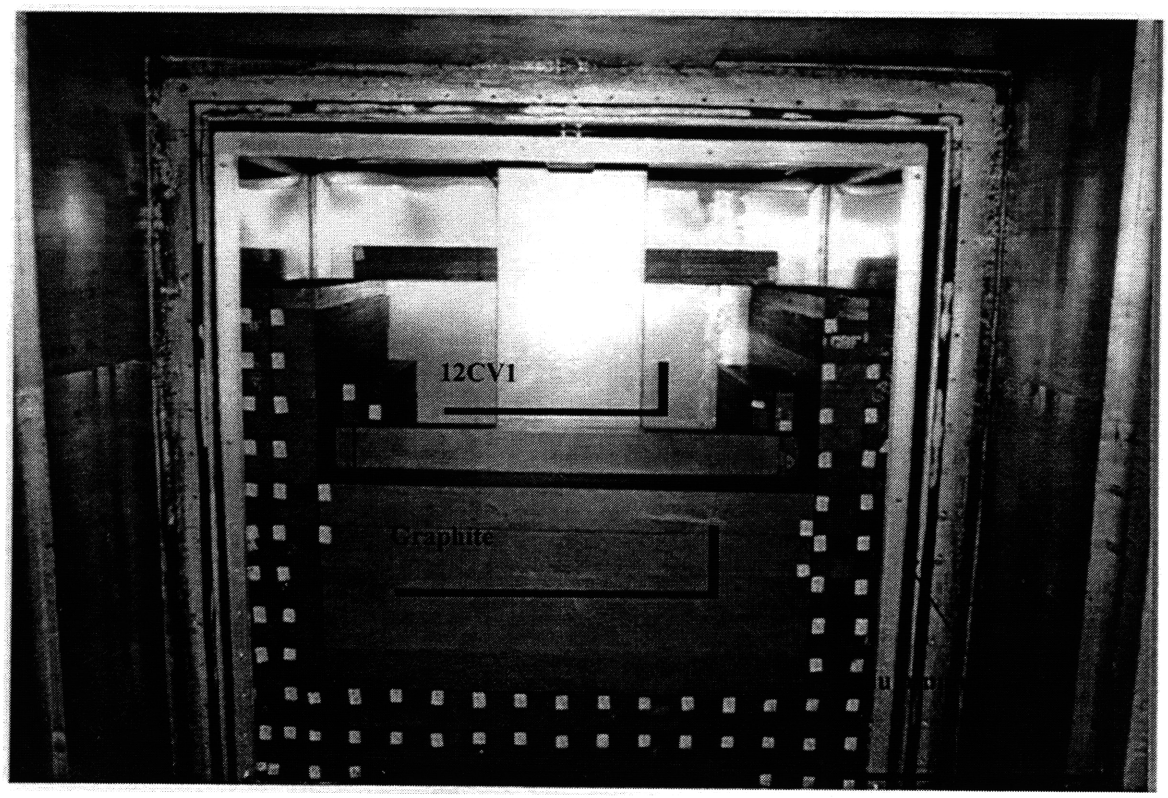

Figure 1.11: The thermal column is viewed from the steel doors, shown in figure 1.7. This picture was taken during the thermal column renovation. An aluminum gasket at the front provides the gas seal between the thermal column and the thermal column vertical duct.

Figure 1.12: The hohlraum is viewed from above during renovation. The steel doors provide access to the thermal column. (Reactor Core is Toward Bottom of Page)

6. References

1. Locher, G.L., *Biological Effects and Therapeutic Possibilities of Neutrons,* Am. J. Roentgenol. Radium Ther., 36: 1-13, 1936.
2. Sweet, W. H., *The Use of Nuclear Desintegrations in the Diagnosis and Treatment of Brain Tumor,* N. Engl. J. Med., 245: 875-878, 1951.
3. Sweet, W. H., Javid, M., *The Possible Use of Neutron- Capturing Isotopes such as Boron-10 in the Treatment of Neoplasms,* I. Intracranial Tumors, J. Neurosurg., 9: 200-209, 1952.
4. Farr, L.E., Sweet, W.H., Robertson, J.S., Foster, S. G., Locksley, H.B., Sutherland, D.L., Mendelsohn, M.L., Stickey, E.E., *Neutron Capture Therapy with Boron in the Treatment of Glioblastoma Multiforme,* Am. J. Roentgenol., 71: 279-291, 1954.
5. Goodwin, G.T., Farr, L.E., Sweet, W.H., Robertson, J.S., *Pathological Study of Eight Patients with Glioblastoma Multiforme Treated with by Neutron Capture Radiation Using Boron-10,* Cancer (Phila.), 8: 601-615, 1955.
6. Asbury, A.K., Ojean, R.G., Nielsen,S.L., Sweet, W.H., *Neuropathological Study of Fourteen Cases of Malignant Brain Tumor Treated by Boron-10 Slow Neutron Capture Therapy,* J. Neuropathol. Exp. Neurol., 31: 278-303, 1972.
7. Hatanaka, H., *Clinical Results of Boron Neutron Capture Therapy,* In: Proceeding of an International Workshop on Neutron Beam Design, Development, and Performance for Neutron Capture Therapy, MIT, Cambridge, March 29-31, 1989.

8. Mishima, Y., Ichihashi, M., Tsui, M., Hatta, S., Ueda, M., Honda, C., Susuki, T., *Treatment of Malignant Melanoma by Single Thermal Neutron Capture Therapy with Melanoma-Seeking [10]B Compound,* Lancet, 2: 388-389, 1989.

9. Rogus, R.D., *Design and Dosimetry of Epithermal Neutron Beams for Clinical Trials of Boron Neutron Capture Therapy at the MITR-II Reactor,* Ph.D. Thesis, Massachusetts Institute of Technology, 1994.

10. Fairchild, R.G., Kalef-Ezra, J., Saraf, S.K., Fiarman, S., Ramsey, E., Wielopolski, L., Laster, B.H., Wheeler, F.J., *Installation and Testing of an Optimized Epithermal Neutron Beam at the Brookhaven Medical Research Reactor (BMRR),* in Neutron Beam Design, Development, and Performance for Neutron Capture Therapy, (Ed. By O.K. Harling et al., Plenum Press, New York, 1990.).

11. Moss, R.L., Stecher-Rasmussen, F., Ravensburg, K., Constantine, G., Watkins, P., *Design, Construction and Installation of an Epithermal Neutron Beam for BNCT at the High Flux Reactor Petten,* in Progress in Neutron Capture Therapy for Cancer (Ed. By B.J. Allen et al., Plenum Press, New York, 1992).

12. Aizawa, O., *Design Study on Triangular-Hexagonal Triga Core for Epithermal Neutron Irradiations,* Cancer Neutron Capture Therapy, (Ed. By Mishima, Plenum Press, New York, 1996)

13. Su, L., Liu, H.Y-W., Peir, J.J., Liaw, F.T., *Eptihermal Neutron Beam Design for Neutron Capture Therapy at Tsing Hua Open-Pool Reactor,* Cancer Neutron Capture Therapy, (Ed. By Mishima, Plenum Press, New York, 1996).

14. Liu, H.B., Brugger, R.M., Rorer, D.C., *Upgrades of the Epithermal Neutron Beam at the Brookhaven Medical Research Reactor,* Cancer Neutron Capture Therapy, (Ed. By Mishima, Plenum Press, New York, 1996).

15. Klee, K.A., Karam, R.A., *Conceptual Design for an Epithermal-Neutron Beam for Boron Neutron Capture Therapy at the Georgia Institute of Technology Research Reactor,* Cancer Neutron Capture Therapy, (Ed. By Mishima, Plenum Press, New York, 1996).

16. Kobayashi, T., Sakurai, Y., Kanda, K., Fujita, Y., *Remodeling of the Heavy Water Facility of the Kyoto University Reactor for Epithermal Neutrons,* Cancer Neutron Capture Therapy, (Ed. By Mishima, Plenum Press, New York, 1996).

17. Mishima, Y., *Cancer Neutron Capture Therapy,* NewYork: Plenum, 1996, Proceedings of the Sixth International Symposium on Neutron Capture Therapy, October 1994, Kobe, Japan.

18. Allen, B.J., Moore, D.E., and Harrington, B.V., *Progress in Neutron Capture Therapy for Cancer,* New York: Plenum, 1992, Proceedings of the Fourth International Symposium on Neutron Capture Therapy, December 1990, Sydney, Australia.

19. Soloway, A.H., Barth, R.F., and Carpenter, D.E., *Advances in Neutron Capture Therapy,* New York: Plenum, 1993, Proceedings of the Fifth International Symposium on Neutron Capture Therapy, September 1992, Ohio, USA.

20. Kiger III, W.S., *Neutronic Design of a Fission Converter-Based Epithermal Beam for Neutron Capture Therapy,* Nucl. E. Thesis, Massachusetts Institute of Technology, 1996.

21. Sakamoto, S., *Sensitivity Studies of the Neutronic Design of a Fission Converter-Based Epithermal Beam for Boron Neutron Capture Therapy,* M. Sc. Thesis, Massachusetts Institute of Technology, 1997.

CHAPTER TWO

FISSION CONVERTER BEAM OVERALL FACILITY DESIGN

1.Overall Design of the Fission Converter Beam Facility

The proposed design of the fission converter beam facility is shown in isometric view in figure 2.1. Eleven MITR-II fuel elements are centered on the 14" cubical window in the graphite reflector to optimize the fuel element exposure to the leakage neutrons from the MITR-II reactor core. These eleven fuel elements are housed in a fission converter tank, which is placed in the thermal column cavity between the graphite reflector and the thermal column. The fission converter tank design is discussed in section 3 of this chapter. The aluminum gas box, the current cadmium shutter frame and the current cadmium shutter will be removed from the thermal column cavity and a new cadmium shutter frame and a new cadmium shutter will be placed in front of the fission converter tank.

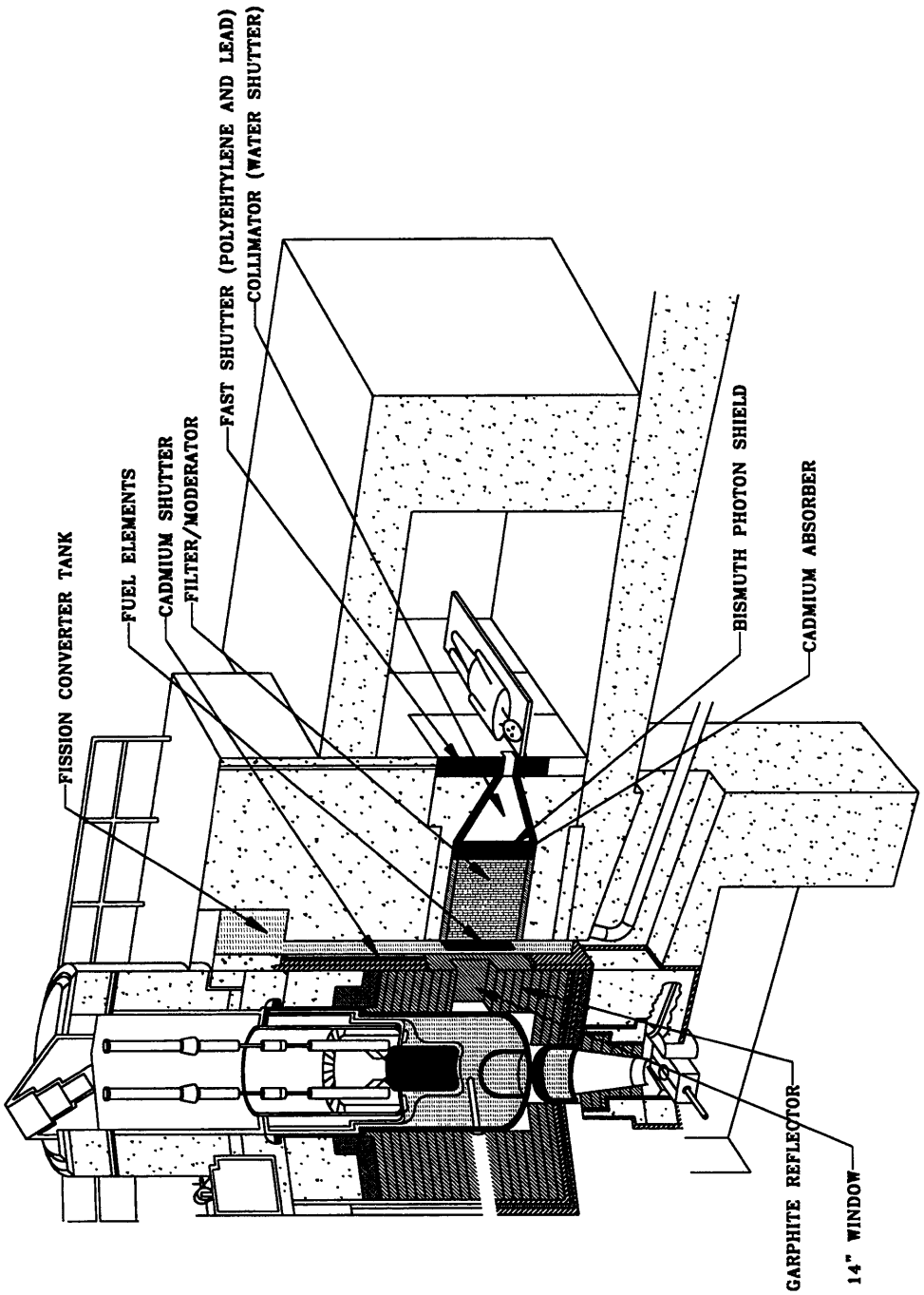

Figure 2.1: Isometric View of the Proposed Design of Fission Converter Facility (Originally drawn by W.S.Kiger and modified by the author)

The cadmium shutter frame may be permanently attached to the front plate of the fission converter tank. The cadmium shutter will be used to reduce the fission rate by a factor of 100 and consequently the heat generation in the eleven fuel elements and also to help control the radiation level in the medical room. The new cadmium shutter and the frame design will be discussed in section 3.2 of this chapter.

Either light water or heavy water or a mixture of both (low quality heavy water) will cool the eleven fuel elements. Different modes of transferring heat from fuel elements to the fission converter's primary coolant in the fission converter tank are analyzed in chapter 3. The generated heat from eleven MITR-II fuel elements is transported to the upper plenum of the fission converter tank by the fission converter's primary coolant. Then, the primary coolant of the fission converter transfers the heat to the MITR-II secondary coolant through a heat exchanger. The MITR-II secondary transports the heat to the atmospheric air through the cooling tower.

W.S. Kiger[1] and S.Sakamoto[2] considered different filter/moderator materials in their fission converter neutronic studies. The beam performances of the different filter/moderator materials are summarized in section 2 of this chapter. The radioactive graphite blocks and other materials, which are presently in the thermal column and the surrounding areas, will be removed to install the filter/moderator and collimator assembly. Lead or nickel reflectors surrounding the

filter/moderator are considered to reduce neutron losses and to improve shielding outside the beam. A thin layer (0.4 mm) of cadmium in the filter/moderator will remove thermal neutrons from the beam. A bismuth or lead shield is placed after the filter/moderator assembly to shield photons. The collimator focuses the neutron beam onto the patient position.

The beam at the patient position is controlled by the cadmium shutter, a light water shutter, and a fast acting mechanical shutter. The empty space in the collimator will be used for a light water shutter by filling or emptying a tank in the collimator. A detailed study of shutters is provided in chapter 4.

The medical room will be located in the current hohlraum area. The hohlraum will be completely removed to build the medical room. The medical room is surrounded by heavy concrete to shield the neutron beam and gamma rays. Entry to the medical room is through a sliding door. There will be a control room outside of the medical room. Most of the instruments will be controlled from the control room. A design study of the medical irradiation room is presented in chapter 4.

2.Summary of Neutronic Studies

W.S.Kiger[1] performed the first neutronic study for the fission converter epithermal beam. His study includes three major components:

developing a methodology for efficient neutronic calculation of the beam design using the Monte Carlo radiation transport code MCNP-4A, validating the MITR-II MCNP-4A model by comparing the calculated results with measurements; and design calculations of various components in the beam. His main objective was to achieve certain beam performance design goals. These beam performance goals are: a high intensity epithermal beam (Φ_{epi} about $1*10^{10}$ n/cm^2 sec at the patient position) to complete an irradiation within few minutes, and negligible contamination from unwanted fast neutrons and photons (D/Φ_{epi} not greater than $2*10^{-11}$ cGycm^2/n). This background level is small compared to the inherent background contamination due to radiative capture of hydrogen. After an extensive series of parametric studies for filter/moderator materials and collimator designs, W.S. Kiger[1] proposed a beam design that is shown in figure 2.2. The reader is encouraged to read Ref. 1 for detailed information about this study.

Although the beam design proposed by Ref. 1 exceeds the design goals of high intensity epithermal beam and low contamination of fast neutrons and photons, further study was performed by S.Sakamoto[2] to provide a better therapeutic ratio and other figures of merit, such as low cost, enhanced safety, flexibility, engineering advantages and the

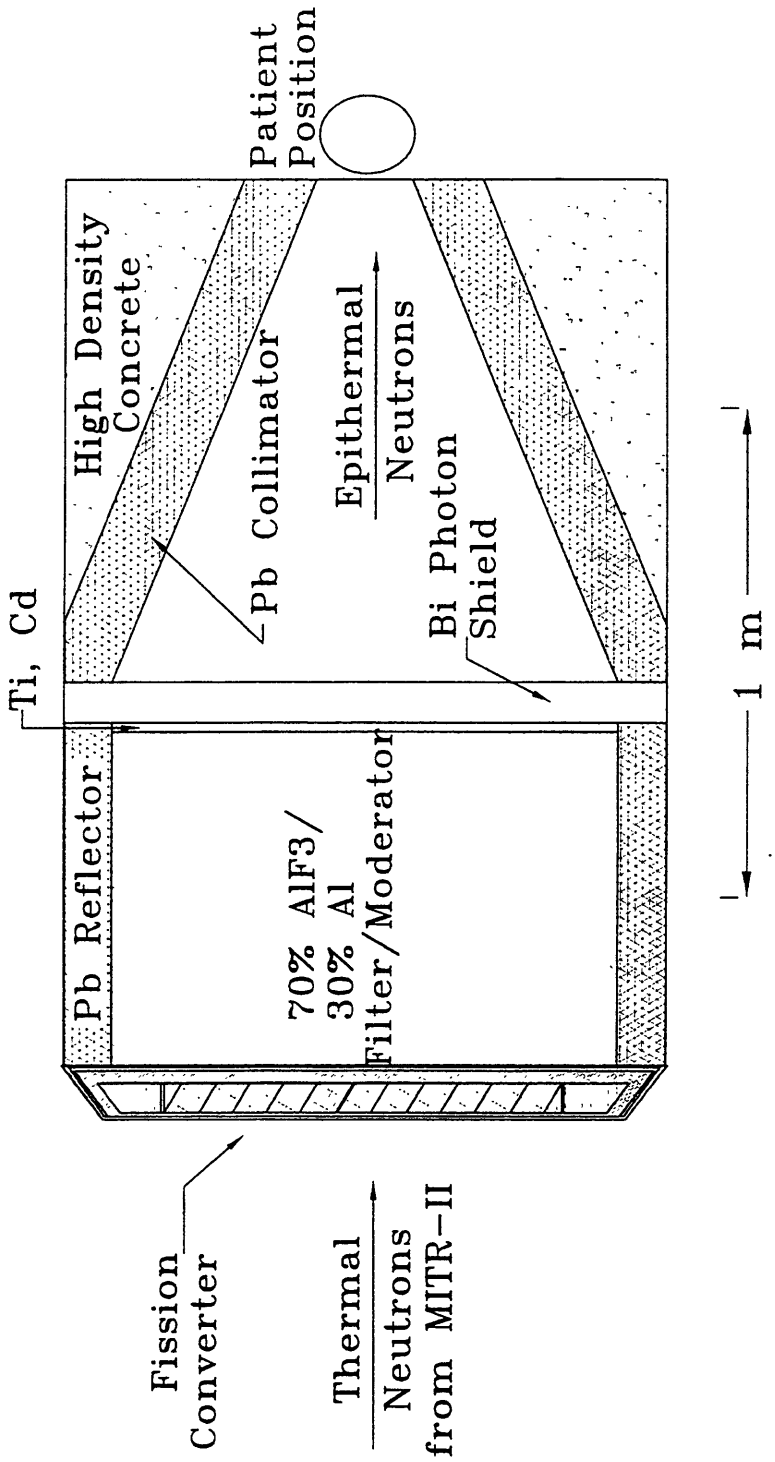

Figure 2.2: Shows the Plan View of the Fission Converter Beam Design Proposed by W.S Kiger (Courtesy of W.S Kiger)

environmental compatibility filter/moderator materials of the facility. S.Sakamoto's main goals were to identify the best configuration of multi-plate reactor type fuel elements, to select the best materials and configuration for the neutron filter/moderator, and to improve the collimator design in terms of directionality, materials and beam aperture size. S.Sakamoto[2] proposed a design that is shown in figure 2.3. Again the reader is encouraged to read Ref. 2 for detailed information about this study.

W.S.Kiger and S.Sakamoto studied many different combinations of filter/moderator materials. A few promising filter/moderator materials are given in Table 2.1. Table 2.1 includes filter/moderator materials, cost of filter/moderator materials, and in-air figures of merit. In-air figures of merit calculations used a D_2O cooled fission converter composed of eleven fuel burned elements (fuel loading is 312 g – ^{235}U per element) at an MITR reactor power of 5 MW. A 10-cm thick lead reflector surrounds the fast neutron filter/moderator. It is followed by a 0.04 cm Cd thermal neutron filter, an 8 cm Bi photon shield and a pyramidal collimator with a 15 cm thick lead lining and a beam aperture size 20 cm square.

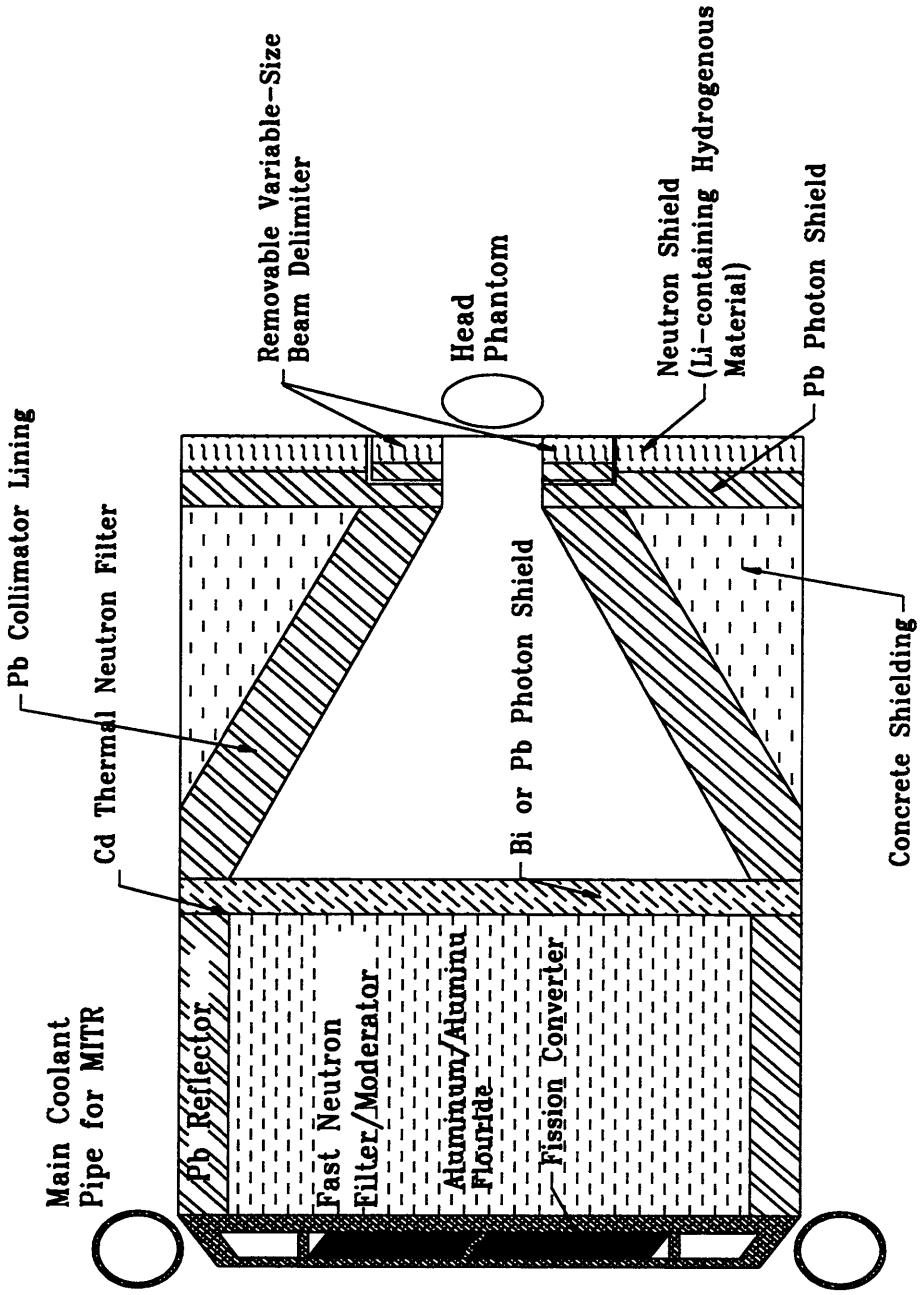

Figure 2.3: Shows the Plan View of the Fission Converter Beam Design Proposed by S.Sakamoto[2] (Courtesy of S.Sakamoto)

Table 2.1: Filter/Moderator Materials, estimated cost, epithermal flux and in-air Figures of Merit D_{fn}/ϕ_{epi} , D_{γ}/ϕ_{epi} and J_{epi}/ϕ_{epi}^2.

Fast Neutron Filter/Moderator	Estimated Cost of Materials	ϕ_{epi} n/cm^2 s X10^{10}	D_{fn}/ϕ_{epi} cGycm^2/ n X10^{-11}	D_{γ}/ϕ_{epi} cGycm^2/n X10^{-11}	J_{epi}/ϕ_{epi} (%)
83 cm Al-17 cm Al_2O_3	$176,500	1.32 ± 1.3%	1.69 ± 2.2%	0.64 ± 2.8%	65 ± 1.8 %
66 cm Fluental w/o LiF	$250,000 (estimated for VTT Chemical Technology)	1.31 ± 0.5%	1.17 ± 0.7%	0.11 ± 0.8%	65 ± 0.8 %
80 cm Al – 17 cm $(CF_2)_n$	$54,510	1.38 ± 1.3%	1.63 ± 2.1%	0.78 ± 2.4%	64 ± 1.8 %
96 cm Al – 12cm C	$17,000	1.20 ± 0.9%	1.73 ± 1.5%	0.87 ± 1.3%	63 ± 1.2 %

The filter/moderator material of 83 cm Al – 17 cm Al_2O_3 provides the highest intensity of epithermal beam at the patient position. FLUENTAL^3 without LiF design has the lowest contaminated beam at the patient position. The FLUENTAL^3 is a metal/ceramic composite, which consists of a mixture of Al and AlF_3, and it may be a commercially available product. Although the in-air figures of merit vary with the choice of filter/moderator material, the difference in beam intensity does not change the irradiation time drastically and the beam contamination is always negligible compared to the inherent background contamination due to radiative capture of hydrogen (about the order of 10^{-10} cGy/epithermal fluence) for all designs in table 2.1. Therefore any choice of filter/moderator design is promising in terms of beam performance. However, the combination of Al – C filter/moderator is attractive, due to its low cost. Moreover, enough graphite is available at the MIT Nuclear Reactor Laboratory (NRL) and graphite is a good engineering material. If the graphite can be used as the filter/moderator, it reduces the cost associated with decommissioning of the radioactive graphite in the thermal column area. For the above reasons, the author proposes that Al-C material be considered as filter/moderator.

3.Fission Converter Tank Design

3.1 Thermal Column Cavity

The fission converter tank should be designed to fill as much space as possible in the thermal column cavity. This minimizes the radiation streaming to the reactor top level. The thermal column cavity region contains two reactor main coolant pipes, the thermal column cadmium shutter and the frame, and the aluminum gas box filled with CO_2 gas. The cadmium shutter frame is attached to the aluminum gas box. The author, with a help of Dr. Bruce Hilton, measured the thermal column cavity length and width. The measured dimensions were compared with those obtained from the thermal column cavity blue prints. Good agreement was found with an error of ±0.25 inches. The clearance height of the thermal column cavity was not measured; therefore the height dimensions were taken from the MITR-II blue prints. A detail side view and cross-section A-A (see figure 2.4) of the thermal column cavity are shown in figure 2.4 and in figure 2.5, respectively.

The current removable lower and upper shield blocks are made of high-density concrete. The current cadmium shutter motor assembly is placed on the top of the upper shield block and the shutter cables run through two small holes in the current upper and lower shield blocks.

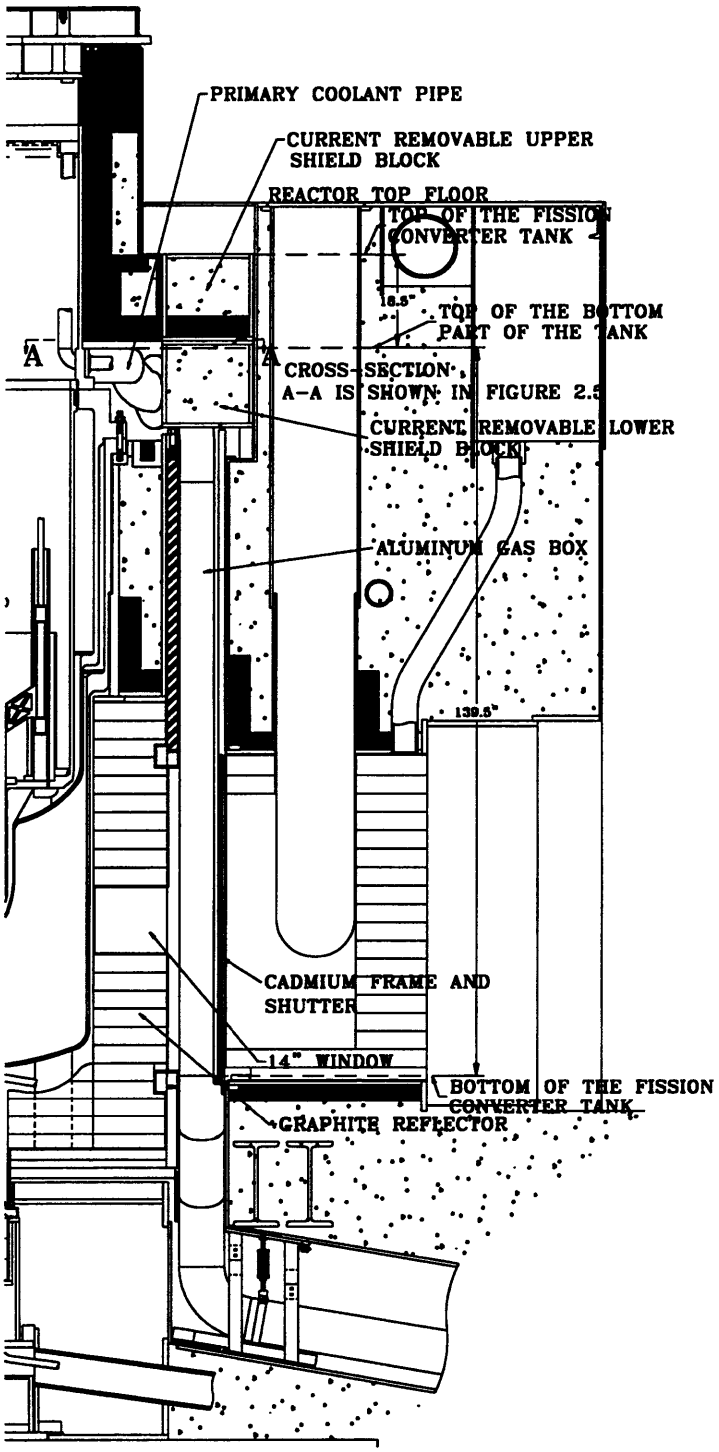

Figure 2.4: Thermal Column Cavity Side View, Showing major components in the thermal column

A side view of fission converter tank installed in the thermal column cavity is shown in figure 2.6. The fission converter tank has two different cross-sectional shapes; the bottom portion of the tank has a trapezoidal shape and the top portion of the tank has a rectangular shape. The height of the trapezoidal portion of the tank is 139.5 inches (3.5 meters), and the height of the rectangular portion of the tank is 18.5 inches (0.5 meters)

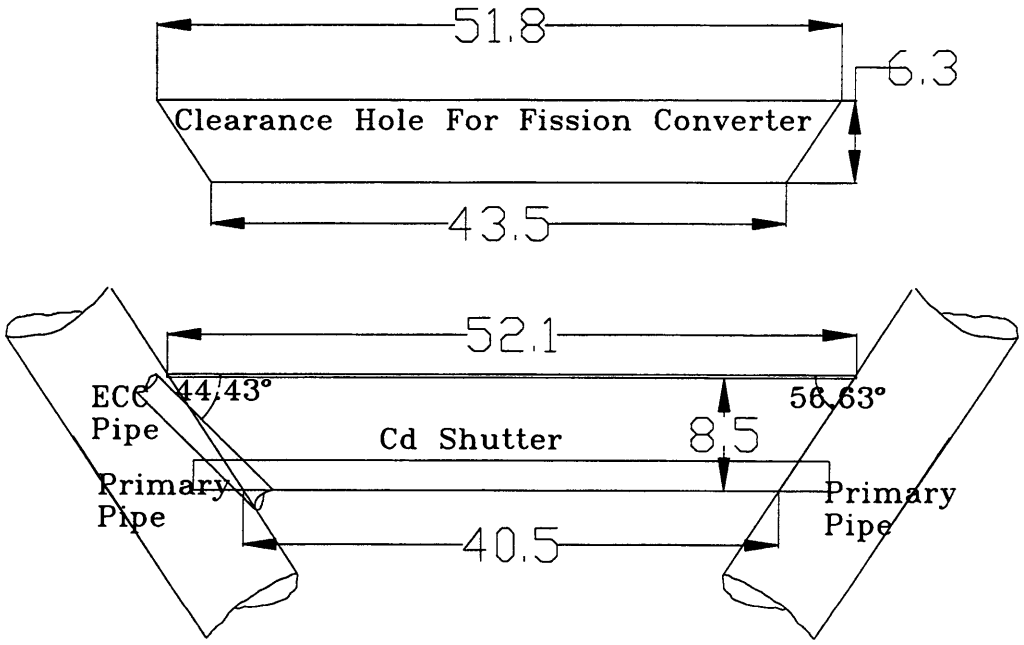

Figure 2.5: View of Thermal Column Cavity Cross- Section A-A. All Dimensions are in inches(A-A is shown in figure 2.4)

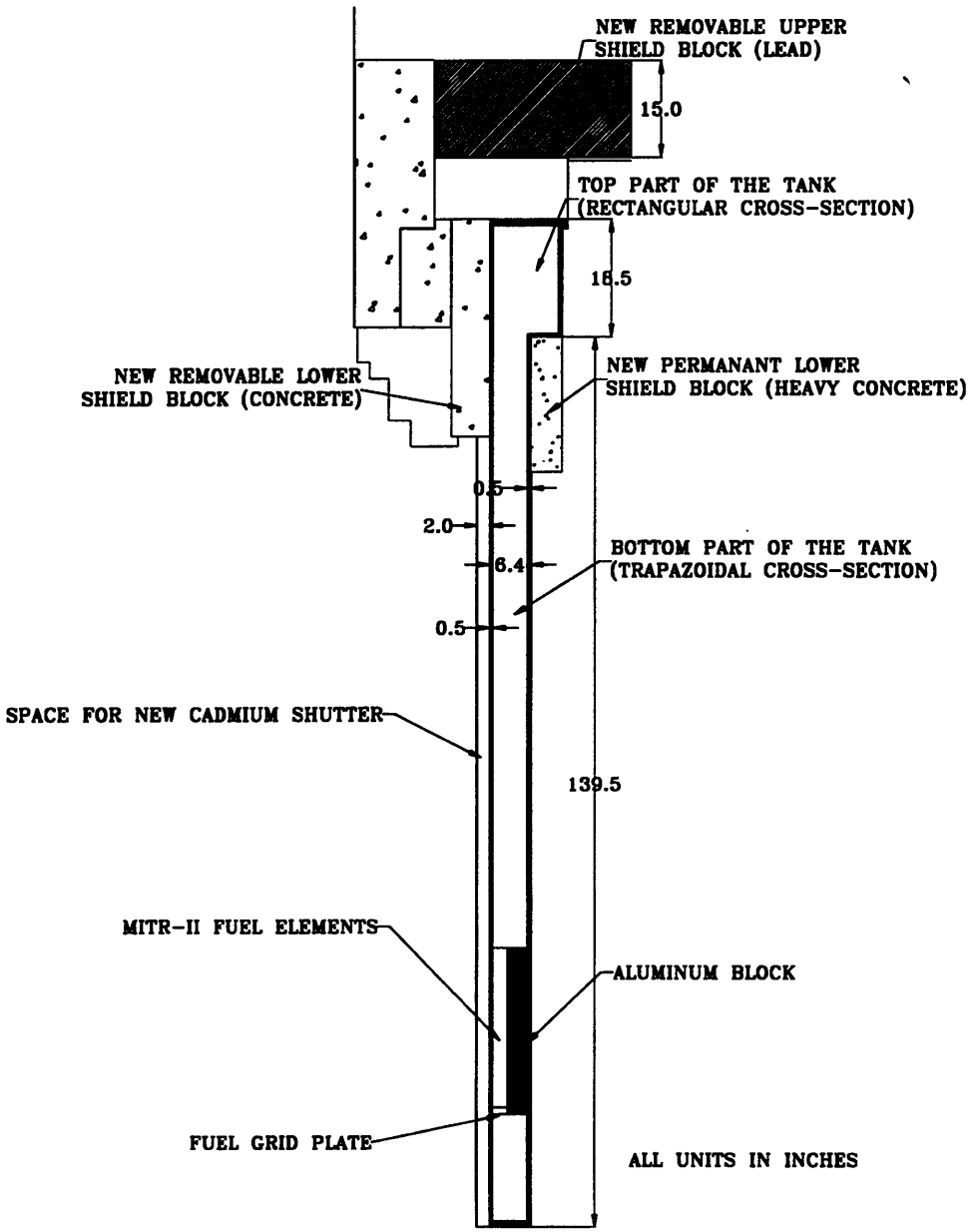

Figure 2.6: Side View of the Fission Converter Tank in the Thermal Column (All dimensions are in inches)

3.2 New Cadmium Shutter and Frame

A new cadmium shutter frame will be permanently attached to the front of the fission converter tank as shown in figure 2.6. The length of the cadmium shutter frame is the same as that of the trapezoidal portion of the fission converter tank. The new cadmium shutter frame and the new cadmium shutter are shown in figure 2.7. The new cadmium shutter frame and the cadmium shutter are similar to the old one except the dimensions are changed so that the cadmium shutter and frame fit between the tank and the graphite reflector.

There are two permanently fixed cadmium pieces and one movable cadmium piece. The cadmium shutter frame will be made of aluminum-6061. The cadmium shutter is made of a 30 mil (0.0762 cm) layer of cadmium sandwiched between two 1/8" (0.3175 cm) layers of aluminum-6061.

Two cables, attached at the top corners of the movable cadmium curtain, connect the curtain to the electric motor. These cadmium shutter cables run through the holes in the movable lower shield block (see figure 2.6). Drive-in and drive-out limit circuits are used to stop the motor and prevent the cadmium curtain from being driven beyond its physical limitations. Limit switches are also used to indicate if the cadmium curtain is either fully closed or fully open.

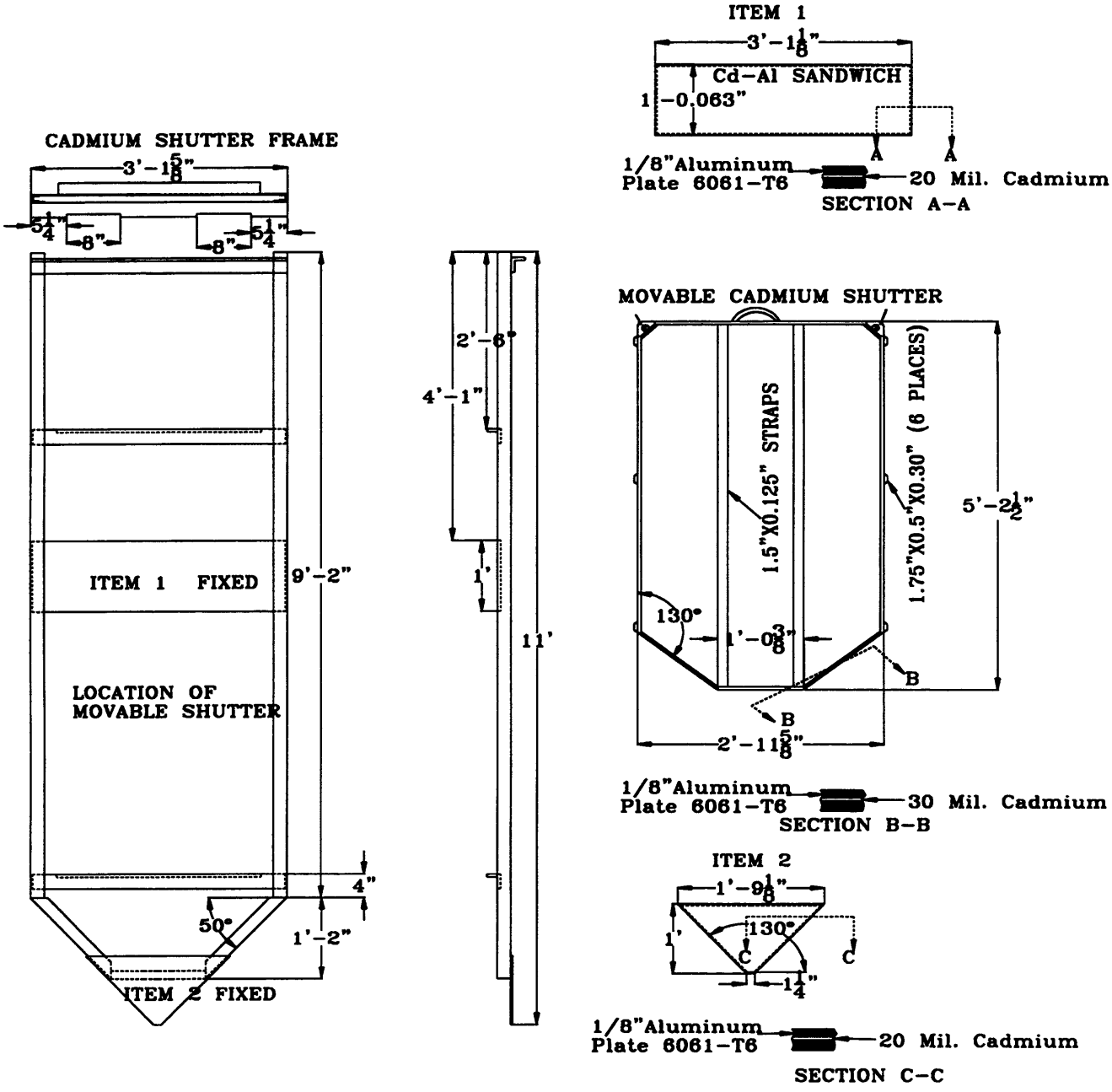

Figure 2.7: Shows the New Cadmium Shutter and Frame

In the event of a failure of the cadmium curtain to close fully, the reactor operator can lower the reactor power or scram the reactor to shut down the fission converter.

The k_{eff} values of the coupled MITR core and converter system were first calculated by W.S.Kiger[1] and then recalculated with a smaller error bar by S.Sakamoto[2]. These calculations were performed using the MCNP-4a K-code option. Criticality calculations to estimate the reactivity insertion to the MITR caused by the fission converter operation were done to assess the potential for interaction between the reactor and the fission converter. These results (calculated by S.Sakamoto[2]) are shown in Table 2.2. The results show that the reactivity insertion to the reactor by opening the cadmium curtain will be 0.00035±0.00060 Δk/k (45±76 mb) for a D_2O system using spent fuel and 0.00125±0.00071 Δk/k (159±90 mb) for a H_2O system using fresh fuel. The reactivity insertion to the reactor will be within the above range for any other combination of fuel burnup and the coolant. The above referenced calculations indicate that it is within the existing technical specification limit (TS# 1) of the MITR-II to use movable experimental facilities (0.002 Δk/k or 254 mb). Therefore, the cadmium shutter can be closed at any speed. However, a variable speed motor will be used to determine reactivity insertion rate during pre-operational testing. If the reactivity insertion is more than 0.002 Δk/k (254 mb), then the following approach will be used. MITR-II Technical Specification No. 6.4 imposes a limit on the allowed period for

experiments related to reactor control research. This approach provides more flexibility because it permits any combination of reactivity and a rate of change of reactivity provided that the period is not less than a certain minimum period. If this approach is used, the fission converter system will be exempt from MITR-II Technical Specification No. 6.1. A reactor period limit of 50 seconds shall be applied during opening of the cadmium shutter. Reactor controls can be used to compensate for the change in reactivity resulting from the presence of the fission converter as long as the reactor period is 50 seconds or greater. Therefore a variable speed motor is necessary to determine the maximum allowed reactivity insertion rate during the pre-operation test. The old cadmium shutter control system (drum and shaft) will be used with a new variable speed drive motor.

Table 2.2: Reactivity Changes Associated with Opening of the Cadmium Shutter to the Fission Converter[2] (Note: The statistical uncertainty listed with each value represents one standard deviation)

Coolant	Fuel (g ^{235}U)	K-effective		Reactivity Insertion ($\Delta k/k$)
		Curtain Closed	Curtain Open	
D_2O	312 (Spent MITR-II fuel)	1.00455±0.00048	1.00490±0.00036	0.00035±0.00060 (45±76 mb)
H_2O	510 (Fresh MITR-II fuel)	1.00417±0.00051	1.00543±0.00050	0.00125±0.00071 (159±90 mb)

The current cadmium shutter opening and closing times were measured with a simple stopwatch. Three measurements were made for each opening and closing time. The average time to either fully close or fully open is about 25 seconds.

The existing shutter cable broke once and slipped from the drum twice since 1975. In the past, the shutter was not used as frequently as the new shutter will be used. Therefore, the new cable drive system may fail more frequently than the old one. It is necessary that the cadmium shutter assembly can be easily accessed to repair any part of the shutter assembly. The cadmium shutter's motor, shaft, and drum will be placed on the top of the fission converter tank. Therefore the shutter motor

assembly and a part of the cable can be accessed after moving the movable upper shield block. The moving cadmium shutter piece and the rest of the shutter cable can be accessed after moving the new removable lower shield block. A round ring is attached on the top of the moving shutter piece (see figure 2.7). If the cable breaks close to the top corner of the movable cadmium piece, the shutter can be pulled up using a hook attached to a long pole.

The current cadmium shutter and frame can be reused if it can be modified to the new dimension. Modification of the current cadmium shutter requires separating the shutter and the frame from the aluminum gas box and reducing the width of the shutter and the frame to fit between the graphite reflector and the fission converter tank. It is a favorable to modify and reuse the current cadmium shutter to avoid some of the high cost associated with disposing of the highly radioactive shutter assembly. However, the cost of modifying the highly radioactive shutter assembly may be higher than that of disposing of it. It is recommended that a cost analysis be performed before choosing the best option.

3.3 New Shield Blocks in the Thermal Column Cavity

There are three types of new shield blocks and each type of new shield block serves different purposes. These three types of shield blocks are:

1.Permanent Lower Shield Block (see figure 2.6)

2.Removable Lower Shield Block (see figure 2.6), and

3.Removable Upper shield Block (see Figure 2.6).

3.3.1 Permanent Lower Shield Blocks

The permanent lower shield blocks will be placed as shown in figure 2.8 (side view is shown in the figure 2.6). The top level of these shield blocks will be just above the coolant pipe height such that the fission converter tank weight (about 1300 kg including the coolant in the tank) will rest on these blocks. This arrangement avoids any pressure on the reactor primary coolant pipes. Moreover, these shield blocks improve the shielding effect and minimize the radiation streaming.

These three permanent shield blocks will be made of high density concrete. Since the fission converter tank's entire weight will rest on these three permanent lower shield blocks, concrete should be manufactured with caution to insure the strength of the blocks.

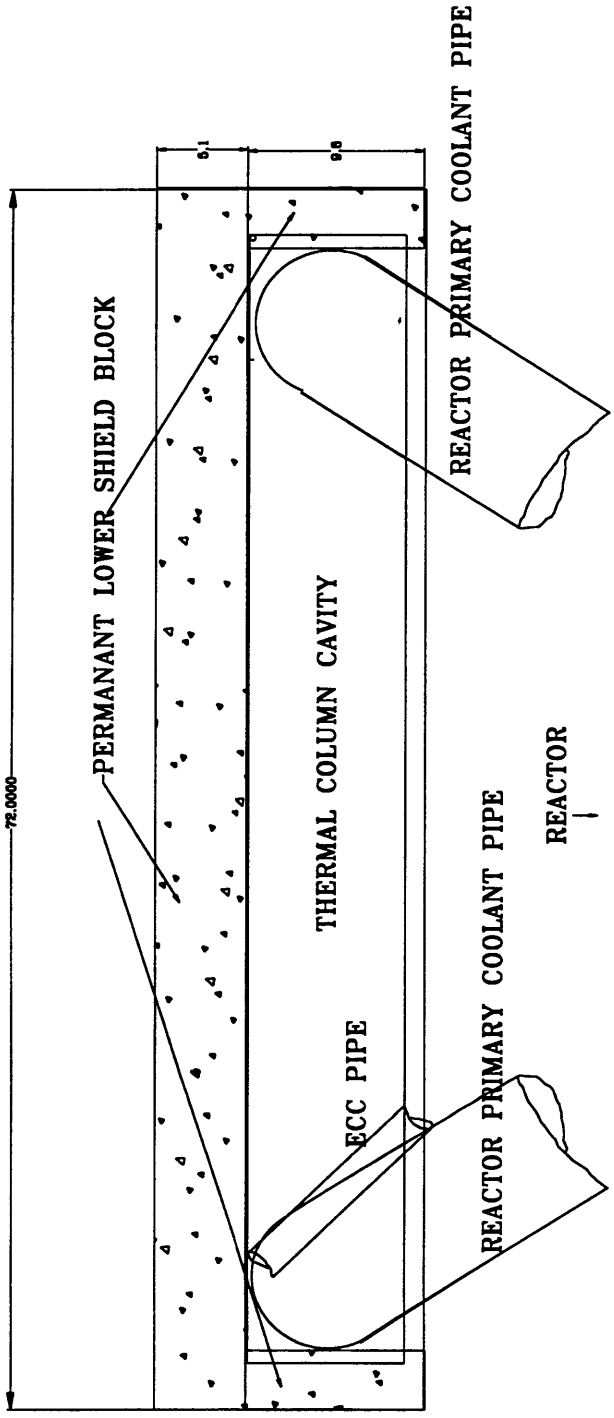

Figure 2.8: Schematic Layout of the Permanent Lower Shield Blocks (A cross-sectional view just below the top portion of the fission converter tank)

3.3.2 Removable Lower Shield Block

The removable lower shield block will be placed in front of the fission converter tank (see figure 2.6, figure 2.9 and figure 2.10). The gap between the removable lower shield block and fission converter tank is minimized as much as possible to minimize the radiation streaming. The top level of the removable lower shield block is at the height of the fission converter tank top.

Two small holes will be made in this block for the cadmium shutter cable to run through it (see figure 2.9). The cadmium shutter and the frame will be under this removable lower shield block. This block can be easily moved if the cadmium shutter needs to be accessed; or for any other purpose. The new removable lower shield block is made of heavy concrete.

3.3.3 Removable Upper Shield Block

The upper removable shield block will be made of two blocks as shown in figure 2.11. These blocks will be placed on the reactor top floor. These removable upper shield blocks provide the final shielding to the reactor top area. These blocks can be moved if any equipment under the block needs to be accessed. The removable upper shield blocks are made of lead. The shield blocks thickness are calculated such that the radiation dose above the removable upper shield blocks is calculated to be less than 1 mrem/hr at 5 MW reactor power.

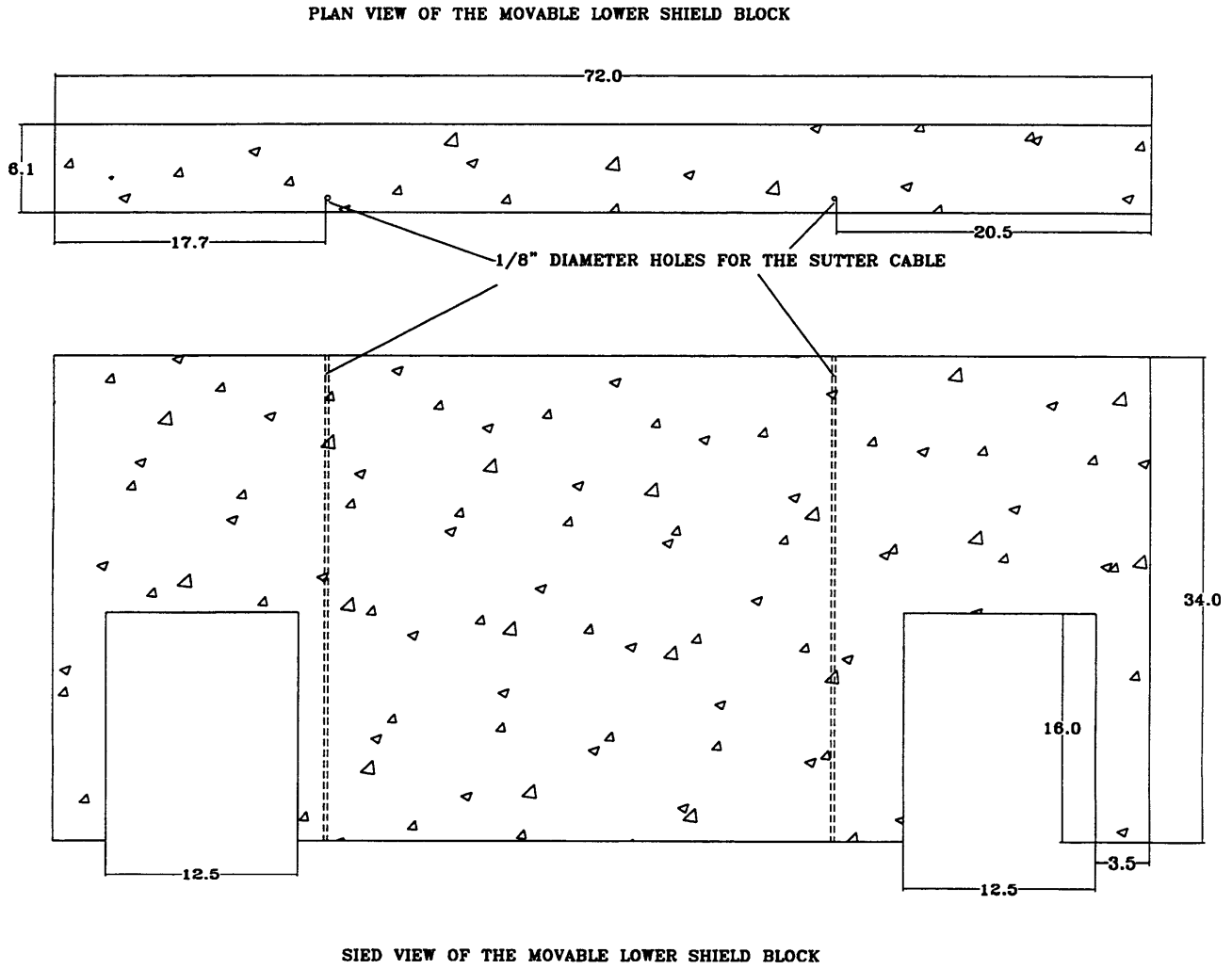

Figure 2.9: Removable lower shield block side and plan views are shown. All dimensions are in inches.

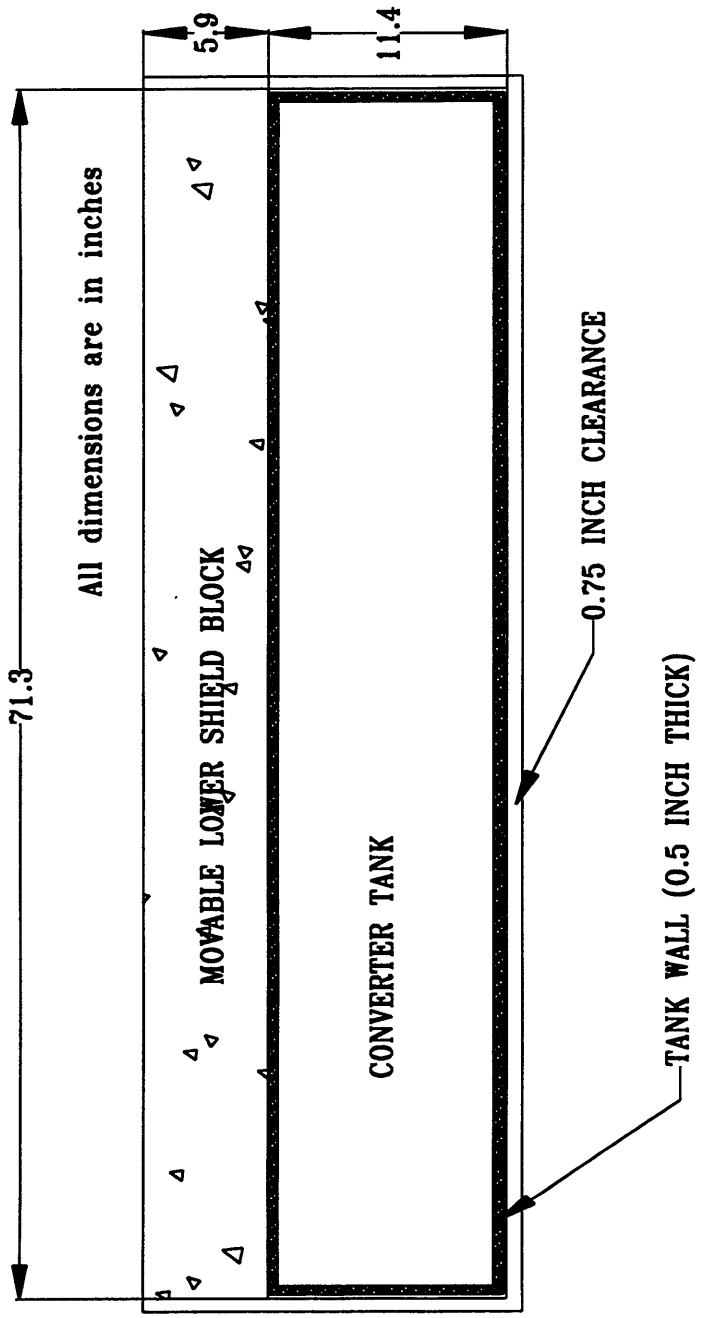

Figure 2.10: Cross Sectional View of the Thermal Column Cavity at the Top of the Tank (All dimensions are in inches)

There are three types of access holes on the removable upper shield blocks as shown in figure 2.11. The center access hole is for lowering the fuel elements into the fission converter tank during fuel handling. The two side access holes are for maneuvering fuel elements from the reactor top floor. There are two holes for the primary inlet and outlet pipe. Since the removable upper shield is made of two blocks, these two blocks can be slide to the opposite sides without interfering with the converter primary pipes.

3.4 Dose Calculation in the Thermal Column Cavity

Radiation doses below and above the movable upper shield block were calculated for fission converter operation and for fueling. The commercially available code MICROSHIELD[4] was used for the above dose calculation. MICROSHIELD is developed by Grove Engineering in Pennsylvania. MICROSHIELD uses a point kernel with numerical integration. The current average radiation dose on the reactor top floor is 5 mR/hr. Therefore, the movable upper shield block thickness is designed such that the radiation dose above the movable upper shield block is about 5 mrem/hr. The gamma source intensity and the spectrum vary with the fission converter operation and fueling.

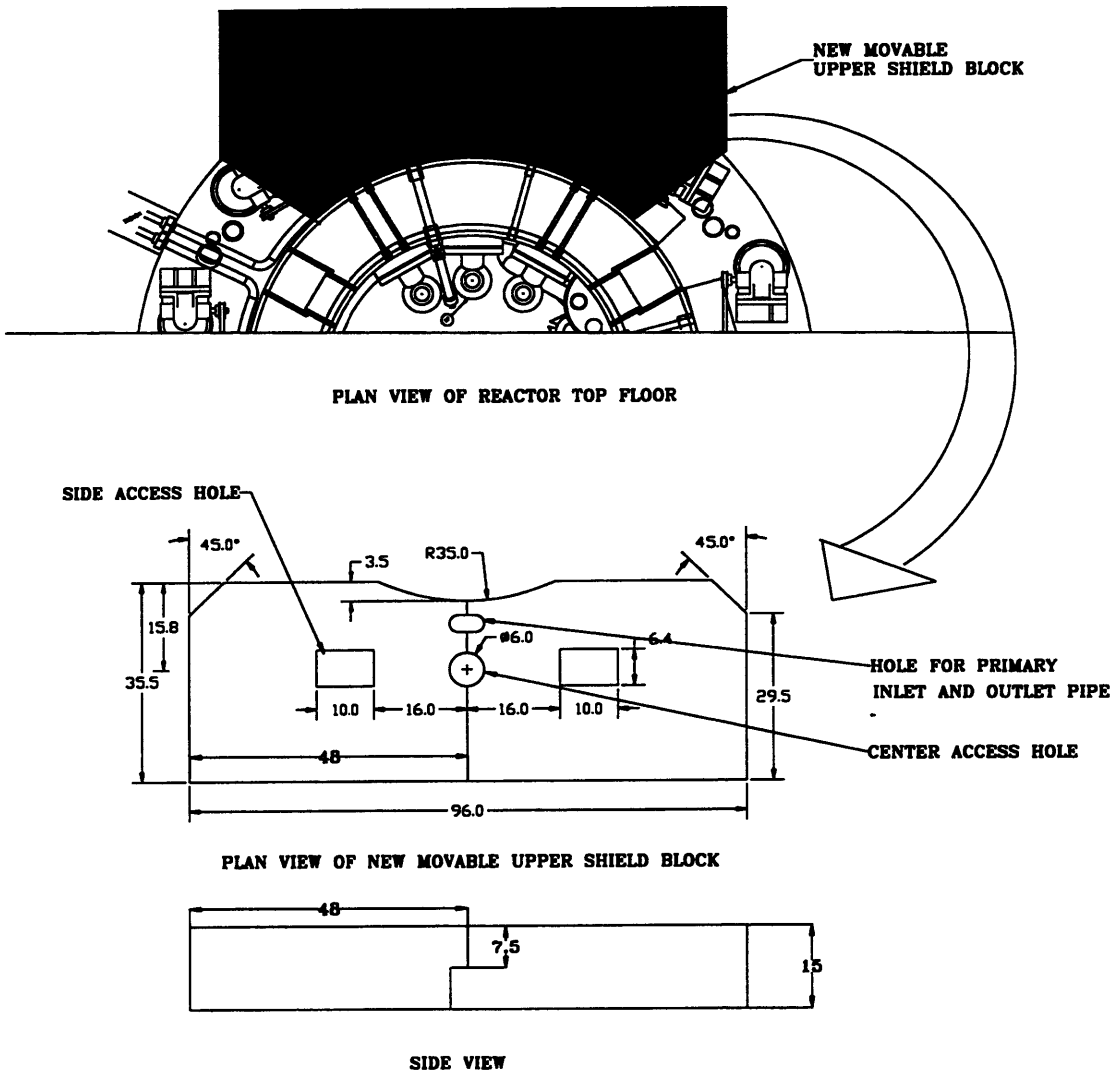

Figure 2.11: Schematic Layout of the New Movable Upper Shield Block (All dimensions are in inches)

When the fission converter is at full maximum power (250 kW), the cadmium curtain will be in the fully opened position. Figure 1.16 in Ref. 1 shows the thermal neutron flux in the thermal column cavity as a function of vertical distance. W.S. Kiger, using MCNP-4A, calculated the thermal neutron flux in figure 1.16. The cadmium shutter will be exposed to neutron flux less than $1X10^{12}$ n/cm^2 sec when the shutter is in the fully opened position. However, it is assumed very conservatively that the whole cadmium shutter will be exposed to thermal neutron flux of $1.0X10^{12}$ n/cm^2 sec for the dose calculation. Table 2.3 shows the gamma spectrum due to the reaction between the cadmium shutter and the thermal neutron flux in the thermal column area. The prompt gamma spectrum produced in the fission converter fuel is also calculated for the maximum power 250 kW and is given in Table 2.4.

The total gamma source during the period of fission converter operation is the gamma from the cadmium shutter plus the prompt gamma from the fission converter fuel. The dose on the reactor top floor due to delayed gamma from the fission converter fuel and the cadmium shutter, gamma from the MITR core, and N-16 production in the fission converter tank are neglected in this calculation, because they are assumed to be small.

Table 2.3: Gamma Spectrum from Cadmium Shutter during the Shutter Fully Opened Position

Energy (MeV)	Activity (photons/sec)
0.5	5.65E+17
1.5	1.82E+17
2.5	5.33E+17
3.5	3.23E+17
4.5	1.67E+17
5.5	1.32E+17
6.5	3.03E+16
7.5	1.42E+16
8.5	4.40E+15
9.5	1.57E+15

Table 2.4: Gamma Spectrum from the Fission Converter Fuel during Operation

Energy (Mev)	Activity (Photons/sec)
0.2	1.03E+15
0.45	1.55E+15
0.8	1.55E+15
1.25	8.80E+14
1.75	4.22E+14
2.25	2.45E+14
2.75	1.42E+14
3.25	8.19E+13
3.75	4.76E+13
4.25	2.73E+13
4.75	1.64E+13
5.25	9.37E+12
5.75	5.46E+12
6.25	3.12E+12
6.75	1.56E+12
7.25	7.80E+11
7.75	6.10E+11
9.25	7.80E+11

The dose due to each source (the cadmium shutter and the fission converter fuel) is calculated separately because the distance between the source and the "detector" location is different. Moreover, the shielding thickness and the shielding materials vary depending on the path of the gamma. Four different conservatively chosen paths are identified in figure 2.12.

The calculated doses are also shown in figure 2.12. As can be seen in figure 2.12, the maximum dose will be observed just above the fission converter tank. The main contributor to the dose is the cadmium shutter because it has higher activity than that of the fuel and it is close to the top of the converter tank. The dose above the movable lower shield block is much smaller than that above the fission converter lid. It is calculated that 15 inches of lead for the movable upper shield block is required to reduce the dose to 2 mrem/hr just above the movable upper shield block. When the cadmium shutter is in the fully closed position, the shutter will be exposed to the thermal neutron flux between the range of $1X10^{12}$ n/cm^2 sec to $2.5X10^{12}$ n/cm^2 sec at 5 MW reactor power and the thermal flux in the fission converter tank will be reduced >99%[2]. On the other hand, the distance between the source (cadmium shutter) and the detector will be increased. Therefore, the net effect will be the same as that of the fully opened position for the cadmium shutter.

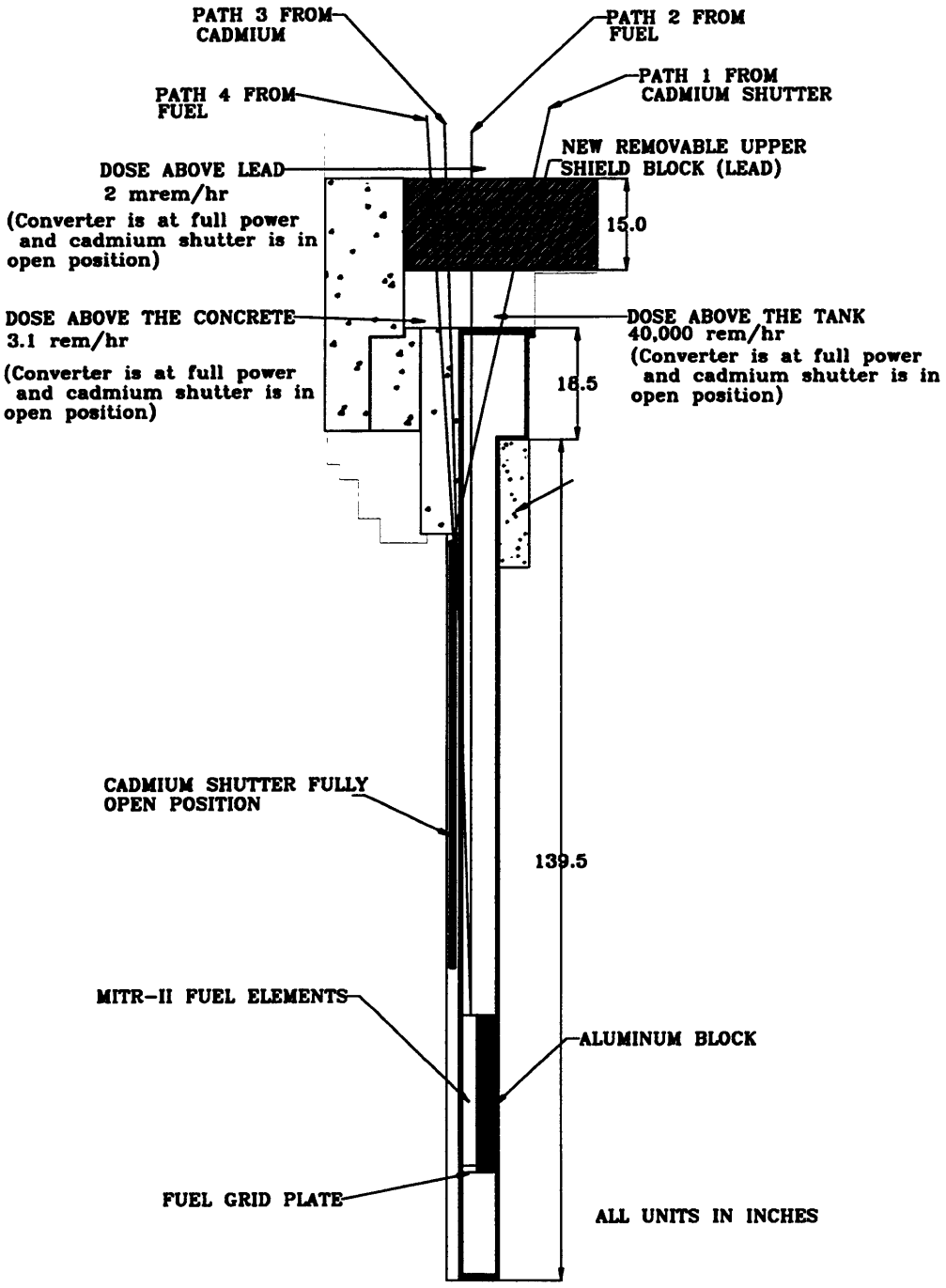

Figure 2.12: Gamma Paths and Shielding Calculation Results

(Side View of the Fission Converter Tank)

The dose just above the fission converter tank is calculated for the fueling condition. During a fueling operation, the MITR reactor and the fission converter will be shut down. The dose due to the cadmium shutter activation and the reactor gamma was measured during the thermal column cavity dimensional measurements. The dose was measured after removing the current lower and upper shield blocks. The dose was 100 mrem/hr at the reactor top floor level. Thus, the dose due to activated cadmium shutter and the reactor will be negligible during the fission converter fueling because there will be extra shielding of 2.6 meters of water and the movable concrete lower shield block. Then, the main source is that from the fission converter fuel delayed gamma. The delayed gamma spectrum is calculated using DKPOWR[5] code. It is calculated for the following conservative conditions; 1) Irradiated fuel from the MITR is continuously irradiated for 5 years in the fission converter tank at a power level of 250 kW, and 2) the gamma spectrum is calculated just after converter shutdown. As was before, the doses are calculated for different paths. The doses are shown in the figure 2.12. As it can be seen from the figure 2.12, the dose above fission converter tank is low enough for work with out the upper shield block. Detailed fuel loading and unloading are discussed in section 4.2.3.

3.5 Equipment in the Thermal Column Cavity

Currently, the cadmium shutter drive motor, the 1 and 6 control blades position controller (Selsen), the regulating rod Selsen and the regulating rod drive motor are placed above the current removable upper shield block in the thermal column cavity. These systems are shown in figure 2.13. These systems except the cadmium shutter control assembly, can be either moved out from the thermal column cavity to other locations or can be left under the removable upper shield block.

If these equipment are kept under the removable upper shield block, the following modifications have to be performed. Since the regulating rod drive motor stands vertically above the reactor top level, it has to be changed to a motor which can be placed horizontally such that it will be below the removable upper shield block. The current control blade drive motor is not rated for high radiation. Since the radiation level above fission converter tank (40,000 rem/hr) will be higher than what it is now (20 – 250 mR/hr), the control blade drive motor should be insulated with a material, which is rated for the high radiation level. Material such as Capton, which is rated for 10^9 rem radiation level, can be used to shield the control blade drive motor. The other option is to move all the systems just above the removable lower shield block where the radiation level (3.1 rem/hr) is much lower than above the fission converter tank lid.

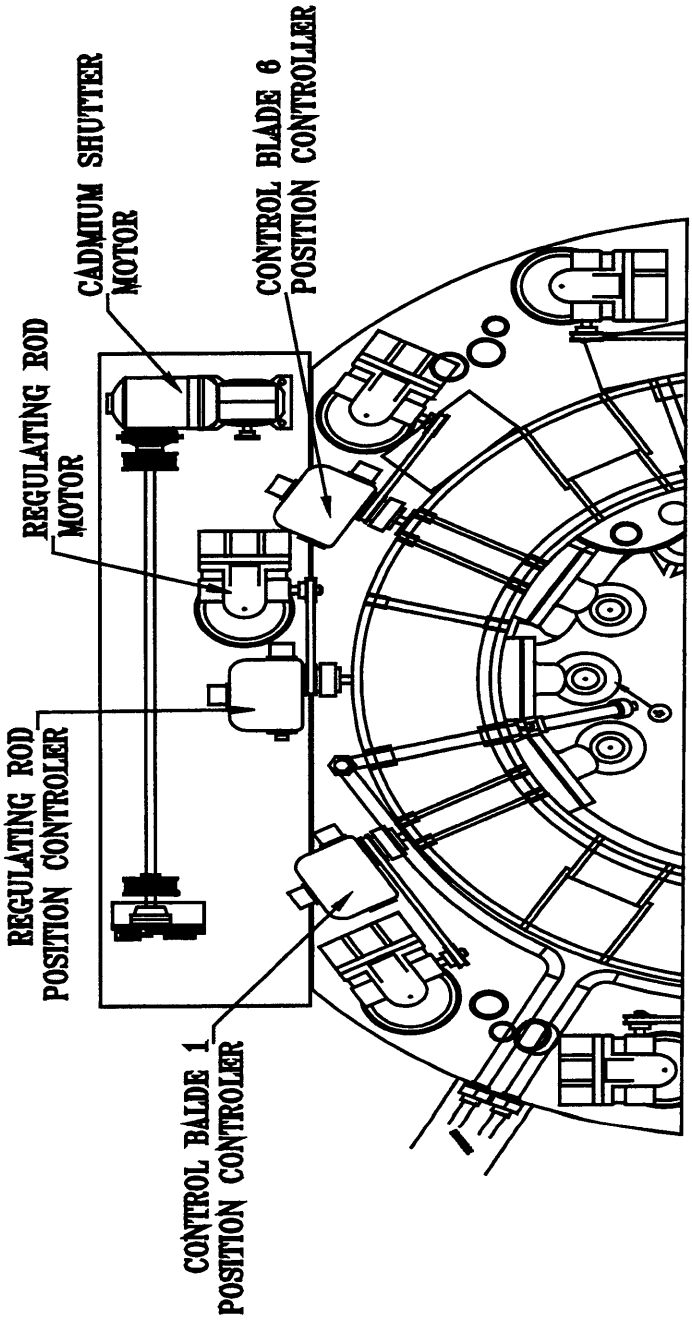

Figure 2.13: Equipment near the Top of the Thermal Column Cavity and above the Current Upper Shield Block

3.6 Fission Converter Fuel Lower Grid Structure

An isometric view of the fission converter tank is shown in figure 2.14. The fission converter tank holds eleven MITR-II fuel elements. A grid plate below the eleven MITR-II fuel elements holds the elements in place. The lower grid plate is shown in figure 2.15. The fuel lower grid plate is designed to tightly fit the MITR-II fuel elements and to keep the fuel plate orientation as is shown in figure 2.15. There is a very minimal space around the fuel inlet nozzle for a coolant flow to bypass. This minimizes the bypass flow.

The fission converter study by S.Sakamoto[2] showed that increasing the coolant thickness between fuel elements does not increase the beam intensity at the patient position, but increases the power per fuel element. The fission converter neutronic study by W.S. Kiger[1] examined the effect of varying coolant thickness in front of and behind the row of fuel elements. It showed that the epithermal neutron flux at the patient position decreases and the specific fast neutron dose at the patient position is unchanged when the coolant thickness is increased. Therefore, the lower grid plate is designed such that;

1. the fuel elements are placed adjacent to the fission converter tank front plate, leaving minimum space between the tank front plate and the fuel elements,

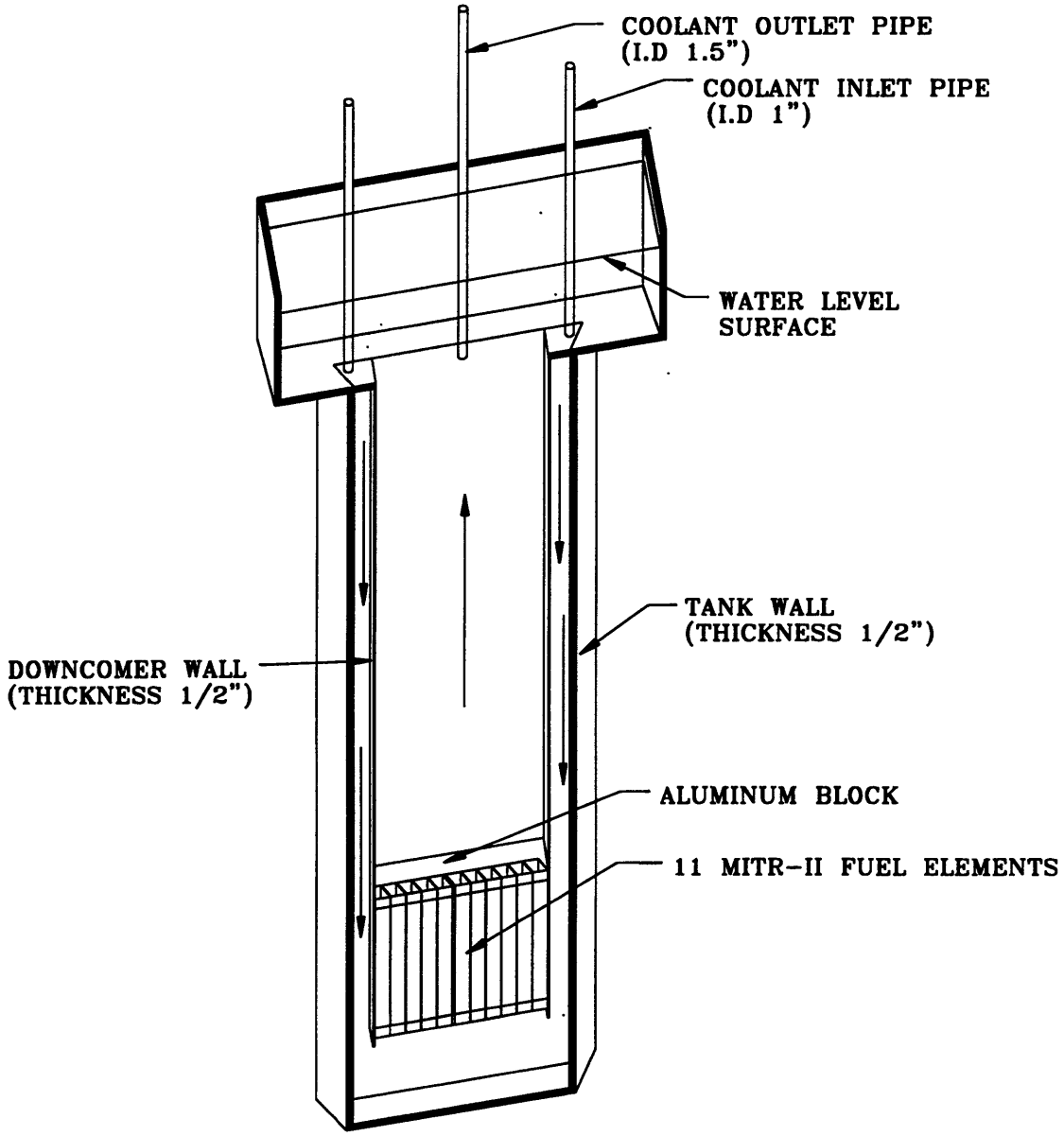

Figure 2.14: Isometric View of Fission Converter Tank

Constructed of Aluminum Alloy Type 6061 T6

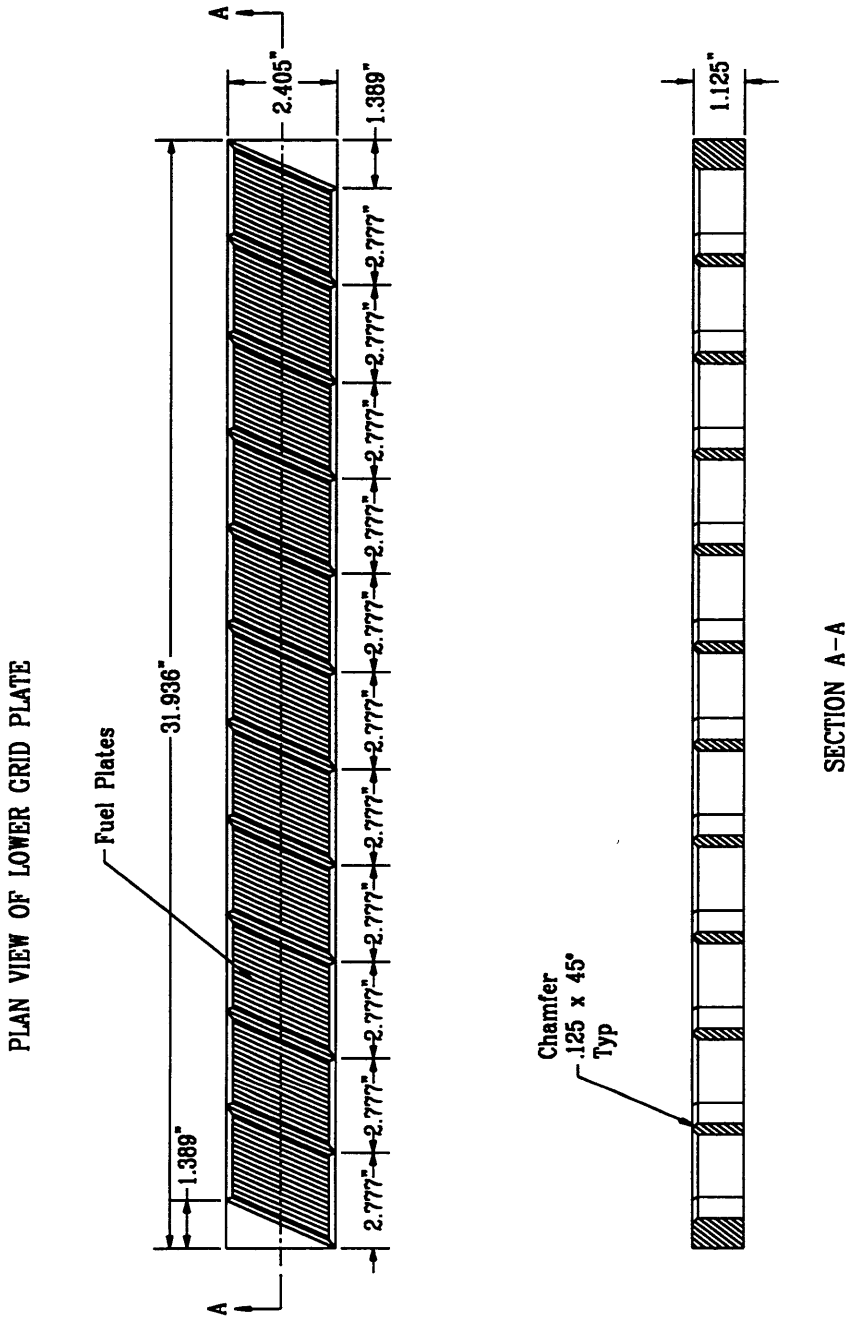

Figure 2.15: Lower Grid Plate for Fission Converter Tank Constructed of Aluminum Alloy Type 6061 T6

2. the space behind the fuel elements are filled with an aluminum block to displace any water behind the fuel, and
3. The space between the neighboring fuel elements is minimized to minimize water between fuel elements.

Hydraulic lift created by coolant flow on the MITR-II fuel elements was calculated for different coolant flow rates and compared with the fuel element weight. This calculation is performed using MathCad. The lifting force on a fuel element as a function of total primary flow rate is given in figure 2.16. The weight of a fuel element is 35 N. The lifting force on a fuel element at the expected operating primary flow rate of 10 kg/s (about 162 gpm) is 3.5 N. If three out of 165 channels were blocked, the lifting force on a fuel element is 7.9 N. Since the lifting force on the fuel element is much smaller than the gravity force on a fuel, fuel lifting should not be a concern. Therefore, a hold down plate is not necessary to hold down the eleven fuel elements.

Blocking a fuel flow path can occur if an object is dropped into the fission converter tank during a fuel loading or unloading. However, the fuel loading and unloading is performed only every 10 to 15 years (Ref. W.S.Kiger[1] and S.Sakamoto[2]) unless elements leak fission products. Furthermore during the fuel loading and unloading the upper movable shield block will cover the fission converter tank which will help prevent any foreign object entering into the fission converter tank.

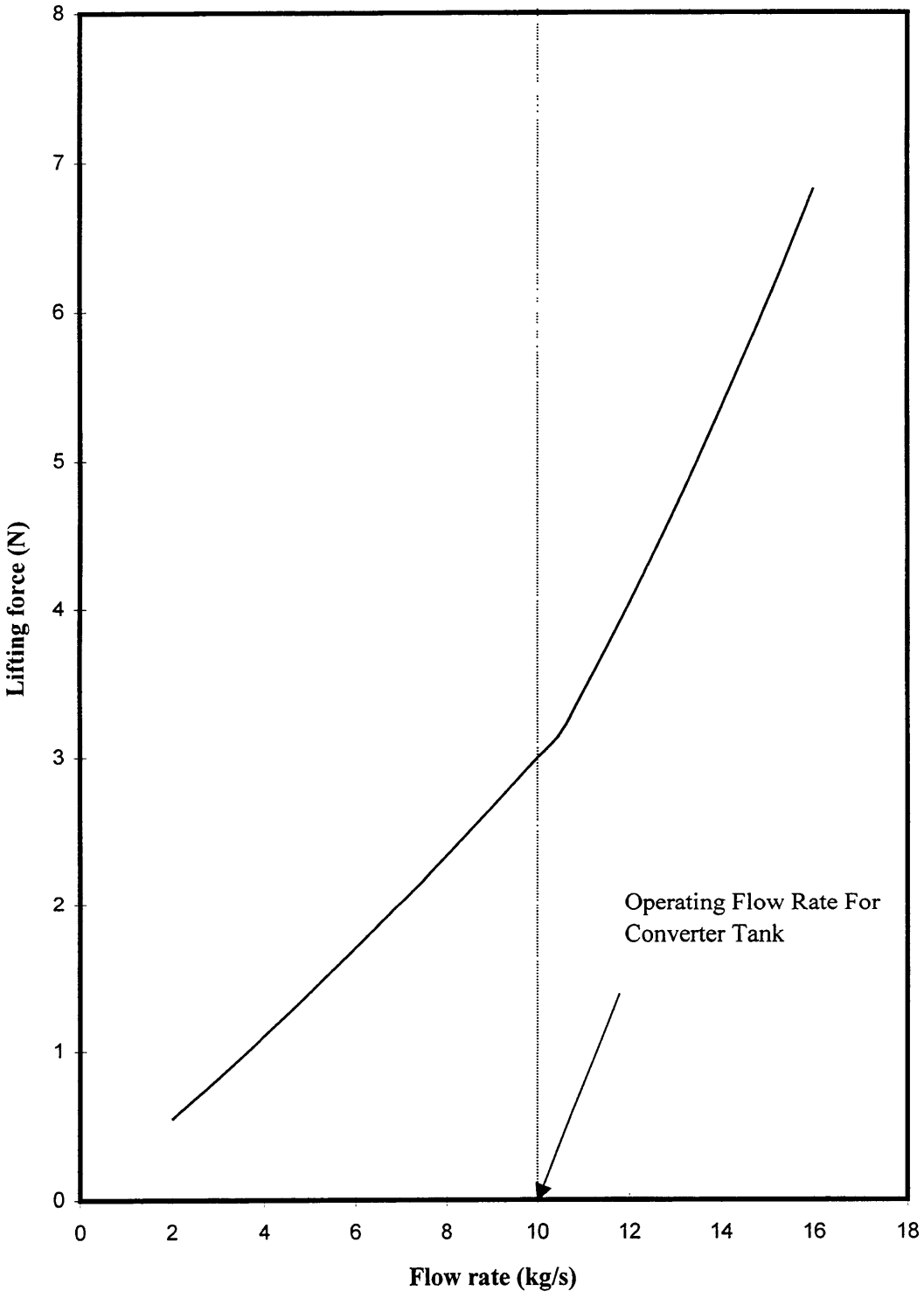

Figure 2.16: Fuel Lifting Force as a Function of Flow Rate

More detailed discussion about fuel loading and unloading is given in the next section of this chapter. Since the fission converter is a closed system, it would be impossible to drop any large object in the fission converter tank during normal operation. The clean up system, filters and ion column, keep the coolant clean, therefore, blockage due to accumulation of small particles in the fuel elements is unlikely. Therefore, fuel channel blockage has a very low probability.

The fuel elements in the fission converter tank are orientated so that the individual fuel plates are "edge-on" towards the MITR as shown in figure 2.15. If the elements were to be rotated, so that the face of the plate is facing the MITR, calculations by S.Sakamoto[2] show that the power peaking in that plate would be significantly greater than in the orientation shown in figure 2.15. Therefore, the hottest channel could experience nucleate boiling on the fuel plate. That is unacceptable. If the elements were to be rotated so that the fuel plate is facing the MITR, the MITR-II fuel elements' nozzles would not fit into the lower grid plate. However, if the MITR-II fuel elements were flipped upside down and were rotated by so that the entire fuel plate was facing the MITR, the MITR-II fuel elements' nozzles would fit into the lower grid plate. This situation is to be avoided for the reasons given above. Administrative procedures will be used to ensure that fuel elements are always loaded with proper orientation (plates edge-on towards MITR).

3.7 Fission Converter Tank

The fission converter tank outside dimensions are chosen such that there is a 1/4" clearance in the front and the back of the fission converter tank and ¼" clearance on each side of the tank between the tank and the cavity in the thermal column. The front, side and cross-sectional views of the fission converter tank are shown in figures 2.17. Each converter tank plate thickness is 1/2". The adjacent converter tank plates are welded on to one another. The tank design shown in the figures 2.6, 2.14, 2.17 is for the forced convection heat removal design. The design of the downcomer wall is different for natural convection and for forced convection with bypass channel designs. The details of these alternative designs are given in the next chapter. It has been decided to use the forced convection heat removal design in the construction. The downcomer wall is 1/2" thick and it is welded onto the front and the back plate of the converter tank. The fuel positioning lower grid plate is welded on to the front and back converter plates and onto the downcomer walls.

The outlet primary pipe extends to just below the top wide portion of the fission converter tank. The downcomer top will be covered by a plate, which will be welded onto the front plate, the back plate, the side plate and the downcomer wall. The cover plate on the top of the downcomer wall will prevent any flow upward. There will be a hole on the cover plate for the insertion of the primary inlet pipe.

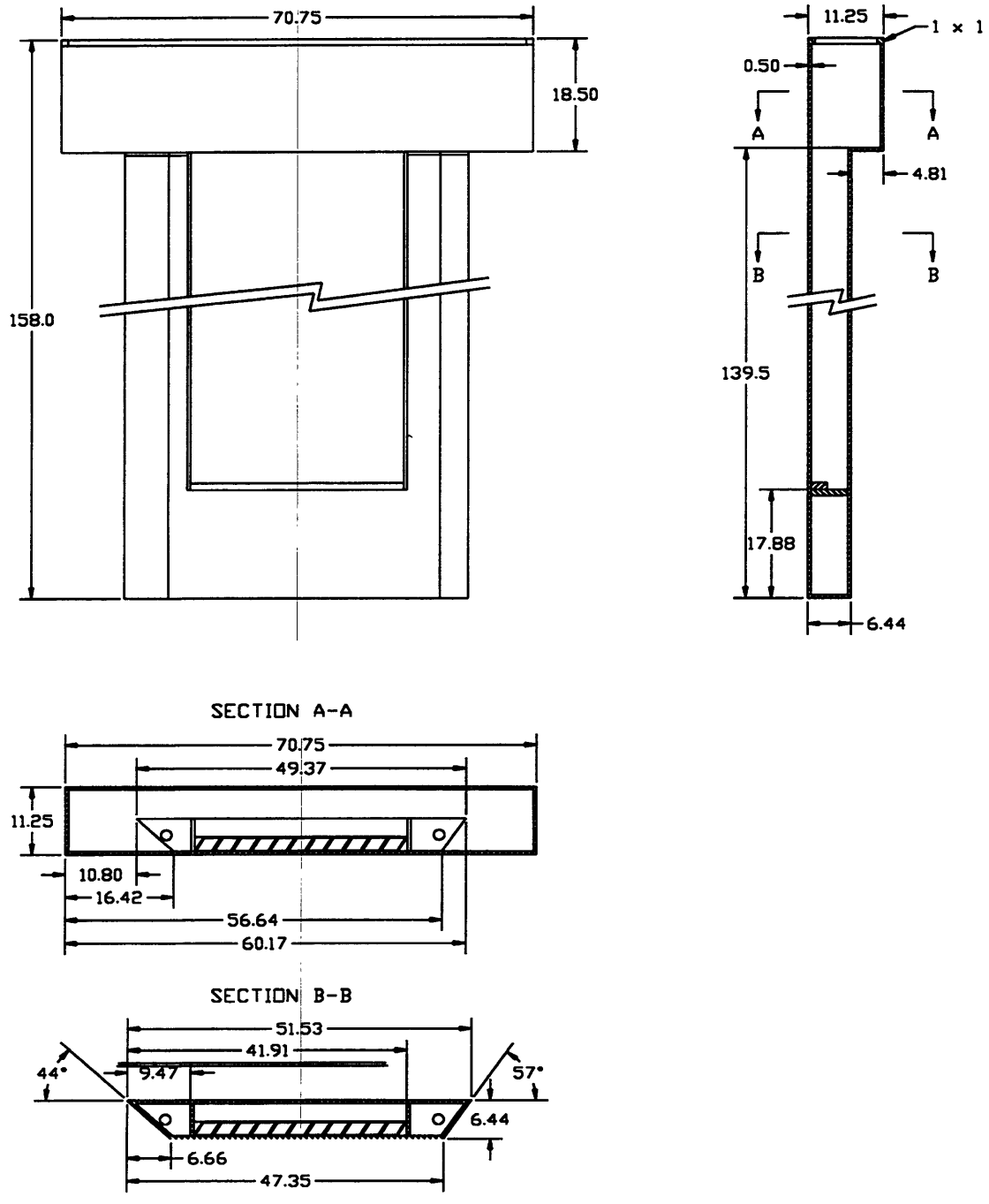

Figure 2.17: Fission Converter Tank Front, Side and Two Cross Sectional Views (All Dimensions are in Inches)

The size of the hole on the cover plate is slightly larger than the size of the outside diameter of the primary inlet pipe. The primary inlet pipe extends just below the cover plate. Bypass flow (flow in the upward direction through the gap at the insertion of primary inlet pipe) was calculated assuming 1) the downcomer top cover plate thickness is ½"; 2) flow in the gap is fully developed, and 3) gap thickness is 1/16". The calculated bypass flow is about 1% of the total primary flow rate. The fully developed flow in the gap is a conservative assumption, because the pressure drop in the developing region is much higher than that of developed region. Therefore, flow through the gap is smaller than that is predicted using assumption 2. Two inlet and one outlet pipes are used as shown in figure 2.14.

The ASME Boiler and Pressure Vessel code has eleven sections. Some of these sections are clearly irrelevant to the fission converter tank. These are: Section I – Power Boilers, Section IV – Heating Boilers, Section VI – Recommended Rules for the Care and Operation of Heating Boilers, Section X – Fiber-Reinforced Plastic Pressure Vessels and Section XI- Rules for Invasive Inspection of Nuclear Power Plant Components. Section III includes nuclear boilers, pressure vessels and containment. Since the fission converter tank is not a nuclear reactor, the fission converter is exempted from Section III. Section II – Materials, Section V – Nondestructive Examination, and Section IX – Welding and Brazing Qualifications are referenced by the other sections of the code and are

relevant only to the extent that is required by such reference. The remaining Section VIII – Pressure Vessels, covers all the remaining pressure vessels that do not fall into the scope of the other sections. The introduction to Section VIII, Part U-1, (c) lists the classes of vessels that are exempt from the scope of this section, including "(6) a vessel for containing water under pressure, including those containing air, the compression of which serves only as cushion, when none of the following limitations are exceeded: (a) a design pressure of 30 psi; and (b) a design temperature of 210 ^{0}F". Therefore the fission converter tank is exempt from this section, because the fission converter design pressure and temperature are below these limits. However, the fission converter tank will be voluntarily build using Sections II and IX for materials and welding specification to help ensure that sound practice is followed in the construction of the tank. Structural mechanical analyses of the fission converter tank plates are given in the following section.

Pressure above the coolant level in the fission converter tank will be at atmosphere pressure. If the whole tank is filled with the coolant, the pressure at the bottom plate due to the hydrostatic head is 5 psi. The tank will be tested for leakage at 10 psi.

The coolant operating temperature will be <60 ^{0}C. The corresponding level increase will be 9" when the coolant temperature changes from 25 ^{0}C to 60 ^{0}C. During operation, the coolant level in the fission converter tank will be kept 10 inches below the lid level. All the

primary pipes and the heat exchanger are above the tank. Therefore the coolant in the primary loop will flow back into the tank if there is a loss of flow condition. This would introduce flooding of coolant into the cover gas system or pressurizing of the tank unless there is sufficient space in the top of the tank. Thus, the following procedures are followed during the start up to avoid any flooding or tank pressurization. The fission converter tank will be filled with coolant up to a level 10 inches below the top of the fission converter tank before starting the pump. Then the coolant is pumped into the primary pipes and the heat exchanger. Once the primary pipes and the primary heat exchanger are filled with coolant, the primary loop will establish a steady flow rate. The amount of coolant needed to fill the primary loop and primary heat exchanger will reduce the coolant level in the tank by 6 inches. Therefore, once steady flow is established in the primary loop, the coolant level in the fission converter will be 16 inches below the top of the fission converter tank. Once the coolant reaches the operating temperature 60 ^{0}C, the coolant level will rise and will leave a space of 7 inches above the coolant level. This 7 inches above the coolant is adequate to accommodate the coolant, which flows back into the tank if there is a loss of flow.

3.8 Fission Converter Tank Lid Design

The converter tank lid is shown in figure 2.18. The fission converter tank lid consists of two separate lids: a permanent lid and a removable lid. The converter tank permanent lid is attached to the top of the converter tank by bolts. A gasket between the converter tank and the permanent lid will provide an airtight seal. This gasket can be made of soft metal (lead or indium wire) to avoid deterioration in the high radiation environment. The fission converter's two primary inlet pipes are fed through the permanent lid and then through the hole on the downcomer top on each side. A pipe coupling is welded on the permanent lid such that the inlet primary pipe can be detached above and below the permanent lid. There are two more access holes on the permanent lid for instrumentation purposes.

The removable lid is bolted to the permanent lid. A gasket is placed between the two lids to assure an airtight seal. The removable lid will be removed during loading and unloading of fuel. The primary outlet pipe is fed through the removable lid and extends to just below the wide part of the upper tank. The outlet primary pipe is fed through the lid by the same approach as the inlet primary pipes are fed through it.

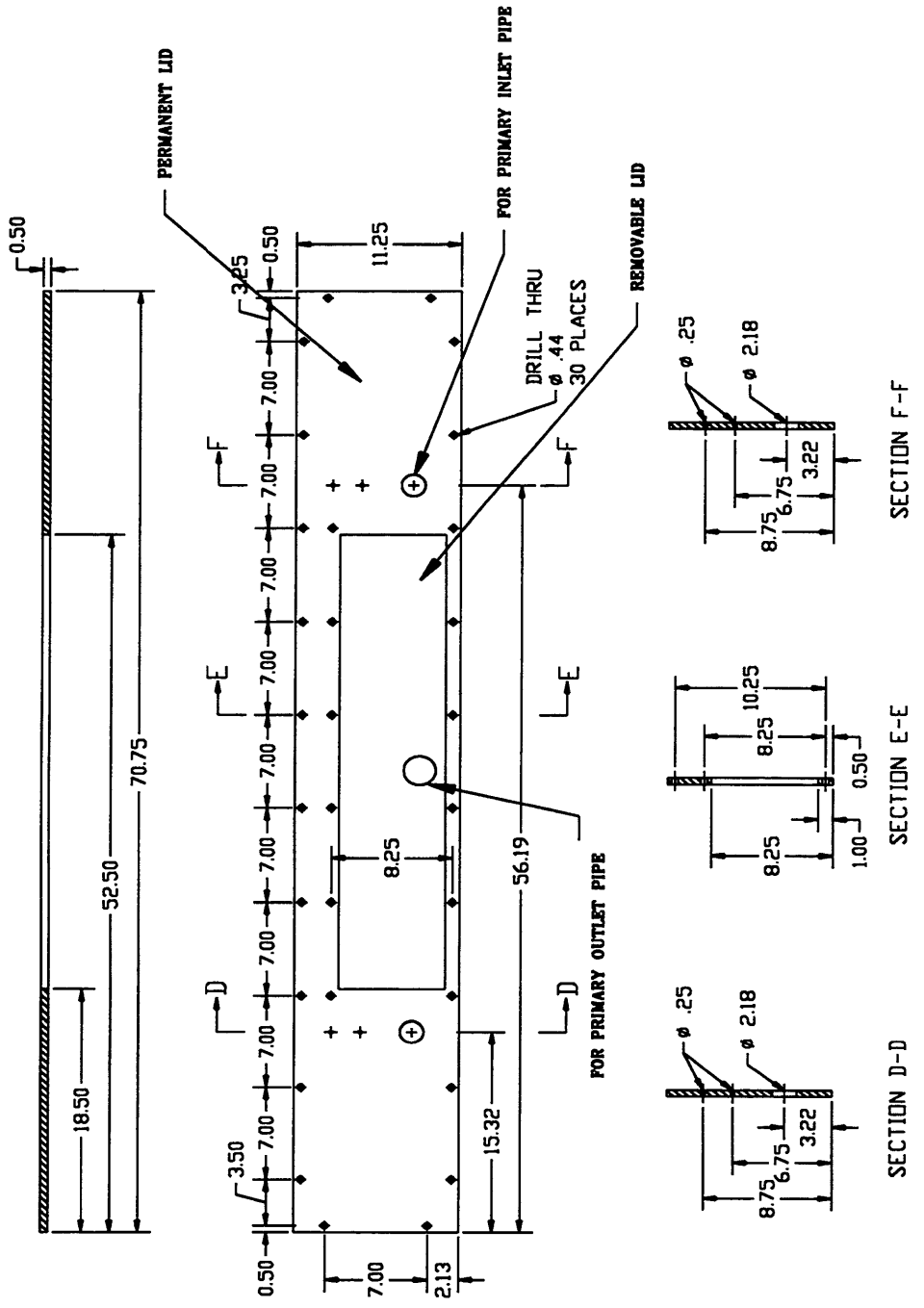

Figure 2.18: Fission Converter Tank Lid Design. All dimensions are in inches (Courtesy of Y. Ostrovsky)

3.9 Structural Analysis of Fission Converter Tank Plates

The fission converter neutronic study by W.S. Kiger examined the effect of the converter tank front and the back plate thickness on the beam performance. When the converter tank back plate thickness is increased, the epithermal flux at the patient position is unchanged because a much larger amount of aluminum is used in the filter/moderator. The epithermal neutron flux at the patient position decreases as the thickness of the fission converter front plate increases because thermal neutrons from the reactor are attenuated. Therefore, the minimum tank's front plate thickness is used such that the converter tank front plate can withstand stresses caused by the hydrostatic pressure, and the deflections are acceptable.

Analytical and numerical structural analysis calculations were performed to obtain a minimum converter tank's front plate thickness. In the following two subsections, the analytical and numerical analyses are presented.

3.9.1 Numerical Analysis

The numerical analysis of fission converter plate structure is performed with a finite element analysis program, ADINA[8]. The ADINA

system of finite element analysis programs allows solving a wide variety of problems in structural, thermal and fluid flow analysis.

The fission converter front plate and the model used for the structural analysis are shown in figure 2.19. The horizontal distance between the two downcomer walls is 32". The downcomer walls are welded onto the front and the back plate of the fission converter tank. There will be zero deflection or bending at the places where the downcomer walls are welded. Furthermore, the slope of the deflection surface, where the downcomer walls are welded, can be assumed as zero or non-zero. However, the slope will be very close to zero. The vertical length between the top of the fission converter tank and the fuel lower grid support plate is 140". The lower grid fuel support plate is welded on to the front and the back plates and onto the two downcomer walls. Similarly, the same assumptions as before can be made about the deflection of the plate and the slope of deflection at the top of the front plate and at the place where the fuel lower grid support plate is welded. The maximum deflection and the maximum shear stresses will be observed on the front plate piece A (see figure 2.19). Therefore, it is only necessary to analyze the front or back plate piece A. The front plate piece, which is analyzed, has dimensions 32"X140". The stresses and deflections were calculated for three different plate thickness of ¼", ½", and ¾".

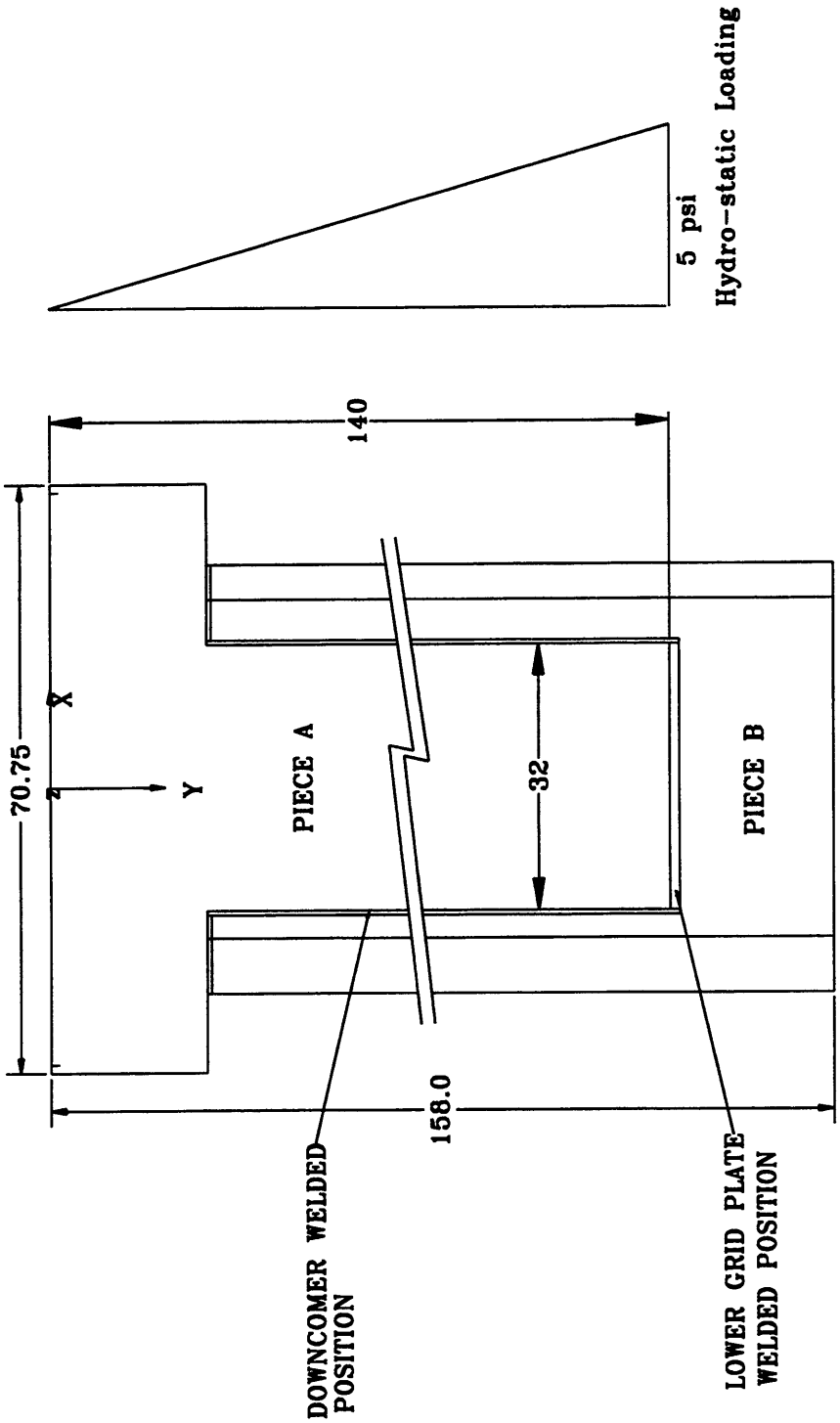

Figure 2.19: The model used for the structural analysis

(All dimensions are in inches)

For each plate thickness two types of boundary conditions were assumed. Those two boundary conditions are:

- Clamped edge conditions, where the deflection and the slope of deflection are zero at the boundary
- Simply supported conditions, where the deflection is zero and the slope of the deflection is non-zero.

Since the tank is filled with water, the loading on the plate is due to the hydrostatic pressure head. The hydrostatic pressure loading varies linearly along the vertical direction from zero at the top to 5.0 psi at the place where the lower fuel grid support plate is welded. The hydrostatic pressure loading is uniform along the horizontal direction.

The aluminum 6061 T6 material properties were obtained from the Handbook of Materials Science[6]. The main mechanical properties of aluminum 6061 T6 material are listed below. The aluminum 6061 T6 material's mechanical properties after welding were obtained from Aluminum and Aluminum Alloys[7] and they are also listed below. Half of the plate is analyzed due to the symmetry along horizontal direction. The calculated primary stresses for clamped edge condition and simply supported condition are shown in figure 2.20(a, b, and c) and 2.21(a, b, and c) respectively.

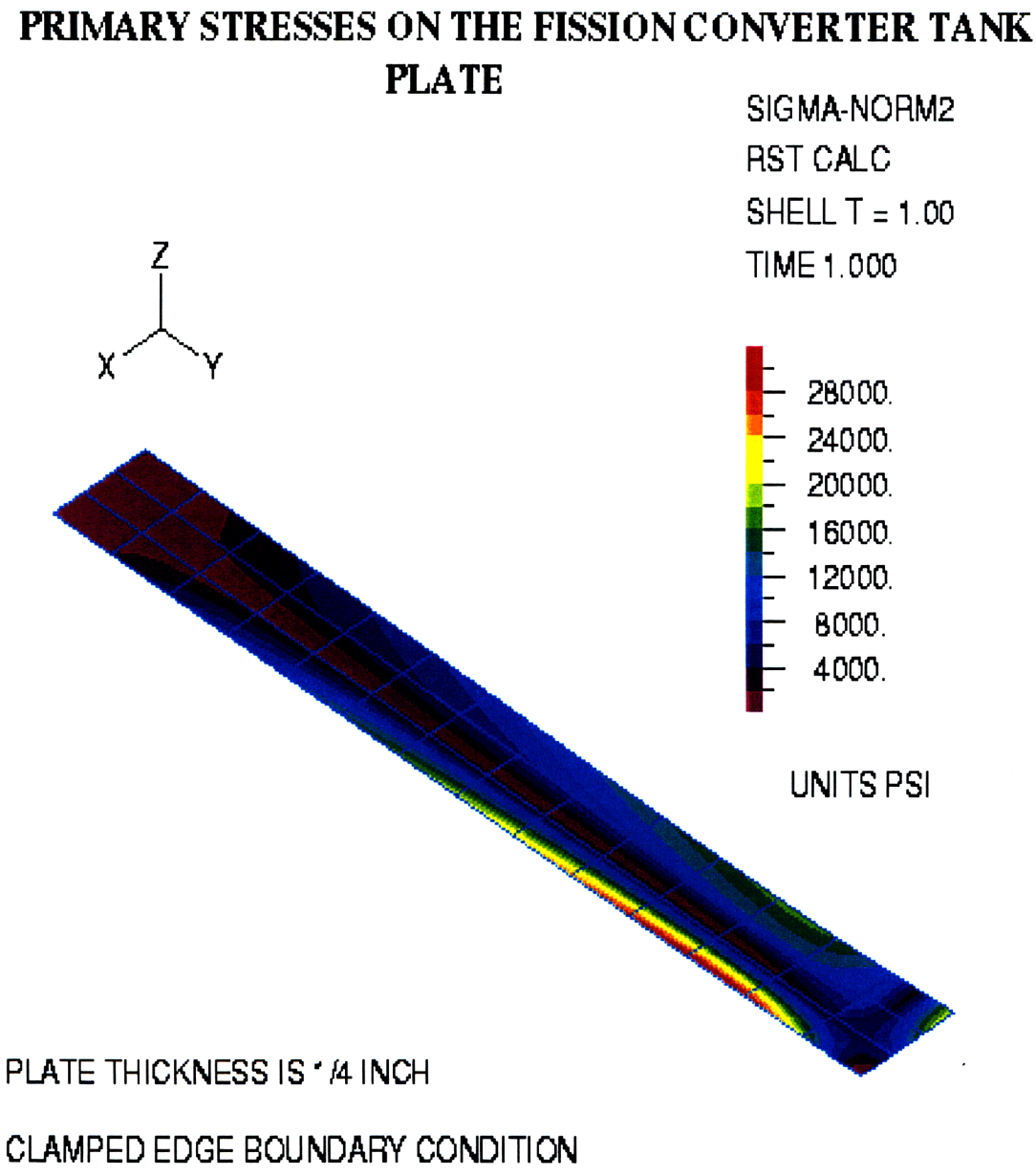

Figure 2.20a: Calculated Primary Stresses for Clamped Edge Boundary Condition

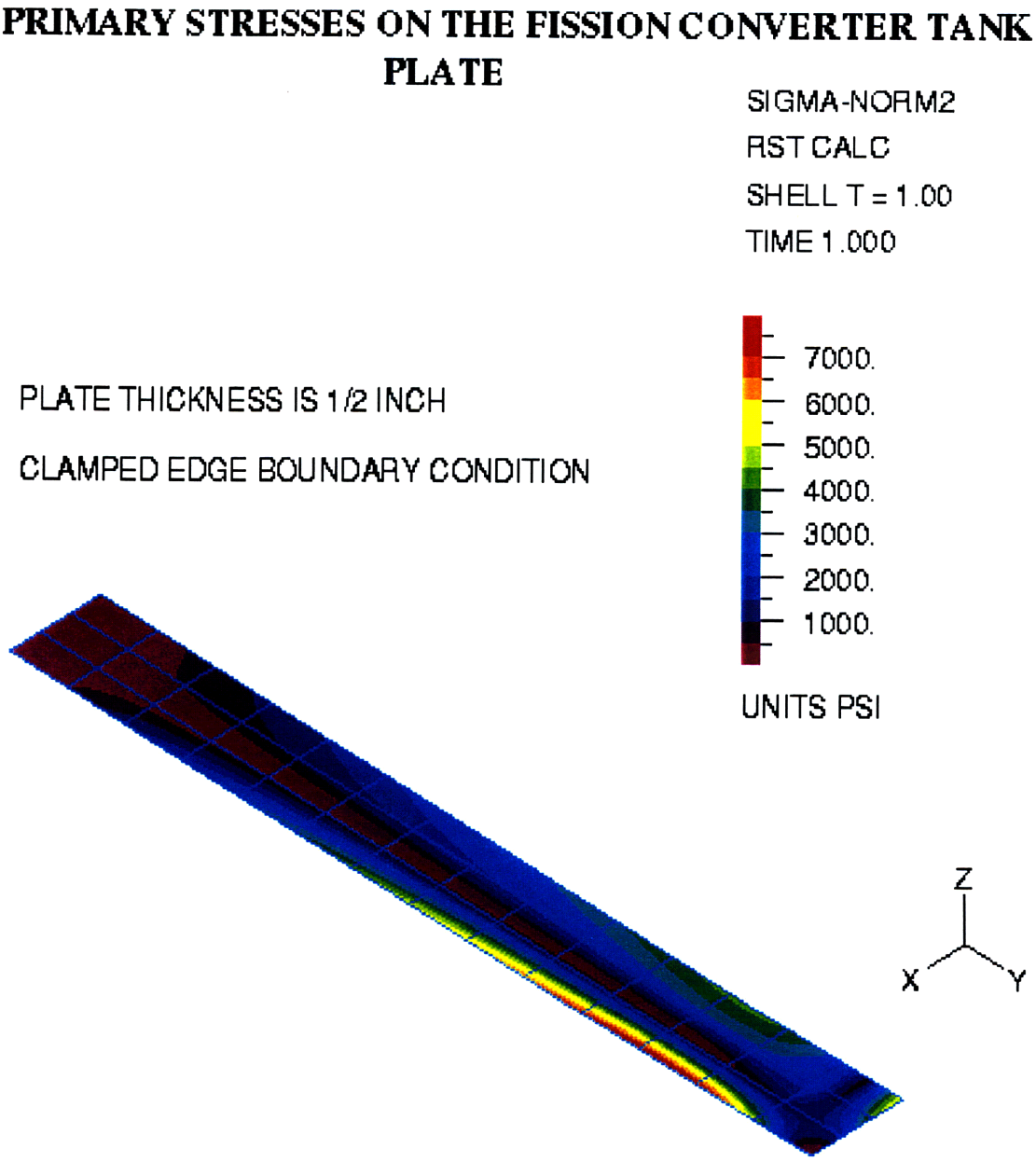

Figure 2.20b: Continuation of Calculated Primary Stresses for Clamped Edge Boundary Condition

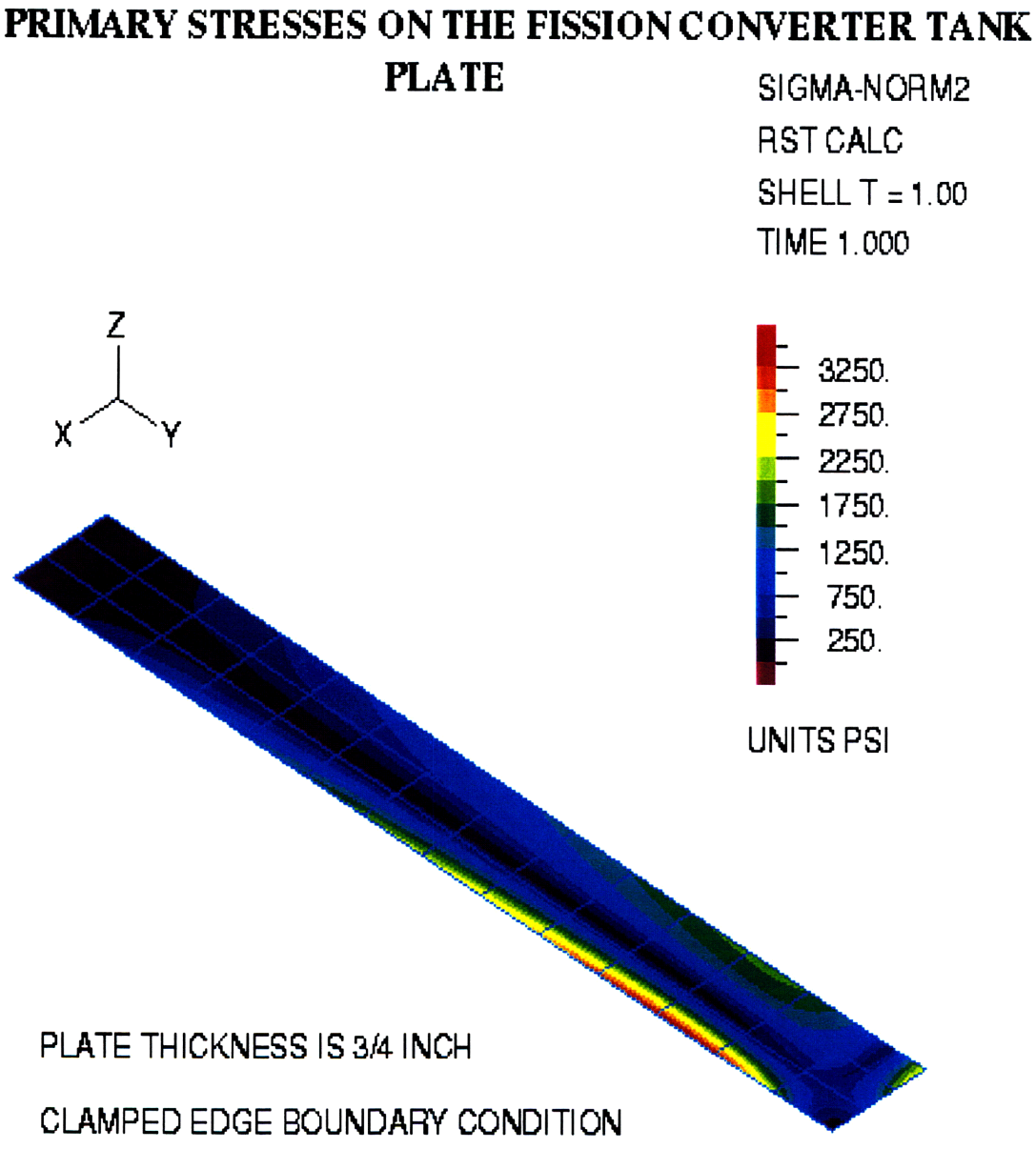

Figure 2.20c: Continuation of Calculated Primary Stresses for Clamped Edge Boundary Condition

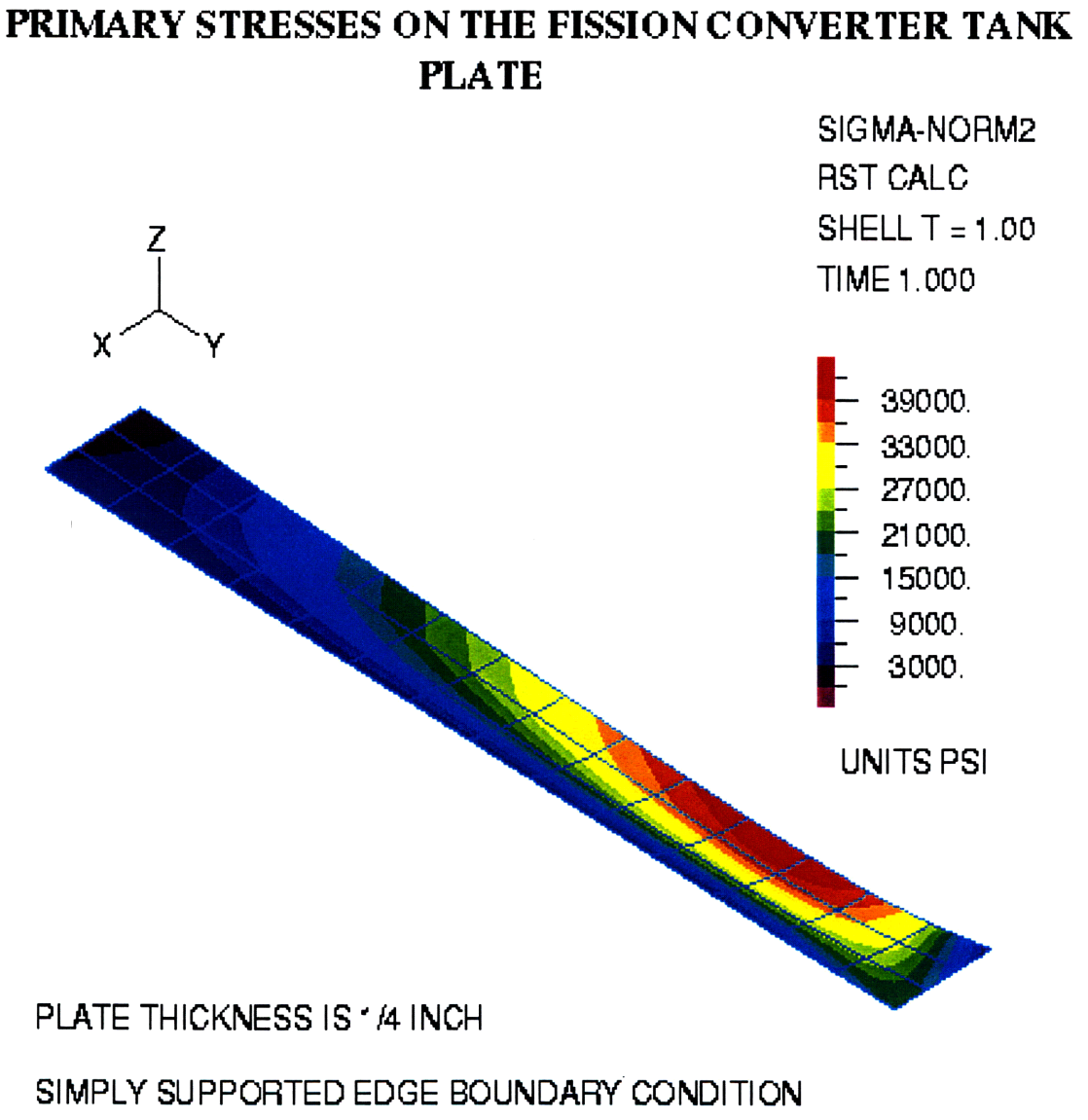

Figure 2.21a: Calculated Primary Stresses for Simply Supported Boundary Condition

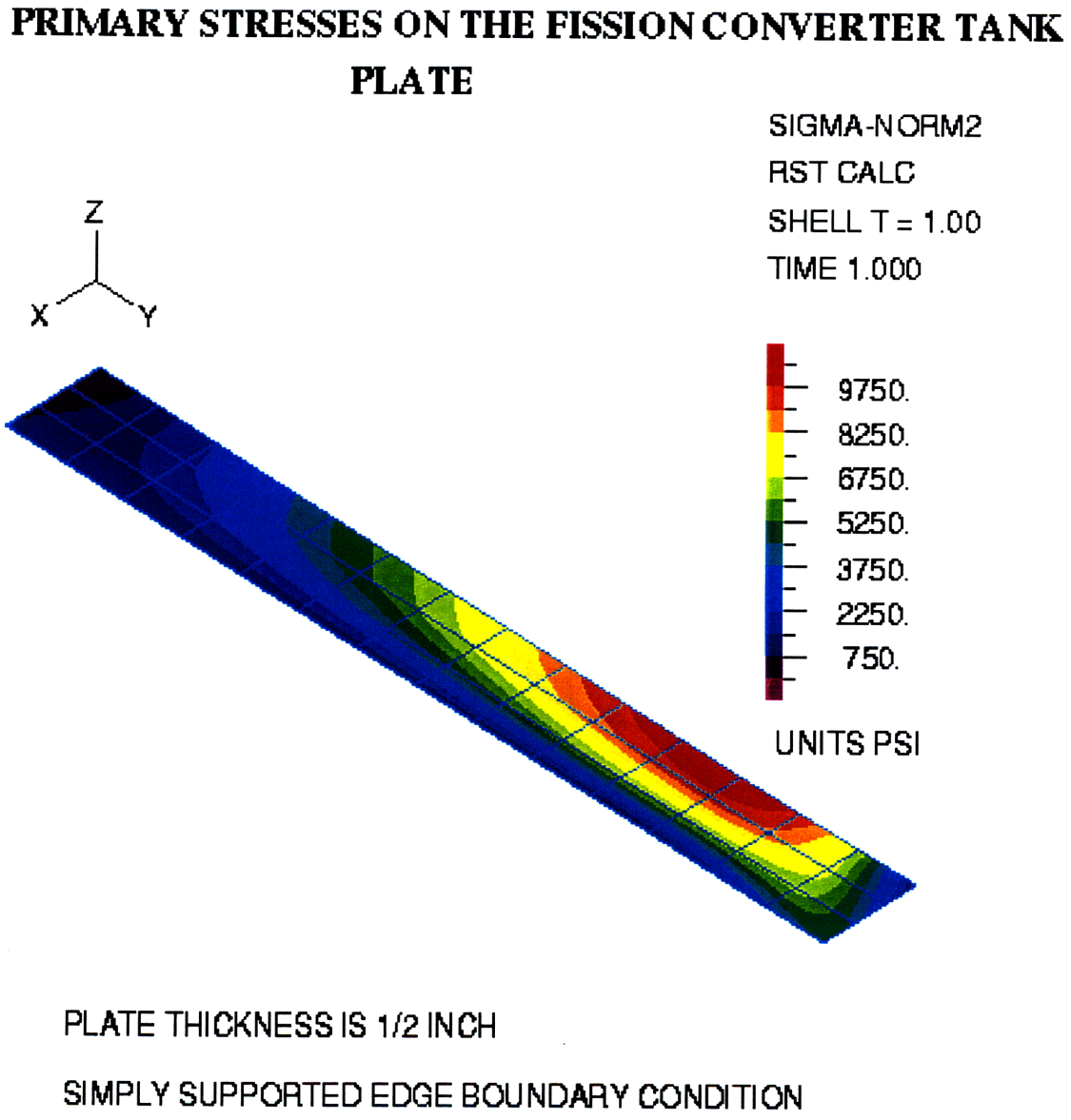

Figure 2.21b: Continuation of Calculated Primary Stresses for Simply Supported Boundary Condition

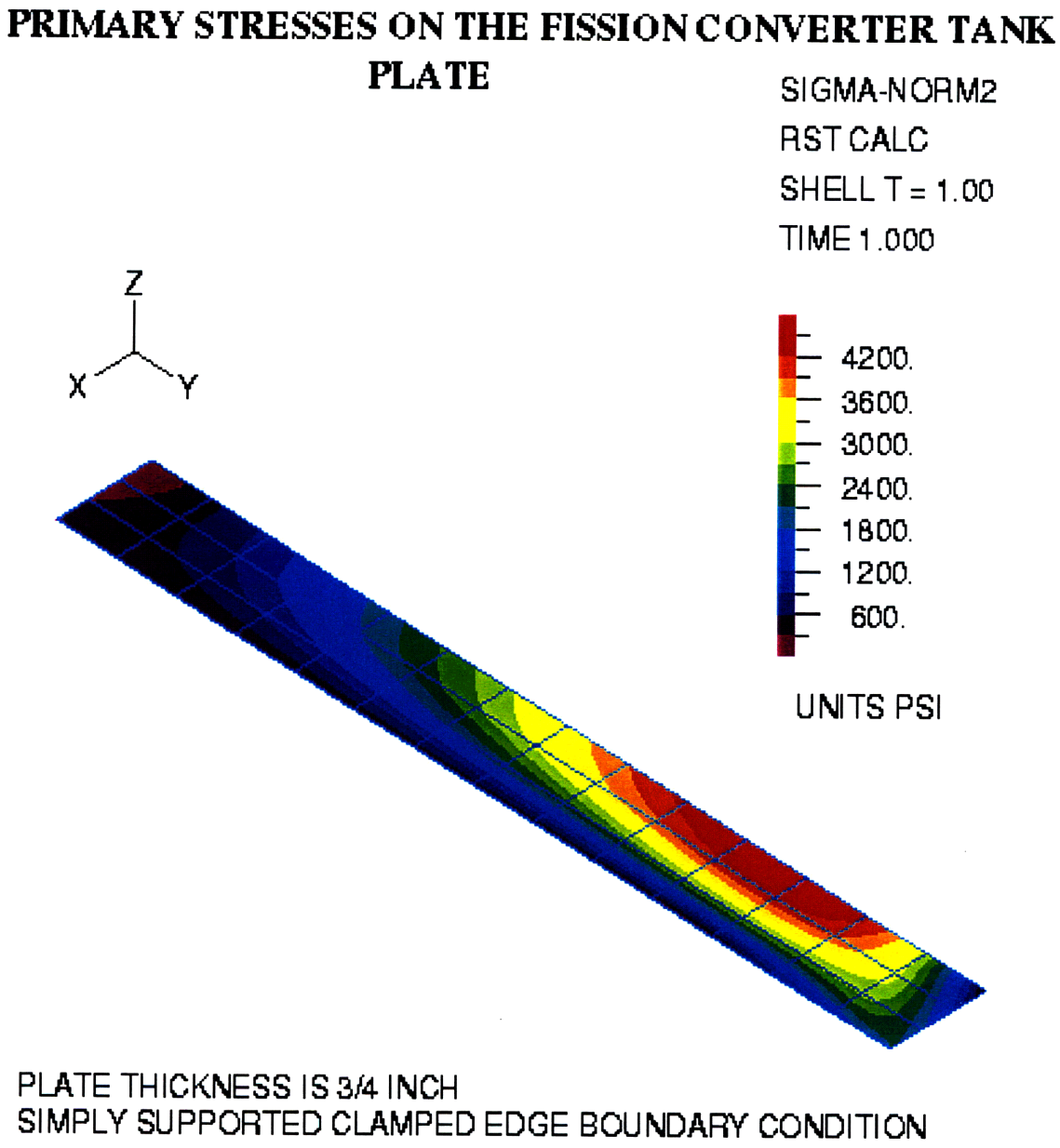

Figure 2.21c: Continuation of Calculated Primary Stresses of Simply Supported Boundary Condition

For the clamped edge case, the maximum primary stress is observed along the boundary, where the downcomer walls are welded. On the other hand, the maximum primary stress is observed along the centerline of the plate for the simply supported boundary condition. According to ASME code, the calculated primary stresses should be less than 2/3 of yield stress of the material. The aluminum 6061 T6 yield stress is 40,000 psi and 27,000 psi before and after welding respectively at 60 ^{0}C. The calculated primary stress should be less than 18,000 psi along the welded boundary or edge and less than 26,000 psi everywhere else. Therefore, the plate thickness should be larger than 1/4" to satisfy the ASME code requirement, because the calculated primary stress (see figure 2.20) is larger than the 2/3 of yield stress.

It is also desired to have low deflection everywhere in the plate. The deflection band plot for ½" plate is shown in figure 2.22. The maximum deflection is observed at 133 inches from the top and 16 inches from the welded side for clamped edge and simply supported boundary conditions. The maximum deflections for clamped edge and simply supported boundary conditions are 0.086" and 0.335" respectively. The actual plate boundary conditions are expected to be very close to the clamped edge case; the deflection and the deflection slope are zero.

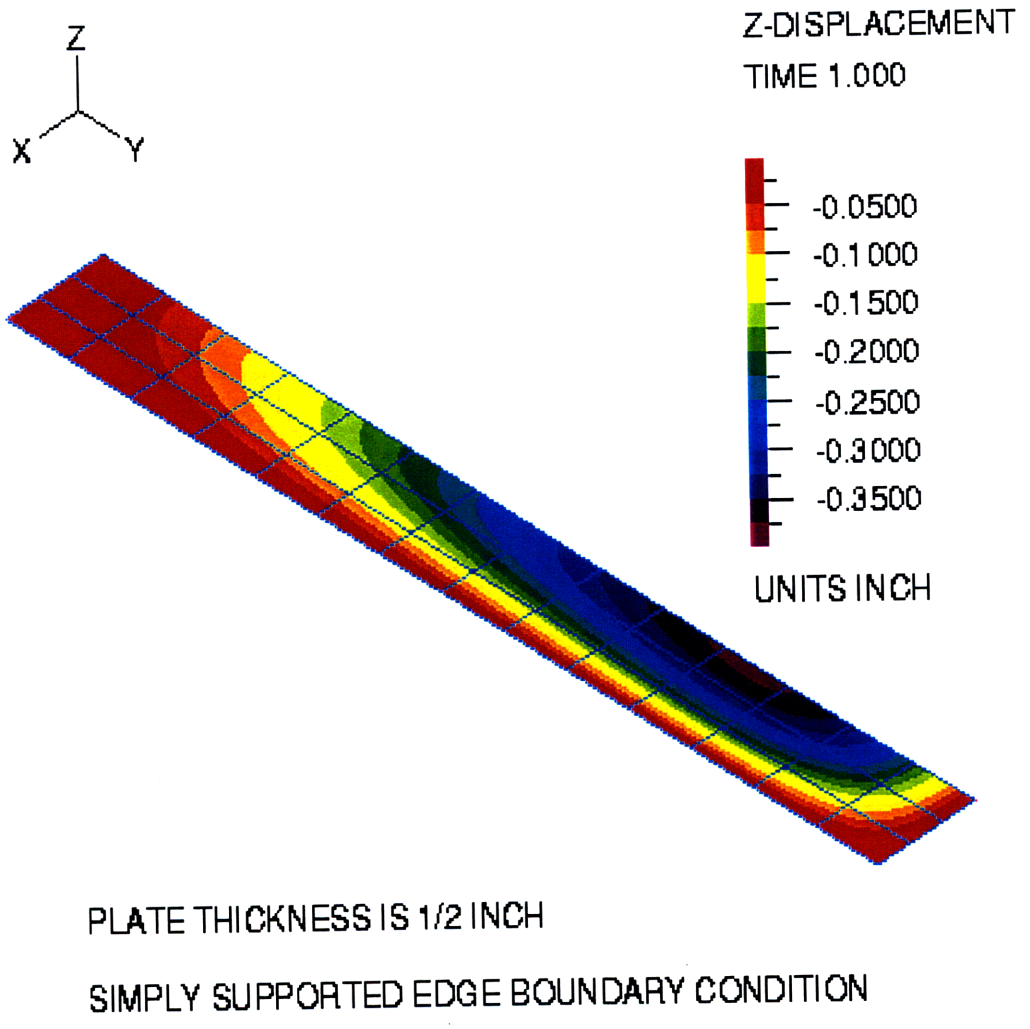

Figure 2.22: Calculated Deflections for Simply Supported Boundary Condition

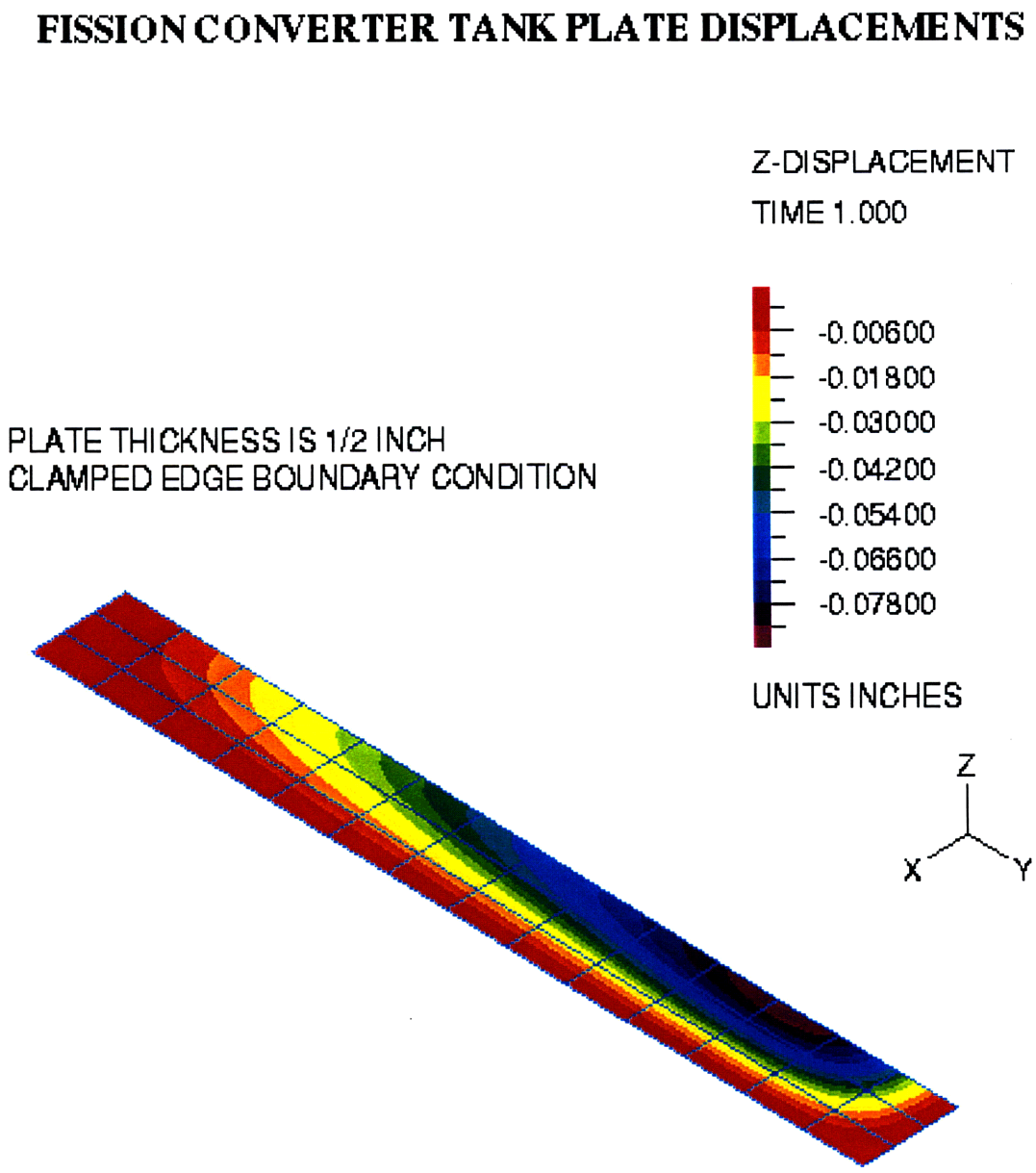

Figure 2.22: Calculated Deflections for Clamped Edge Boundary Condition

Therefore, it is safe to assume that the maximum deflection will be less than ¼". As is obvious, the maximum deflection occurs along the centerline. The deflection along the centerline for ¼", ½", and ¾" thick plates are shown in figure 2.23.

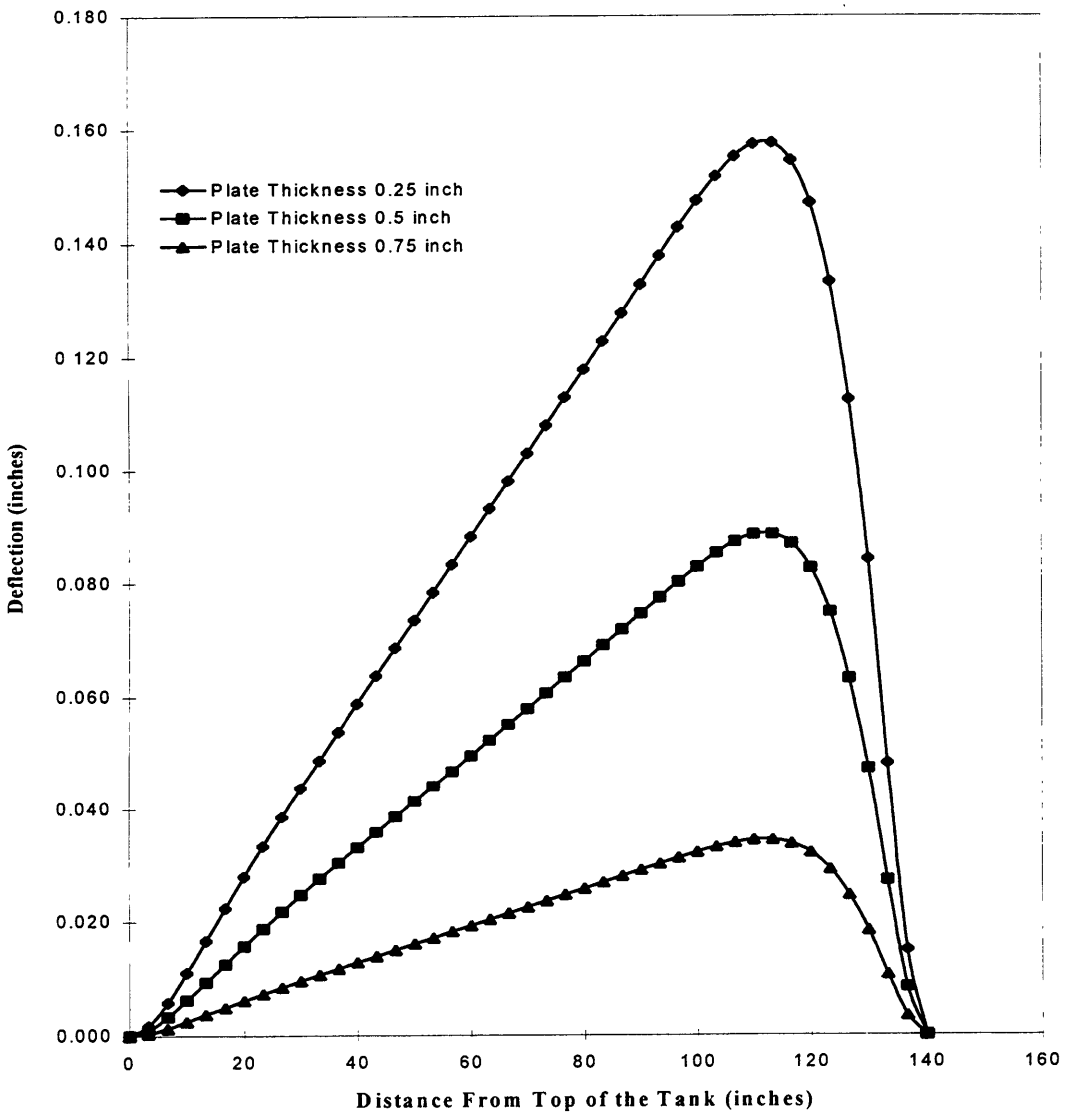

Figure 2.23: Deflections for Different Thickness of Plates

3.9.2 Analytical Calculation

The analytical calculation is performed to verify the plate bending results obtained from numerical analysis. Verification of the plate bending results give us confidence in the numerical analysis and the mathematical model used for the numerical analysis.

The fission converter tank's front plate is modeled as shown in figure 2.19. The hydrostatic pressure head at x=0 (top of the converter tank) is zero and linearly increases to 5.0 psi at x=140 inches (where the fuel lower grid support plate is welded on to the converter tank front plate). In the Y direction, only the front plate between the two-downcomer wall is modeled. Since all the boundaries are welded, clamped edge boundary conditions are assumed.

The deflection w, the load q(=5.0 psi), and the flexural rigidity of the plate $D(=Eh^3/12(1-\nu^2))$ are related by the following differential equation;

$$\frac{\partial^4 w}{\partial x^4}+2\frac{\partial^4 w}{\partial x^2 \partial y^2}+\frac{\partial^4 w}{\partial y^4}=\frac{q}{D} \qquad (2.1)$$

with the following boundary conditions for clamped edges:

$$(w)_{x=\pm b/2}=(w)_{y=a}=(w)_{y=a}=0, \text{ and } \left(\frac{\partial w}{\partial x}\right)_{x=\pm b/2}=\left(\frac{\partial w}{\partial y}\right)_{y=0}=\left(\frac{\partial w}{\partial y}\right)_{y=a}=0$$

Here a = length of plate in x direction,

b = length of plate in y direction,

h = thickness of plate

E = modulus of elasticity of plate material,

ν = Poisson's ratio.

The solution to equation (2.1) is obtained by combining the solution for the simply supported plate with the solution for the plate bent by moments distributed along the edges. The values for the edge moments are determined from the condition that at the boundaries the slope of the deflection is equal to zero. The solution for the deflection surface w, of the plate is

$$w=w_1+w_2+w_3+w_4$$

Here w_1, w_2, w_3 and w_4 are given by the following equations:

$$w_1 = \frac{2qb^4}{\pi^5 D}\sum_{m=1,3,5..}^{\infty}\frac{(-1)^{(m-1)/2}}{m^5}\cos\frac{m\pi x}{b} * \frac{1}{\sinh\beta_m}\left(\frac{2y\sinh\beta_m}{a} - \left(\beta_m\coth\beta_m + 2\right)\sinh\frac{m\pi y}{b} + \frac{m\pi y}{b}\cosh\frac{m\pi y}{b}\right)$$

$$w_2 = \frac{a^2}{2D}\sum_{n=1,2}^{\infty}\frac{E_n}{n^2\pi^2\cosh\alpha_n}(\alpha_n\tanh\alpha_n\cosh\frac{n\pi x}{a} - \frac{n\pi x}{a}\sinh\frac{n\pi x}{a})\sin\frac{n\pi y}{a}$$

$$w_3 = \frac{b^2}{2D}\sum_{m=1,3}^{\infty}\frac{F_m}{\pi^2 m^2}\left(-\frac{m\pi y}{b}\sinh\frac{m\pi y}{b} - \frac{\beta_m}{\sinh^2\beta_m}\sinh\frac{m\pi y}{b} + \coth\beta_m\frac{m\pi y}{b}\cosh\frac{m\pi y}{b}\right)\cos\frac{m\pi x}{b}$$

and,

$$w_4 = \frac{b^2}{2D}\sum_{m=1,3}^{\infty}\frac{G_m}{m^2\pi^2\sinh\beta_m}\left(\beta_m\coth\beta_m\sinh\frac{m\pi y}{b} - \frac{m\pi y}{b}\cosh\frac{m\pi y}{b}\right)\cos\frac{m\pi x}{a}$$

Here $\alpha_m = n\pi b/2a$, $\beta_m = m\pi a/b$ and En, Fm and Gm can be determined from the following three equations;

$$\frac{2qa^2(-1)^{n+1}}{n^3\pi^3}\left(\alpha_n - \tanh\alpha_n\left(1+\alpha_n\tanh\alpha_n\right)\right) + E_n\left(\tanh\alpha_n\left(\alpha_n\tanh\alpha_n - 1\right) - \alpha_n\right)$$

$$= \frac{4b^3}{a^3}\left(\sum_{m=1,3}^{\infty} m(-1)^{\frac{m-1}{2}}\frac{F_m}{n^2\pi^2}\frac{1}{\left(\frac{b^2}{a^2}+\frac{m^2}{n^2}\right)^2}\right)$$

$$\frac{4qb^2}{m^3\pi^3}(-1)^{\frac{m-1}{2}}\left(\frac{2}{\beta_m}-\frac{\beta_m\coth\beta_m+1}{\sinh\beta_m}\right)+F_m\left(\coth\beta_m-\frac{\beta_m}{\sinh^2\beta_m}\right)+\frac{G_m}{\sinh\beta_m}\left(\beta_m\coth\beta_m-1\right)$$

$$=-\frac{8b}{a}\sum_{n=1,2}^{\infty}\frac{E_n}{n^3\pi}m^2(-1)^{\frac{m-1}{2}}\left(\frac{1}{\frac{b^2}{a^2}+\frac{m^2}{n^2}}\right)^2$$

and,

$$\frac{4qb^2}{m^3\pi^3}(-1)^{\frac{m-1}{2}}\left(\frac{2}{\beta_m}-\frac{\beta_m}{\sinh^2\beta_m}-\coth\beta_m\right)-\frac{F_m}{\sinh\beta_m}\left(\beta_m\coth\beta_m-1\right)-G_m\left(\coth\beta_m-\frac{\beta_m}{\sinh^2\beta_m}\right)$$

$$=\frac{8b}{a}\sum_{n=1,2}^{\infty}\frac{E_n}{n^3\pi}(-1)^{n+1}m^2(-1)^{\frac{m-1}{2}}\frac{1}{\left(\frac{b^2}{a^2}+\frac{m^2}{n^2}\right)^2}$$

These equations are solved numerically by neglecting terms higher than n=4 and m=7, which results in a system of simultaneous equations. The maximum deflection is along the axis of x=0. The deflection of the plate along the axis of x=0 is calculated and shown in figure 2.24 along with the numerical analysis results. As it is obvious from the figure 2.24, that the numerical and analytical results agree reasonably well.

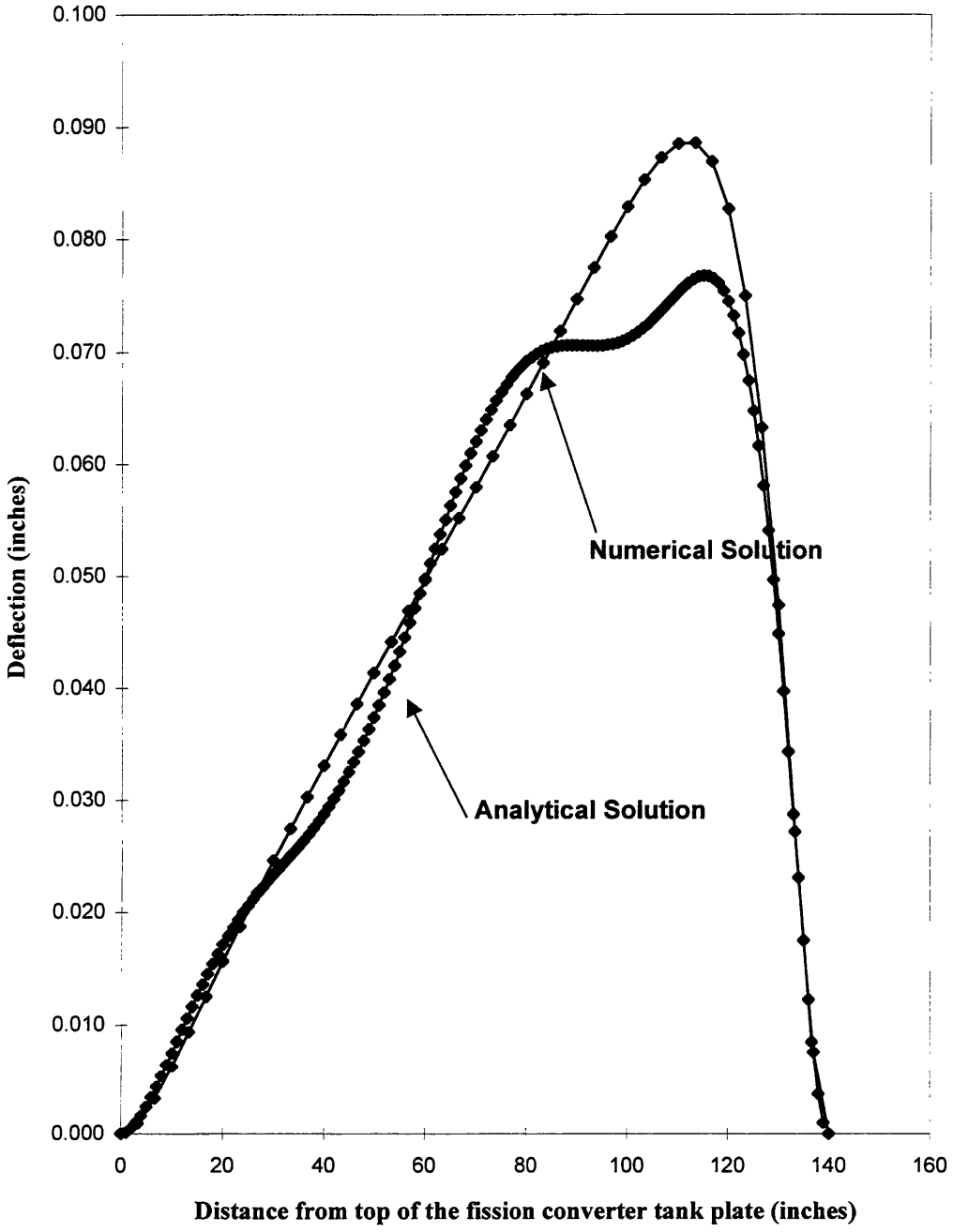

Figure 2.24: Numerical and Analytical Deflection Results for the 0.5 inch Thick Fission Converter Tank Front Plate

4.Fission Converter Fuel Handling

The fission converter will either use fresh or irradiated (partially burnt) MITR-II fuel elements. Thus, the same procedures as for the MITR can be used for the fission converter fuel regarding fuel storage and fuel handling. A unique issue to fission converter fuel is "self-protection" of the fuel because the fission converter operates at a maximum power of 250 kW. This and other related topics are discussed in the following sub sections.

4.1 Fuel Element self-protection

Self-protection fuel should have a radiation level of 100 R/hr at one meter away from the fuel. Calculations and measurements show that discharged MITR-II fuel from the MITR (average overall depletion ~ 40%) will remain self-protecting for at least a decade. Thus self-protecting criteria can be met if the discharged fuel from the MITR is used for the fission converter. However, if relatively fresh MITR-II fuel elements have to be used as the fission converter fuel, fuel can be maintained self-protecting if the following strategy is followed:

- Fresh fuel elements will be first irradiated in the MITR-II core before they are to be used in the fission converter. Calculations show that if a fresh fuel element is irradiated in the MITR-II core at 5 MW power (25 elements in the core, 200 kW average power output per element)

for 150 hours, it will remain self-protecting for 300 days. This is equivalent to a burn up of $3X10^4$ kW-hr per element.

- Then the irradiated fuel will be placed in the fission converter. The element with a burn up of $3X10^4$ kW-hr per element will remain self-protecting if the fission converter is operated at 80 kW for at least 60 hours (minimum burn up of 436 kW-hr for each fuel element) every month.

Fresh unirradiated fuel elements can also be used in the fission converter provided that the total number of non self-protecting elements on site conforms to the MITR security plan.

4.2 Fuel Loading and Unloading

According to the MITR Technical Specification 3.10.4, a fuel element shall not have been operated in the reactor core at a power level above 100 kW for at least four days prior to removal. Since the MITR core and fission converter core have different numbers of fuel elements, the above requirement can not be directly transferred to the fission converter tank. In addition, it might be desirable to operate the fission converter at a power of 100 kW and refuel within less than four days, provided that the power history is acceptable. The following conditions are equivalent to the limit given in the MITR Technical Specification 3.10.4 for the fission converter:

- Continuous operation at or below 50 kW for four days prior to refueling.
- A maximum operating time of 4.8 hours per day at or below 250 kW during the four days prior to refueling.
- A maximum burn up of 436 kW-hr per fuel element during the four days prior to refueling.

The first of these conditions is equivalent to MITR Technical Specification 3.10.4. The second and third are based on an equivalent power history for the fission converter. However, fuel elements can be removed immediately from the fission converter tank during emergency conditions, such as fuel leakage.

The maximum fuel plate temperatures were calculated for the normal fuel removal and for emergency fuel removal conditions. It was assumed that the fission converter was operated continuously for 5 years at the maximum power of 250 kW until four days prior to fuel removal of the fuel elements for the normal fuel removal condition. For the emergency fuel removal condition, it was assumed that the fission converter was operated continuously for 5 years at the maximum power of 250 kW until removal of the fuel element. These assumed power histories are much more intensive than is likely to be the case for the fission converter fuel. Moreover, it was assumed that all heat transfer from the fuel element was by radiation alone. The maximum clad temperature was calculated to be 340 ^{0}C and 383 ^{0}C for normal removal

and emergency removal conditions, respectively. The calculation procedure is given in the appendix.

During refueling of the fission converter, depleted or partially depleted fuel elements may be removed from the fission converter and stored in the fuel storage pool in the MITR. It is also possible to move the partially depleted fuel element within the fission converter from one position to another. Then, new or spent fuel from the fuel storage pool can be inserted into the fission converter. The fuel transfer cask, which is used for MITR fuel transfer, will also be used for the fission converter fuel movements. The fuel transfer cask will provide the necessary gamma shielding during the fuel movements.

The setup and the arrangement for fuel handling are shown in figure 2.25. Detailed information about each piece of equipment is given in the following subsections.

4.2.1 Fuel Transfer Cask

The fuel transfer cask for transferring spent fuel is a steel weldment, filled with lead shielding and equipped with shutters at the bottom and the top. The cavity in the center has a diameter of 6.75 inches and a length of 40 inches between the shutters. The weight of lead in the transfer cask is 12,767 pounds and the weight of the steel is 1,286 pounds.

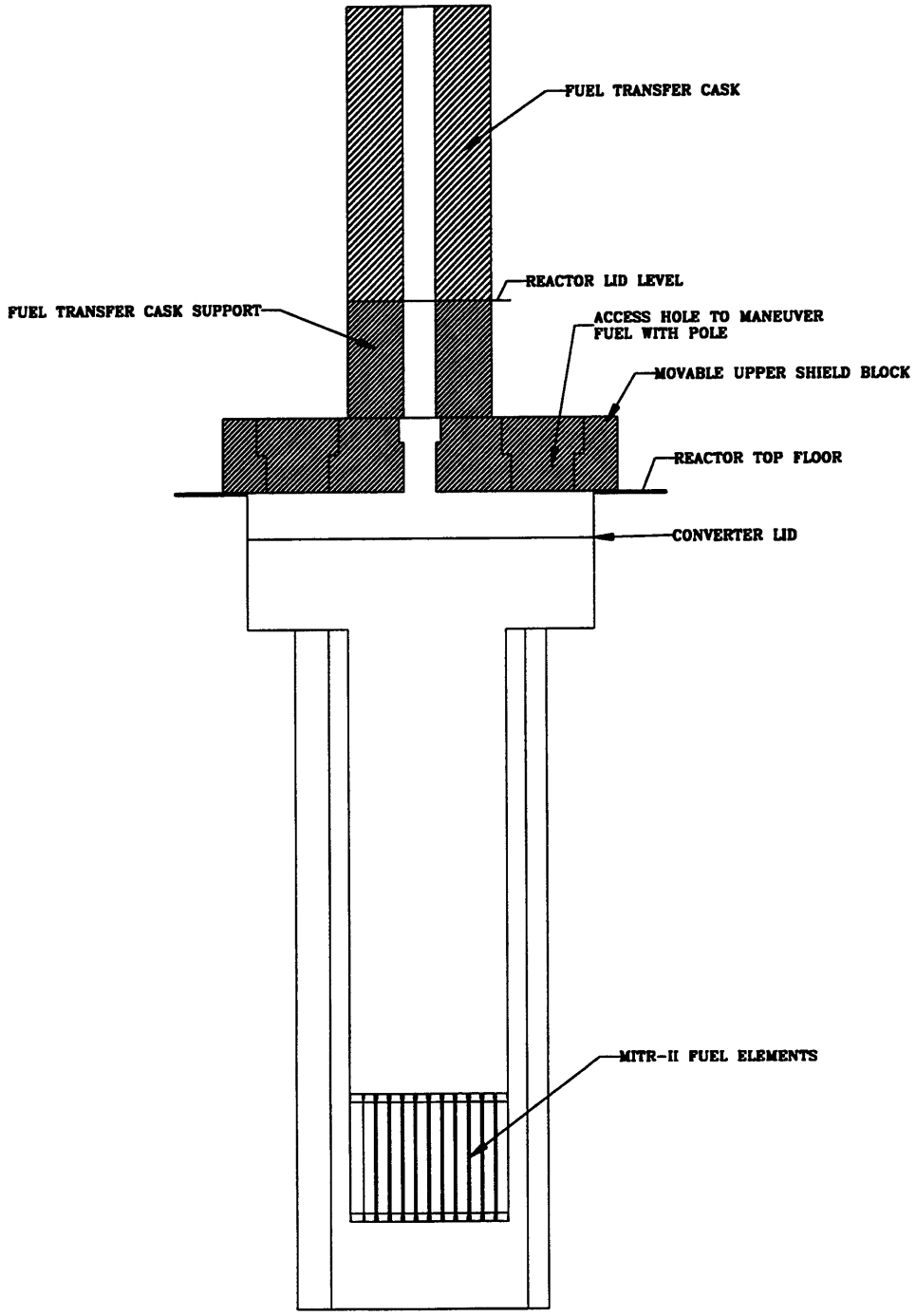

Figure 2.25: Schematic Setup for Fuel Handling, Showing the Fuel Transfer Cask and Fuel Transfer Cask Support

Any transfer of irradiated fuel elements out of the fission converter tank will be made by lifting the fuel elements into the transfer cask and then closing the bottom and top shutters of the transfer cask. The fuel transfer cask will be positioned such that the hole in the transfer cask and the hole in the fuel transfer cask support are aligned.

During loading of fuel, there will be a fuel element in the fuel basket, which will be in the fuel transfer cask. Once the transfer cask is positioned, the bottom shutter will be opened and the basket will be lowered into the fission converter tank. Then the fuel element will be transferred to the fuel grid plate by a pole with a grappling hook fitted at the end of the pole.

During unloading of fuel, the empty basket will be lowered into the fission converter tank, and the fuel element will be transferred to the basket from the fuel grid by a pole with a hook at the end. Then the basket with the fuel element will be lifted up into the transfer cask and both shutters will be closed. Once the fuel and basket is in the transfer cask, the bottom shutter will be closed. Then the transfer cask will be moved to the fuel storage well and the fuel will be discharged into the storage pool.

The above fuel loading and unloading procedures are the same as those for the MITR.

4.2.2 Fuel Transfer Cask Support

The fuel transfer cask must be aligned with the center access hole in the removable upper shield blocks due to the interference of the reactor top ring above the reactor floor. Therefore the fuel transfer cask support will serve as a middle piece to align the holes in the movable upper shield blocks and the hole in the fuel transfer cask. The fuel transfer cask height is determined such that the reactor lid top level and the fuel transfer cask support level will be the same. The fuel transfer cask support will be placed onto the removable upper shield blocks and the removable upper shield blocks center access hole and the fuel transfer cask support hole will be aligned. Then the fuel transfer cask will be placed on top of the fuel transfer cask support such that all the holes are aligned vertically. Therefore a small part of the fuel transfer cask will be placed on top of the reactor lid.

The fuel transfer cask support will be made of a steel weldment filled with lead for shielding purpose.

4.2.3 Fuel Loading and Unloading Procedures

The author is proposing two options for refueling the fission converter tank. Either of these options can be adopted by the operator to refuel the fission converter tank. These two options are described below.

Option1

Step1: The upper removable shield blocks are removed first, then the movable part of the fission converter lid and the primary outlet pipe are removed.

Step2: The upper removable shield blocks are moved back to its original position. The fuel transfer cask support is placed on top of the upper removable shield blocks such that the center access hole in the upper removable shield blocks and the hole in the fuel transfer cask support are aligned vertically.

Step 3: Irradiated or unirradiated fuel is placed in the fuel basket in the fuel storage tank. Then the fuel transfer cask is moved above the fuel storage tank, and the cable with a hook is lowered from the fuel transfer cask into the fuel storage tank. Once the fuel basket is attached to the hook on the rope, the fuel is raised into the fuel transfer cask and the bottom shutter in the fuel transfer cask is closed.

Step 4: The fuel transfer cask is placed on top of the fuel transfer cask support such that all three holes in the upper shield blocks, fuel transfer cask support and the fuel transfer cask are aligned vertically.

Step 5: The bottom shutter in the fuel transfer cask is opened and the fuel is lowered into the fission converter tank.

Step 6: The fuel transfer cask is moved away but the fuel is kept in the same position by adjusting the cable length. Once the fuel transfer cask is moved, the fuel transfer cask support will be moved allowing the cable to slide through the slit. Then the removable upper shield blocks will be moved by sliding side ways. The dose is low at the reactor top level after removing the upper shield blocks. The dose calculation during the refueling is given in the section 3.4.

Step 7: The fuel is moved from the fuel basket and placed into the lower grid plate with an aid of a pole with a hook attached.

Option 2

Step 1 to Step 5: Same as the option 1

Step 6: Open the side accesses holes in the movable upper shield blocks. Then insert the grappling pole into the fission converter tank and move the fuel from the basket into the fuel lower grid plate. There are two access holes each side and total of four holes on the removable upper shield blocks. One hole is to maneuver the fuel with the pole and the other one is to look inside the fission converter tank.

Option 1 makes it easier to move the fuel within the fission converter tank, because there is more space to maneuver fuel from the reactor top

floor. However, the movable upper shield blocks, the fuel transfer cask support and the fuel transfer cask have to be moved for each fuel element transfer. Therefore, option 1 requires more labor compared to option 2.

5. References

1. Kiger, W.S., *Neutronic Design of a Fission Converter-Based Epithermal Beam for Boron Neutron Capture Therapy*, Nucl. E. Thesis, Massachusetts Institute of Technology, 1996.
2. Sakamoto, S., *Sensitivity Studies of the Neutronic Design of a Fission Converter-Based Epithermal Beam for Boron Neutron Capture Therapy*, SM Thesis, Massachusetts Institute of Technology, 1997.
3. Auterine, I., and Hiismaki, P., "Epithermal BNCT Neutron Beam Design for a TRIGA II Reactor", *Advances in Neutron Capture Therapy*, Edited by A.H. Soloway et. al., Plenum Press, New York, 1993.
4. Negan, C., Fricke, V., and Owrutsky, S., *Microshield3.12: a Program to Calculate the Dose from Direct gamma Irradiation*, Rockville, MD, 1987.
5. Wilson, W.B., England, T.R., LaBauve, R.J., and George, D.C., *DKPOWR: A Code for Calculating Decay Power, Energy, Activity, and $\beta+\gamma$ Spectra in LWR Fuel Using Fission Pulse Functions*, Los Alamos National Laboratory, Los Alamos, New Mexico, 1984.
6. Lynch, C.T., Summitts, R., and Sliker, A., *CRC Handbook of Materials Science*, CRC Press, Cleveland, 1974.
7. Phillips, A.L., *Aluminum and Aluminum Alloys*, 5th Edition, New York, 1966.
8. Bathe, K-J, *Adina: A Finite Element Program for Automatic Dynamic incremental nonlinear analysis*, Cambridge, 1978.

CHAPTER THREE

THERMAL-HYDRAULIC ANALYSIS

1.INTRODUCTION

The fission converter can be thought as a subcritical power reactor. The power generated by the eleven fuel elements in the fission converter should safely be transported to the coolant without degrading the fuel elements or the fission converter structure. Specifically, the temperature should be prevented from reaching the melting point temperature of the fuel or the clad, during steady state operation or transients due to anticipated accidents.

The fission converter is designed to accommodate either light or heavy water as a coolant/moderator (the design is described in the Chapter 2). The power generated by the eleven fuel elements is tabulated in the table 3.1 for two different MITR-II research reactor power levels (5 MW and 10 MW) and two different coolant/moderator (light and heavy

water). The total converter power given in the table 3.1 is for the fresh MITR-II fuel elements. The total power and the power profiles were calculated using Monte Carlo code MCNP-4A by W.S. Kiger[1] and S.Sakamoto[2].

Table 3.1: The fission converter power generation[1,2].

Coolant/Moderator	**MITR II Power 5 MW**	**MITR II Power 10 MW**
Light Water	125 kW	250 kW
Heavy Water	103 kW	206 kW

Three different designs, natural convection, forced convection with bypass channel and simple forced convection, are explored to remove the generated heat from the eleven fuel elements. All three designs should satisfy the design goals to consider as a viable option to remove the heat from the eleven fuel elements. The design goals are:

1. An anti-siphon valve should not be required in the downcomer region. Anti-siphon valve requires regular visual inspection and frequent maintenance according to Nuclear Regulatory Commission (NRC) regulations. Hence, avoiding anti-siphon valve will minimize the required maintenance. Lack of space in the downcomer area and design simplicity are the other reasons to avoid an anti-siphon valve.

2. Normal coolant operation temperature should be low (hot channel exit temperature should be less than 60 ^{0}C). Since the finned MITR-II fuel element's clad is made of aluminum alloy, continuous high operating temperature may enhance corrosion. Moreover, lower normal operating temperature provides higher heat sink capacity for accident conditions.
3. During a Loss Of Flow (LOF), it is preferred that the fission converter primary coolant in the tank remains in the single-phase region for more than 10 minutes when the converter is at full power. This preferred condition would allow patient treatment to continue and to finish even if a LOF accident occurs at the beginning or during the treatment. S.Sakamoto[2] and W.S.Kiger[1] have estimated the treatment time to be less than 2 minutes. Therefore, ten minutes is sufficient time to complete the patient treatment. It is unacceptable to operate the system in normal operating mode when it is in two-phase region, because boiling on the MITR-II fuel plates will cause corrosion.

After the calculation of steady state thermal-hydraulic results for the three designs, transient thermal hydraulic analysis is performed and the results are compared among the three designs. The following transients are considered in the analysis;

- Loss of Flow with Cadmium Shutter Closure
- Pump failure

- Outlet pipe break
- Inlet pipe break

- Loss of Flow with Cadmium Shutter Failure
  - Pump failure
  - Outlet pipe break
  - Inlet pipe break
- Loss of Coolant

The countermeasures and lines of defenses are outlined for each anticipated accident. A suitable design is chosen among the three designs.

Even though the maximum converter power is 250 kW, 300 kW is chosen to perform the thermal hydraulic analysis. The converter power of 300 kW is chosen to accommodate any error in the neutronic calculations and to allow any future changes in the design. These future changes may include the number of fuel elements, the orientation of fuel elements, and the configuration of fuel elements.

2.THERMAL-HYDRAULICS DESIGN LIMITS

The design limits are different for the steady state and for the anticipated accidents. For the steady state operating condition, the design limits are no nucleate boiling and no recirculation within the core or the upper plenum. The MITR-II fuel is made of aluminum-6061 cladding and each fuel element has 15 plates. Both surfaces of each plate are finned. Enhanced corrosion is possible on the MITR-II fuel elements if boiling occurs on the fuel plates for a long period of time. Therefore, the temperature of the coolant should be below its saturation temperature to prevent boiling during the steady state operating condition. The fuel cladding temperature for the incipient boiling condition is calculated and then compared with the fuel cladding temperature expected during steady state operation.

Since the anticipated or the credible accidents occur very rarely and for short periods of time, brief periods of boiling is acceptable during such events. However, the temperature must be prevented from reaching the softening temperature of the fuel cladding (450 ^{0}C) during all accidents to prevent any fuel disruption.

3. NATURAL CONVECTION DESIGN (DESIGN I)

3.1 DESCRIPTION OF COOLING SYSTEM

The schematic of fission converter's heat removal system, which includes the primary and part of the secondary loop, is depicted in the Figure 3.1. The power generated in the eleven MITR-II fuel elements is transported to the primary coolant by natural convection. The arrows in the fission converter tank (see figure 3.1) show the primary coolant flow directions for the natural convection. The coolant in the upper plenum is removed from the converter through an outlet pipe. It is then returned to the downcomer region in the tank through an inlet pipe, after it has been cooled to the temperature of 40° C.

The coolant entrance velocity into the outlet pipe is same as the coolant velocity in the upper plenum region near the entrance of the outlet pipe. As a result, the suction power created by the pump in the primary outlet pipe will not disturb the natural convection in the fission converter tank. The detail calculations of the flow rate in the primary loop and the diameters of inlet and outlet pipe are performed in subsection 3.4.

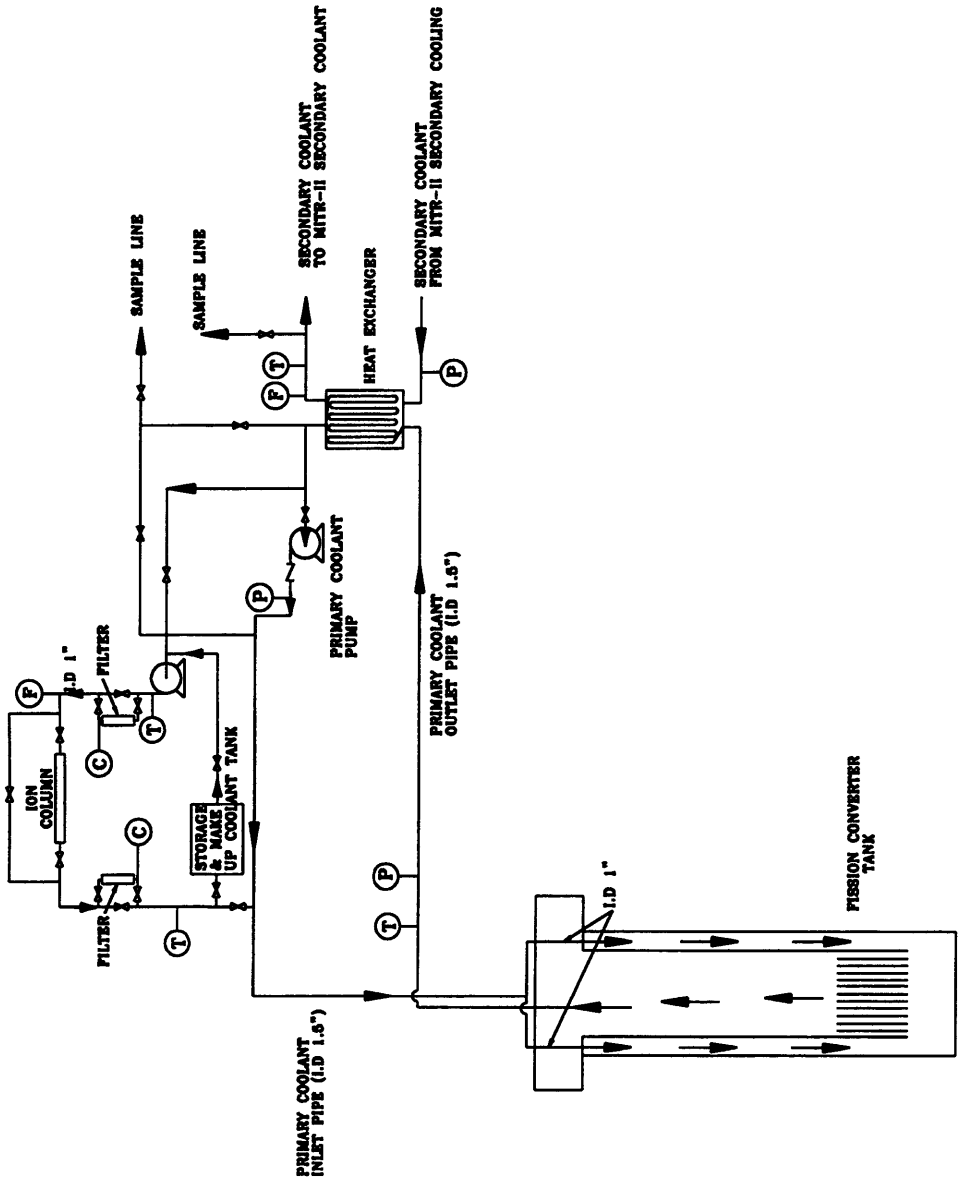

Figure 3.1: Schematic Drawing of Fission Converter Heat Removal System for Natural Convection Design (Design I)

All of the primary piping, some of the secondary piping and the primary heat exchanger will be located above the level of the fission converter tank. This obviates the need for anti-siphon valves, which would be required to prevent coolant loss in the event of a pipe break if the coolant system were below the level of the coolant in the fission converter tank. The secondary coolant is sent to the existing MITR-II cooling tower where it is cooled by the air circulation in the cooling tower.

The primary cooling system has a primary pump, a heat exchanger, a coolant clean up system, and a make up coolant system. One percent of the primary coolant flow is diverted to the coolant clean up system to clean and to control the water chemistry. The make up coolant system adds the coolant to the primary loop if the coolant is lost by evaporation or by other means. The clean up loop is also designed to remove residual heat during the fission converter shut down (the primary pump is off and the cadmium shutter is closed). It was calculated that the residual heat in the eleven fuel elements is 1% of the full power when the cadmium shutter is closed. Therefore, the 1% of the total flow rate (flow through the clean up loop) has a capability of removing the generated heat while keeping the exit temperature from the tank the same as that during normal operation. During the fission converter shut down (the primary pump is off and the cadmium shutter is closed), the 1% of the total flow rate is continued through the primary outlet pipe,

the primary heat exchanger, the clean up loop and back into the tank through the primary inlet pipe.

3.2 THERMAL-HYDRAULIC ANALYSIS OF NATURAL CONVECTION DESIGN (DESIGN I)

As a first step, an analytical calculation was performed with the aid of MathCad software to calculate the total flow rate through the eleven fuel elements and the average temperature difference across a fuel element. In the analytical calculation, a mass flow rate through the eleven MITR-II fuel elements was assumed and then the total pressure loss (Δp_t) due to skin friction and form pressure losses along the flow path were calculated for the assumed flow rate. Under natural circulation conditions, a system operates without a pump, and the flow is driven entirely by the buoyancy generated pressure head (Δp_b). Thus, the steady state momentum equation can be reduced to:

$$\Delta p_t = \Delta p_b. \qquad (3.1)$$

Then a mass flow rate was calculated that corresponds to the above buoyancy pressure head. This procedure was iterated until the mass flow rate for the total pressure loss and the mass flow rate for the buoyancy pressure head were same.

The analysis and the results are given in the Appendix A3.1. The average temperature difference across the fuel element was calculated to be 26 ^{0}C. Since the inlet temperature to the fission converter core is 40 ^{0}C, the coolant exit temperature from the fuel elements should be 66 ^{0}C. This is a very encouraging result because 66 ^{0}C is much below the saturation temperature (106 ^{0}C) of the coolant. The saturation temperature at the fuel level is elevated to 106 ^{0}C because of the water column above the fuel elements. It is also important to note that the dominant pressure loss is in the core (see the results given in the appendix A3.1).

However the analytical calculation can only provide the total flow rate and the average temperature difference. The complete temperature and the velocity fields within the fission converter are valuable information to identify the hot spot, irregular flow patterns, the mixing effects and the flow path. They also help to determine the outlet pipe diameter, and to design the downcomer region.

The thermal hydraulic code "TEMPEST" was chosen to perform the detailed calculation and to provide a complete temperature, velocity and pressure fields within the fission converter tank. Researchers (D.S. Trent and L.L. Eyler) at Battelle, Pacific Northwest Laboratories have developed the TEMPEST computer code. The TEMPEST stands for Transient Energy Momentum and Pressure Equation Solution in Three dimensions. TEMPEST can analyze a broad range of coupled fluid dynamic and heat

transfer systems and is being used to simulate transient turbulent flow and heat transfer in various complex, three-dimensional geometry that can be modeled using Cartesian or cylindrical coordinate systems.

The researchers at Battelle have used TEMPEST to analyze the waste tanks at Hanford and have predicted the flow and the temperatures within the waste tank with reasonable accuracy. Since the waste tank problems are similar to the fission converter problem, TEMPEST is chosen over other existing computational fluid dynamics codes. The code ability to perform transient calculation, continuous support from Dr. Trent and the fact that TEMPEST is supplied free of charge are the other factors favoring the TEMPEST code.

3.3 FISSION CONVERTER INPUT MODEL FOR TEMPEST

The TEMPEST code uses the following independent variables to analyze the fission converter. These independent variables are:

- Power profile,
- Geometry, and
- Inlet temperature.

Author of this report provided the appropriate friction factors for the different regions and the code provided the output of the velocity field, the temperature field and the pressure field.

The fission converter is modeled in the Cartesian coordinate system. The modeled region must be divided into finite-difference cells arranged in rows/columns/tiers in three dimensions as indicated by the figure 3.2. Gravity is in the negative Z direction. The number of cells specified in each direction must always include an extra plane of cells on each side to accommodate boundary conditions. The boundary cells are not shown in figure 3.2. There are 9 cells in the X direction, 35 cells in the Y direction and 96 cells in the Z direction. The cell thickness varies from 0.8 inches to 3.8 inches.

The modeling of the MITR-II fuel in the fission converter is shown in figure 3.3. Two cells in the Y direction model one fuel element where each element consists of 15 fuel plates; one cell represents the 15 fuel plates lumped together (the clad and the fuel) and the other represents the lumped flow area of a fuel element. There are 13 cells in the Z direction. Eleven of 13 cells are active fuel cells. One on the top and the other on the bottom are exit and entrance cells, respectively. Form loss coefficients were supplied to the entrance and exit cells to calculate the pressure losses.

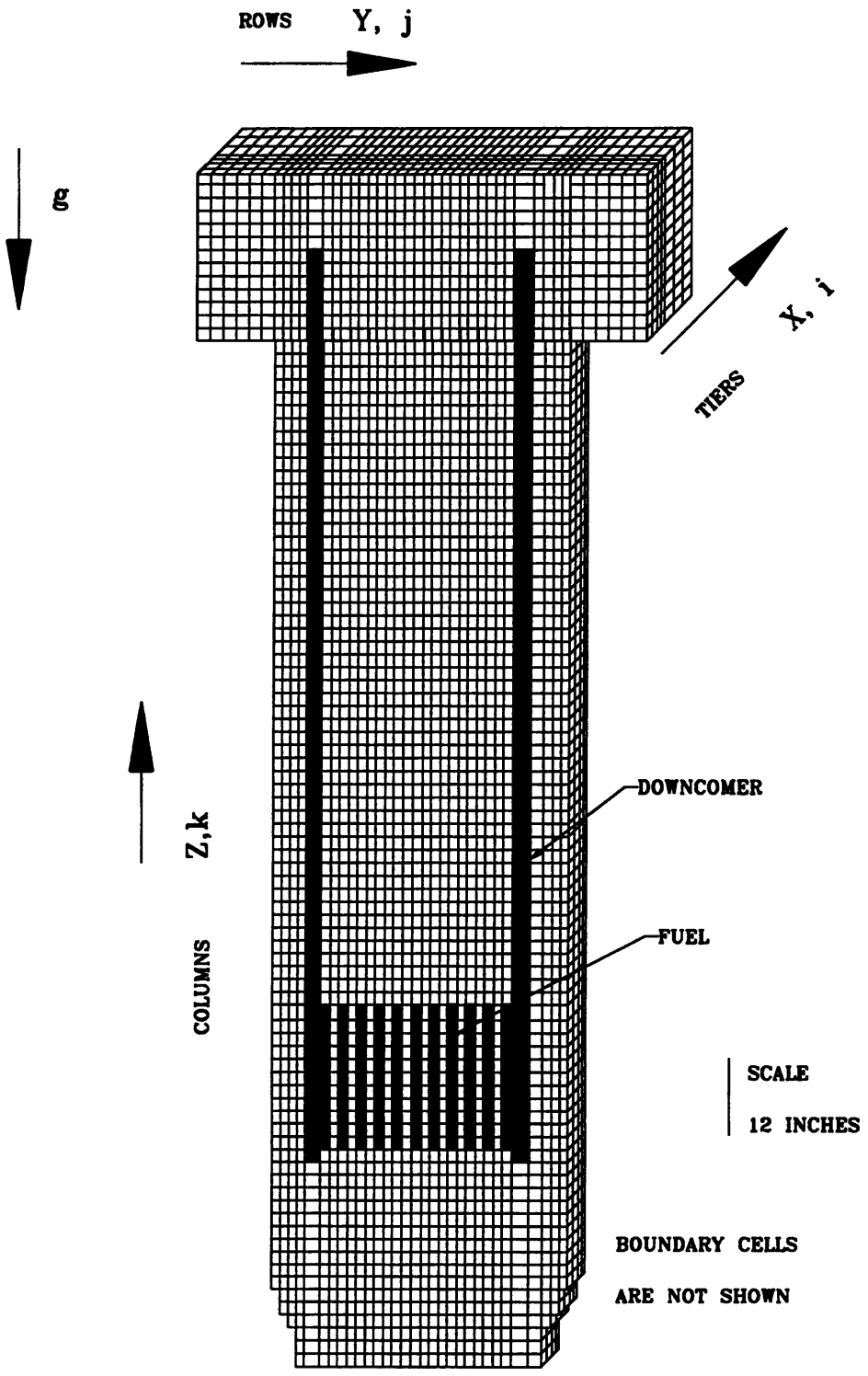

Figure 3.2: Fission Converter Finite Difference Cell Structure

Two cells in the X direction model each fuel element. The fuel elements are modeled, such that the flow cross sectional area, solid cross sectional area and the length, are the same as the real fuel elements. However, the hydraulic diameter is not same as the real fuel elements, because the wetted perimeter is not the same as the real fuel element. This difference in the wetted perimeter (or hydraulic diameter) will affect the pressure loss calculation, because the pressure loss, Δp_{loss}, is equal to;

$$\Delta p_{loss} = \frac{f}{2D_h} L\rho V^2 \qquad (3.2)$$

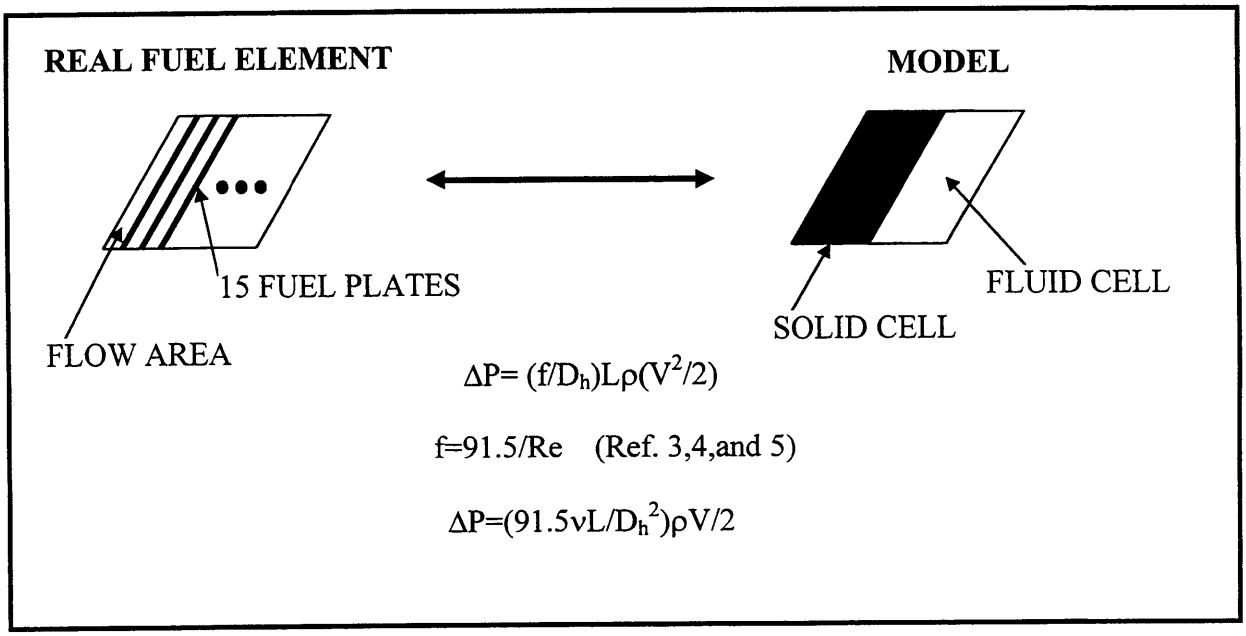

Figure 3.3: Fuel Model for the TEMPEST Input

However as explained in the following, this difference is corrected by inputting K_i and N_i values. The TEMPEST provides the flexibility of specifying the drag coefficient (K_i or $\left(\frac{f}{D}\right)_i$) and the velocity exponent N_i in two different forms.

These two forms are;

1. $\Delta p = K_i \frac{\rho}{2} V^{N_i}$ (3.3)

2. $\Delta p = \left(\frac{f}{D}\right)_i \frac{\rho}{2} V^{N_i}$ (3.4)

If the flow is assumed to be laminar (this assumption is checked after obtaining the final results), the friction factor, f, is:

$$f = \frac{91.5}{\mathrm{Re}} \quad \text{(Ref. 3,4and 5)} \qquad (3.5)$$

If the equation (3.5) is substituted into the equation (3.2) for the friction factor, f, the equation (3.3) becomes,

$$\Delta p_{loss} = \left(\frac{91.5\nu L}{D_h^{\,2}}\right)\frac{\rho}{2} V \qquad (3.6)$$

By comparing the equations (3.3) and (3.6), the constants K_i and N_i can be obtained.

$$K_i = \frac{91.5\nu L}{D_h^{\,2}}, \text{ and } N_i = 1 \qquad (3.7)$$

By specifying the K_i and the N_i as shown in the equation (3.7), the difference in the hydraulic diameter will not affect the pressure loss calculation.

If the flow in the core is laminar, the hydrodynamic entrance length is equal to $0.05*D_h*Re_{Dh}$. Since the hydraulic diameter, D_h, for a MITR-II fuel element is $2.24*10^{-3}$ meters and the Reynolds number in the core is about 600-700, the hydrodynamic entrance length for the core (0.0672 - 0.0784 meters) is negligible compare to the MITR-II fuel length of 0.667 meters.

The downcomer is modeled as 4 cells in the Y direction, 77 cells in the Z direction and starts from the front plane to the last plane in the X direction. The pressure loss in the downcomer region was calculated internally. The internal pressure loss calculation for laminar flow was performed by calculating the shear stress using the velocity profile. There are adequate numbers of cells in the Y- direction and in the X- direction to establish the correct velocity profile. Similarly, the pressure losses in the upper plenum and lower plenum were internally calculated.

The aluminum block in the back of fuel elements is modeled by 2 cells in the X direction, 13 cells in the Z direction and from the first fuel element to the last fuel element in the Y direction.

The external primary loop acts as a heat sink for the fission converter internal buoyancy driven flow. This external primary loop takes the liquid from the upper plenum, cools it down to 40^0C and brings it back to the downcomer. Code running time is saved by modeling the whole primary loop and the pump as heat sink cells in the downcomer.

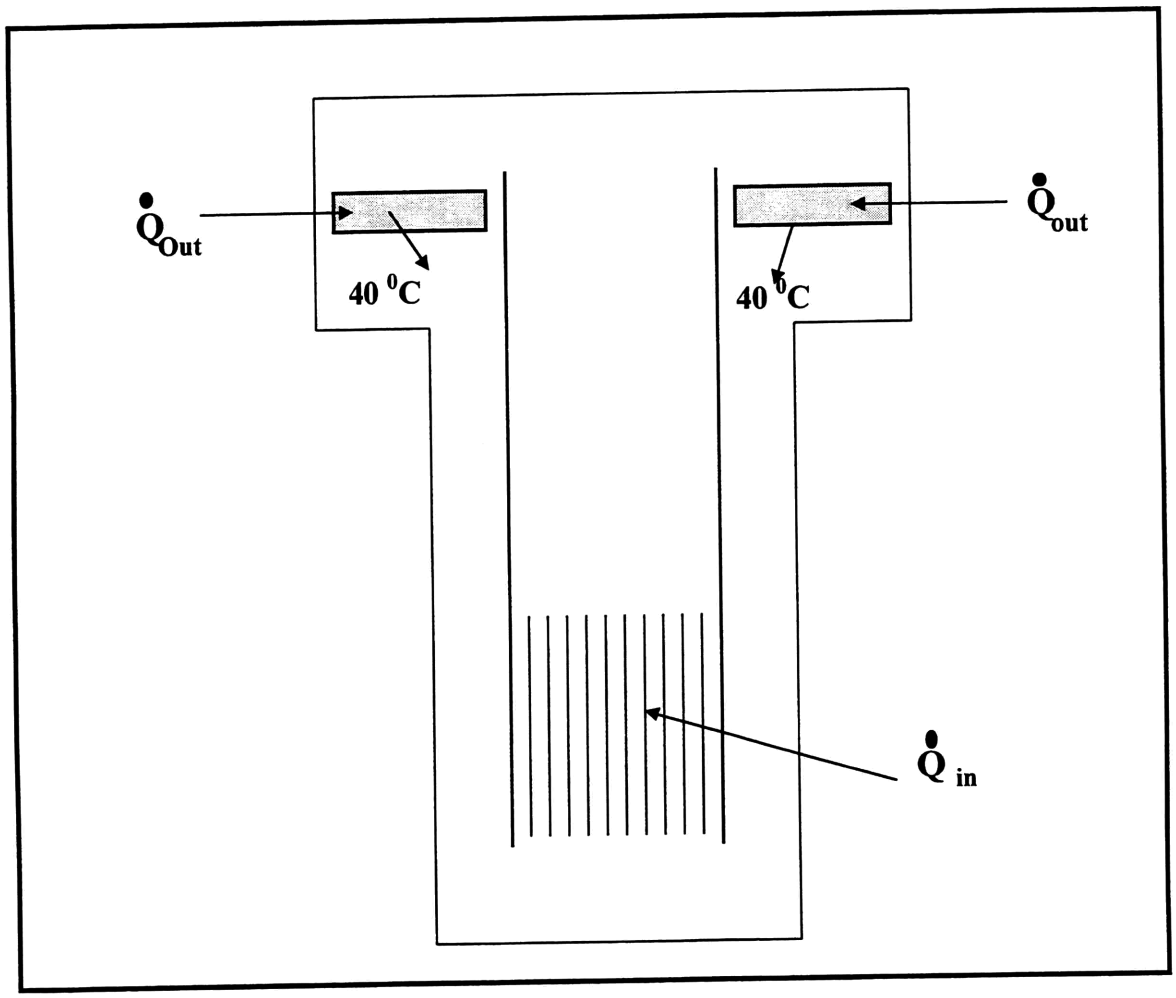

Figure 3.4: Heat Sink Cell Model

The purpose of these heat sink cells is to cool the incoming liquid into the downcomer to the temperature of 40°C. Therefore, any flow into these heat sink cells will be cooled to 40°C, as shown in the figure 3.4. TEMPEST does not have the capability of performing the above calculation, but the author modified the code to perform the above task. The modification was carried out by the author with the permission and help from Dr. Trent.

As mentioned before, the perimeter of the fuel elements is not the same as that of the real fuel elements. Therefore, heat transfer area from the 15 plates to the coolant is also not the same as that of the real fuel elements. The difference in heat transfer area will affect the heat transfer calculation. However, it is compensated for by inputting the heat generation into the fluid cells. Since heat conduction calculations performed on a solid cell increase the run time, the solid cells in this model are specified as empty cells, within which the code does not perform any calculation. Therefore, inputting heat generation into the fluid cells not only saves computational time but also compensates for the effect of the different heat transfer area. The solid cell temperatures can be obtained after knowing the velocity and the temperature fields of the coolant close to the solid cells.

The heat generation rate for the eleven fuel elements was calculated using MCNP-4A by W.S. Kiger[1] for the reactor power of 5 MW. The total power generated by the 11 fuel elements is 125 kW. Therefore the heat generation rate for each fuel element is multiplied by the factor of 2.42 (=300/125) to adjust the total heat generation rate to be 300 kW. The adjusted heat generation rate for the eleven fuel elements is given in the table 3.2. Again by knowing the temperature, the velocity and the heat generation rate, the fuel and the fuel cladding temperatures can be calculated externally.

Table 3.2: The Adjusted Heat Generation Rate

Element	Power (kW)
1	19.8
2	21.9
3	26.6
4	31.0
5	33.9
6	35.0
7	34.2
8	30.8
9	25.8
10	21.1
11	19.3
Total	299.4

3.4 RESULTS FROM THE TEMPEST CODE

The first few runs were performed by modeling the downcomer wall with the thermal conductivity equal to the aluminum. When the downcomer wall is modeled with aluminum properties, the coolant near

to the wall in the upper plenum is cooled by the coolant in the downcomer. As a result, the coolant near the wall in the upper plenum has temperature less than the rest of the coolant in the upper plenum. This temperature difference induced the flow downward near the wall, while the coolant leaving the fuel elements with higher velocity pushed the coolant upward. This induced a recirculation near the wall. A sketch of the circulation flow path is shown in figure 3.5.

The recirculation increased the pressure loss in the upper plenum. As a result, the total pressure loss within the fission converter increases and the total flow rate decreases. Therefore, the exit coolant temperature from the fuel elements increases. To reduce the heat transfer across the wall, the wall is made of two sheets of aluminum with a small gap between them, which is filled with stagnant coolant. The cross sectional view of the wall from the top is also shown in figure 3.5.

The design with above change was reanalyzed with TEMPEST. Figure 3.6 shows the inlet and outlet temperature from each fuel element. Figure 3.7 shows the velocity of the coolant in the fuel elements. In the above two figures (figure 3.6 and figure 3.7) the power profile is also plotted to compare the shapes of power, temperature, and velocity profiles.

The average temperature in the upper plenum is 72^0 C. The maximum coolant temperature is 80^0 C. This hottest spot was observed at the exit of the hottest fuel element. The hottest fuel element is the

center fuel element (6th fuel element from left to right). The Reynolds number in the downcomer and the average Reynolds number in the fuel elements are 600 and 700 respectively.

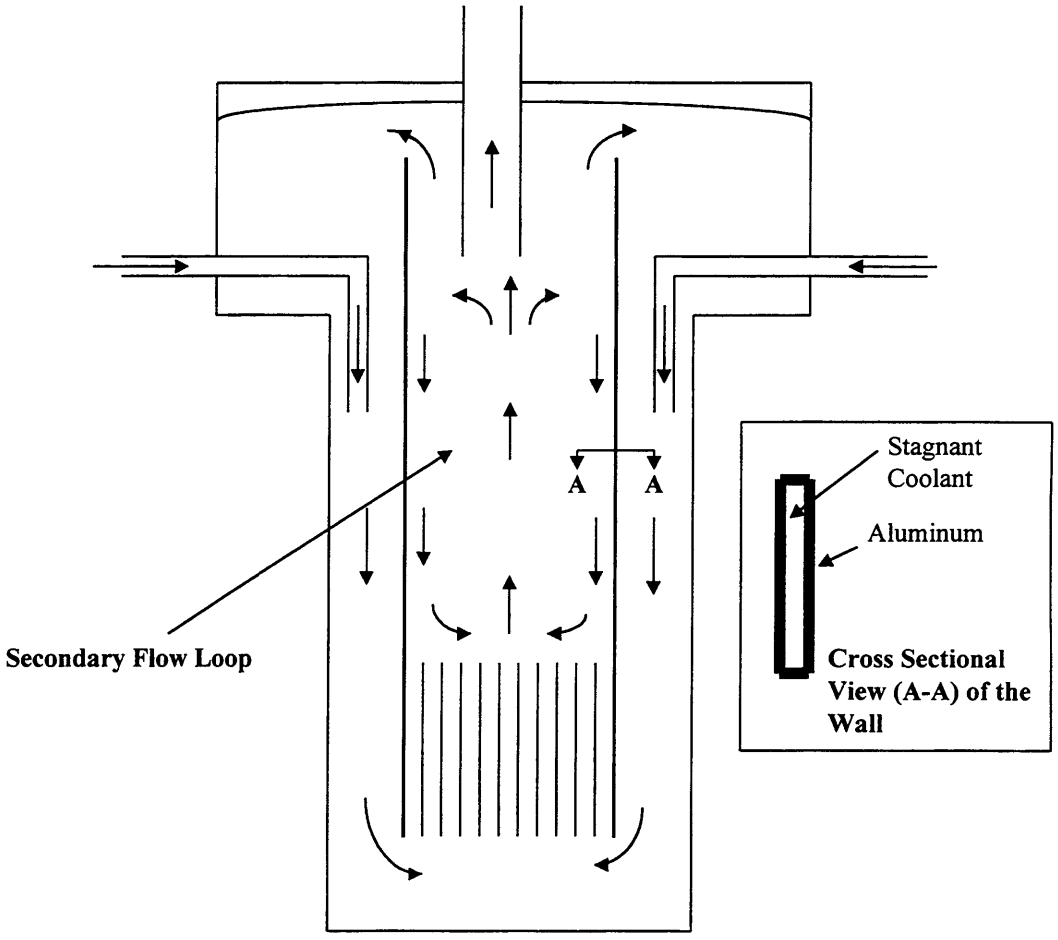

Figure 3.5: Recirculation Flow Path near the Downcomer Wall and the Cross section View of the Downcomer

The flow inside the fuel element is laminar. The thermal entrance length for laminar flow can be calculated from $0.017*D_h*R_{Dh}*Pr$. Since the Reynolds number, the Prandtl number and the hydraulic diameter are 700, 3 and $2.24*10^{-3}$ respectively, then the thermal entrance length is equal to 0.08 meters. The thermal entrance length of 0.08 meters is negligible compare to the fuel length of 0.667 meters. The Nusselt, Nu, number in the developed region is smaller than that in the developing region. The fuel cladding surface temperature, which is calculated using the Nu in the developed region, is a conservative value. The fin effect was neglected in the surface temperature calculation.

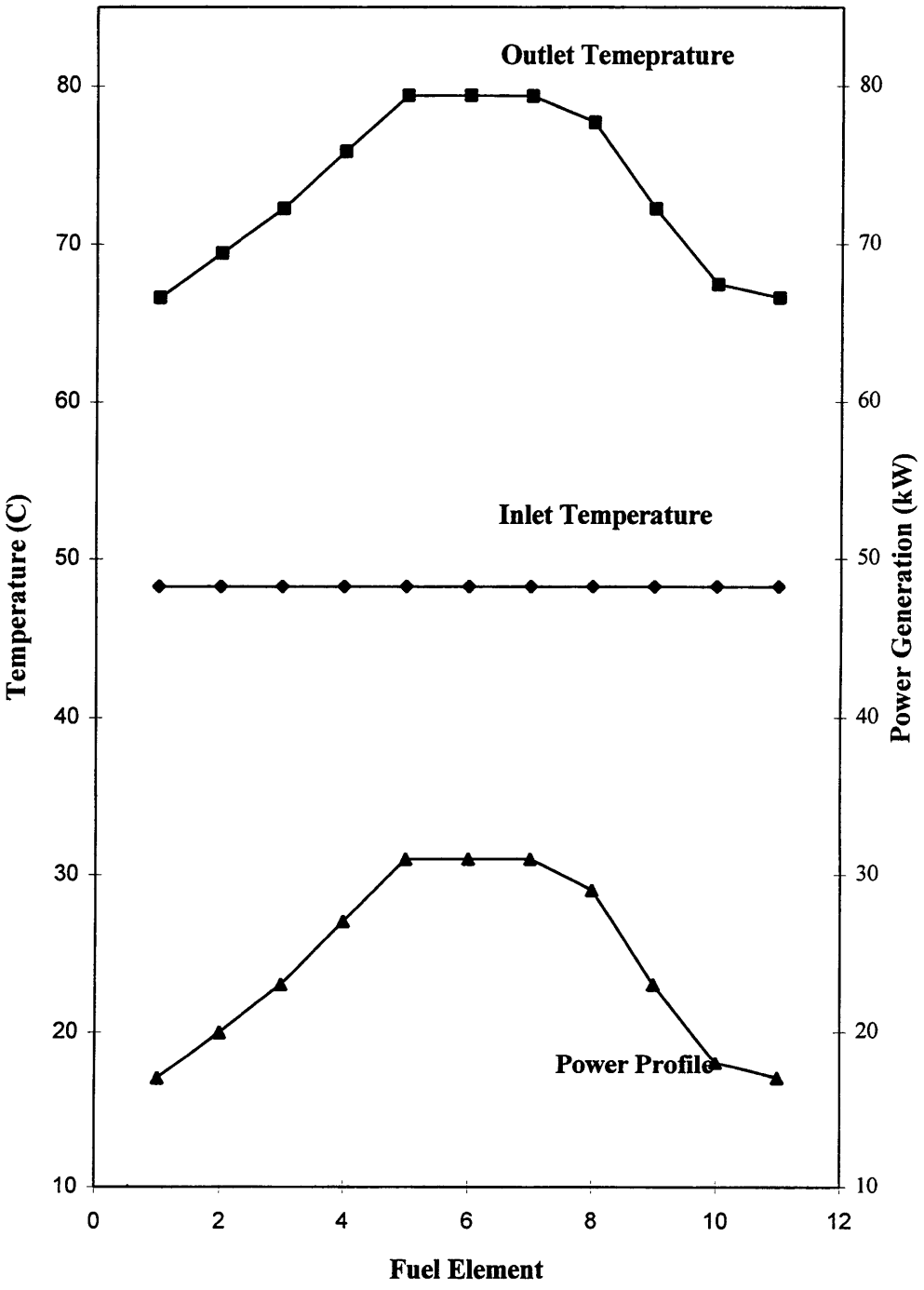

Figure 3.6: Inlet and Outlet Temperature from Each Fuel Element

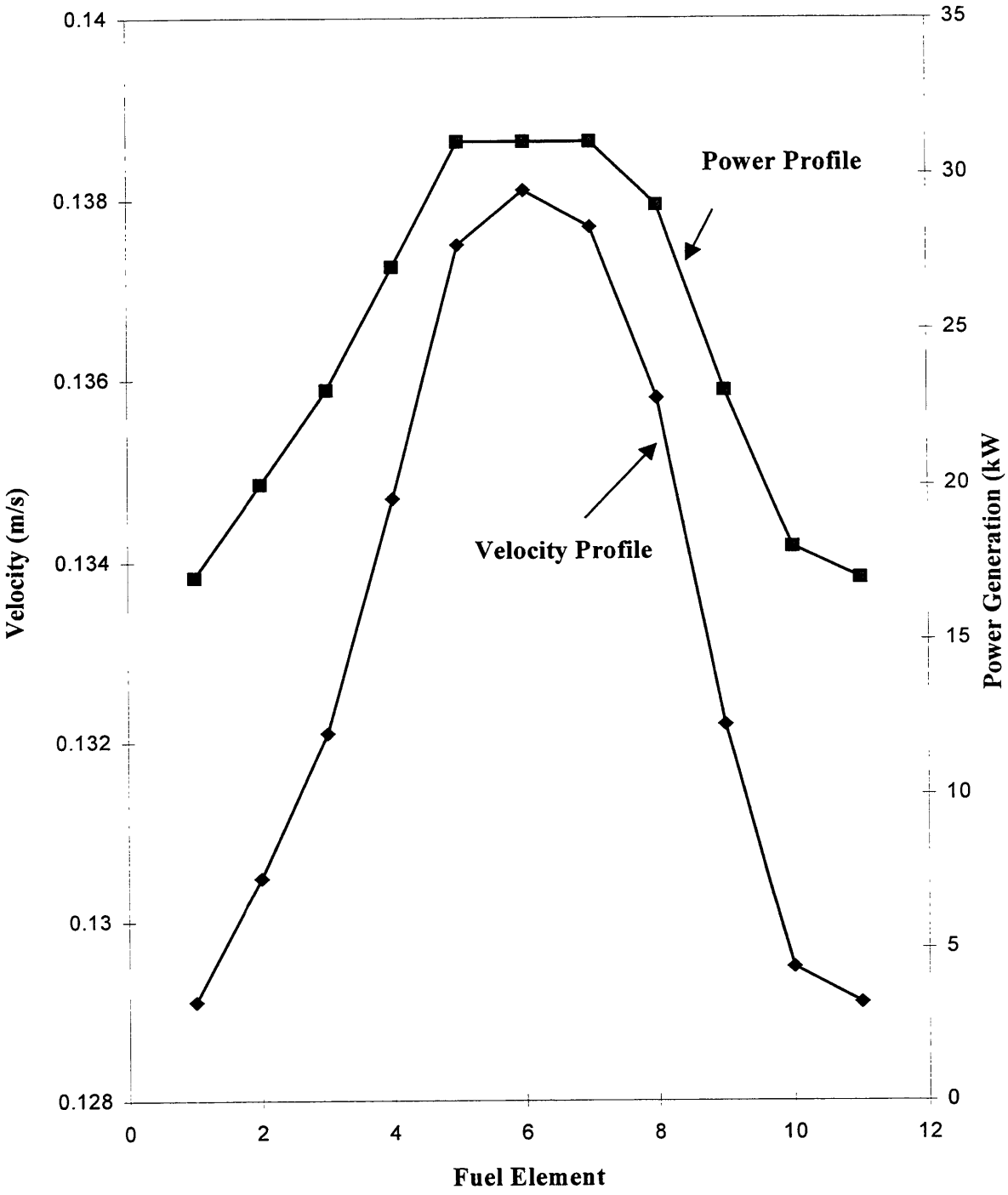

Figure 3.7: Coolant Velocity and Heat Generation in Each Fuel Element

However the extended area was included. The Nu for a developed laminar flow in a rectangular duct is given by equation 3.8.

$$Nu = hD/k = 8.235 \quad \text{(ref. 7)} \qquad (3.8)$$

Then the heat transfer coefficient, h, is 2.4 kW m^{-2} C^{-1}. Hence for thermal conductivity k =0.662 W m^{-1} C^{-1} and real fuel element hydraulic diameter D=2.24E-3 meters. The hottest channel heat flux (q''_{max}) is 19.5 kW/m^2, which is assumed to be constant axially. The maximum clad surface (T_{max_clad}) temperature can be expressed as;

$$T_{max\_clad} = T_{max\_coolant} + q''_{max} / h \qquad (3.9)$$

Here $T_{max\_coolant}$ is the coolant exit temperature from the hottest channel. From equations (3.8) and (3.9), the maximum clad temperature is calculated to be 88^0 C.

For the following discussions, nomenclatures used for flow rates are defined in figure 3.8. The total power produced in the fission converter is 300 kW; therefore the primary loop has to extract energy of 300 kW from the upper plenum. The coolant in the outlet pipe leaves the fission converter with the temperature of 72^0 C and returns in the downcomer with the temperature of 40^0 C. Therefore the flow rate ($\dot{m}_P$) can be calculated using the following equation;

$$\dot{m}_P = \frac{\dot{Q}}{C_P \Delta T} \qquad (3.10)$$

Here $\dot{Q}$(=300 kW) is the total power, C_p (=4.18 kJ/kg K) is the average heat capacity between the temperatures 72^0 C and 40^0 C, and ΔT (= 32^0

C) is the temperature difference between the outlet and inlet. From equation 3.10, the primary loop mass flow rate is calculated to be 2.24 kg/s. The natural circulation flow rate, which extracts the heat from the eleven fuel elements is 2.8 kg/s (from TEMPEST calculation).

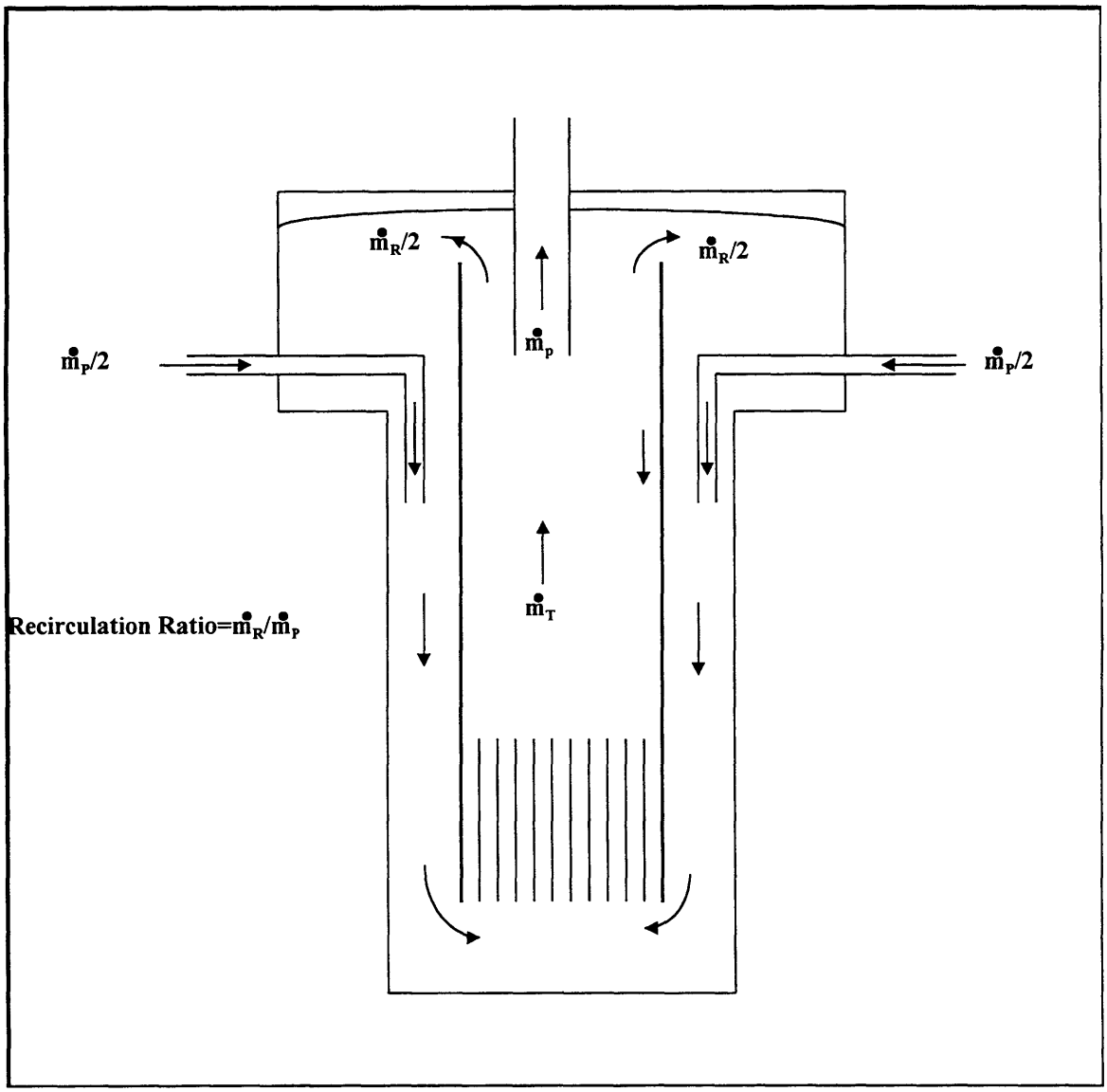

Figure 3.8: Flow Rate Nomenclature

The diameter of the outlet pipe is determined such that the primary loop volumetric flow rate does not disturb the buoyancy driven flow in the fission converter. If the coolant velocity, which enters the outlet pipe, is much higher than that of the upper plenum coolant, the suction power in the outlet pipe will disturb the buoyancy driven flow in the fission converter. Therefore, the coolant velocity in the outlet pipe should be equal to or less than that of the upper plenum coolant velocity. The coolant velocity in the upper plenum ranges from 0.10 to 0.13 m/s in the vertical direction. Since the primary loop volumetric flow rate should be $2.3X10^{-3}$ m^3/s (i.e. $\dot{m}_P / \rho = 2.24/974$) and the coolant velocity in the outlet pipe should be 0.1 m/s, the inside diameter of the outlet pipe should be 0.17 m (6.8 inches).

The average inlet temperature to the fuel element is 48^0 C (from TEMPEST calculation), rather than 40 ^{0}C. This is due to the mixing between the cooled liquid from the heat sink cells and the hot liquid from the upper plenum. In real case, the flow of hot liquid from the upper plenum to the downcomer can be controlled by the flow rate in the primary loop. The primary flow rate of 2.24 kg/s corresponds to the fuel inlet temperature of 48^0 C. If the primary coolant flow rate in the primary pipe and the buoyancy flow rate are equal, then the fuel inlet temperature will be 40 ^{0}C. This means none of the upper plenum liquid flows directly into the downcomer region. The average inlet temperature as function of recirculation ratio is shown in figure 3.9.

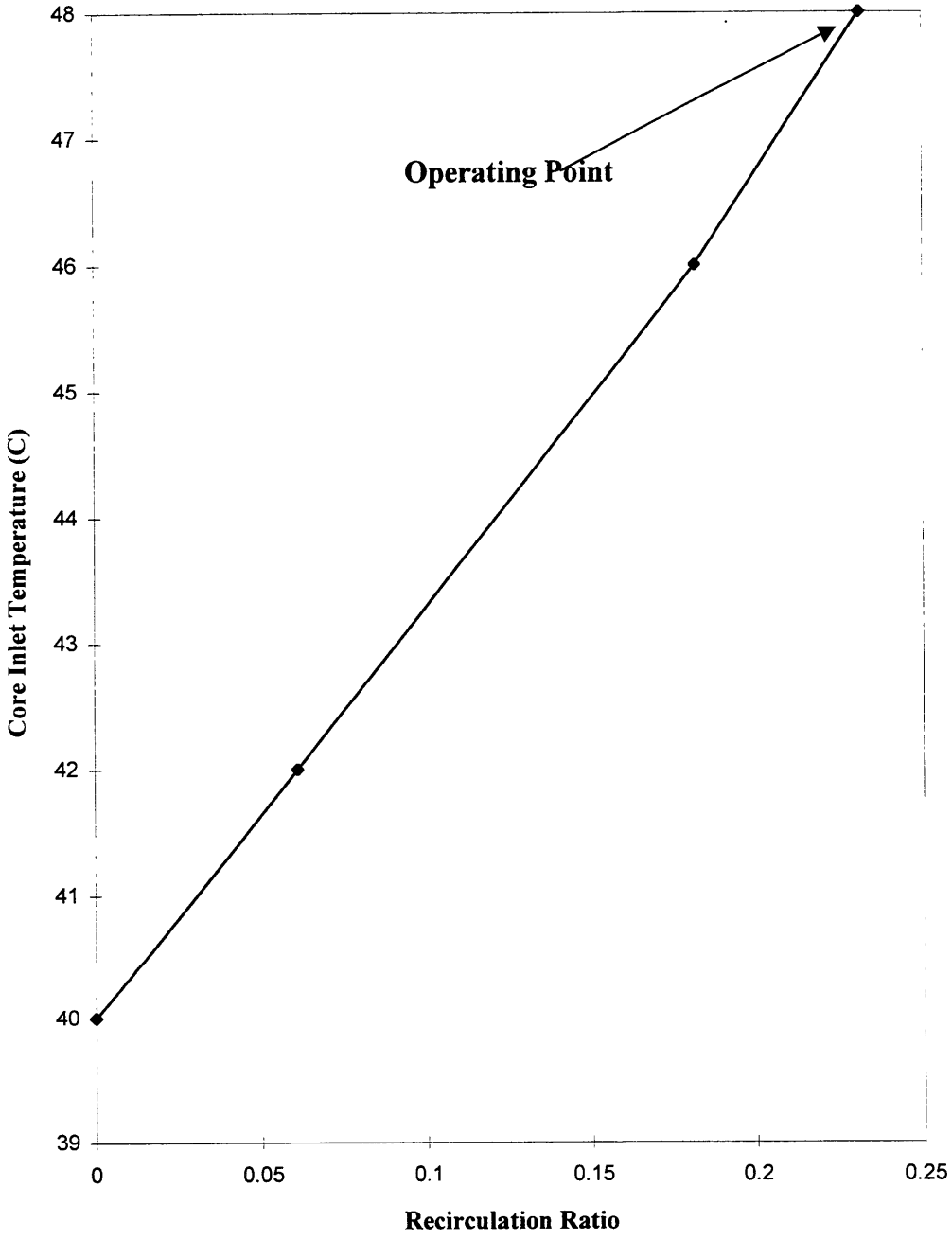

Figure 3.9: Core Inlet Temperature as a Function of Recirculation Ratio

A sketch of the cross sectional view of the flow channel and the finned fuel plates are shown in figure 3.10. The heat transfer coefficient between the coolant and the clad surface was calculated (see equation 3.8) to be $2.434X10^3$ W/m.^{0}C. The clad surface temperature and the fuel centerline temperature (the maximum temperature inside the fuel) are 87.55 ^{0}C and 87.6 ^{0}C respectively. Therefore, the maximum clad surface temperature is less than the design limit of 106 ^{0}C.

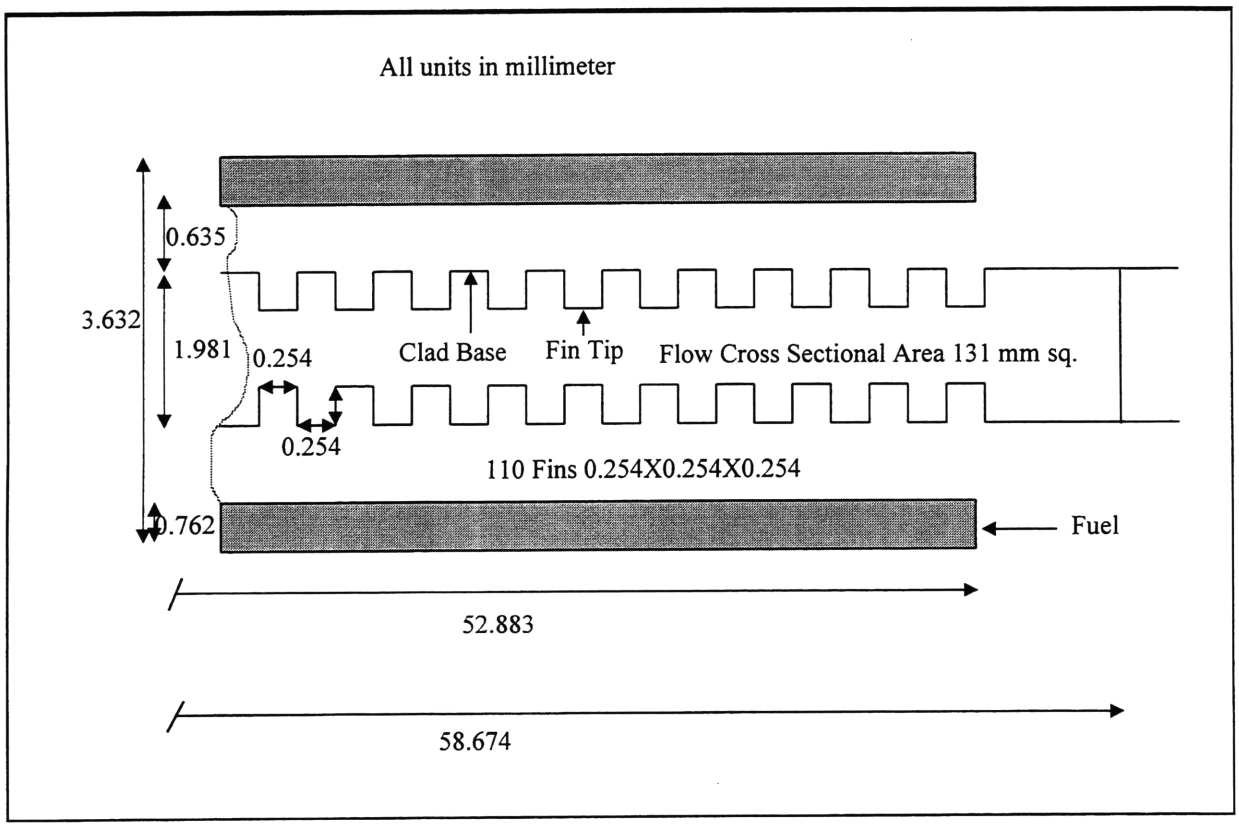

Figure 3.10: Cross Sectional View of a Flow Channel and Finned Fuel Plates

In this subsection, the author has demonstrated that during the steady state operation none of the limiting conditions will be reached. The coolant and the clad surface temperatures are about 18 ^{0}C below the boiling condition, if the fission converter power is 300 kW.

3.5 Validity of the Calculated Results

It is always important to know how accurate are the results. The results were checked by two means: 1) total flow rate and the temperature difference across the fuel element calculated by the analytical calculations and the numerical calculations are compared, and 2) the pressure loss in the fuel and the downcomer calculated by the analytical calculations and the numerical calculations are compared.

Table 3.3: Comparison of Analytically and Numerically calculated Results.

	Temperature Difference Across a Fuel Element (^{0}C)	Total Flow Rate Through Eleven Fuel Elements (kg/s)
Analytical Calculation	**26**	**2.74**
Numerical Calculation	**25**	**2.8**

The limiting condition for the normal steady state operation is no boiling on the fuel elements. Therefore comparison of the temperature difference and the flow rates are valuable to confirm the no boiling condition. The results obtained by the analytical calculation and the numerical calculation are listed in the table 3.3. As it is obvious from the table 3.3, the hand calculated and the code calculated results agree reasonably well.

Since the flow in the fission converter is driven by the buoyancy, the friction pressure loss is a very important parameter in determining the flow rate and the maximum temperatures of the coolant and the fuel. It was shown by the analytical calculation that the pressure loss in the downcomer and the fuel are large compare to skin friction pressure loss in the upper plenum and in the lower plenum, and form losses due to expansion and contraction. Therefore the pressure losses in the downcomer and in the fuel are compared between the analytically calculated and numerically calculated results. It can be seen in the table 3.4 that the differences between the results are negligible.

Table 3.4: Comparison of Pressure losses

	Analytical Calculation	**Numerical calculation**
Pressure loss across the fuel elements	542 Pa	538 Pa
Pressure loss in the downcomer	60 Pa	58 Pa

The good agreement between analytically calculated and numerically calculated results is a favorable indication of the validity of the results. It is also shown that there is a 18 ^{0}C margin from the limiting condition, when the fission converter power is assumed as 300 kW. The steady state results and the appropriate limiting conditions for the natural convection design are summarized in the table 3.5.

Table 3.5: Summary of Natural Convection Design steady state results

	Analytical Calculation	Numerical Calculation	Limiting Conditions
Average Temperature Difference across a fuel element	**26 ^{0}C**	**25 ^{0}C**	
Total Flow rate through 11 fuel elements	**2.74 kg/s**	**2.8 kg/s**	
Maximum Coolant Temperature		**80 ^{0}C**	
Maximum Clad Temperature		**88 ^{0}C**	**106 ^{0}C**

4.FORCED CONVECTION WITH BYPASS CHANNEL (DESIGN II)

4.1 DESCRIPTION OF FORCED CONVECTION WITH BYPASS CHANNEL DESIGN

One of many advantages of the natural convection design is that the design does not require an anti-siphon valve in the downcomer region to create a natural circulation during accidents. However, the hot

channel coolant exit temperature will be higher than that for a forced convection case. Furthermore, increasing or decreasing the forced convection flow rate can control the hot channel coolant temperature. On the other hand, most of forced convection designs require an anti-siphon value to provide a flow path for natural convection cooling during loss of flow accident. It is our design goal not to have an anti-siphon valve in the fission converter tank, because of space constraint and extensive labor involvement for required frequent inspection. Therefore, a design providing forced convection cooling during normal operation, natural convection cooling during loss of flow accident, and no anti-siphon valve in the downcomer is preferred for the fission converter tank.

A proposed forced convection with bypass channel design, which has forced convection cooling during steady state operation, natural convection cooling during loss of flow accidents and no anti-siphon valve, is shown in figure 3.11. During steady state operation (forced convection cooling), part of the coolant will be bypassed through the two bypass channels located adjacent to the core.

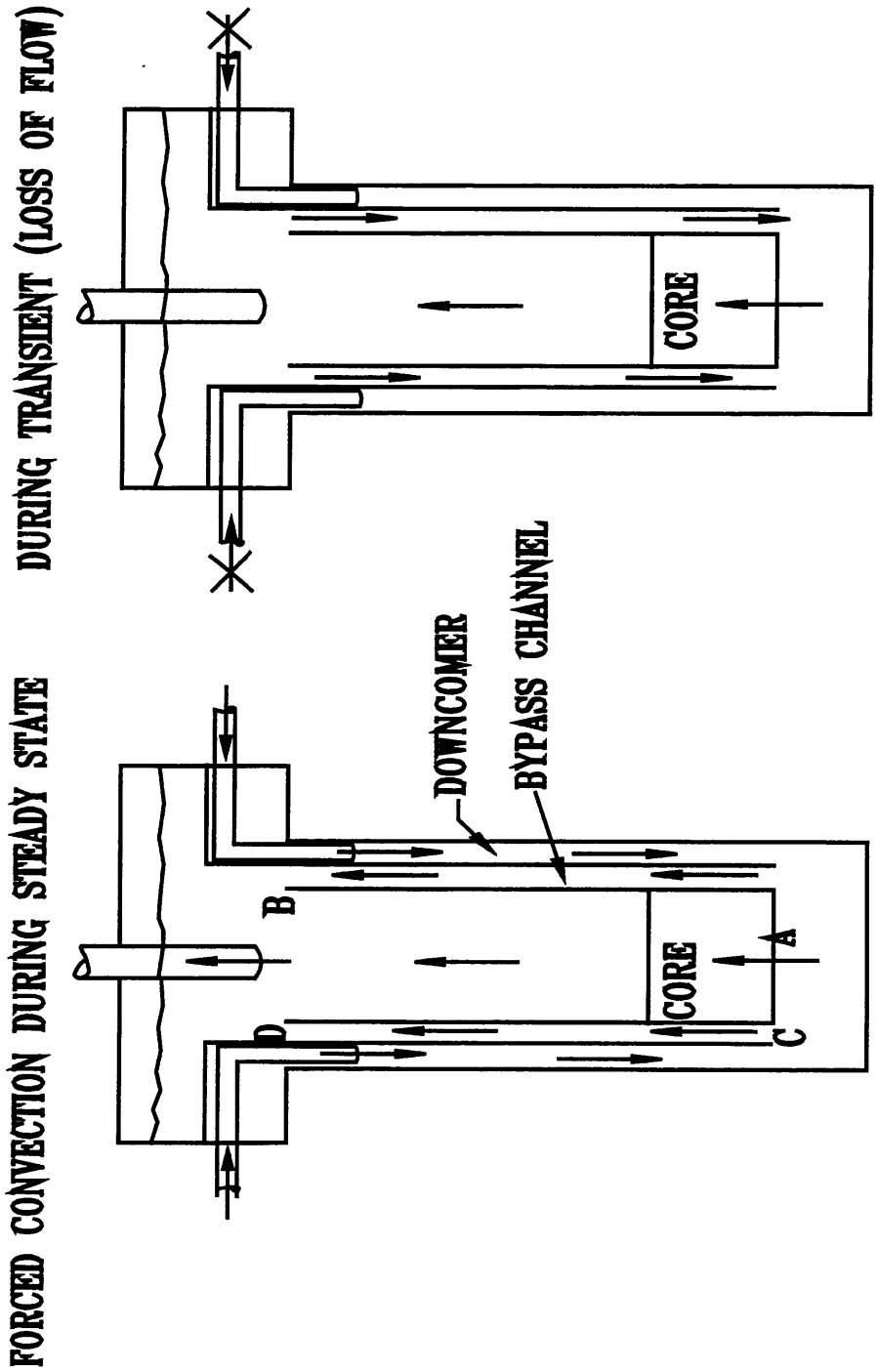

Figure 3.11: Forced Convection with Bypass Channel Design

(Design II)

The amount of coolant, which is bypassed through the two bypass channels, can be suppressed by reducing the bypass channel width. On the other hand, reduction of the bypass channel width will reduce the natural convection flow rate during loss of flow accidents. Therefore, a detailed study was performed to optimize the bypass channel width.

The external primary and secondary loop for the forced convection with bypass channel are the same as that of the natural convection loop (shown in figure 3.1).

4.2 OPTIMIZATION OF BYPASS CHANNEL WIDTH

Three steady state cases were modeled and simulated using TEMPEST. These three cases are;

1. Inlet primary flow rate (m_{total}) of 4.17 kg/s and a bypass channel width of 0.5 inches (0.0127 m)
2. Inlet primary flow rate of 4.3 kg/s and a bypass channel width of 1 inch (0.0254 m)
3. Inlet primary flow rate of 4.4 kg/s and a bypass channel width of 1.5 inches (0.038 m)

Inlet primary coolant velocities are same for the three cases. However, inlet primary flow rates are different because of different densities. A similar approach as for the natural convection (described in section 3.3)

was used to model these three cases. For the above three cases TEMPEST inputs are;

- Power profile
- Inlet flow rate and temperature (40 ^{0}C)
- Bypass channel width
- Geometry
- Friction coefficients

From TEMPEST output, the hot channel coolant exit temperature for these three cases are found to be 66 ^{0}C, 74 ^{0}C and 80 ^{0}C respectively.

For the same three cases, an analytical calculation was performed. In the analytical calculation, the bypass channel width was calculated using the inputs of inlet primary flow rate, inlet primary coolant temperature and hot channel coolant exit temperature. The following steps were followed for the analytical calculation to obtain the bypass channel width.

1. The hot channel coolant flow rate, which is required to keep the hot channel coolant exit temperature at the prescribed value (either 66 ^{0}C or 74 ^{0}C or 80 ^{0}C), was calculated.
2. The total flow rate through the core was calculated by multiplying the hot channel flow rate by eleven (because of eleven elements). It was assumed that the flow rate is same for each fuel element and equal to hot channel coolant flow rate.
3. The pressure loss from A to B (see figure 3.11) was calculated.

4. The flow rate through the two bypass channels was calculated by subtracting total core flow rate from the total prescribed inlet flow rate. Then the pressure drop from C to D (see figure 3.11) was calculated as a function of the bypass channel width.
5. By setting the pressure loss from C to D (see figure 3.11) equal to the pressure loss from A to B (see figure 3.11), the bypass channel width was selected from the results of Step 4.

The above calculations were performed with MathCad and the MathCad calculation procedure is given in appendix A3.2. It is obvious from figure 3.12 that the TEMPEST and the analytically calculated results agree reasonably well.

For further analysis of forced convection with bypass channel, the analytical calculation results were used because it is less time consuming and the result agrees reasonably well with TEMPEST result. As a next step, core coolant exit temperature as a function of inlet primary flow rate was calculated with MathCad for different bypass channel widths (see appendix A3.3). The results are shown in figure 3.13.

One of the design goals is to keep the hottest fuel element coolant exit temperature to be less than 60 ^{0}C. The other design goal is to keep the system in single-phase more than 10 minutes for a LOF accident.

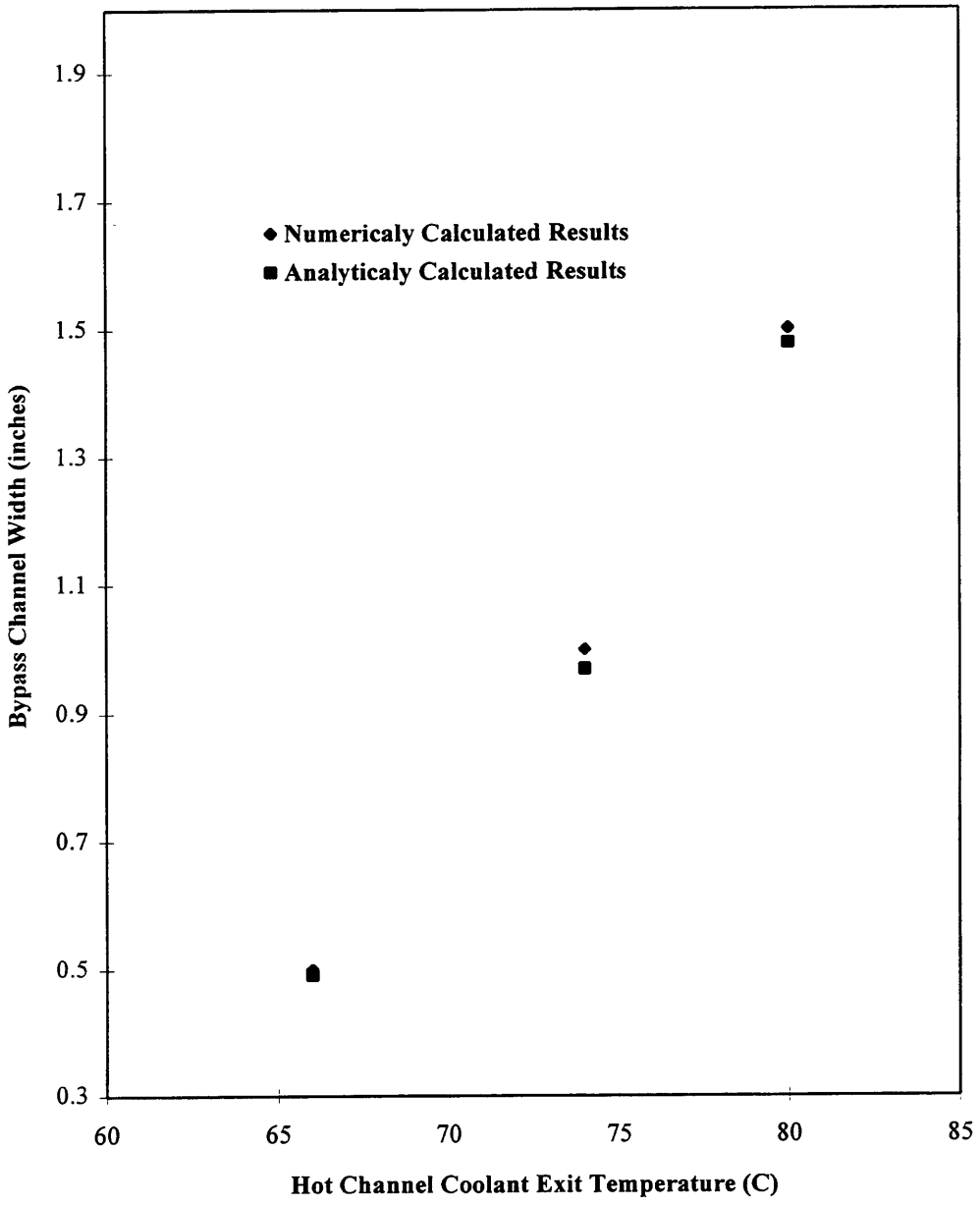

Figure 3.12: Comparison of Analytically and Numerically Calculated Results

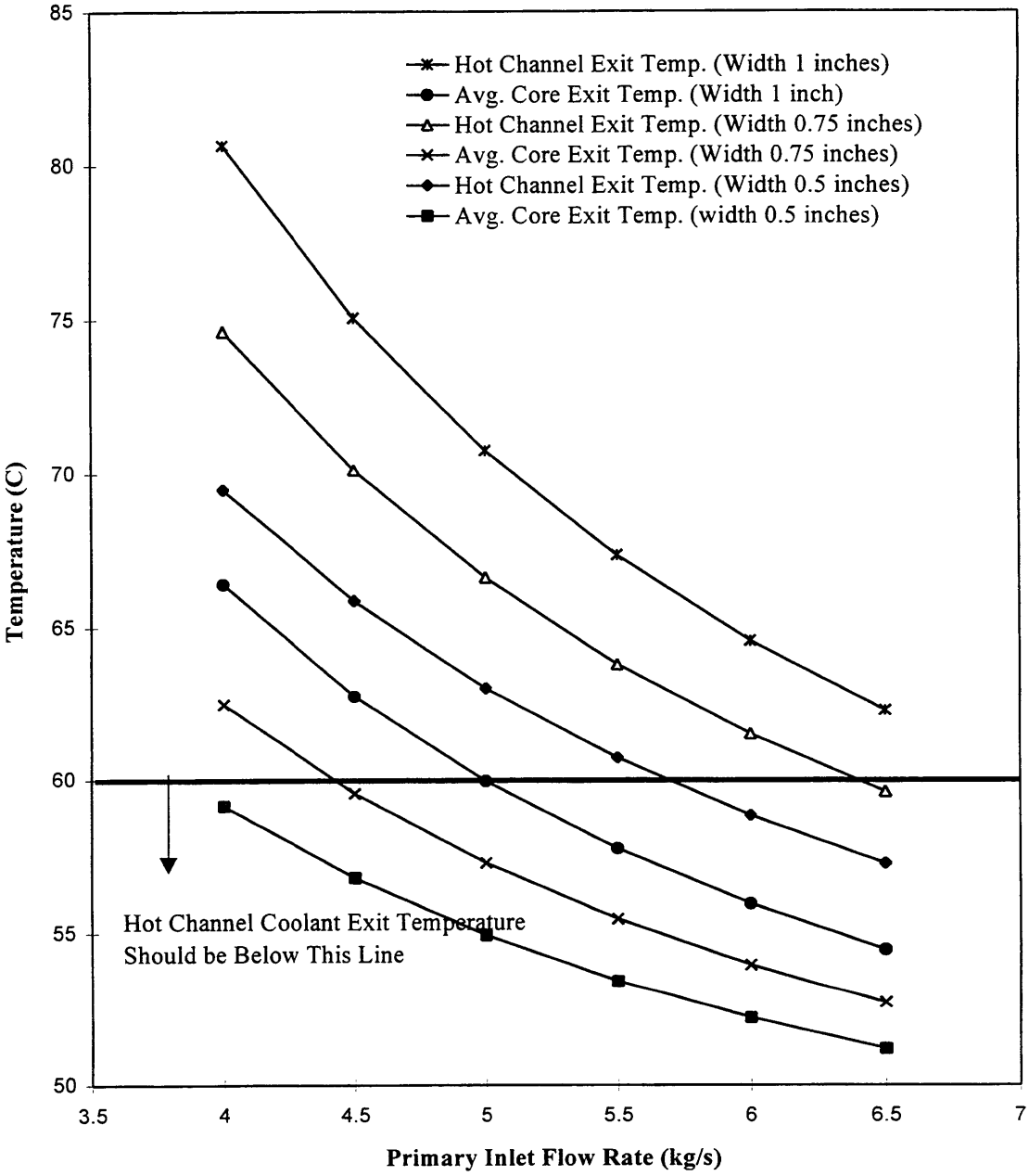

Figure 3.13: Temperature as a Function of Primary Flow Rate for Different Bypass Channel Widths

However, if the system experiences boiling after the loss of primary flow, then it is important to confirm attainment of the minimum condition of no critical heat flux until the coolant level drops below the top of bypass channel wall during loss of flow. It is not necessary to calculate the coolant and fuel temperatures after CHF, because fuel is assumed to overheat. If we neglect the pump coast down period, the primary inlet flow rate will drop instantaneously from steady state flow rate value to zero. The instant at which the primary forced flow is lost; and hydrodynamic steady state condition after some time into the loss of flow transient are shown in figure 3.14.

4.2.1 Instant at Which the Primary Forced Flow is Lost

This subsection describes the calculations, which were performed to check whether the system is in the single-phase or two-phase regime at the instant of LOF. If the system is in the single phase, the duration of the single phase regime is calculated and compared with the design goal of 10 minutes.

As shown in figure 3.14, coolant temperature in the downcomer, lower plenum and bypass channel will be at 40 ^{0}C, because the inlet primary coolant temperature during the forced convection is 40 ^{0}C. Since the core coolant average exit temperature during forced convection is below 60 ^{0}C, coolant in the upper plenum will be below 60 ^{0}C at the instant when the primary forced flow is lost. As a conservative assumption, the coolant in the bypass channel and in the upper plenum is assumed to be at 60 ^{0}C.

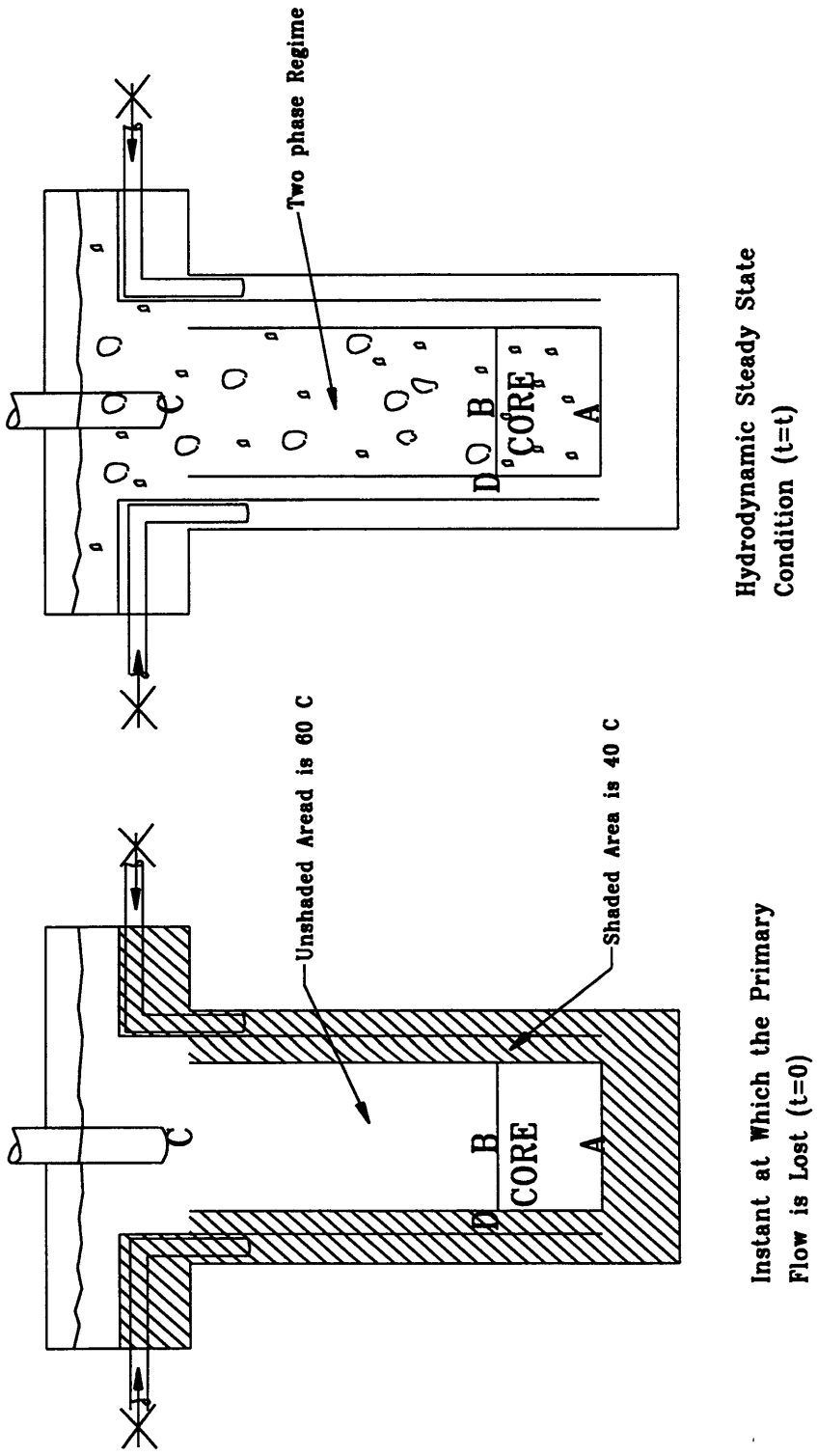

Figure 3.14: Loss of Flow Transient of Design II

Therefore the buoyancy pressure head from B→C→D (see figure 3.14) is zero. The total pressure loss (i.e. skin friction, form losses, and acceleration losses) and the buoyancy pressure head are calculated along the flow path (A→B→C→D (see figure 3.14)) and they are shown in figure 3.15 for different assumed flow rates. The center fuel element (hot channel) will go into the two-phase regime first. Therefore, the pressure loss and the buoyancy pressure head in the core (A→B (see figure 3.14)) was calculated for assumed flow rates by calculating the pressure loss and the buoyancy pressure head in the hot channel. The MathCad worksheet for this calculation procedure is given in Appendix A3.4. Figure 3.15 shows the total pressure loss and the total buoyancy head for the flow path A→ B→C→D (see figure 3.14) as a function of flow rates for different bypass channel widths. The natural circulation flow rate through hot channel is the point where the total pressure loss curve and the buoyancy pressure head curve intersects. Since the natural circulation flow rate is in the two-phase regime, there is a boiling in the hot channel as soon as the primary pump coast down flow rate is equal or less than the intersect point shown in figure 3.15.

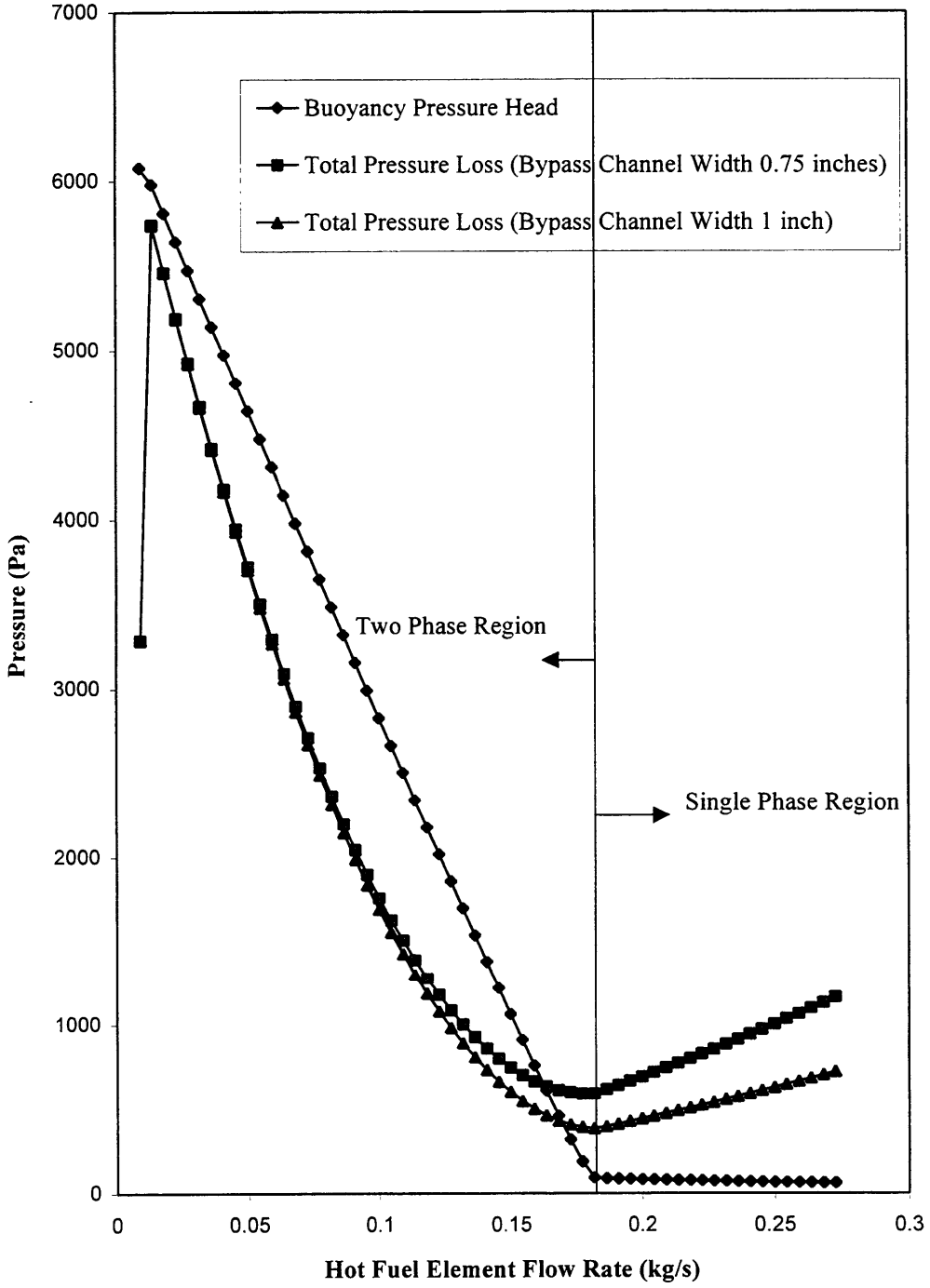

Figure 3.15: Total Pressure Losses and Buoyancy Pressure Head for Instant of LOF

Until the hydrodynamic steady state condition is reached, the bubbles leaving the core will collapse in the upper plenum and will heat the coolant in the upper plenum.

The pump coast down period is very short compare to the 10 minutes. Therefore the system will be in the two phase region for a short period after pump failure.

4.2.2 Hydrodynamic Steady State Condition ($t < t < t_{CHF}$)

After some time (t = t) into the loss of flow transient, the coolant in the fission converter tank will reach the temperature of 106 ^{0}C (saturation temperature). Therefore, the bubbles leaving from the core will not collapse in the upper plenum. The bubbles from the core rise through the upper plenum and escape the system through the primary coolant outlet pipe and the cover gas outlet pipe as shown in figure 3.14. The total pressure loss and total buoyancy pressure head for the flow path A$\rightarrow$ B$\rightarrow$C$\rightarrow$D (see figure 3.14) were calculated for different bypass channel widths and for different assumed flow rates (see figure 3.16). The MathCad spreadsheet is given in Appendix A3.5.

It is obvious from figures 3.15 and 3.16 that the hot channel will not starve for flow at the instant of loss of flow and the hydrodynamic steady state condition.

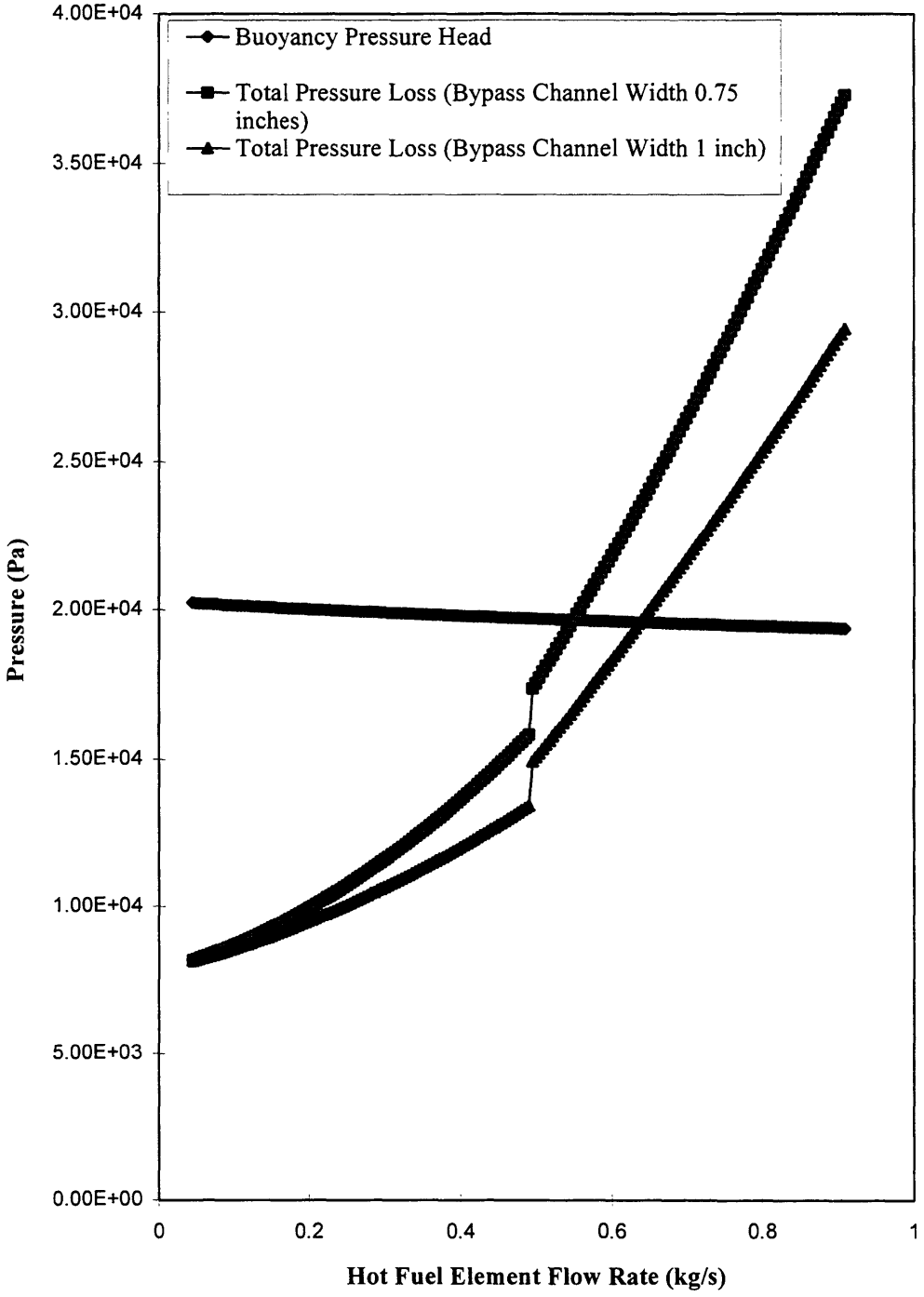

Figure 3.16: Total Pressure Losses and Buoyancy Pressure Head for Hydrodynamic Steady State Condition

The buoyancy pressure head as a function of time is shown in figure 3.17. The buoyancy pressure heads at the instant of loss of flow (t = 0) and after the hydrodynamic steady state conditions (t>t) are calculated. The buoyancy pressure head between the instant of loss of flow and the hydrodynamic steady state condition increases from its initial value to the hydrodynamic steady state condition value. Therefore, coolant flow rate will increase from its initial value at the instant of loss of flow to the hydrodynamic steady state value. If the bypass channel width is 1 inches, the hot channel flow rate will increase from its initial value of 0.16 kg/s (see figure 3.15) to hydrodynamic steady state value of 0.64 kg/s (see figure 3.16). Therefore, the hot channel will not starve for flow during the loss of flow transient. When the coolant level drops below the level of the bypass channel wall, there will not be a bulk flow path ($A \rightarrow B \rightarrow C \rightarrow D$).

The CHF for the flow rates 0.16 kg/s and 0.64 kg/s were calculated using equation 3.11 (in section 7.1.1.1). The calculated values are 277 ± 91 kW/m^2 for 0.16 kg/s and 647 ± 213 kW/m^2 for 0.64 kg/s. Since the flow rate increases from 0.16 to 0.64 kg/s, the CHF will also increase from 277 ± 91 to 647 ± 213 kW/m^2. Therefore, the operational heat flux (=19 kW/m^2) is much smaller than the CHF values. Hence it is evident that the design II will not experience CHF condition during LOF accident.

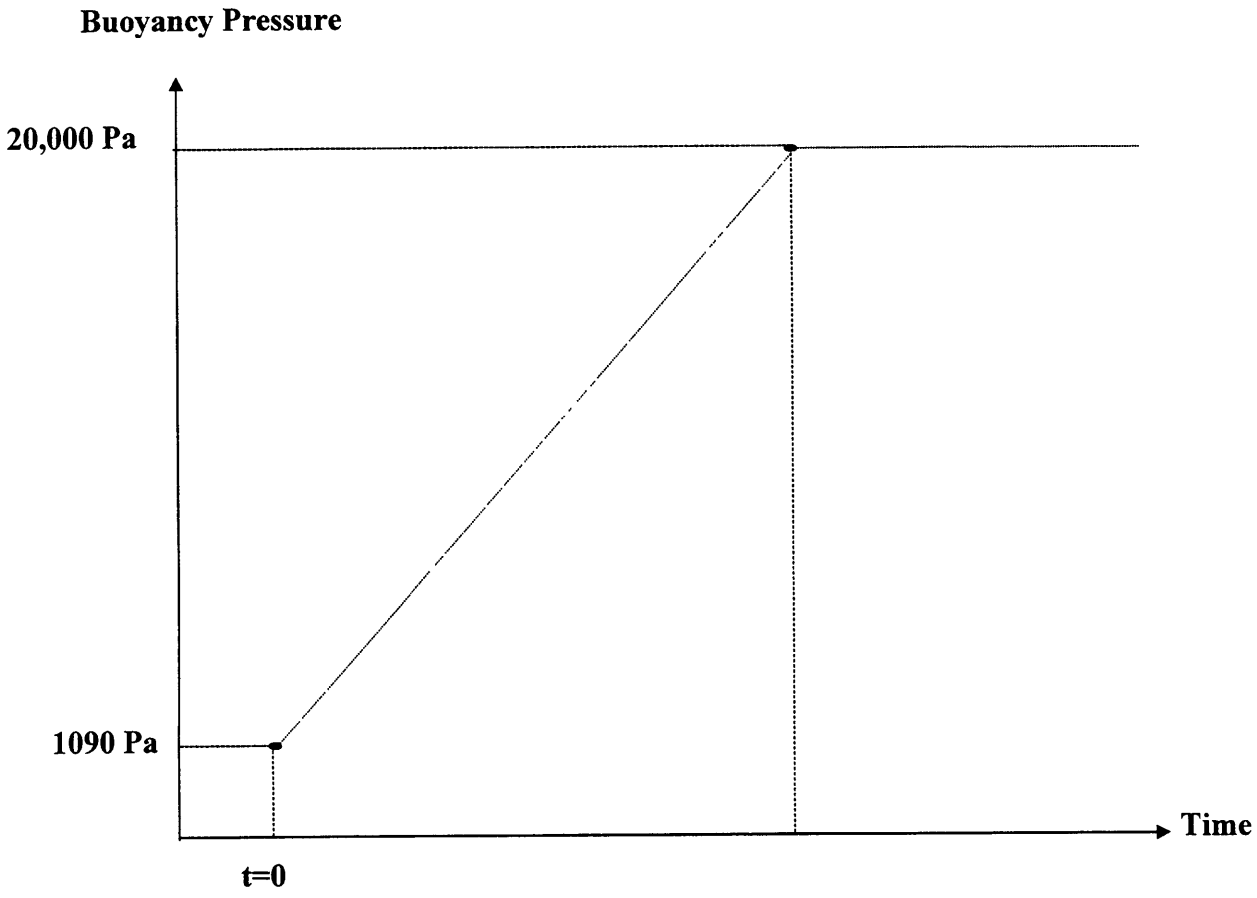

Figure 3.17: Sketch of Buoyancy Pressure Head as a Function of Time

However when the coolant level drops below the bypass channel top wall, the CHF drops to 25 ± 7 kW/m^2 (calculated using equation 3.12), because natural convection flow around the loop drops to zero. Therefore, the system can reach the CHF condition after the coolant level drops below the bypass channel wall top.

It is evident from above analysis that the system will experience boiling condition much before 10 minutes into the loss of flow accident. However, the fuel will not be damaged until the coolant level drops below the bypass channel top, because critical heat flux will not be experienced during that period.

5.SIMPLE FORCED CONVECTION (DESIGN III)

Schematic of design III heat removal system is show in figure 3.18. There are two pumps in parallel and each has the capability of pumping half of the primary flow rate. Here primary coolant is sucked through the outlet pipe and passed through the heat exchanger. Once it is cooled to 40^0C, it is returned to the downcomer region. Since the downcomer top is closed for this design, the upper plenum coolant will not flow into the downcomer nor will the downcomer coolant flow into the upper plenum. The only difference in the external loop compare to the other two designs is that this design has two primary pumps in parallel.

This design is easier to analyze analytically. The required primary flow rate is calculated for the hottest fuel element coolant exit temperature of 60^0C. The calculated primary flow rate is 4.6 kg/s.

6.SUMMARY OF STEADY STATE RESULTS

The steady state results for all three designs are summarized in the table 3.6. Except for the natural convection design (design I), the normal operational temperature can be kept under the design goal (60^0C). However, design II requires a much higher flow rate than design III to keep the temperature under 60^0C. The exit cooling temperatures of all three designs are much below the design limit of 106^0C (no boiling).

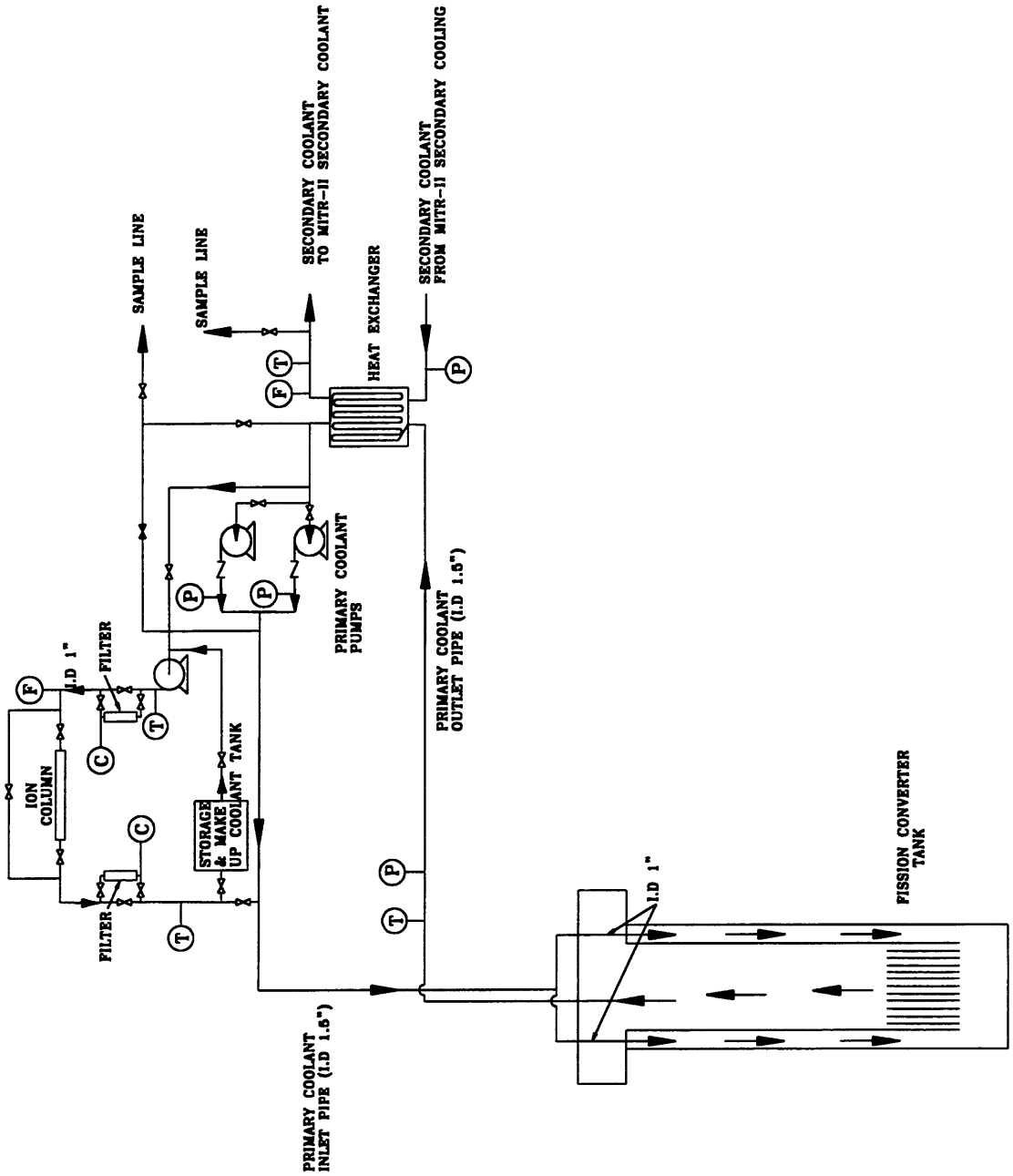

Figure 3.18: Schematic Drawing of Design III (Forced Convection Design) Fission Converter Heat Removal System

Table 3.6: Summary of steady state results

	Design I (Natural Convection Design)	**Design II (Forced Convection with Bypass Channel)**	**Design III (Forced Convection Design)**
Total Flow Rate Through the Core	2.8 kg/s	6.5 kg/s (bypass channel width 0.75 inches)	4.6 kg/s
Temp. Difference Across the Hottest Fuel Element	32 ^{0}C	20 ^{0}C	20 ^{0}C
Exit Coolant Temp. From Hottest Fuel Element	80 ^{0}C	60 ^{0}C	60 ^{0}C

7.ANTICIPATED ACCIDENTS ANALYZED

The author has tried to analyze all possible anticipated accidents for each of the three designs and then checked the results with the anticipated accident design limits and design goal. The analyzed anticipated accidents are;

1. Loss of Flow with cadmium shutter closure
   - Pump Failure
   - Outlet Pipe Break
   - Inlet Pipe Break
2. Loss of Flow with cadmium shutter failure
   - Pump Failure
   - Outlet Pipe Break
   - Inlet Pipe Break

7.1 Loss Of Flow with cadmium shutter closure

Although aluminum-6061 melts at approximately 660 ^{0}C (1200 ^{0}F) it begins to soften significantly at about 450 ^{0}C (842 ^{0}F) and this temperature is, therefore, a suitable criterion for guaranteeing the

structural integrity of the fuel elements** and containment of radioactive fission products.

Primary coolant flow to the fission converter can be lost due to loss of pumping power or break in the inlet pipes or break in the outlet pipes. As soon as any of the above accidents occur the cadmium shutter can be lowered to absorb most of the thermal neutrons which come from the MITR-II reactor. The new cadmium shutter can either open or close in 15 seconds. The length of travel is 1.64 meters. Therefore the speed of cadmium shutter is 0.11 m/s. When cadmium shutter is in the fully closed position, the steady state fission converter power is 2 kW (0.67% of full power[1]). The fission converter power decreases from 300 kW as the cadmium shutter starts to close. However, as a conservative assumption, the fission converter power is assumed to be 300 kW until the cadmium shutter is fully closed. After full closure of the cadmium shutter, decay power will start at 18.8 kW and decay exponentially to the steady state fission converter power of 2 kW. The power history for the loss of flow with cadmium shutter closure is shown in figure 3.19.

The decay power is calculated using the code called DKPOWR. DKPOWR is a code for calculating decay power, energy, activity, and $\beta + \gamma$ spectra in LWR fuel using fission pulse functions and was prepared by Los Alamos National Laboratory, Applied Nuclear Science Group, Theoretical Division, University of California, Los Alamos, New Mexico.

** Taken from safety Analysis Report for the MIT Research Reactor (MITR-II)

The basic DKPOWR code was prepared originally to incorporate the 1979 ANSI/ANS 5.1 decay power standard using U.S Department of Energy funding.

In the following subsections, detail analysis of each of the loss of flow anticipated accidents are presented for each design.

7.1.1 **Pump Failure**

7.1.1.1 Design I

When the pumping power is lost, the primary coolant is not flowing into or out of the fission converter tank. Therefore, the fission converter will lose its external heat sink. The figure 3.20 is a sketch of different phases which the fission converter will experience during this transient. Phase 1, where there is no inflow or outflow to or from the fission converter, is a single-phase region. The coolant temperature will be rising with time due to the heating by 300 kW for the first 15 seconds, by decay power till 134 minutes and then by constant 2 kW. When the temperatures of the coolant and the fuel clad reach the boiling condition, there will be boiling on the fuel plates. This is shown as phase 2. When the hottest fuel channel reaches the Onset of Nucleate Boiling (ONB) condition, the coolant temperature in the upper plenum, in the downcomer, in the lower plenum and in the most of the coolant channels is less than the saturation temperature.

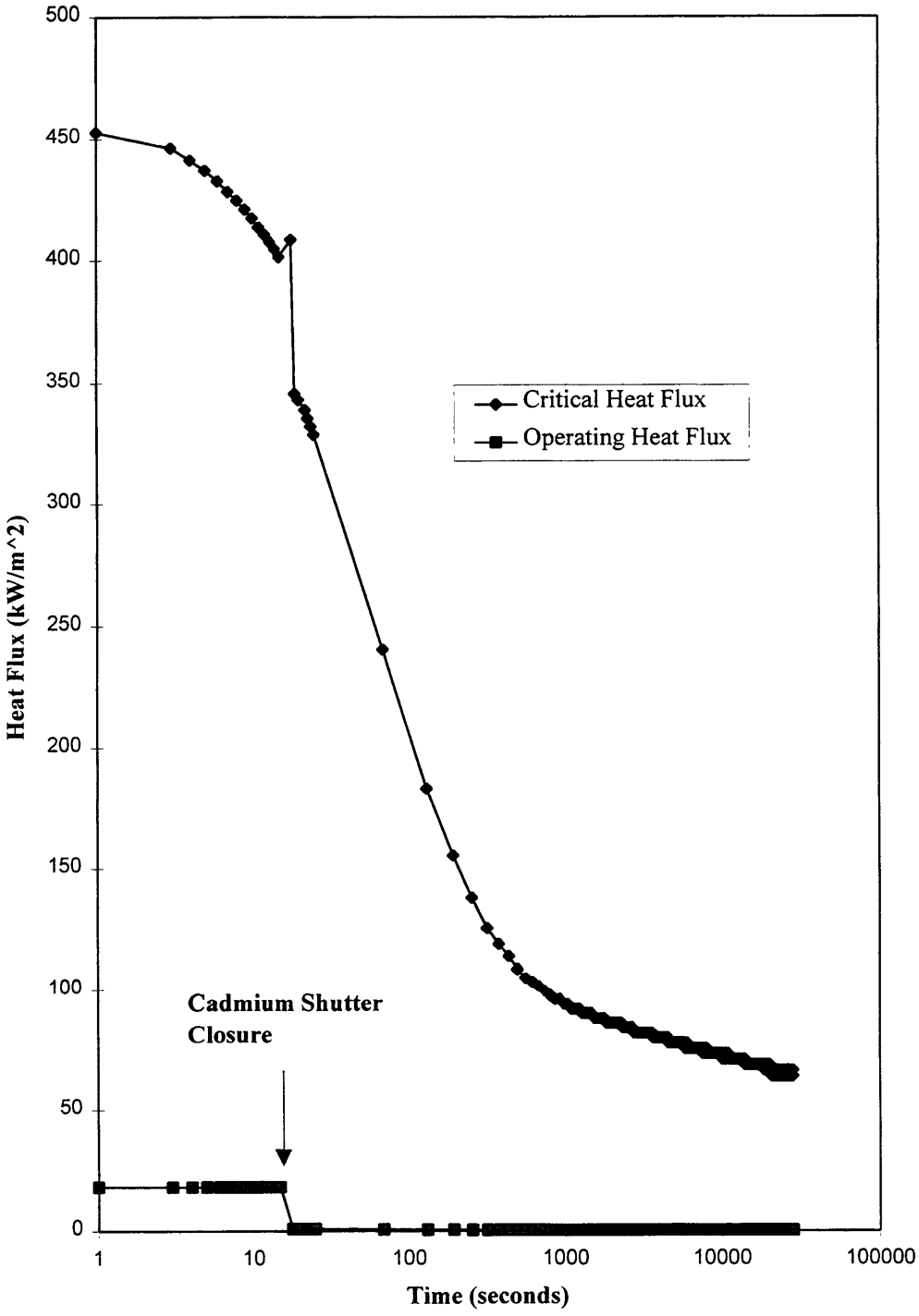

Figure 3.19: Power History for Loss of Flow with Cadmium Shutter Closure

Hence, the vapor bubbles that leave the hottest channel will collapse in the upper plenum. In phase 3 the temperature of all the coolant in the fission converter tank is at the saturation temperature and the vapor bubbles leave the fission converter tank without collapsing in the upper plenum. When the liquid level in the fission converter drops below the top of the downcomer wall, bulk recirculation flow will cease in the fission converter. This can be classified as a pool-boiling region. In the figure 3.20, this pool boiling region (no bulk flow) is shown as phase 4. In phase 5, the liquid level drops below the fuel element top and the fission heat is extracted by the liquid below the liquid level and by the vapor above the liquid level. In phase 6, the liquid level drops below the fuel element bottom edge and vapor is not generated. Therefore, the heat from the fuel elements is transferred by either air circulation or by the radiation heat transfer to the surrounding structures.

Temperature calculations for phases 1 through 3 were performed by a program written by the author. Detail about this program is given in section 7.3.

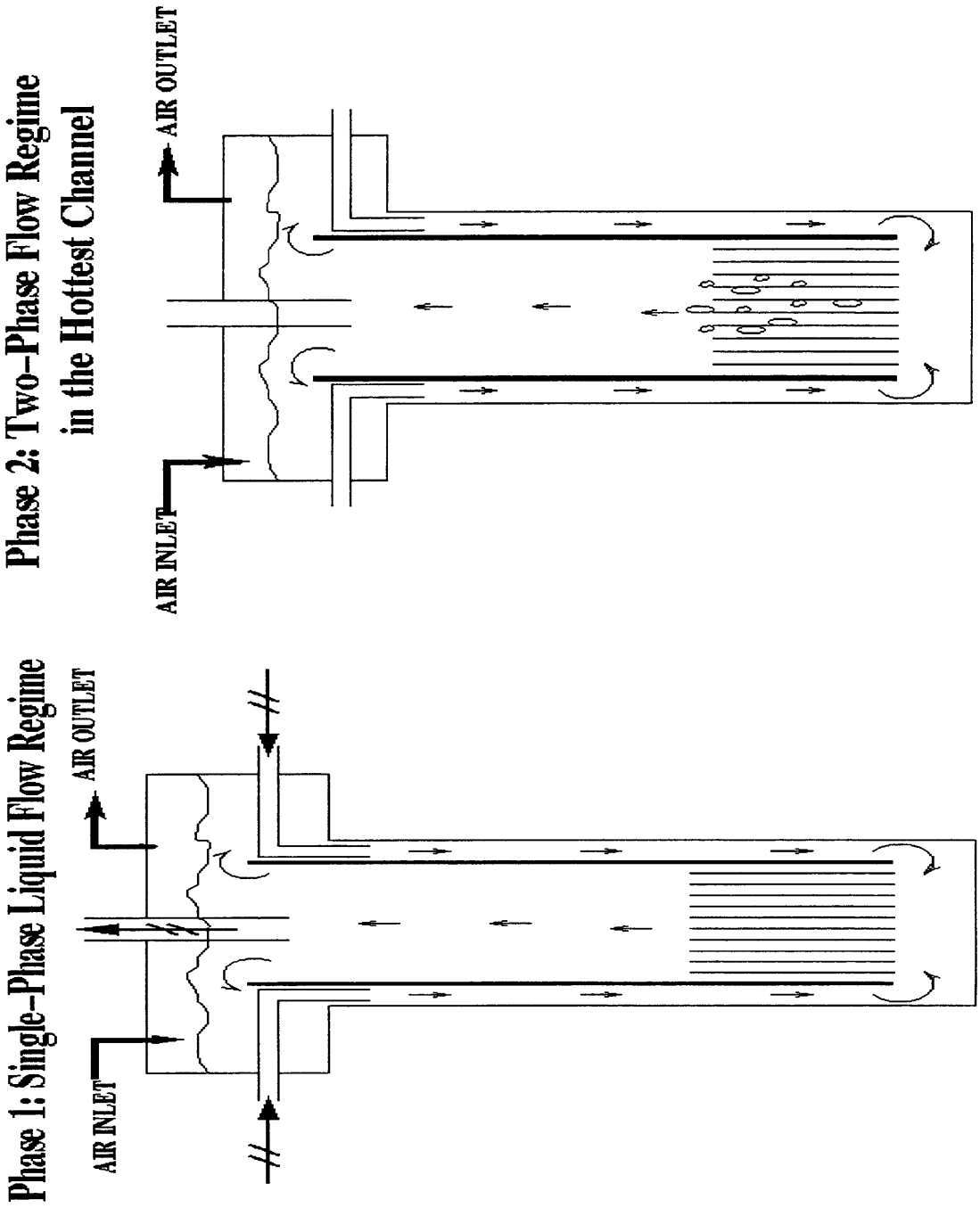

Figure 3.20:Sketch of Different Phases (Continues on next page)

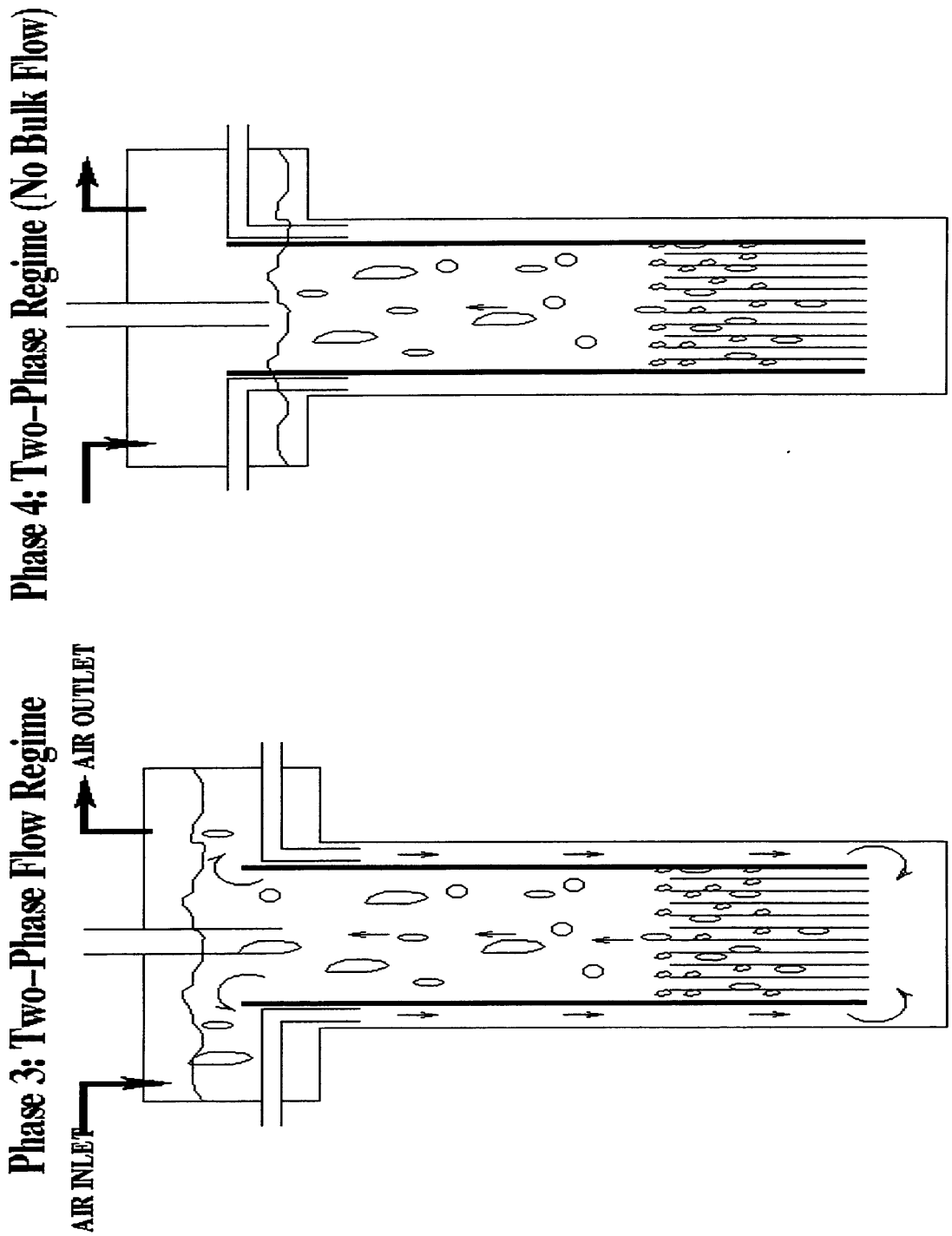

Figure 3.20: Continuation of Sketch of Different Phases (Continues on next page)

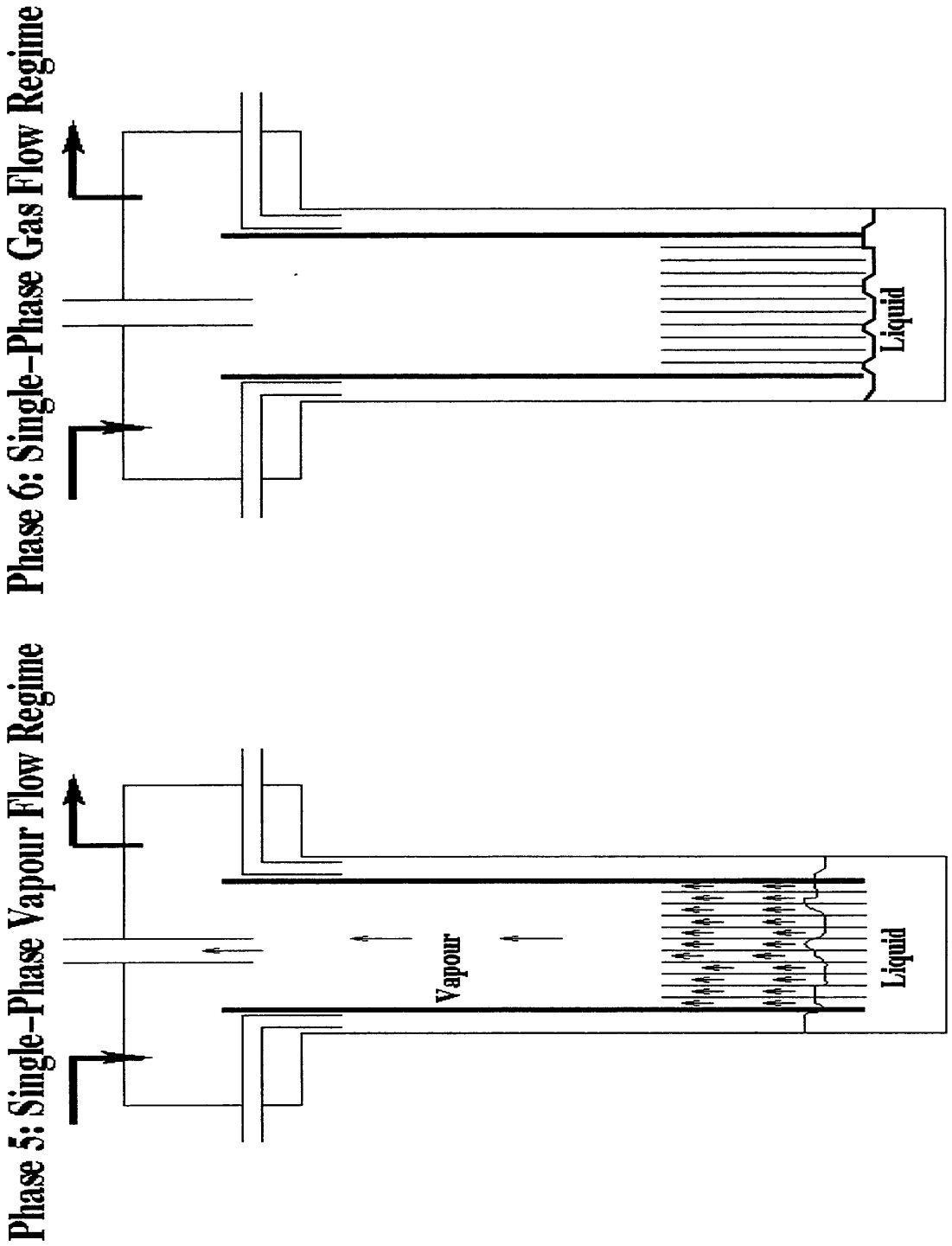

Figure 3.20: Continuation of Sketch of Different Phases

This program requires the following inputs:

1. Initial conditions:

- Normal operation upper plenum coolant temperature (T_u)
- Normal operation lower plenum coolant temperature (T_L)
- Normal operation coolant exit temperature from the hottest fuel channel (T_h)
- Normal operation heat transfer coefficient from the clad surface to the coolant (h)
- Normal operation mass flow rate ($\dot{m}$)

2. Heat generation rate as a function of time (Q_{gen})
3. Hot channel factor (F_h).

The program will provide the temperatures of the upper plenum coolant, the lower plenum coolant, the coolant exiting from the hottest channel, the hottest fuel clad surface, and the hottest fuel center line as outputs for the phases 1 through 3.

The equations used in the program are only applicable in the phases 1 to 3, if the critical heat flux (CHF) condition is not reached. Therefore, CHF is calculated for the phases 1 to 3; and then compared with operating heat flux. The correlation proposed by Y.Sudo and M.Kaminaga[6] was used to calculate the CHF in the phases 1 to 6. Equation (3.11) is applicable in the phases 1 to 3, where bulk flow exits and equation (3.12) is applicable for the phases 4 to 6, where no bulk flow exits. CHF predicted by these two equations have $\pm 33\%$ error.

$$q^*_{CHF} = 0.005G^{*0.611} \tag{3.11}$$

$$q^*_{CHF} = 0.7\frac{A}{A_H}\frac{\sqrt{W/\lambda}}{\left(1+(\rho_g/\rho_l)^{1/4}\right)^2} \tag{3.12}$$

with,

$$G^* = \frac{G}{\sqrt{\lambda g \rho_g(\rho_l - \rho_g)}}$$

$$q^*_{CHF} = \frac{q_{CHF}}{h_{fg}\sqrt{\lambda g \rho_g(\rho_l - \rho_g)}}$$

and

$$\lambda = \left(\frac{\sigma}{(\rho_l - \rho_g)g}\right)^{1/2}$$

Here A =flow area of channel (m^2),

A_H = heated area of channel (m^2),

g = acceleration of gravity (m/s^2),

G = mass flux ($kg/m^2.s$),

G* = dimensionless mass flux,

H_{fg} = latent heat of vaporization (J/kg),

W = width of the channel (m),

and σ = surface tension (N/m).

The critical heat flux and operating heat flux are presented in the figure 3.21. From these results it is predicted that the fission converter system will never experience CHF condition during the phases 1 to 6.

After some time, the coolant level in the fission converter drops below the downcomer top if the vapor escapes from the system as it boils. A conservative assumption would be that the vapor generated due to

boiling escapes the fission converter through the primary outlet pipe and the cover gas system without condensing. Hence, the vapor condensation is neglected. If the vapor condensation is neglected, the liquid level in the fission converter will drop below the downcomer wall top after about 2 days into the transient. This region is classified as the phase 4. Phase 4 can be classified as the pool boiling region since there is no fluid being circulated out of the upper plenum region. Phase 4 can be classified as nucleate boiling because the system will not reach the CHF condition. The coolant temperature is at the saturation temperature. The fuel clad surface temperature can be calculated using Rohsenow's correlation (Ref. 8).

$$Nu = \frac{Ja^2}{C_{nb}^3 \, \mathrm{Pr}_l^m}$$

with,

$$Ja = \frac{c_{pl}(T_w - T_{sat})}{h_{fg}}$$

and

$$q'' = h(T_w - T_{sat}).$$

Here C_{nb} (=0.013) is an experimentally determined value for horizontal aluminum-water surface.

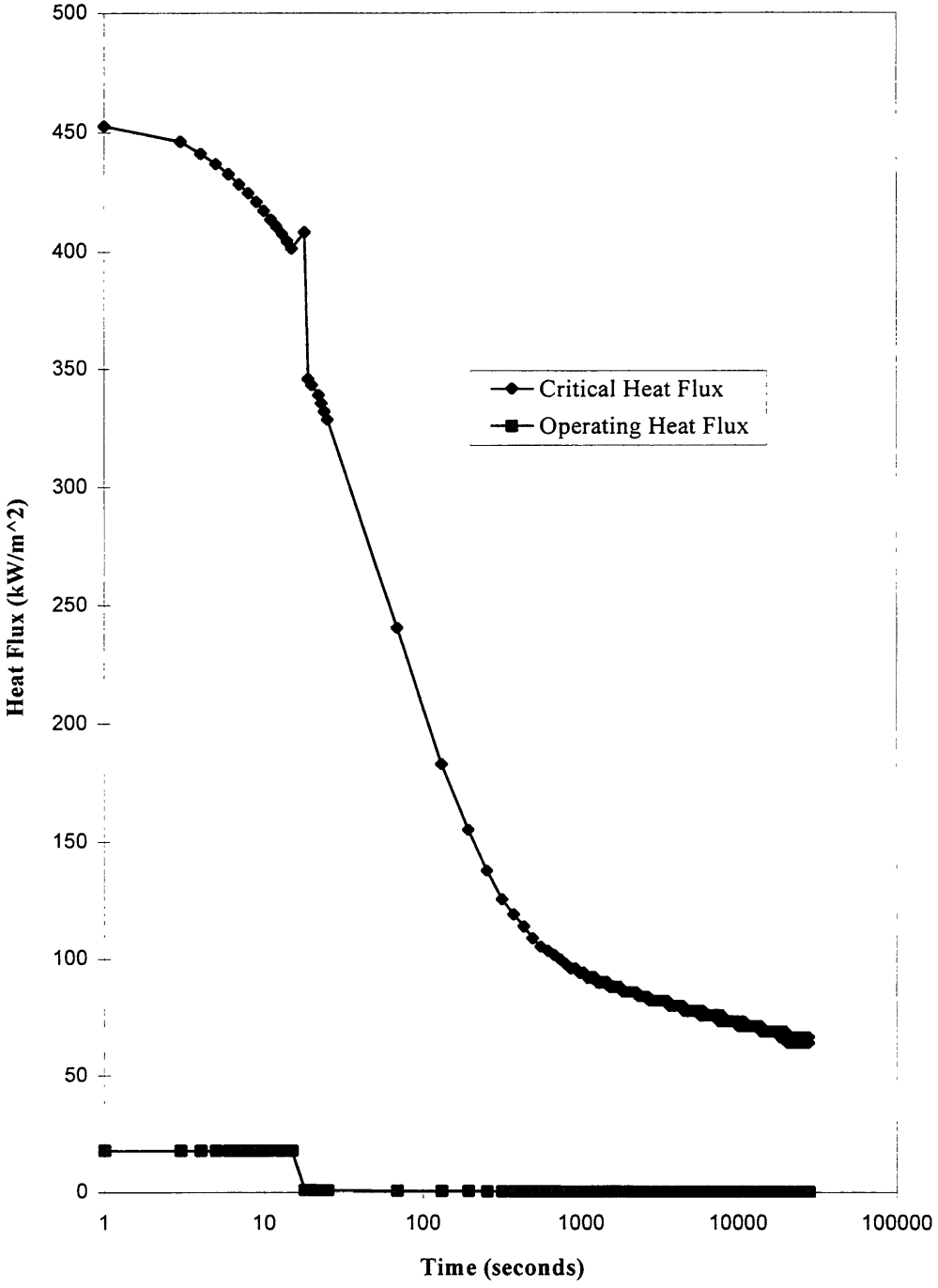

Figure 3.21: Critical Heat Flux and Operating Heat Flux for the Loss of Coolant Accident

As before, if the vapor condensation is neglected, after about 9 days into the transient the liquid level in the fission converter will drop below the fuel elements (phase 5). In the phase 5, the decay heat in the fuel is extracted by the liquid below the liquid level, by the vapor above the liquid level and by radiation heat transfer to the surrounding structure. Then, the liquid level drops below the bottom of the fuel elements (phase 6). In the phase 6, the generated heat is removed by the radiation heat transfer to the surrounding structures. The surrounding structures are conservatively assumed to have a temperature of 150 ^{0}C. Most of the surrounding structure is made of heavy concrete. In phase 6 calculations, the heat removed by air circulation is assumed to be negligible.

The temperature history for the phases 1 to 4 is shown in figure 3.22. The temperature histories for the hottest channel coolant exit temperature, the hottest channel fuel clad surface temperature, and the hottest channel fuel center line temperature are shown in figure 3.22 for the pump failure with cadmium shutter closure. The temperature histories for the phases 5 and 6 are similar to the loss of coolant accident analyzed later in section 7.4. Therefore, the phases 5 and 6 temperature histories are not shown in the figure 3.22.

The temperature histories shown in the figure 3.22 are only true if the primary pump and the clean-up pump fail and the cadmium shutter closes simultaneously.

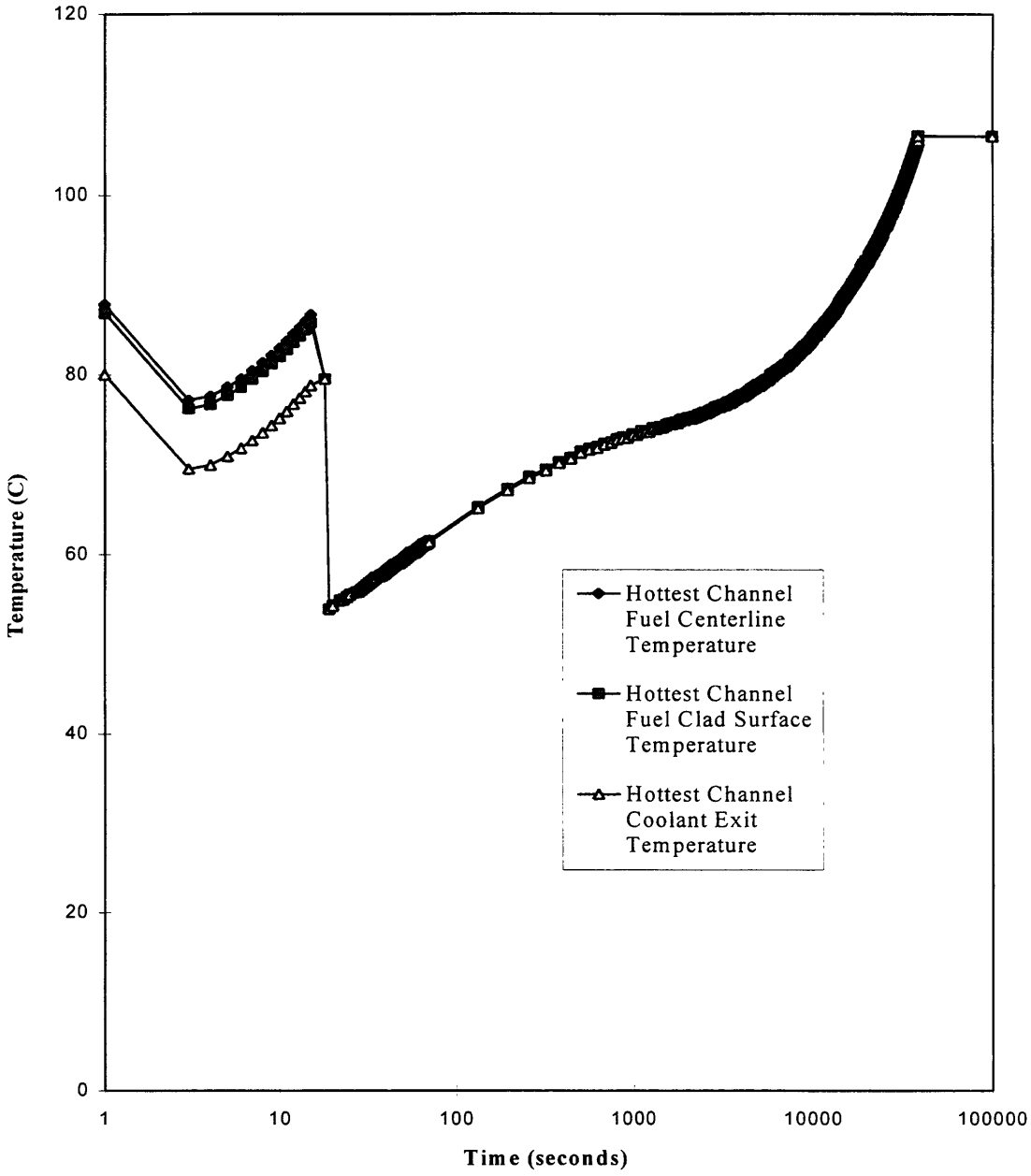

Figure 3.22: Temperature History for Primary Pump and Cleanup Pump Failure Accident, Cleanup Pump Flow Available (Design I)

However, if only the primary pump fails and the clean up pump continues to operate, there will be a 1% of total primary flow rate in and out of the fission converter tank. This scenario is analyzed by the author using the program (see section 7.3 for description of the program) with some minor changes. The temperature histories for this scenario are shown in figure 3.23. As is obvious from the figure 3.23, the system never reaches the two-phase region.

7.1.1.2 DESIGN II

As it is shown in figure 3.11, a natural circulation will be established within the fission converter tank after the primary pump and the clean up pump failure. The system will go through all the phases shown for the design I. However the design II reaches the two-phase system faster than the design I. Also the design II single phase flow rate is smaller than the design II single phase flow rate. The hottest fuel centerline temperature, the hottest fuel clad surface temperature and the coolant exit temperature from the hottest channel can be calculated with the aide of the program written by the author. The same inputs are used as the ones used for the design I calculation. These temperature histories are shown in figure 3.24.

The temperature histories for the accident scenario of the primary pump failure, the clean up pump continuous operation, and the cadmium shutter closure are shown in the figure 3.25.

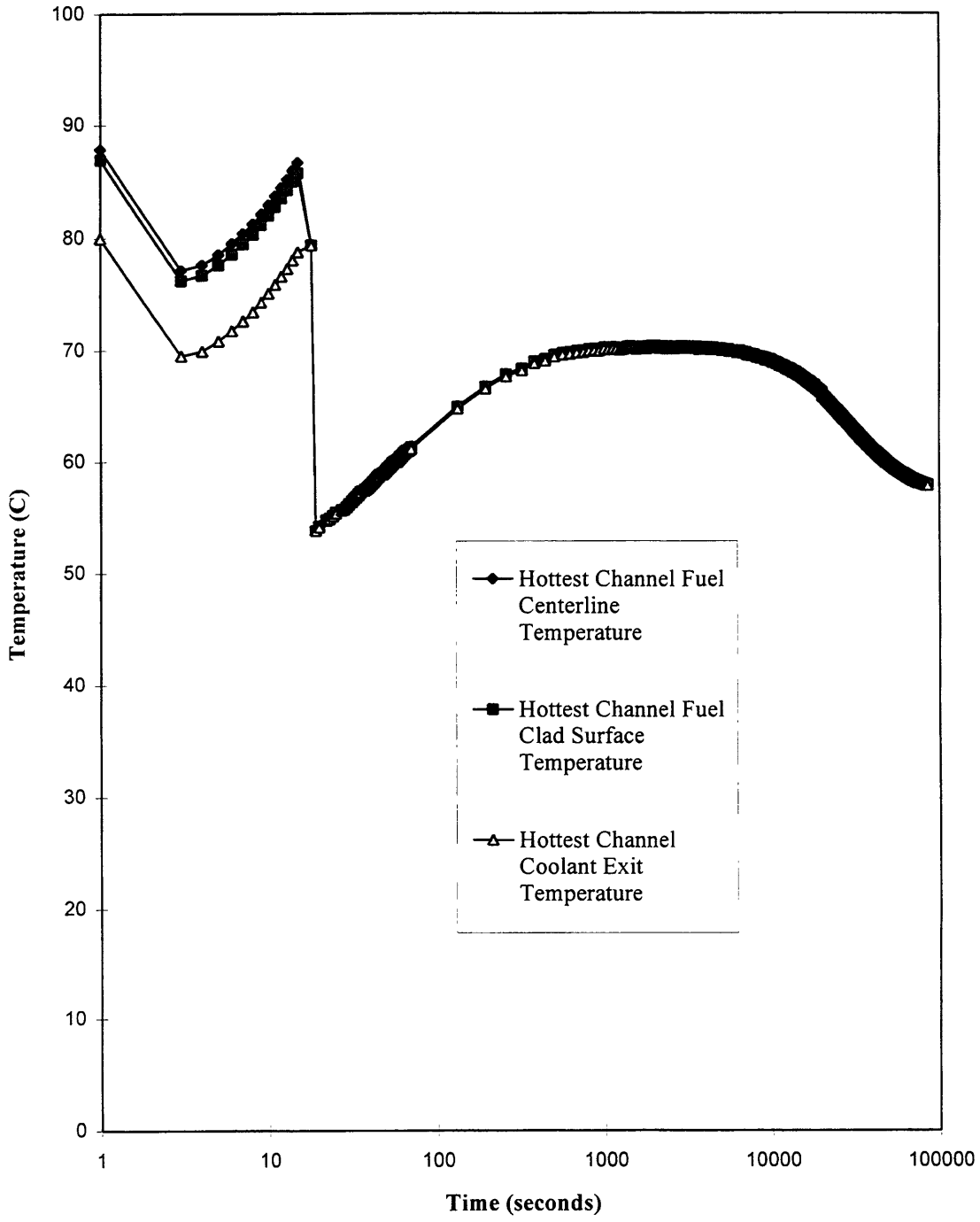

Figure 3.23: Temperature History for Primary Pump Failure Accident (Design I)

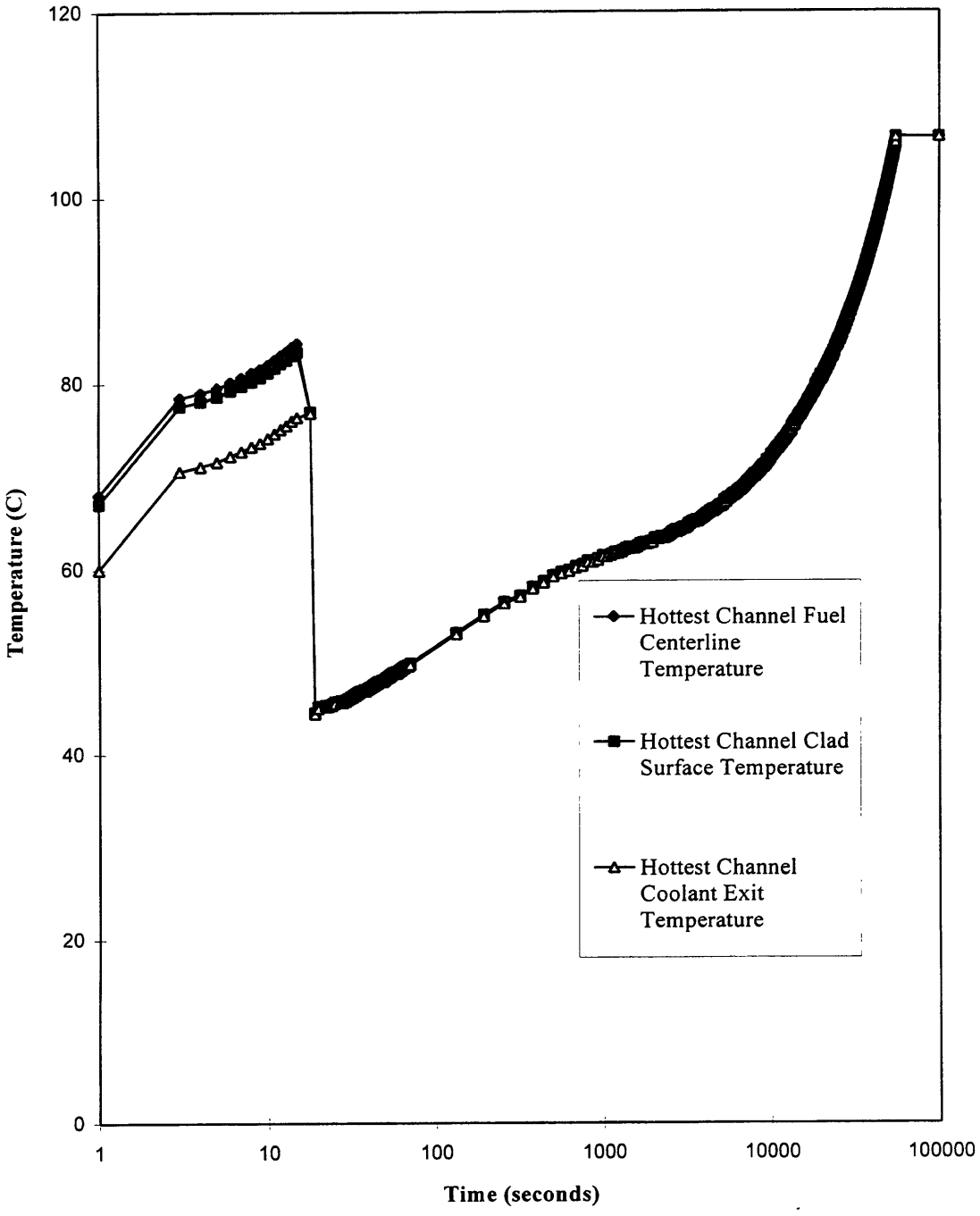

Figure 3.24: Temperature History for Primary Pump and Cleanup Pump Failure Accident (Design II)

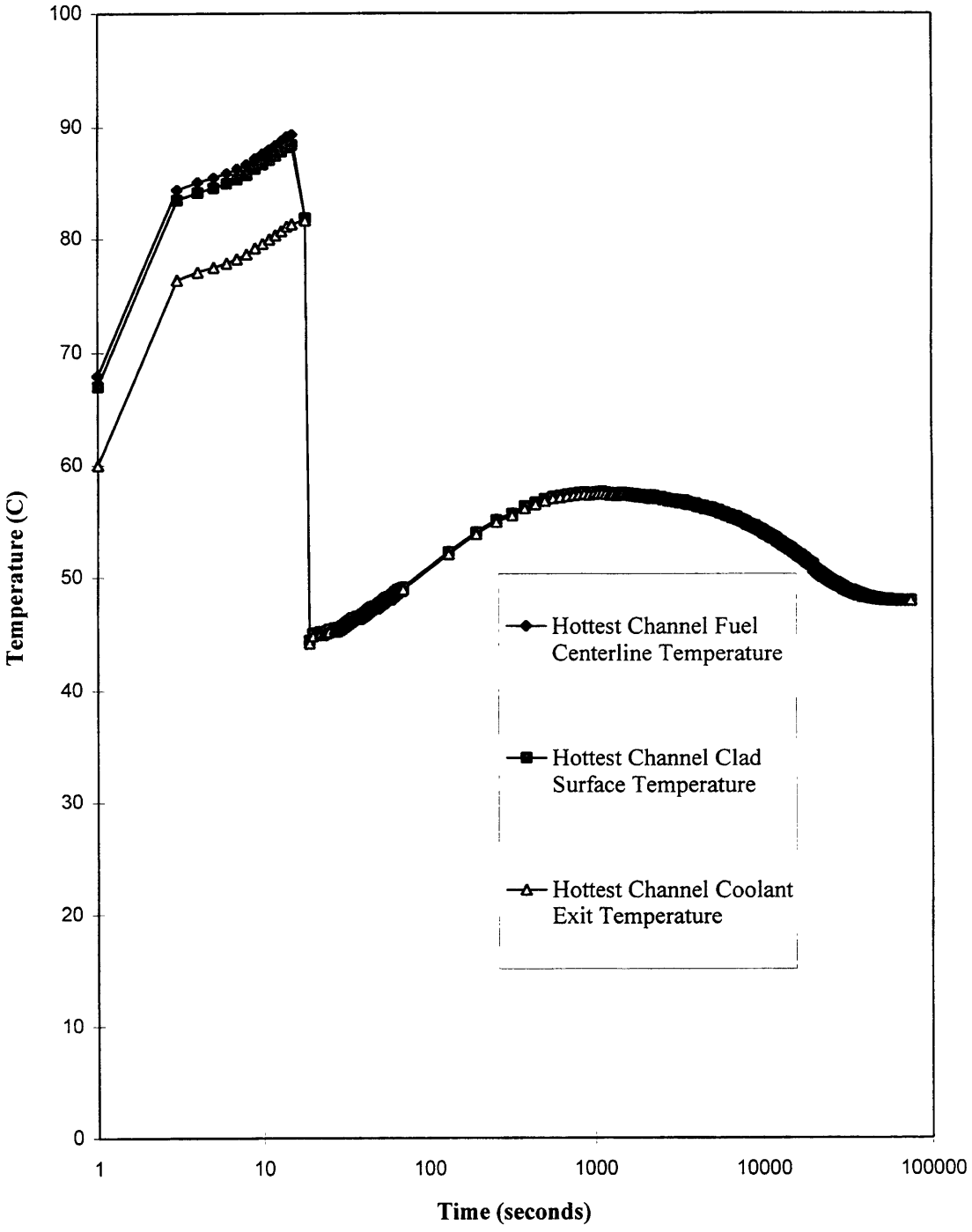

Figure 3.25: Temperature History for Primary Pump Failure Accident, Cleanup Pump Flow Available (Design II)

7.1.1.3 DESIGN III

In design III, there will not be any bulk flow after the simultaneously failure of all three pumps (two primary pumps and one clean up pump). It is an unlikely event to fail all three pumps simultaneously. However, if all three pumps fail simultaneously, then the reactor will be automatically scrammed. Since the reactor can be scrammed within in a second, the fission converter power will be due to decay power after the loss of pumps. The operational heat flux and the CHF are shown for this condition in the figure 3.26. As it is obvious from the figure 3.26, there will not be CHF situation during this accident scenario. Since there is no path to establish bulk flow, the fuel elements will stay in the pool of coolant and raise the coolant temperature. In figure 3.27, the hottest channel clad surface temperature is shown for this transient. As it is evident from figure 3.27, the system will reach ONB condition.

If only one primary pump is failed, then the system temperature will rise and will come to new steady state temperature. Since each primary pump has the capability of pumping half of the total primary flow rate, the temperature difference across a fuel element will be double the difference when both pumps are operating.

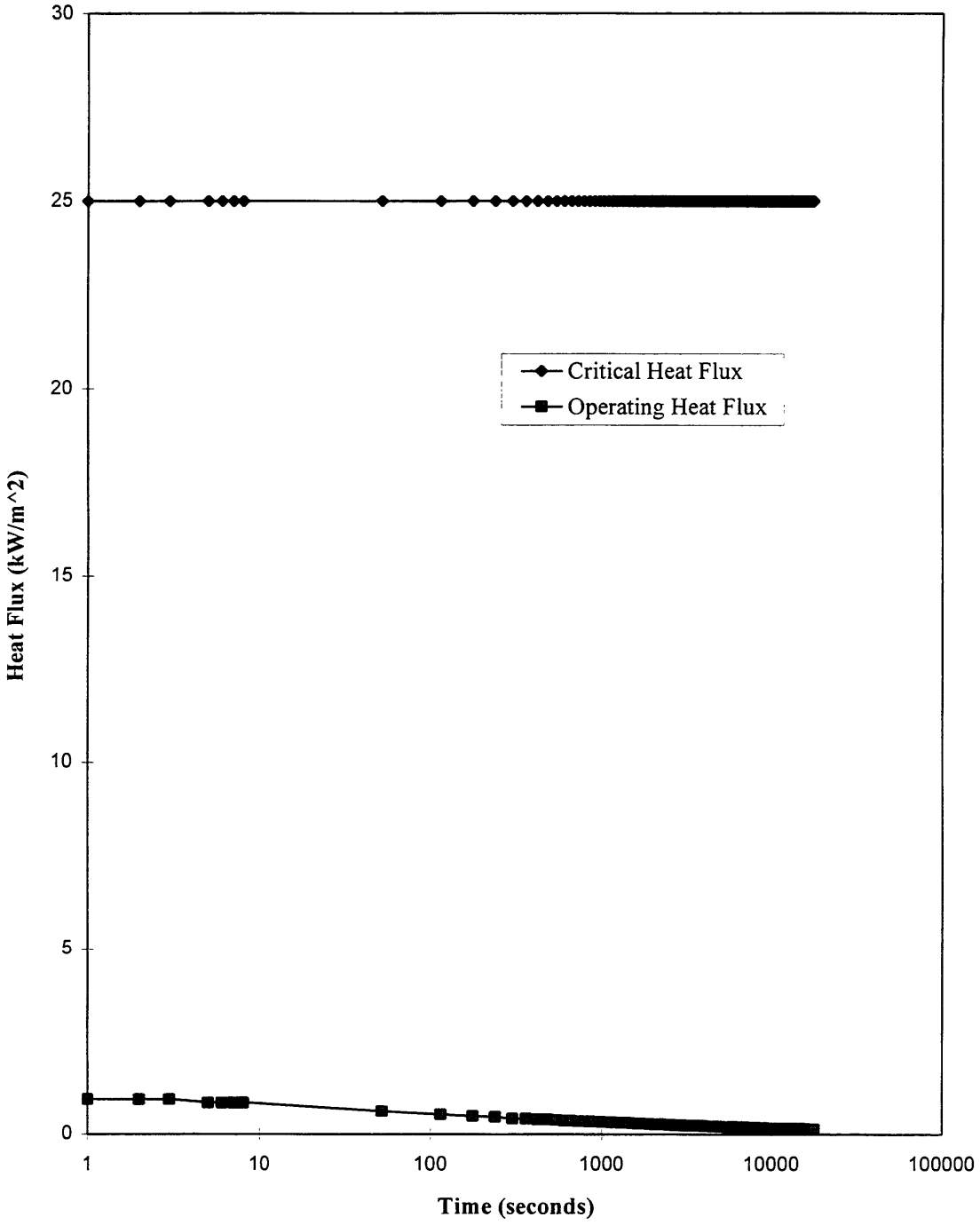

Figure 3.26: Critical Heat Flux and Operating Heat Flux for All Pumps Failure Accident (Design III)

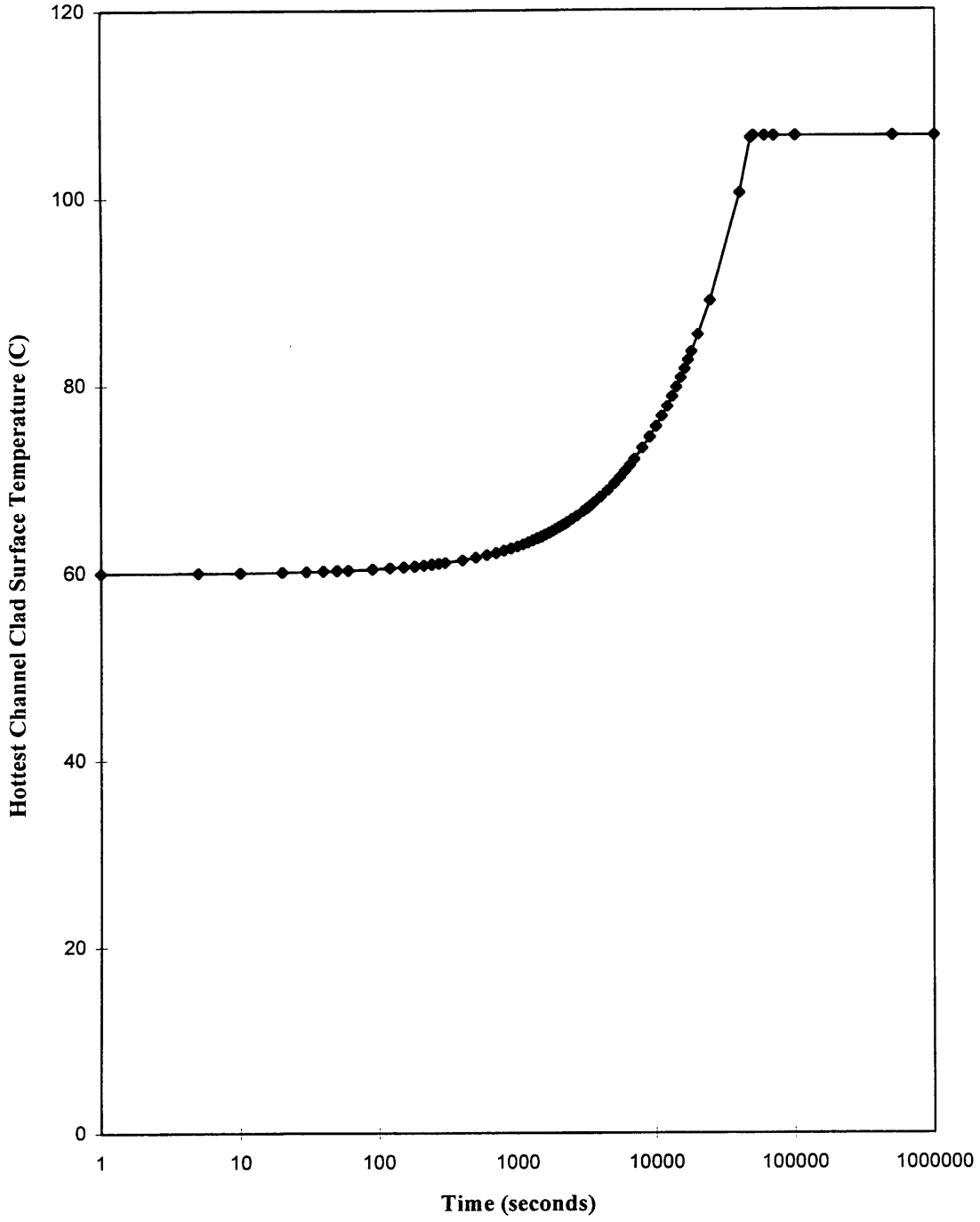

Figure 3.27: Temperature History for All Pumps Failure with Reactor Scram (Design III)

Hence, the system coolant maximum temperature will be 80 ^{0}C. Since the clad temperature is much less than the ONB temperature, there will not be any boiling on the fuel plates. Hence, the system can be operated continuously during the failure of single primary pump.

If both primary pump fails and the clean up pump continue to operate, again the reactor will be scrammed. The clean up has a capability of pumping 1% of the total primary flow rate. Again this accident scenario is analyzed with the program written by the author and the results are shown in the figure 3.28. As is obvious from figure 3.28, there will be no ONB condition.

7.1.2 OUTLET PIPE BREAK

Outlet pipe break is a break anywhere from the outlet of the fission converter tank to the inlet of the primary pumps. During the outlet pipe break, the flow to and out of the fission converter tank will be lost. Therefore, outlet pipe break accident is similar to the all pump failure accident. All the temperatures and calculations procedures given in the primary pump failure are valid for the outlet pipe break accident.

7.1.3 INLET PIPE BREAK

Inlet pipe break is a break anywhere between the outlet of the primary pump(s) to the inlet of the fission converter tank. During this accident, the coolant will be pumped out until the coolant level drop below the outlet pipe level in the fission converter tank.

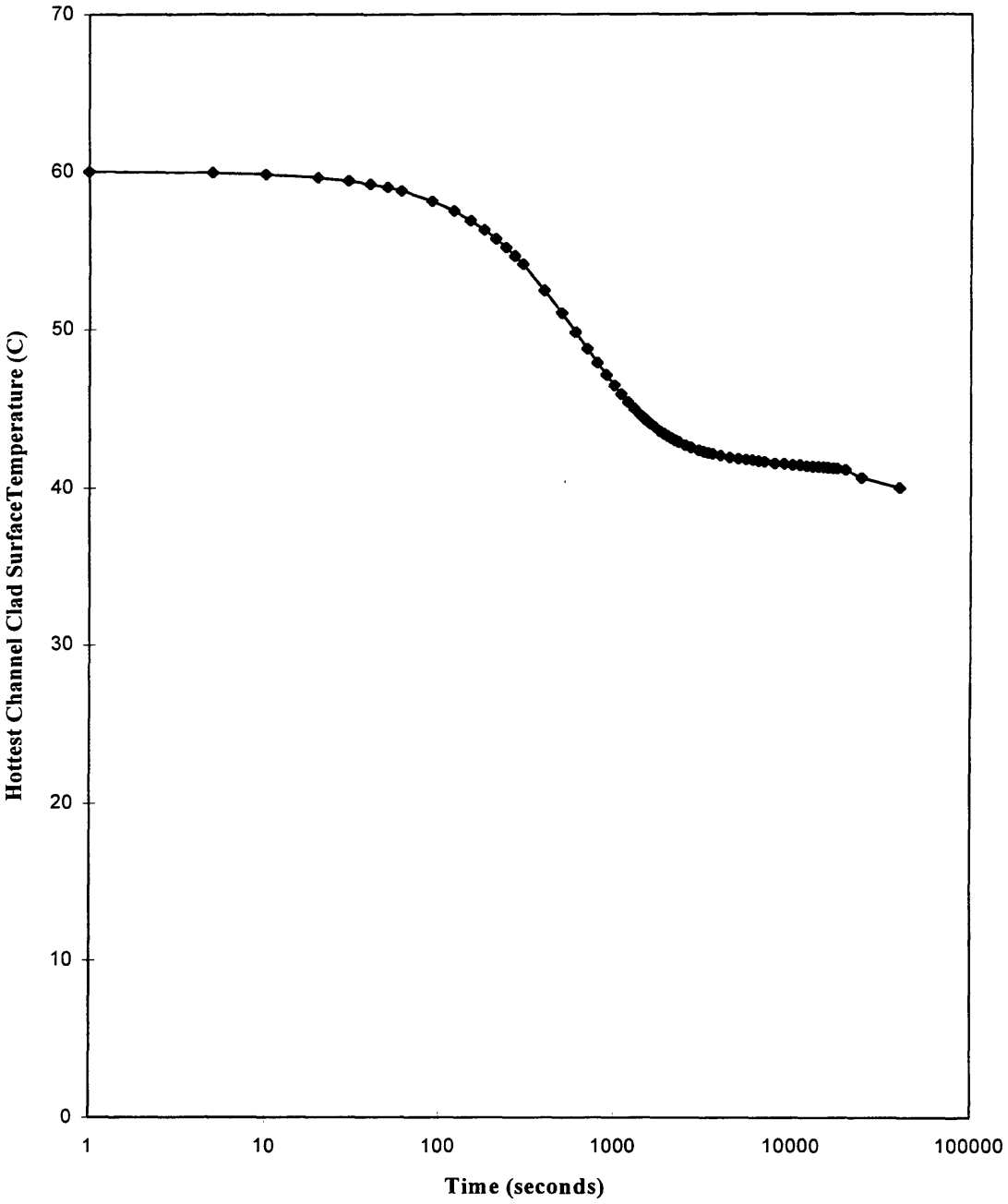

Figure 3.28: Temperature History for Two Primary Pumps Failure, Cleanup Pump Operates and Reactor Scrams (Design III)

The reactor will be automatically scrammed if the coolant level drops below the outlet pipe level in the fission converter tank. The hottest channel fuel clad surface temperature history is shown in figure 3.29. These calculations were performed analytically.

7.2 LOSS OF FLOW WITH CADMIUM SHUTTER FAILURE

The other anticipated accident associate with loss of pump is the failure of the cadmium shutter. It is assumed that the failure of cadmium shutter can only be detected after 15 seconds into the loss of pump transient. If the cadmium shutter and the pump failed simultaneously, the MITR-II reactor will automatically be scrammed. It requires about less than a second to scram the reactor. Therefore, during the failure of cadmium shutter and the pump, the power history will be identical to the one shown in the figure 3.19, except at the end power continues to decay rather than remain at a steady value of 2 kW. Hence, all the temperature histories shown for the pump failure with cadmium shutter closure are applicable for this accident scenario.

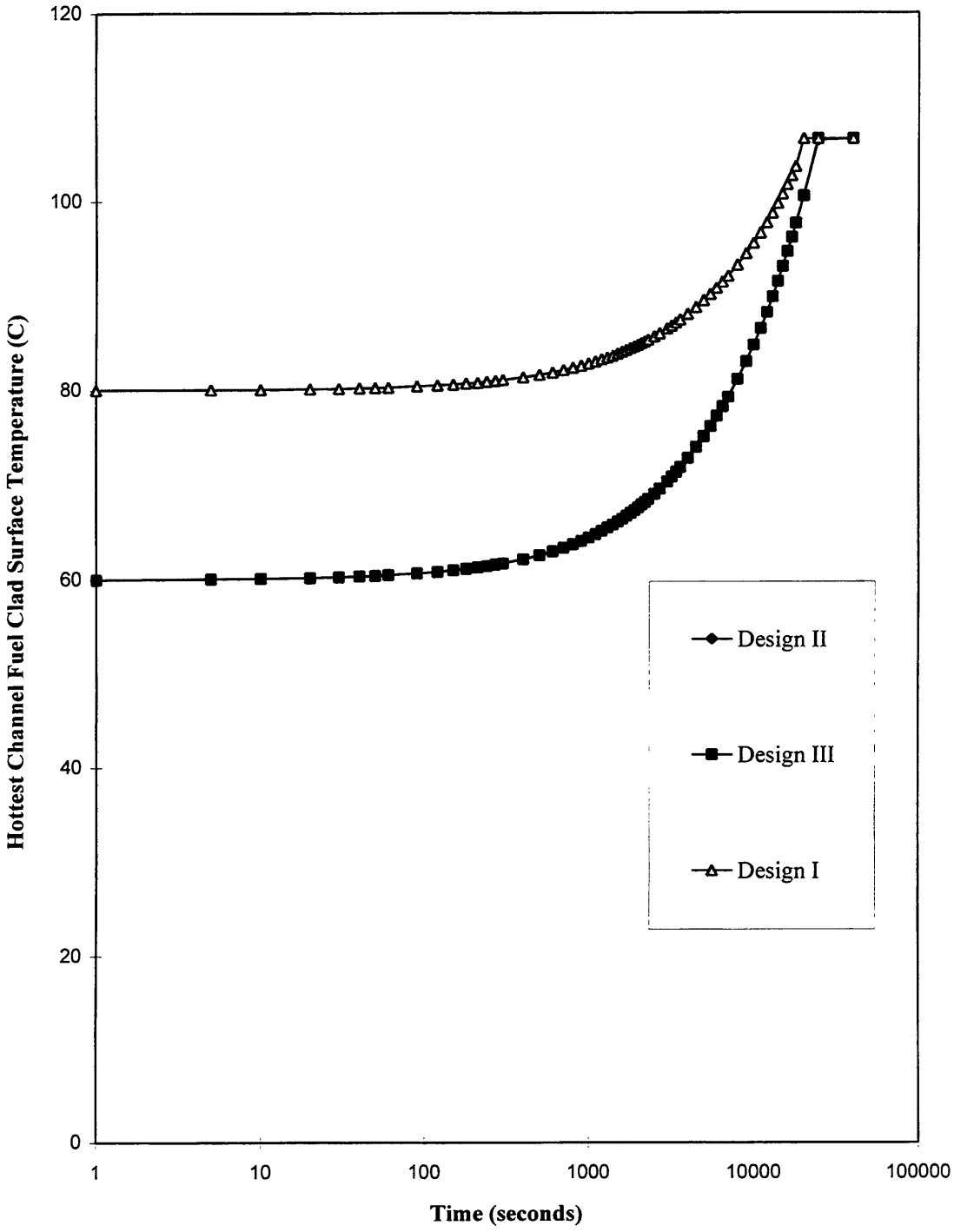

Figure 3.29: Temperature History for Inlet Pipe Break

7.3 LOSS OF FLOW AND CONVERTER AT FULL POWER

One of the design goals is that the fission converter coolant remain in single phase more than 10 minutes during a LOF for the case converter power equals to 300 kW. As can be seen in the figure 3.30, the hottest channel in Design I starts to boil after 64 seconds into the LOF transient. Design II will start to boil as soon as pump coast down is completed (see section 4.2.1). The same is true for the design III. Hence, none of these designs will satisfy this third design goal listed in section 1.

7.4 DESCRIPTION OF THE PROGRAM USED FOR LOF ANALYSIS

The flow chart for the program is given in the figure 3.31. The downcomer region coolant and the lower plenum coolant are assumed to be at same temperature. It is also assumed that all the coolant in the upper plenum at same temperature. This program requires following the initial conditions;

1. Upper plenum coolant temperature (T_u),
2. Lower plenum coolant temperature (T_L),
3. Coolant exit temperature from the hottest channel (T_h),

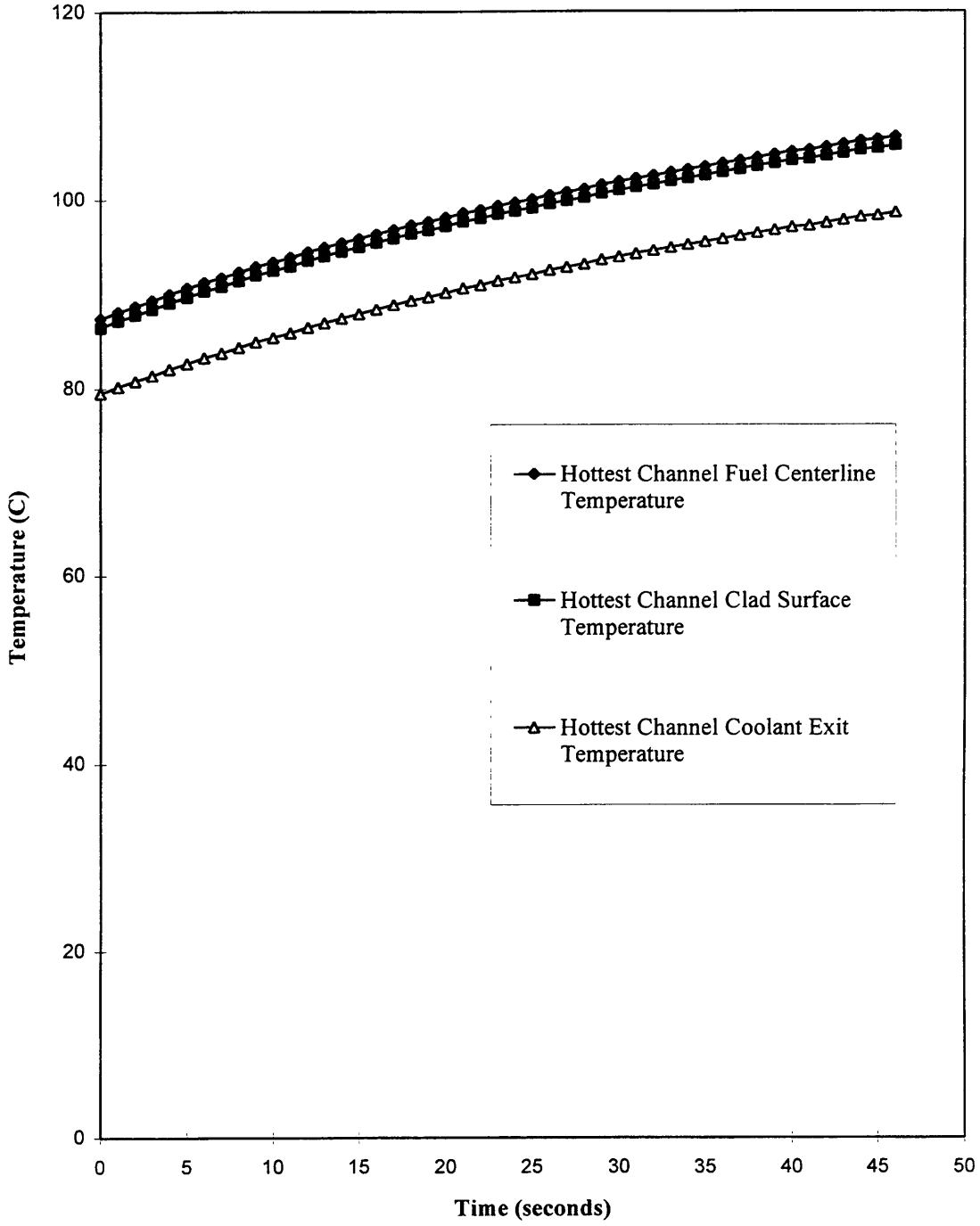

Figure 3.30: Temperature History for Design I LOF (Converter is at full power 300 kW)

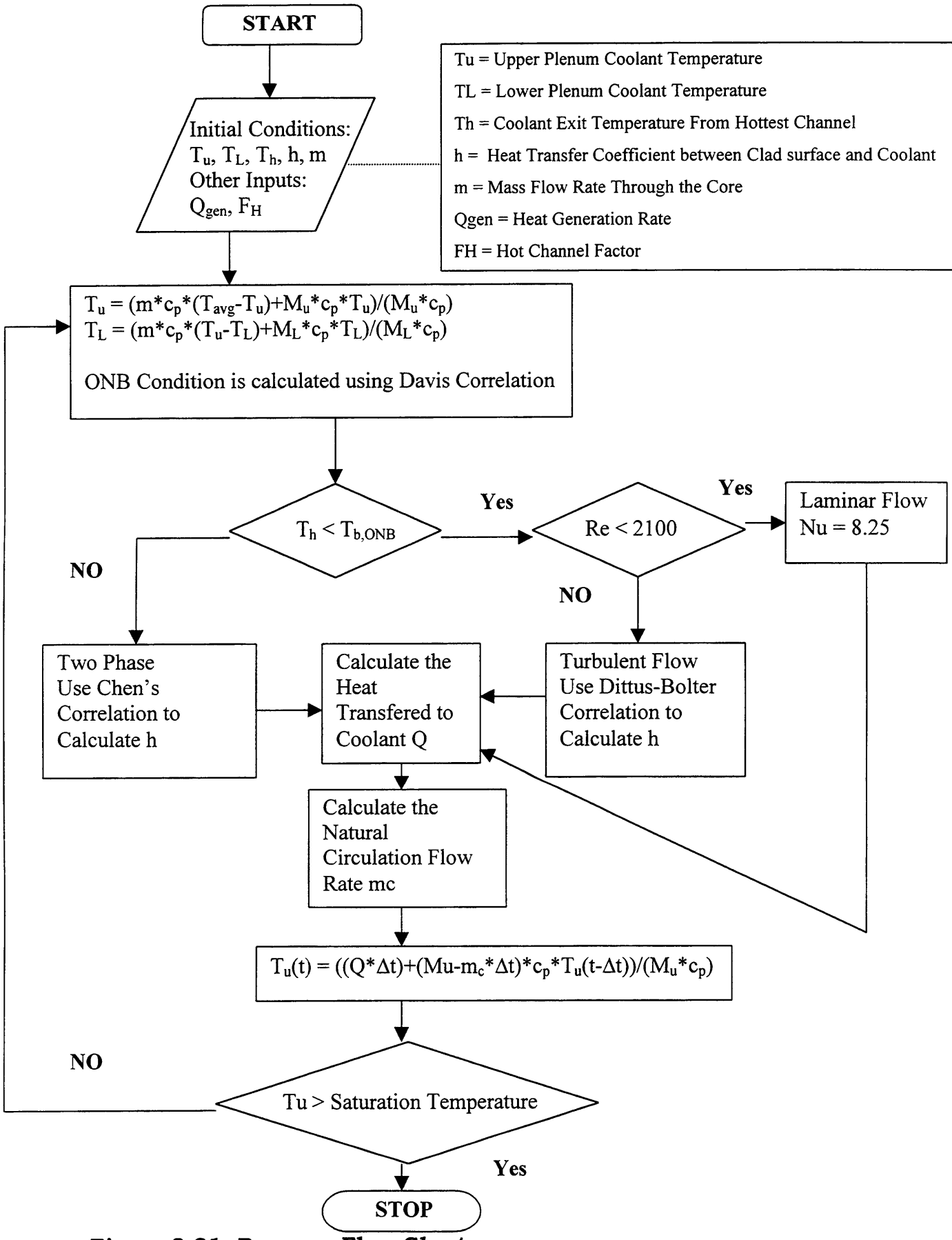

Figure 3.31: Program Flow Chart

4. Mass flow rate through the core ($\dot{m}$), and

5. Heat transfer coefficient between the fuel clad surface and the coolant (h).

The program also requires inputs of upper plenum coolant mass (M_u) lower plenum coolant mass (M_L), heat generation rate (Q_{gen}), and the hot channel factor. As a first step, new upper plenum and lower plenum coolant temperatures are calculated using the prior time step information. Then flow conditions are checked to see whether flow is single phase or two phase and laminar or turbulent.

Single phase or two phase is determined by comparing ONB condition bulk temperature to the hot channel coolant exit temperature. The ONB condition bulk temperature is calculated following manner. The surface clad temperature at the ONB is calculated using the Davis's and Anderson's[9] correlation, with the constant (c=12.5) found by experiments on finned fuel plates (Ref. 3).

$$T_{W,ONB} - T_{sat} = \left[\frac{12.5q''\sigma T^{*}_{sat}}{h_{fg}k_l(\rho_l - \rho_v)}\right]^{1/2} \qquad (3.13)$$

Where, $T_{W,ONB}$ = Wall temperature required for nucleation (^{0}C)

T^*_{sat} = Coolant saturation absolute temperature (K)

T_{sat} = Coolant saturation temperature (^{0}C)

Then the coolant bulk temperature can be calculated using the following equation;

$$T_{w,ONB} - T_{b,ONB} = q''/h \qquad (3.14)$$

If the flow condition is single phase and laminar, the new heat transfer coefficient between the coolant and the finned surface is calculated using the following equation;

$$h = 8.25 \frac{k_l}{D_h} \tag{3.15}$$

Here k_l = liquid thermal conductivity

and D_h = hydraulic diameter.

If the flow is single phase and turbulent, the new heat transfer coefficient is calculated using the Dittus-Boelter equation. If the flow is two phase, the new heat transfer coefficient is calculated using Chen's correlation,

$$h = h_{NB} + h_c \tag{3.16}$$

Where, h_{NB} = Nucleate boiling heat transfer coefficient

h_c = Convective heat transfer coefficient.

The convective term is calculated with Dittus-Boelter correlation, with convection to the liquid phase only and a factor to account empirically for the contribution of vapor to the convective heat transfer.

$$h_c = 0.023\left[\frac{G(1-x)D_h}{\mu_l}\right]^{0.8} \mathrm{Pr}_l^{0.4} \frac{k_{ls}}{D_h} F \tag{3.17}$$

with the factor F is given by,

$$F=1 \qquad \text{For } 1/X_{tt} < 0.1 \tag{3.18}$$

$$F = 2.35(0.213 + \frac{1}{X_{tt}})^{0.736} \qquad \text{For } 1/X_{tt} > 0.1 \tag{3.19}$$

with,

$$\frac{1}{X_{tt}} = \left(\frac{x}{1-x}\right)^{0.9}\left(\frac{\rho_l}{\rho_v}\right)^{0.5}\left(\frac{\mu_v}{\mu_l}\right)^{0.1} \tag{3.20}$$

Where, G = Mass flux

x = Vapor quality

D_h = Equivalent heated diameter

μ_f = Saturated liquid viscosity

μ_v = Saturated vapor viscosity

k_{ls} = Saturated liquid conductivity.

The nucleate boiling heat transfer coefficient, h_{NB}, has the same form as the Forster-Zuber correlation, but contains a factor, S, to suppress it during low-quality flow.

$$h_{NB} = S(0.00122)\left[\frac{K_{ls}^{0.79} c_{pl,s}^{0.45} \rho_l^{0.49}}{\sigma^{0.5} \mu_l^{0.29} h_{fg}^{0.24} \rho_l^{0.24}}\right] \Delta T_{sat}^{0.24} \Delta P_{sat}^{0.75} \qquad (3.21)$$

with,

$$S = \frac{1}{1 + 2.53 \times 10^{-6} \left(\frac{G(1-x)D_h}{\mu_l}\right)^{1.17} F^{2.42}} \qquad (3.22)$$

The equilibrium quality x is calculated at the exit of the hottest element using the following equation;

$$x = \frac{q'(L_{fu} - L_b)}{\dot{m} h_{fg}} \qquad (3.23)$$

Here $q' = Q/L_{fu}$

Q = heat generation rate in the fuel element

L_{fu} = Length of fuel element

L_b = boiling length

The new clad surface temperature (T_s) is calculated at the inlet of the hottest channel. The temperature T_s is calculated using the heat

transfer coefficient, lower plenum coolant temperature and the prior heat flux (q").

The new and the old temperature profiles in the fuel plate are calculated assuming uniform heat generation within the fuel plate. The fuel clad surface temperature and heat flux which is zero at the fuel centerline are used as boundary conditions for the temperature profile calculation. The shaded area shown in figure 3.32 is the amount of heat that required by the fuel to establish the new temperature profile from the old temperature profile. By subtracting this amount of the heat from the input heat generation rate, the heat transferred to the coolant can be obtained (Q). By knowing the heat transferred to the coolant and the hot channel factor, the coolant exit temperature from the hottest channel is calculated. From the coolant exit temperature from the hottest channel, the maximum fuel centerline temperature and the maximum clad surface temperature are calculated. These procedures are continued until the coolant level drops below the downcomer top.

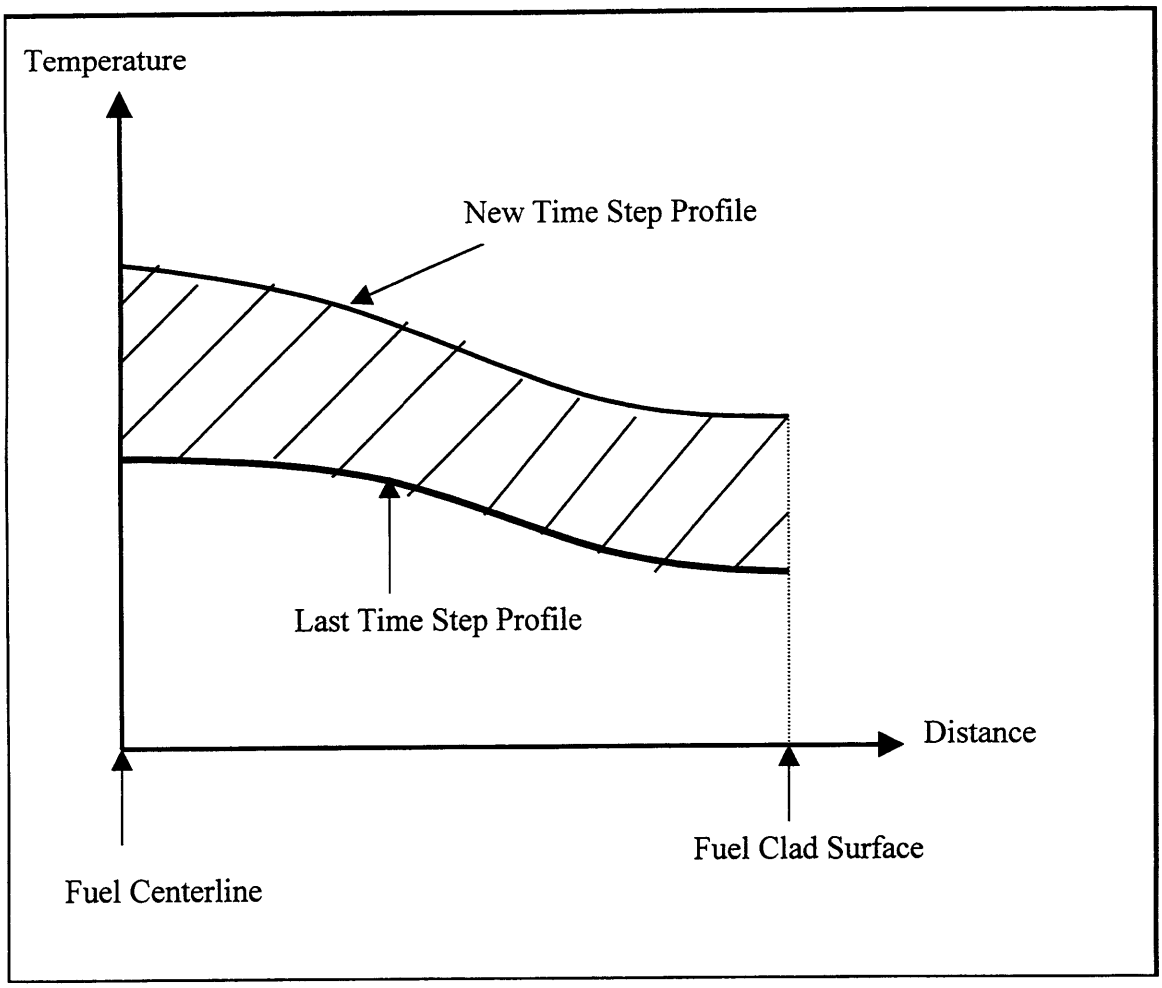

Figure 3.32: Demonstration of Heat Flux Calculation

7.5 Loss of Coolant Accident (Bounding Analysis)

The fission converter tank is made of 1/2 inch thick aluminum-6061. The structures around the fission converter tank are made of concrete and graphite. No sharp protruding objects are located near the

fission converter tank. It is impossible to identify a hole size in the fission converter tank that could be caused by a sharp object. Furthermore, the location of a hole on the fission converter tank cannot be identified. Hence the loss of coolant analysis is performed assuming that the fission converter tank's bottom plate fails completely and the coolant in the fission converter is drained within a second. The level detector in the fission converter will automatically actuate the MITR-II scram and the MITR-II reactor can be scrammed within a second. Therefore, heat generation in the fission converter is due to decay power during the period that the coolant in the fission converter tank is drained.

The maximum converter power is 250 kW when the MIT reactor power is 10 MW, coolant/moderator in the fission converter tank is light water, and fission converter fuel is fresh fuel. However, the decay power history is calculated assuming that the fission converter has operated at a full power of 300 kW for 5 year before it is shut down.

In a realistic case, the fission converter power will be at full power only during the irradiation of patient. An approximate patient irradiation time is 5 minutes. During the non-radiation period, the fission converter power will be at 2 kW or less (0.67% of full power). Therefore, the decay power history, which is calculated assuming fission converter power of 300 kW for a continuous 5 year period, is a very conservative value. The decay power history is shown in figure 3.33.

When there is no coolant in the fission converter tank, heat transfer from the converter fuel to the surrounding air by conduction and convection is neglected. It is assumed that the generated heat in the converter fuel is transferred by conduction to the front and the back end plates (along the X axis of figure 3.34), from the end plates heat is transferred to the front and the back plates of the fission converter tank, and from tank plates heat is transferred to surrounding structures by radiation heat transfer. As shown in figure 3.34, the heat flux q''_2 is negligible compare to the heat flux q''_1, because the composite resistance to radiation heat transfer in the Y direction is much higher than the resistance in the X direction. The surrounding structure in

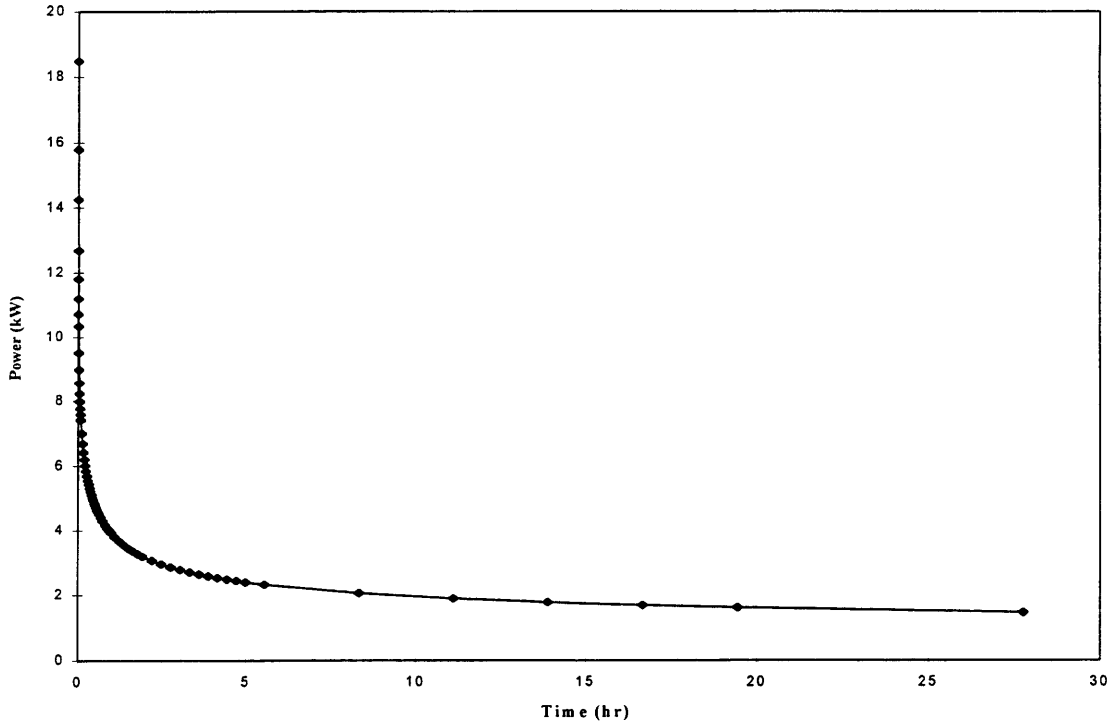

Figure 3.33: Decay Power in the Fission Converter after MITR-II Reactor Scram

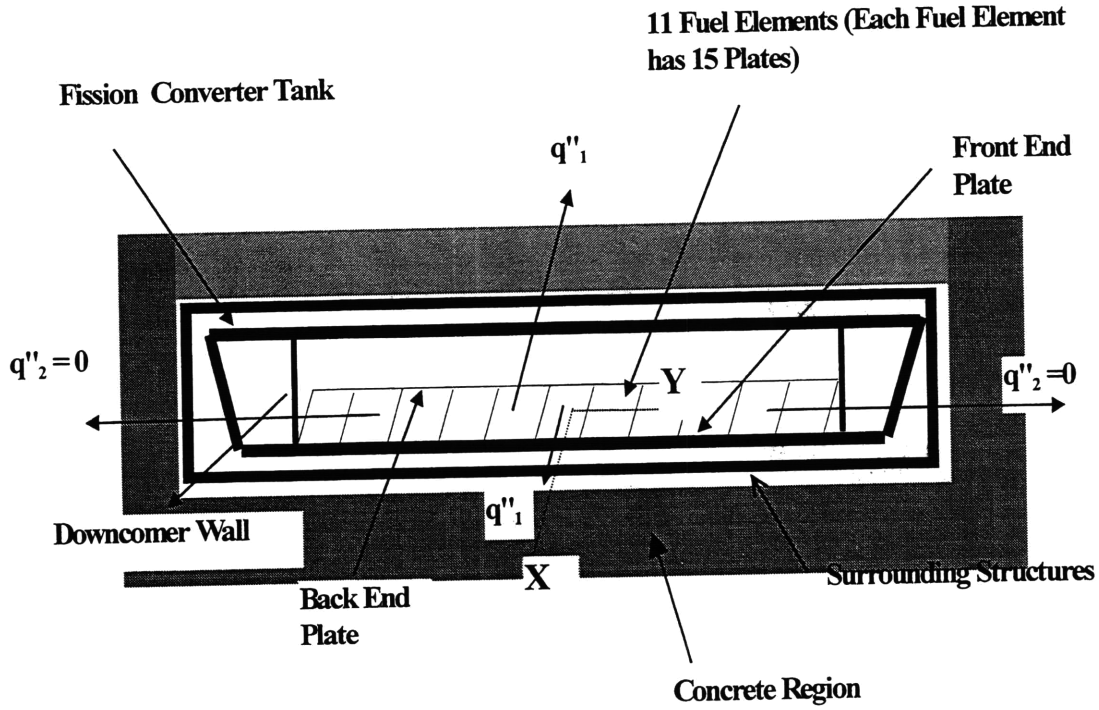

Figure 3.34: Plan View of Fission Converter Tank

the graphite region is at 150 ^{0}C and the concrete region temperature is less than 150 ^{0}C. For this analysis, the graphite and concrete region temperature is assumed to be 150 ^{0}C. All of the above assumptions are conservative. Therefore, the predicted fuel temperature will be higher than the real case. Since the maximum temperature will be observed on the hottest fuel plate (center fuel plate in the 6th fuel element from right to left), the hottest fuel plate temperature history has been calculated. The hottest fuel plate is depicted in figure 3.35. Due to symmetry, only ¼ of the fuel plate is modeled.

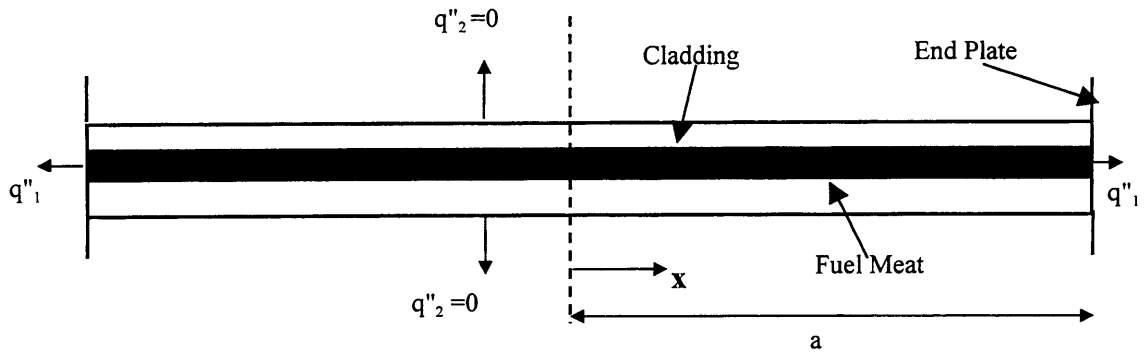

Figure 3.35: Hottest Fuel Plate

7.5.1 Initial Heat Up of Fuel Plate to 150 ^{0}C

There is no radiation heat transfer from the fuel to the surrounding structures until fuel temperature reaches 150 ^{0}C. During this period, the radiation heat transfer from the surrounding structures to the fission converter is negligible compared to the heat generation rate. Therefore the time for the fuel temperature to reach 150 ^{0}C from the 106 ^{0}C initial condition can be obtained from the following equation.

$$\left[\left(\rho c_p A\right)_f + \left(\rho c_p A\right)_c\right]\frac{dT}{dt} = q'''(t)\left(A_f + A_c\right) \qquad (3.24)$$

Here $q'''(t)$ is the heat generation rate in the hottest fuel plate, which is uniform in the X and Y directions. The subscripts f and c represent fuel and clad respectively. The expression for the heat generation rate was obtained by curve fitting the decay power history for the first 150 seconds. The decay power history for the first 150 seconds and the curve fit are shown in figure 3.36. Hence

$$q'''(t) = \frac{1120}{125}\left(\frac{2*10^{-7}*t^4 - 7*10^{-5}*t^3 - 0.0085*t^2 - 0.4301*t + 18.47}{4}\right)$$ (unit is watts) from t=0 to t=150 seconds. (3.24a)

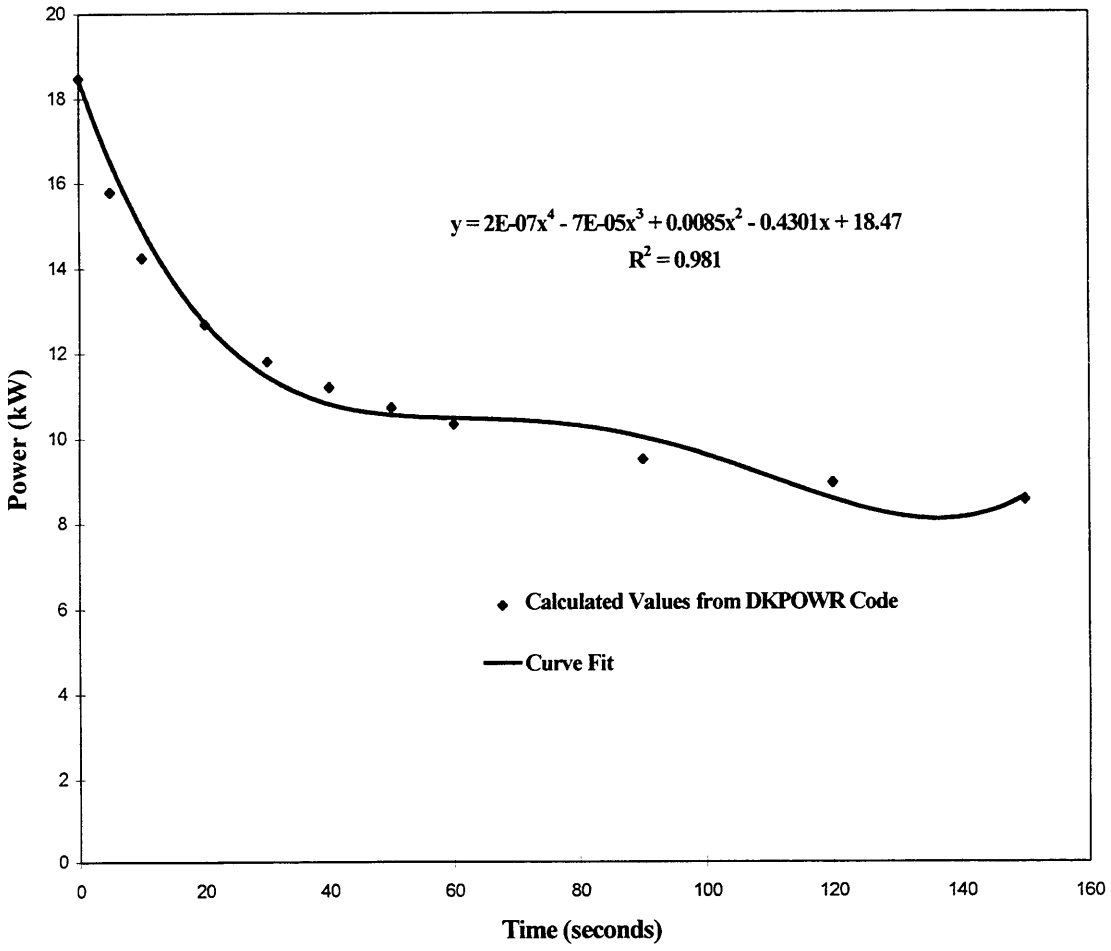

Figure 3.36: Decay Power in the Fission Converter From t=0 to t=150 seconds

The time for the fuel temperature to reach 150 ^{0}C from 106 ^{0}C is calculated to be 56 seconds (calculation is shown in the MathCad Worksheet in appendix B).

7.5.2 Calculation of Temperature History After Initial Heat Up

The temperature on the fuel plate (T (x, t)) can be obtained from the following partial differential equation after 56 seconds;

$$\left[\left(\rho c_p A\right)_f + \left(\rho c_p A\right)_c\right]\frac{\partial T(x,t)}{\partial t} = \left[\left(kA\right)_f + \left(kA\right)_c\right]\frac{\partial^2 T(x,t)}{\partial x^2} + q'''(t)\left(A_f + A_c\right) \qquad (3.25)$$

with the following boundary and initial conditions;

B.C. 1. $\frac{\partial T(x=0,t)}{\partial x} = 0$

B.C. 2. $-\left[\left(kA\right)_f + \left(kA\right)_c\right]\frac{\partial T(x=a,t)}{\partial x} = A_{rad} q_1'' = F_{12}\sigma(T(x=a,t)^4 - T_{sur}{}^4)$

I.C. T(x,t=0) = T_i (=423 K).

In equation (3.25a), the heat generation rate $q'''(t)$ is in the hottest fuel plate and it is taken uniform in the X and Y directions. The following expression for heat generation rate is obtained by curve fitting the decay heat after 56 seconds.

$q'''(t)$ = 48*(exp(-0.006*t)+exp(-0.00007*t)) (unit is watts) . from t=56 to t=35000 seconds (3.25a)

F_{12} is a radiation transfer factor between the fuel end plate and the surrounding structure (concrete and graphite). T_{sur}(=423 K) is the temperature of the surrounding structures. Here the unit of the temperature T(x, t) is Kelvin. The radiation heat flux is linearised as follows:

$$q_1'' = h_{rad}(T(x=a,t) - T_{sur})$$

$$\text{Here } h_{rad} = F_{13}\sigma 4\frac{1}{A_{rad}}\left(\frac{T(x=a,t)+T_{sur}}{2}\right)^3$$

Here A_{rad} is the surface area of a fuel plate for radiation heat transfer and

$$F_{13} = \frac{1}{\left(\frac{1-\varepsilon_1}{\varepsilon_1 A_{rad}}\right)+\left(\frac{1}{A_{rad} f_{12}}\right)+2\left(\frac{1-\varepsilon_2}{\varepsilon_2 A_{\tan k}}\right)+\left(\frac{1}{A_{\tan k} f_{23}}\right)+\left(\frac{1-\varepsilon_3}{\varepsilon_3 A_{wall}}\right)} \qquad (3.25b)$$

In equation (3.25b), ε_1 and ε_2 is a emissivity of aluminum oxide, ε_3 is a emissivity of concrete, A_{tank} is surface area of the tank front plate and also the tank back plate, A_{wall} is a surface area of the surrounding concrete structures and f_{12} and f_{23} are view factors from fuel plate to tank wall and tank wall to surrounding structures respectively. The subscripts 1, 2, and 3 represent the fuel end plate, the fission converter tank front and back walls, and the surrounding structures respectively. The h_{rad} is calculated for each time step using the prior time step temperature. The formulation of the problem in terms of $\theta = T - T_i$ is

$$\frac{1}{a_t}\frac{\partial\theta(x,t)}{\partial t} = \frac{\partial^2\theta(x,t)}{\partial x^2} + \frac{A_t q_0''(t)}{kA} \qquad (3.26)$$

with the following boundary and initial conditions

B.C. 1. $\dfrac{\partial\theta(x=0,t)}{\partial x} = 0$,

B.C. 2. $-kA\dfrac{\partial\theta(x=a,t)}{\partial x} = h_{rad}A_{rad}\theta(x=a,t)$

I.C. $\theta(x,t=0) = 0$.

Here $a_t = \frac{(kA)_f + (kA)_c}{(\rho c_p A)_f + (\rho c_p A)_c}$, $A_t = A_f + A_c$ and $kA = (kA)_f + (kA)_c$.

According to Duhamel's superposition integral, the solution for the equation(3.26) is

$$\theta(x,t) = D(0) * \psi(x,t) + \int_0^t \psi(x,t-s)\frac{dD(s)}{ds} ds \tag{3.27}$$

Here ψ(x,t) is a solution for equation (3.26) after replacing $q'''(t)$ by $q'''(t=0)$, $D(t) = \frac{e^{-bt} + e^{-dt}}{2}$, b=0.006 and d=0.00007.

We eliminate the difficulty arising from nonhomogenity of equation (3.26) by replacing $q_0''(t)$ by $q_0''(t=0)$, and expressing the fuel temperature as the sum of two temperatures in the form of

$$\psi(x,t) = \phi(x) + \vartheta(x,t)$$

Hence $\phi(x)$ satisfies

$$\frac{d^2\phi(x)}{dx^2} + \frac{A_t}{kA} * q_0''' = 0, \text{ with B.C.'s } \frac{d\phi(0)}{dx} = 0, \quad -kA\frac{d\varphi(a)}{dx} = h_{rad}A_{rad}\phi(a), \tag{3.28}$$

and $\vartheta(x,t)$ satisfies

$$\frac{\partial\vartheta}{\partial t} = a_t\frac{\partial^2\vartheta}{\partial x^2}, \text{ with B.C.'s } \frac{d\vartheta(0,t)}{dx} = 0, \; -kA\frac{d\vartheta(a,t)}{dx} = h_{rad}A_{rad}\vartheta(a,t), \text{and I.C}$$

$$\vartheta(x,0) = -\phi(x) \tag{3.29}$$

Here $q_0''' = q_0'''(t=0)$. The solution for equation (3.28) is

$$\phi(x) = -\frac{A_f q_0'''}{2kA}x^2 + \frac{A_f q_0''' a}{h_{rad} A_{rad}} + \frac{A_f q_0''' a^2}{2kA}.$$

A product solution $\vartheta(x,t) = X(x)\tau(t)$ is applied to equation (3.29) which upon application of the B.C.'s yields

$$\vartheta(x,t) = \sum_{n=0}^{\infty} C_n \cos(\alpha_n x) e^{-\alpha^2 n a_f t}$$

Here $\alpha = \frac{h_{rad} A_{rad}}{kA}\cot(\alpha a)$, and C_n is given by the following equation after applying the initial condition to $\vartheta(x,t)$;

$$\int_0^a -\phi(x)\cos(\alpha_n x)dx = C_n \int_0^a \cos^2(\alpha_n x)dx.$$

$$C_n = \left[\frac{A_f q_0''' \sin(\alpha_n a)}{2kA\alpha^3 n a}\left((\alpha_n a)^2 + \frac{2\alpha^2 n akA}{h_{rad} A_{rad}} - 2\right) - \frac{\sin(\alpha_n a)}{\alpha_n}\left(\frac{q_0''' a A_f}{h_{rad} A_{rad}} + \frac{q_0''' A_f a^2}{2kA}\right)\right]\left[\frac{1}{\frac{a}{2} + \frac{\sin(2\alpha_n a)}{4\alpha_n}}\right]$$

The solution for equation (3.26) after replacing $q'''(t)$ by $q'''(t=0)$ is

$$\psi(x,t) = -\frac{A_f q_0'''}{2kA}x^2 + \frac{A_f q_0''' a}{h_{rad} A_{rad}} + \frac{A_f q_0''' a^2}{2kA} + \sum_{n=0}^{\infty} C_n \cos(\alpha_n x) e^{-\alpha^2 n a_f t} \qquad (3.30).$$

After substituting expressions for $\psi(x,t)$, D(0) and D(s) into equation (3.27), the solution of equation (3) can be obtained. The solution, $\theta(x,t)$, is

$$\theta(x,t) = \vartheta(x,t) + \phi(x)\left(\frac{e^{-bt}}{2} + \frac{e^{-dt}}{2}\right) - \sum_{n=0}^{\infty} C_n \cos(\alpha_n x) e^{-\alpha^2_n a_t t}\left[\frac{b}{2}\left(e^{\left(\alpha_n^2 a_t - b\right)t} - 1\right) + \frac{d}{2}\left(e^{\left(\alpha^2_n a_t - d\right)t} - 1\right)\right] \tag{3.31}$$

The maximum temperature within the hottest fuel plate will be observed at x=0. The temperature history at x=0 is shown in figure 3.37 which indicates a maximum temperature of 337 at 3887 seconds.

7.5.3 Alternate Simple Calculation Approach

Another simple approach was taken to obtain the temperature history of the fuel clad. In this approach, all of the fuel plates are lumped together as a one solid mass. As before, conduction and convection heat transfer from this solid mass to the surrounding air is neglected compared to the radiation heat transfer. There is no radiation heat transfer from surrounding structures to the solid mass when the solid mass temperature is less than 150 ^{0}C. Until the temperature of the fuel mass reaches 150 ^{0}C, the solid mass temperature history can be obtained by equation (3.24). After the fuel reaches the temperature of 150 ^{0}C, there will be radiation heat transfer to the surrounding structures from the solid mass. During this period, the solid mass temperature history can be obtained from the following equation,

$$\left[\left(\rho c_p A\right)_f + \left(\rho c_p A\right)_c\right]\frac{dT}{dt} - q'''(t) + F_{12}\sigma(T(t)^4 - T_{sur}{}^4) = 0 \tag{3.32}$$

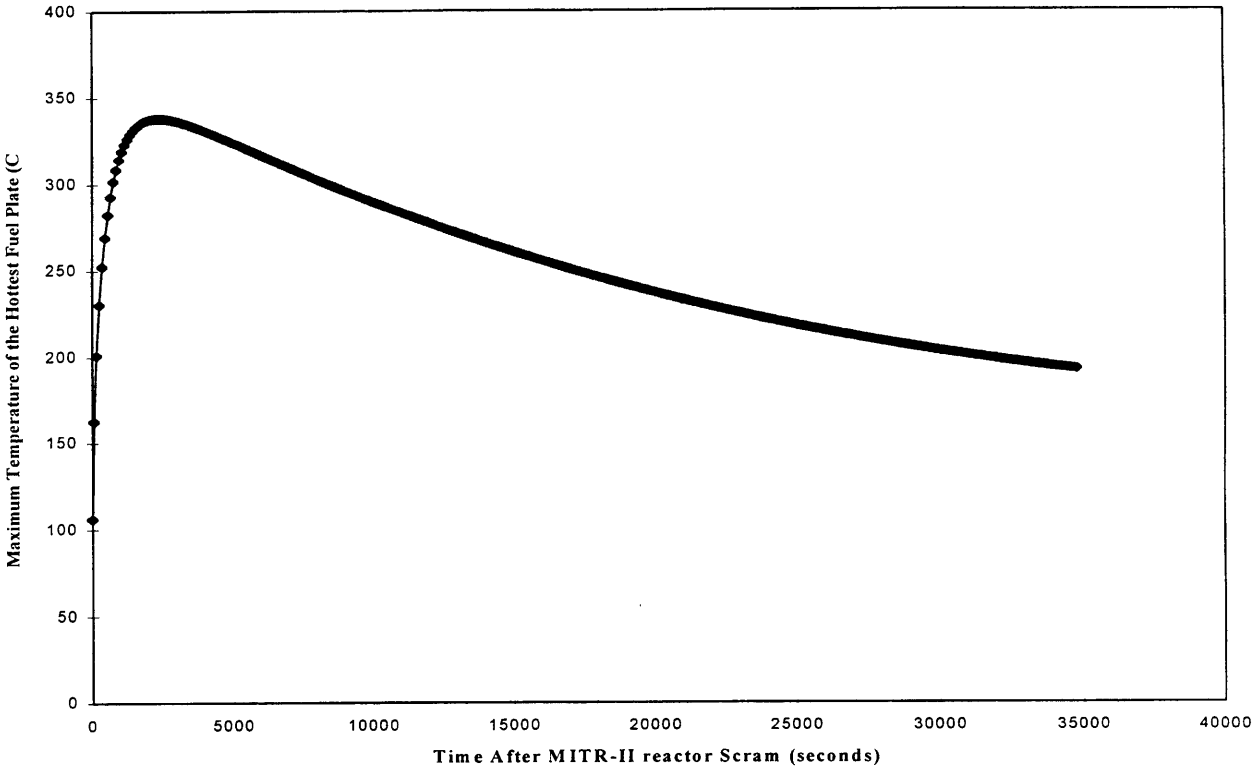

Figure 3.37: Temperature History Calculated from Equation 3.31

Even though it is hard to obtain an analytical solution for equation (3.32), the temperature history of solid mass can be obtained by calculating each term using prior time step information. This can be done in an EXCEL spread sheet. Figure 3.38 shows the resulting temperature history of the solid mass.

It is important to compare the solid mass assumption to the real case geometry which is shown in figure 3.34 and figure 3.35 since the solid mass temperature is different from the desired temperature, that of the centerline of the hottest fuel plate. Hence a further step is necessary in this simple analysis method to calculate this desired temperature.

Hence the center line (x=0, see figure 3.35) temperature is calculated at the

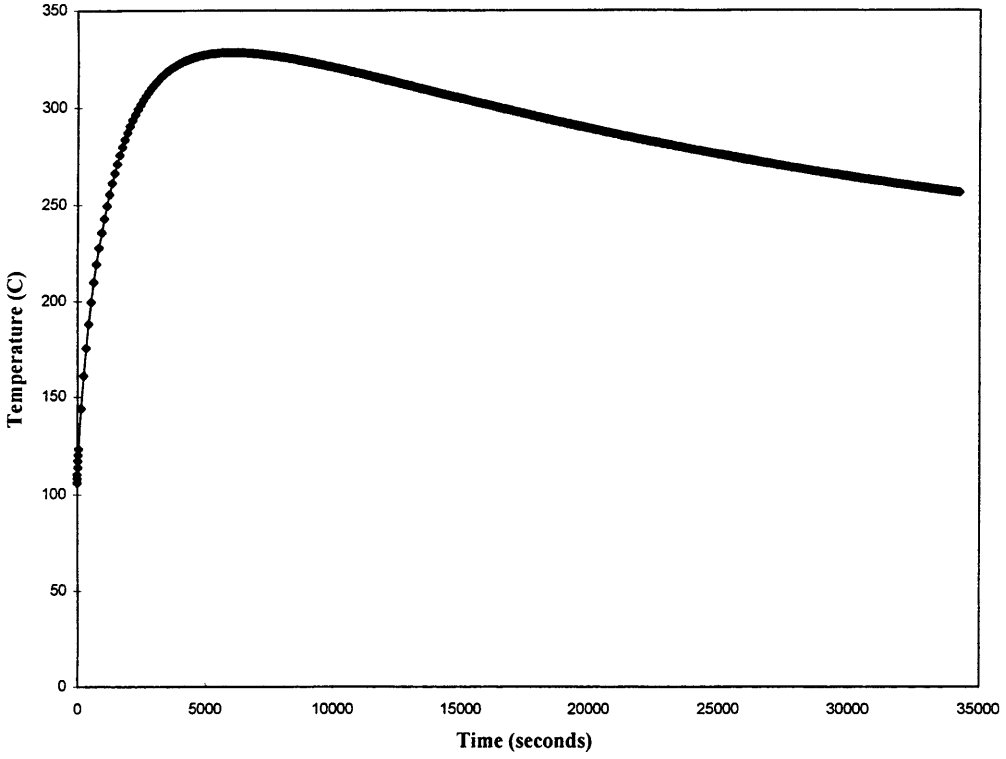

Figure 3.38: Solid Mass Temperature History

instant the solid mass temperature is maximum. The center line temperature for the hottest fuel plate is obtained by the following equation;

$$\left[(kA)_f + (kA)_c\right]\frac{d^2T}{dx^2} + q'''(t = t_m)\left(A_f + A_c\right) = 0, \qquad (3.33a)$$

subject to boundary conditions $\frac{dT(x=0)}{dx} = 0$, and $T(x=a) = T_m$ (3.33b)

Again due to symmetry only ¼ of the hottest fuel plate is analyzed. Here T_m is the maximum end plate temperature (taken as maximum solid mass temperature) and t_m is the time when the end plate temperature is at a maximum. The solution for the equation (10) is;

$$T(x) - T_m = \frac{-q'''(t = t_m)A_f}{2kA} x^2 + \frac{q'''(t = t_m)A_f}{2kA} a^2 \qquad (3.34)$$

The maximum temperature within the hottest fuel plate can be calculated by setting x=0 in equation(3.34). The temperature difference ($T(x=0)-T_m$) is obtained from equation (3.34) and added to the solid mass temperature history to obtain the center line temperature history. For comparison, the center line temperature histories calculated using two different approaches are plotted in figure 3.39. As can be seen in figure 3.39, the maximum temperatures calculated using two different approaches agree reasonably well. The time to reach the maximum temperature is different, because the hottest fuel plate will reach the maximum temperature first. The second approach is the average time for all of the fuel plates to reach the maximum temperature.

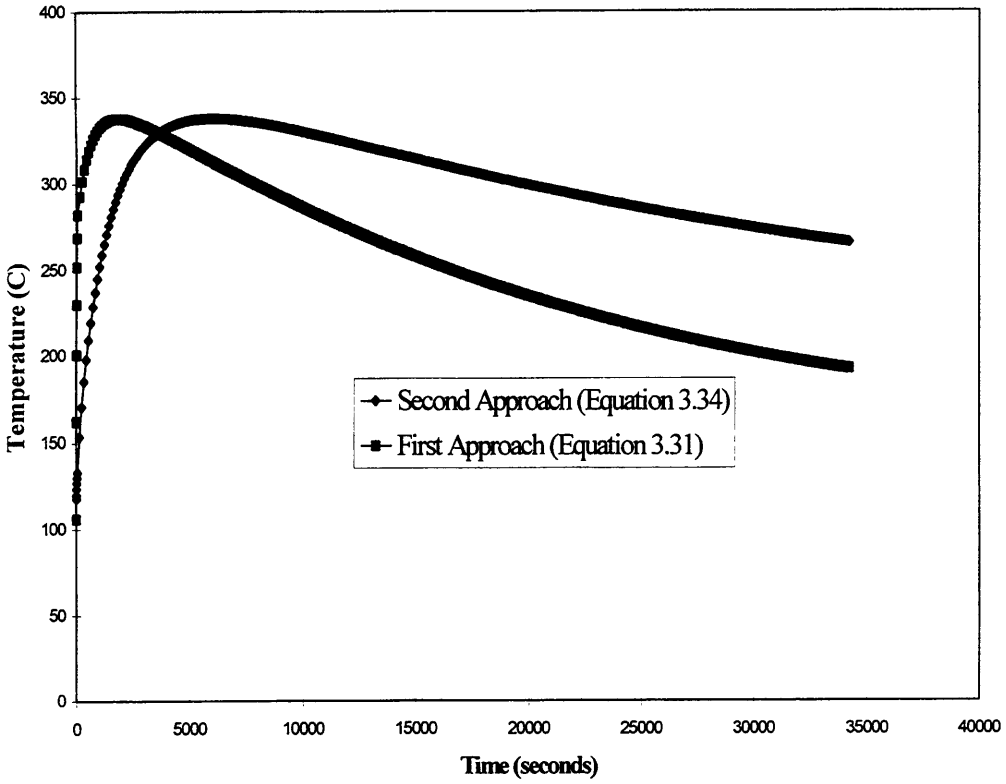

Figure 3.39: Comparison of Temperatures Obtained from Two Different Approaches

7.5.4 Effect of Emissivity Value Uncertainties

Different emissivity values for the aluminum oxide layer on a aluminum wall were found in the literature. The emissivity value ranges from 0.22 to 0.61[10]. In figure 3.40, the temperature histories calculated using first approach and different emissivity values are shown. As can be seen from the figure 3.40, the maximum temperature of the hottest plate does not rise above 450 ^{0}C, which is the aluminum softening point temperature.

7.5.5 Conclusions

The author has shown that during a massive LOCA the fuel clad temperature will not exceed 450 ^{0}C, after making the following conservative assumptions;

1. The fission converter power is assumed to be 300 kW,
2. The fission converter bottom fails and the coolant in the fission converter drains within a second,
3. The decay power in the fission converter is obtained assuming the fission converter is operated at a full power of 300 kW for 5 years,
4. The heat loss to the surrounding air due to conduction and convection is neglected.

Therefore it is safe to say that during LOCA fuel disruption will not occur.

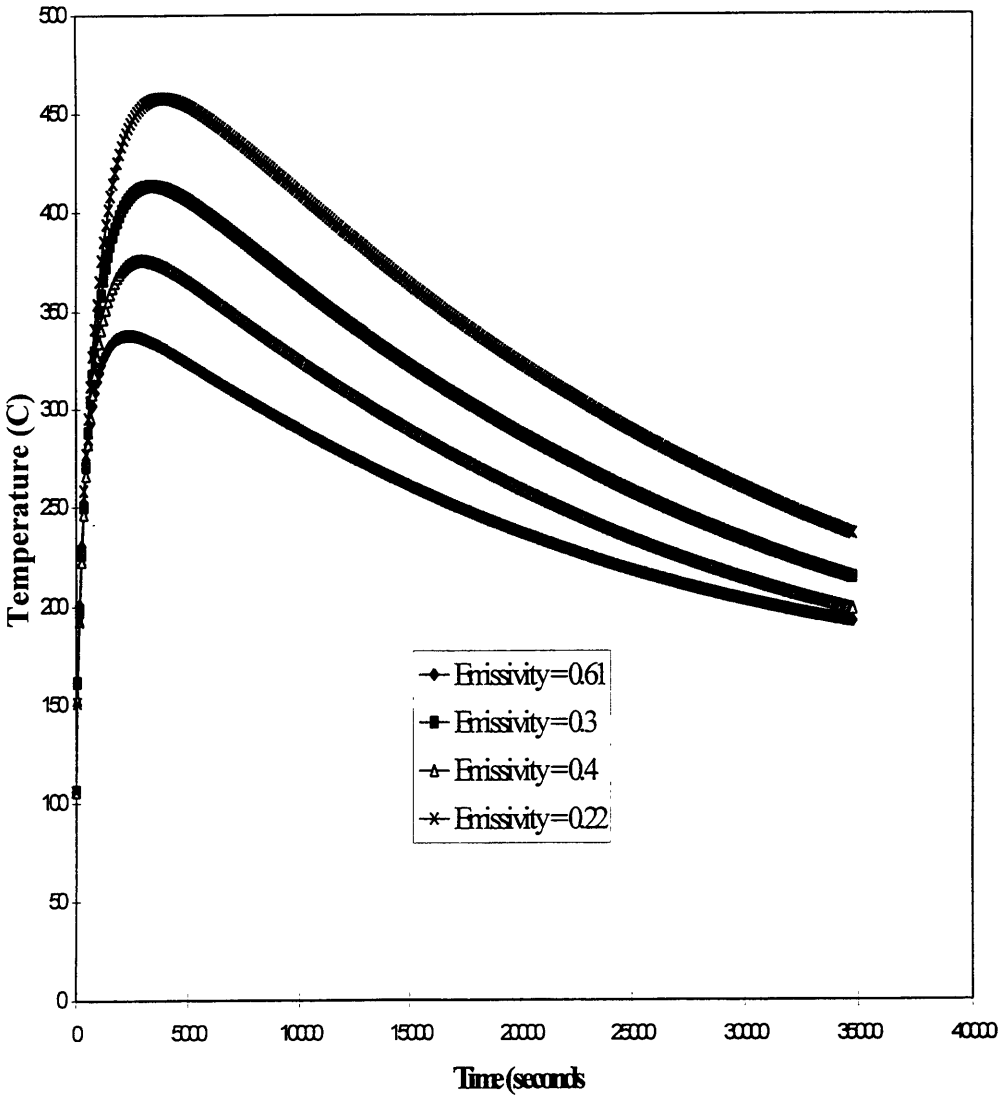

Figure 3.40: Temperature Histories for Different Aluminum Oxide Emissivity

8. CONCLUSION

As it has been demonstrated, all three designs satisfy the steady state and accident criteria design limits. All three designs satisfy the first design goal of no anti-siphon valve. However, for design I the normal operation hottest channel coolant exit temperature is higher than that of the design goal temperature of 60 ^{0}C. Hence, design I is not a viable option. It is also important to note that none of these three designs satisfy the third design goal of a limit of 10 minutes duration in the single phase region during LOF accident.

The design III was chosen as a viable design, because it is a simple design compare to the design II. Moreover, the primary flow rate is much smaller than that for the design II. Since the design III has two primary pumps, it can continue to be operated if one of them fails. Therefore, design III partially satisfies the third design goal. It is also important to note that it is an unlikely event for both primary pumps to fail simultaneously.

Even though the maximum converter power is 250 kW, it has been demonstrated that the converter system is safe for a power of 300 kW. All of the possible accidents have been analyzed and it has been shown that the fuel will not be disrupted.

9. References

1. Kiger III, W.S., *Neutronic Design of a Fission Converter-Based Epithermal Beam for Neutron Capture Therapy,* Nucl. Eng. Thesis, Massachusetts Institute of Technology, 1996.
2. Sakamoto, S., *Sensitivity Studies of the Neutronic Design of a Fission Converter-Based Epithermal Beam for Boron Neutron Capture Therapy,* SM Thesis, Massachusetts Institute of Technology, 1997.
3. Allen, G.C., *The Reactor Engineering of the MITR-II Construction and Startup,* Ph.D Thesis, Massachusetts Institute of Technology, 1976.
4. Kays, W.M., *Convective Heat and Mass Transfer,* McGraw-Hill Book Co., New York, 1966.
5. McGwire, M.J., *An Analysis of the Proposed MITR-III Core to Establish Thermal-Hydraulic Limits at 10 MW,* Ph.D. Thesis, Massachusetts Institute of Technology, 1995.
6. Sudo, Y., and Kaminaga, M., *A New CHF Correlation Scheme Proposed for Vertical Rectangular Channels Heated from Both Sides in Nuclear Research Reactors,* Trans. ASME, 115, 1993.
7. Mills, A.F., *Heat and Mass Transfer,* Richard D. Irwin, INC., 1995.
8. Rosenhow, W.M., *A Method of Correlating Heat Transfer Data for Surface Boiling of Liquids,* Trans. ASME, 74, 969-976, 1952.
9. Davis, E.J., and Anderson, G.H., *The Incipient of Nucleate Boiling in Forced Convection Flow,* AIChE J. 14:4:775,1966.
10. *CRC Handbook of Chemistry and Physics,* 53rd Edition, 1972-73.

CHAPTER FOUR

SHUTTERS AND MEDICAL ROOM DESIGN STUDIES

1.Introduction

Design studies of three shutters, cadmium shutter located between the reactor and the converter tank, water shutter and fast shutter, located in front of the patient irradiation position, and medical room are presented in this chapter. The purpose of having shutters is to control the dose rate in the medical room. These three shutters must attenuate fast neutrons by a factor of approximately 2.5E7 and gamma rays by a factor of approximately 6E6 such that the total dose rate at the patient position is in the range of one mrem/hr. These three shutters must be fully opened during the treatment period without altering the beam characteristics and should have a fail-safe mechanism. Detailed design studies of three shutters are given in subsection 2.

The medical room design studies involve design of shielding around the medical room so that personnel exposure outside the medical room is as low as reasonably achievable. The design of the medical room also includes design of an access door to the

The medical room design studies involve design of shielding around the medical room so that personnel exposure outside the medical room is as low as reasonably achievable. The design of the medical room also includes design of an access door to the medical room. Details about these shielding studies are given in subsection 6 of this chapter. Figures 4.1 and 4.2 are plan and side views of overall fission converter beam facility. In these figures, the shutters and the medical room layouts are also shown.

Description of computational tool and methods, which were used for the particle transport computation, are given in section 4 of this chapter.

2.Design Studies of Shutters

As was mentioned before, there are three shutters along the beam line. The first shutter, the cadmium shutter, is placed between the fission converter tank and the graphite reflector. The purpose of having a shutter before the fission converter tank is to control the thermal neutron flux incident on the converter fuel plates. The shutter is similar to control blades that are used to start up and to shut down a reactor. The cadmium shutter absorbs the incident thermal neutrons from the MITR-II reactor so that the fission converter power is reduced by 99.3%[1]. Since the thermal neutron flux incident on the converter fuel plates is reduced, fast neutron generation in the fuel elements is also reduced.

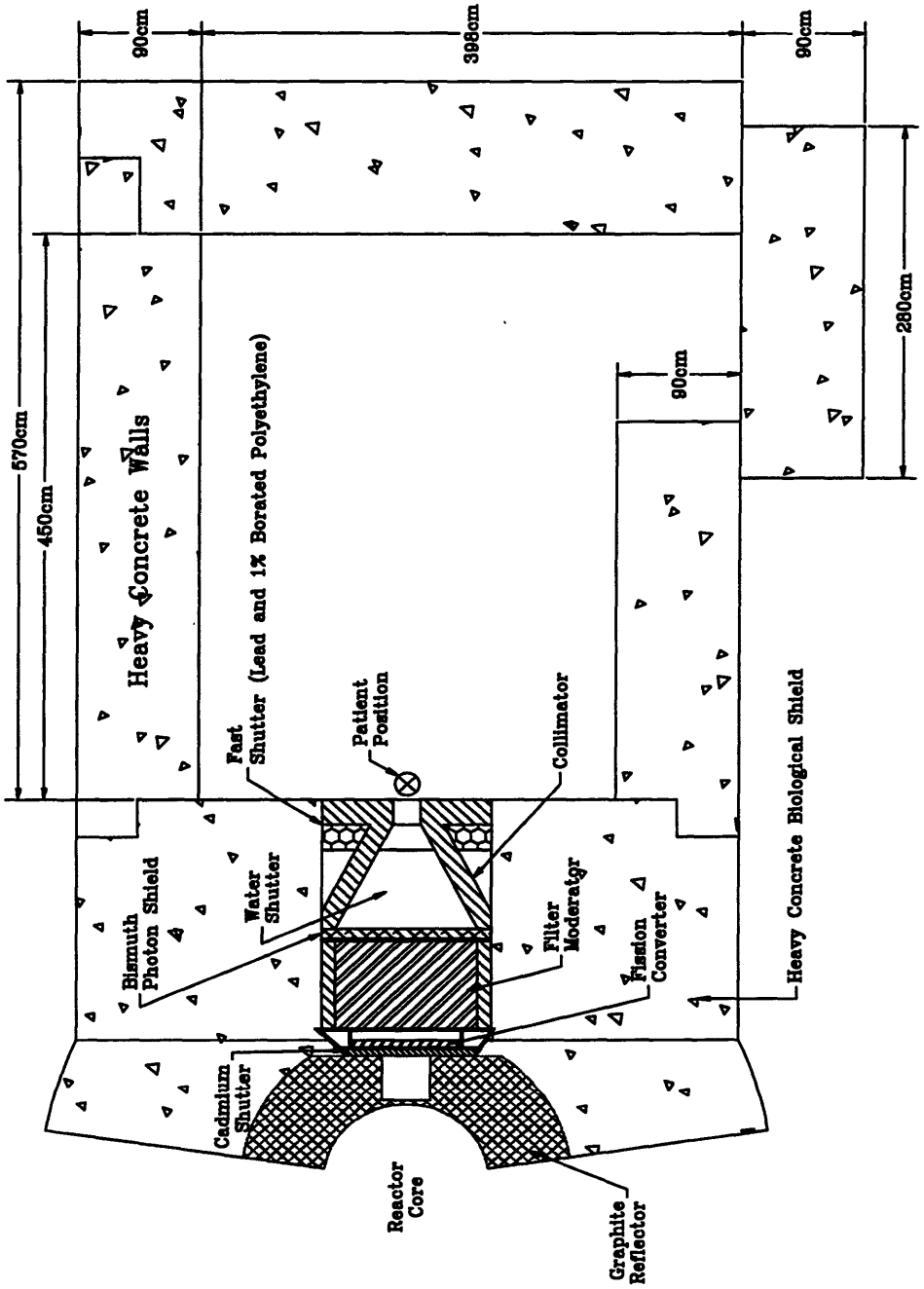

Figure 4.1: Plan view of the final shielding design of the fission converter beam facility, showing part of the MITR-II reactor and the converter facility in the thermal column.

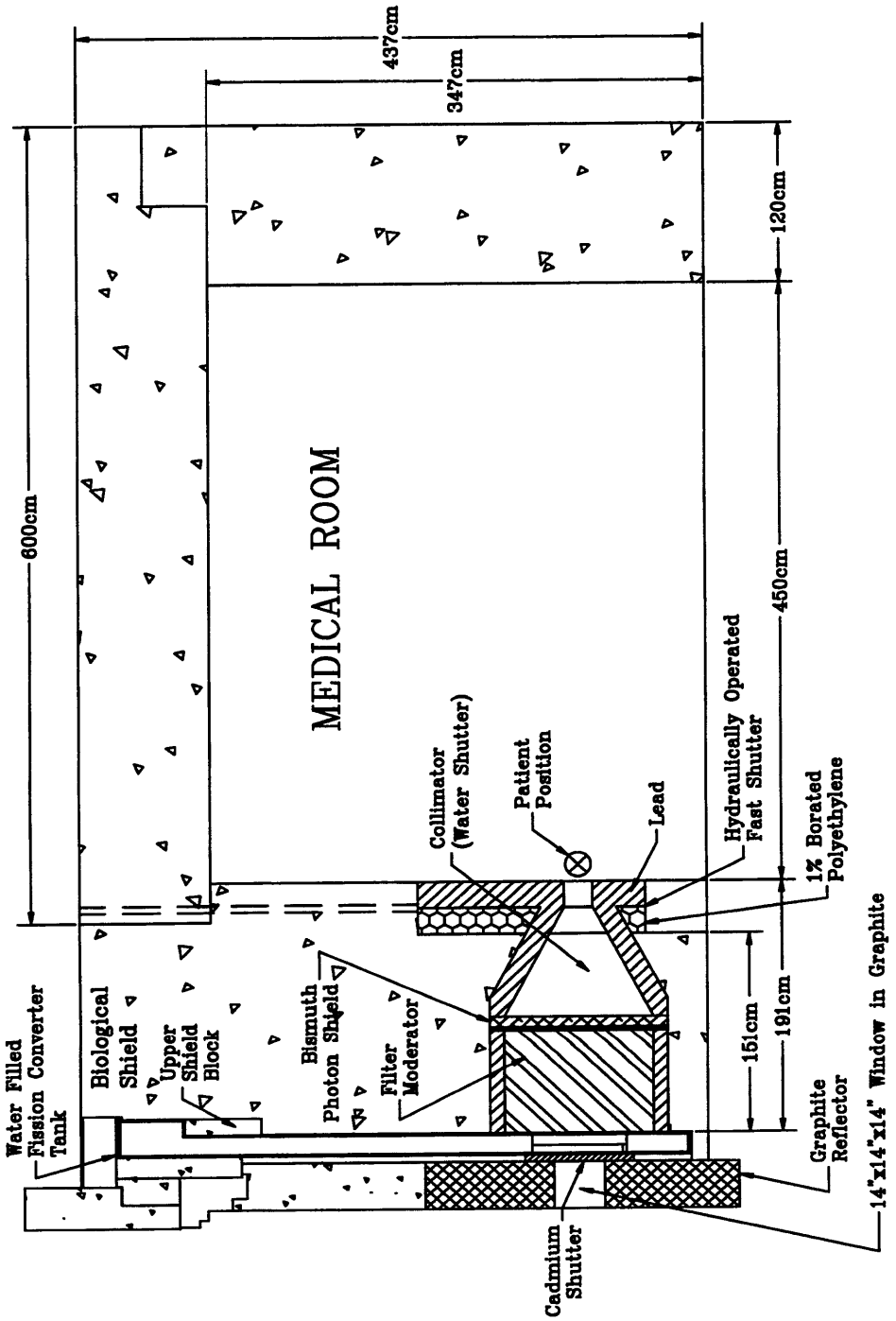

Figure 4.2: Side view of the final shielding design of the fission converter facility, show part of the MITR-II and the converter facility in the thermal column.

Therefore, the cadmium shutter serves two purposes; 1) reduces the power generation in the fission converter fuel elements to 0.7% by absorbing incident thermal neutrons and 2) reduces the fast neutron dose rate approximately by a factor of $\approx$100 at the patient position. The design and operating procedures for the cadmium shutter are given in the chapter 2.

The dose rate at the patient position when the cadmium shutter is fully closed is approximately 2E5 mrem/hr due to fast neutrons and 3E4 mrem/hr due to gamma rays. The quality factors used for these dose calculations are given in section 3. Therefore, it is evident that the cadmium shutter alone can not reduce the dose rate at the patient position to the design goal of 1mrem/hr. Therefore it is important to have more shutters before the patient position to further reduce the dose rate at the patient position. These shutters should have materials which attenuate fast neutrons and gamma rays. It is also evident that these shutters should attenuate fast neutrons and gamma rays by factors of 2E5 and 3E4 respectively.

The patient irradiation time can be less than two minutes. Since the irradiation time is short, it is important to control the beam as quickly as possible. Hence this shutter should be able to open or close quickly. Most importantly, the dose delivered to the patient during opening and closing of the shutters should be negligible compared to the target dose to the patient. Since it must be a fast acting shutter, the author will mention this shutter as a fast shutter in the proceeding text.

Since the fast shutter controls the dose rate to the patient and to the other personnel who work in the medical room, the fast shutter must have a fail-safe mechanism.

The patient position is shown in figures 4.1 and 4.2. The fission converter beam performances were calculated assuming the patient position shown in the figures 4.1 and 4.2. Moving the patient position further from the reactor core (moving towards medical room back wall) degrades the beam performance. Moving away 20 cm from the current position will reduce the epithermal neutron beam intensity by a factor of 1.7(see figure 5.23 in Ref. 1). Therefore, the fast shutter should be placed in front of the current patient position shown in the figures 4.1 and 4.2. However it is not a viable option to place the fast shutter in the space where the filter/moderator assembly is located. Placing the fast shutter in the filter/moderator assembly space requires to move the shutter and filter/moderator assembly vertically or horizontally during closing and opening of the beam. It is impossible to move the shutter and the filter/moderator assembly vertically or horizontally without major modification to the reactor biological shield and to the reactor floor. It is a design goal to avoid any major modification to the reactor biological shield. Therefore, the fast shutter should be placed within the collimator space to avoid any major modifications to the reactor biological shield.

Other additional requirements are that the shutter materials should be relatively inexpensive, readily available, and have good engineering properties.

2.1 Optimization of Shutters

The major objective of the shutter design study is to find an optimum arrangement of shutter or shutters to sufficiently reduce the dose rate at the patient position. The optimization should be found with regard to special quantities such as shutter weight, cost and thickness. It is also important to consider the constraints; dose rate at the patient position, geometry and structural consideration of the shutter and the shutter region, during the optimization process. The absolute optimum of the shutter arrangement can only be obtained if the considered optimization quantity is varied in all control variables such as materials and geometric consideration of shutter. This is practically impossible to attempt because it is a time consuming process and will also contribute to the total costs of the design. Therefore the number of variables must be reduced by reasonable preliminary decisions. It is also important to note that some of these variables are fixed in the shutter design due to the constraints. The other control variables, which are not fixed by constraints, are reduced by analyzing either with engineering judgement or simple analytical calculations. This reduces the number of control variables being analyzed to the capacity, which can be analyzed with a

numerical analysis code in a reasonable time frame. The analysis of each of the control variables is described in the following subsections.

2.1.1 GEOMETRIC CONFIGURATION OF THE SHUTTERS

As was mentioned before, the shutter position is somewhat fixed by the beam performance constraint. The fast shutter has to be before the patient position and after the photon shield (bismuth layer) in the filter/moderator arrangements. Since the shutter occupies the collimator space, it has to reconstitute the collimator shape when it is in open position and it should completely shut the beam when it is in closed position. Three possible shutter arrangements were considered for this design. These three shutter arrangements are:

1. Classic Slab Shielded Door
2. Rotating Collimator
3. Water Shutter plus Fast Shutter.

2.1.1.1 Classic Slab Shielded Door

Classic slab shielded door shutter is made of single material slab or succession of materials' slabs. A scaled vertical section of thermal column, filter/moderator assembly and a classic slab shielded door shutter design are shown in figure 4.3. One of the advantages of this design is that it is a simple design. The shutter moves up to open the beam and down to close the beam.

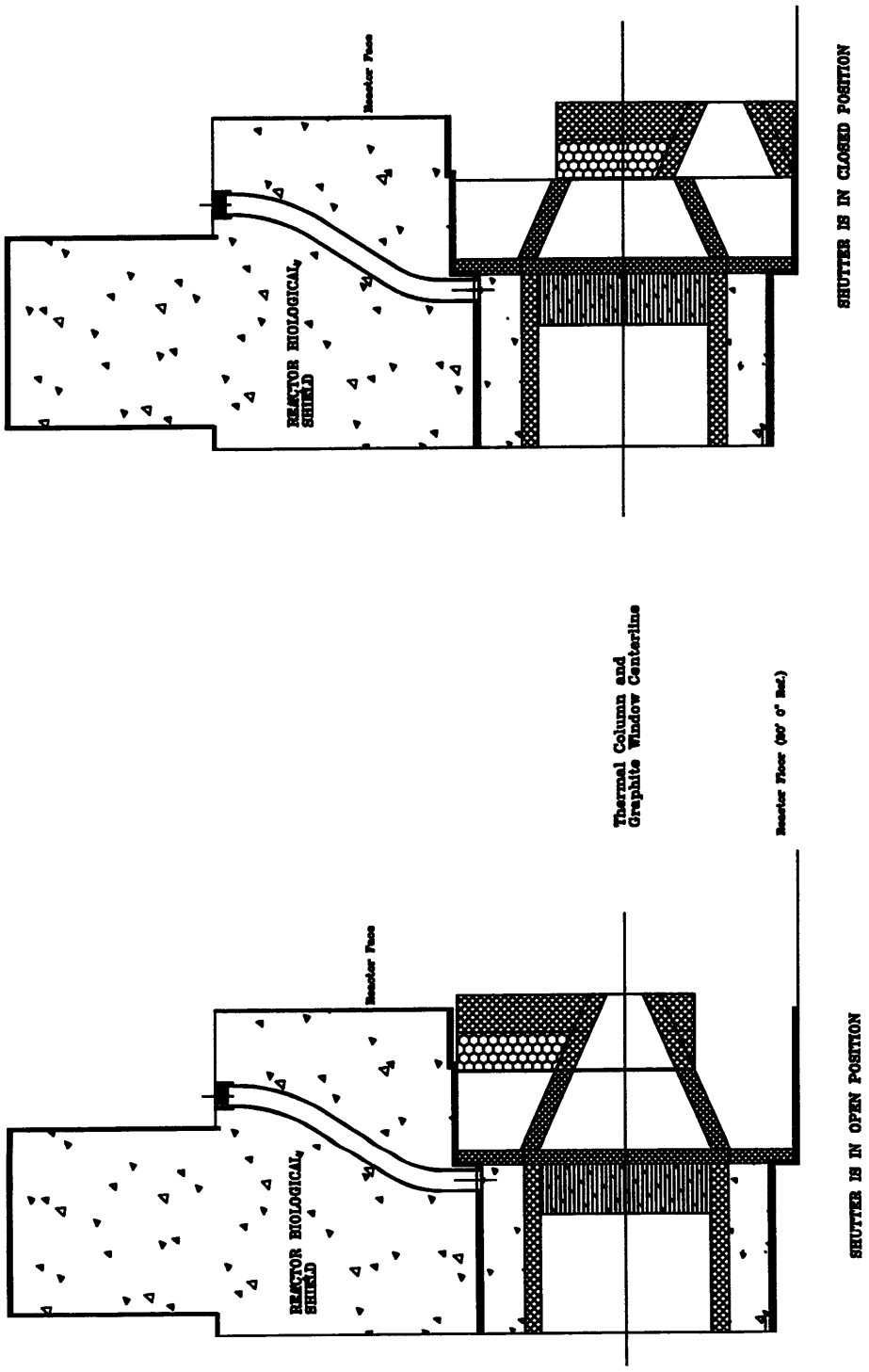

Figure 4.3: Vertical cross section of the thermal column, filter/moderator assembly, and fast shutter, showing in the open and close positions

Since the shutter moves down to close, it can close by its weight during any adverse conditions. Hence it has a fail-safe mechanism. Specially, during power failure conditions it can close the beam by its weight and assures the patient safety.

The figure 4.3 shows a part of the converter facility in the thermal column. Figure 4.3 depicts the shutter in the open and closed positions. If the shutter thickness is thicker than that shown in figure 4.3 (about 40 cm), the reactor floor and the reactor biological shield must be mined out to allow full closure and opening of the beam. If the shutter thickness exceeds the thickness shown in the figure 4.3, it is a disadvantage because the reactor biological shield and the reactor floor have to be modified.

As a next step, the slab thickness was calculated for different selected materials. An analytical calculation was carried out by Marc Ledieu (Exchange Student from Ecole Superieure D'Electronique DE L'Ouest) to determine the shutter thickness. It was calculated that 77 cm thick polyethylene and 38 cm thick lead slabs are required to reduce the dose rate at the patient position to about 0.1 mrem/hr. The calculation procedures are discussed in section 2.2. The total shutter thickness is much higher than that shown in figure 4.3. Therefore it is not a suitable design because it requires modifying the reactor biological shield and the reactor floor.

2.1.1.2 Rotating Collimator

The basic idea behind the rotating collimator is shown in figure 4.4. The whole collimator rotates to provide shielding when it is in the closed position. In the open position, the collimator shape is reconstituted, therefore no detriment to the beam performance is expected. As is obvious from the figure 4.4, it obviates the space requirements above and below the collimator, as is required in the classic slab shielded door design.

However, amount of shielding on the beam line is not sufficient in the closed position (shown by an arrow in the figure 4.4). There is no rotational position that can correct the lack of shielding. Therefore this is not a suitable design for further considerations.

2.1.1.3 Water Shutter plus Fast Shutter

The two geometric configuration studied above could not provide an acceptable design for the beam shutter. However, most of the shutter thickness in the classic slab shielded door design is due to the polyethylene thickness. Polyethylene was used to attenuate and to slow down fast neutrons. Since polyethylene and light water have a similar effect in stopping fast neutrons, a part of the polyethylene can be replaced by light water to reduce the slab thickness. This shutter arrangement is presented in figure 4.5. The analytical calculation for the classic slab shielded door design showed that the capture gamma ray dose is too high.

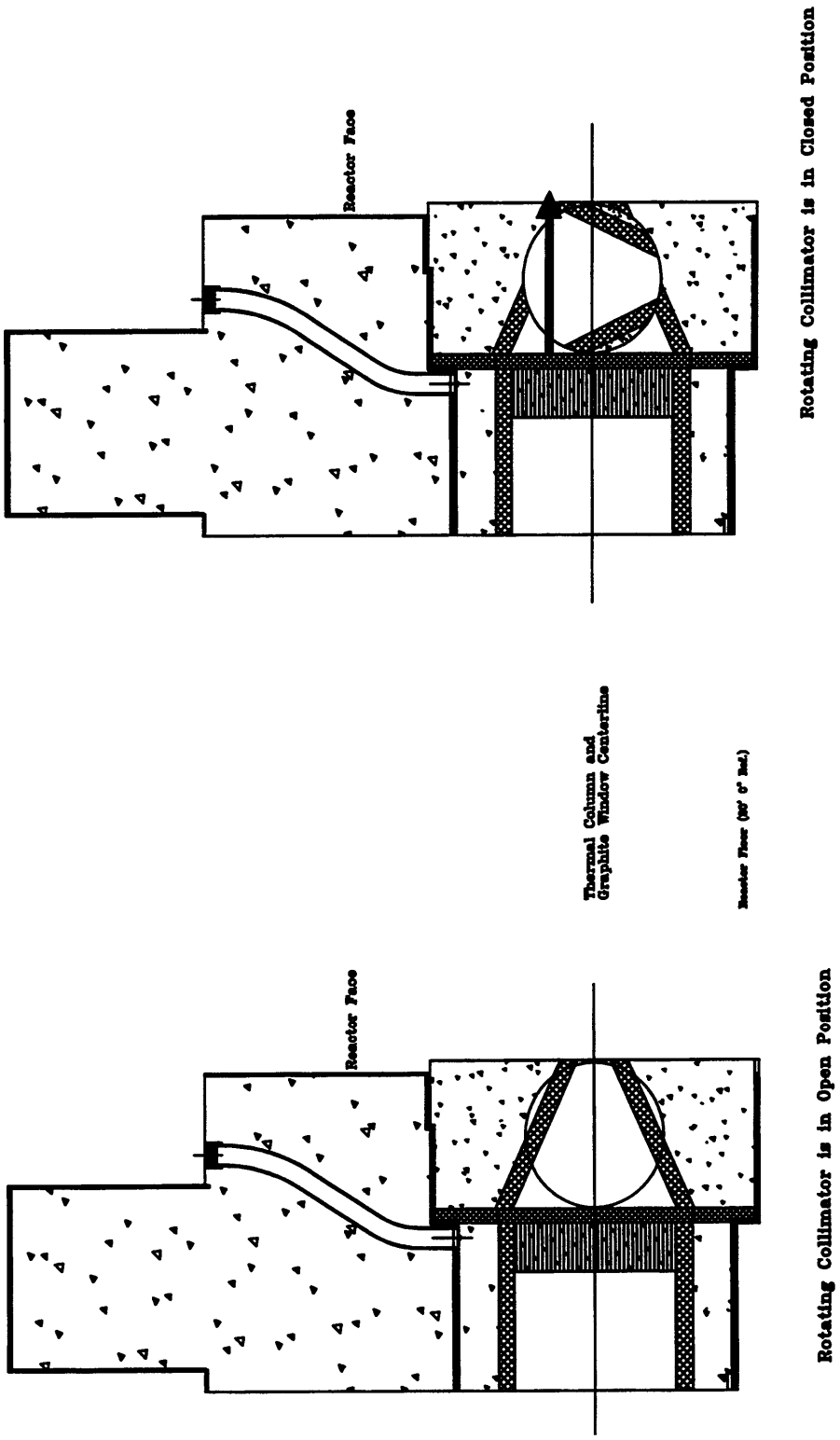

Figure 4.4: Showing rotating collimator arrangement in the opened and closed positions.

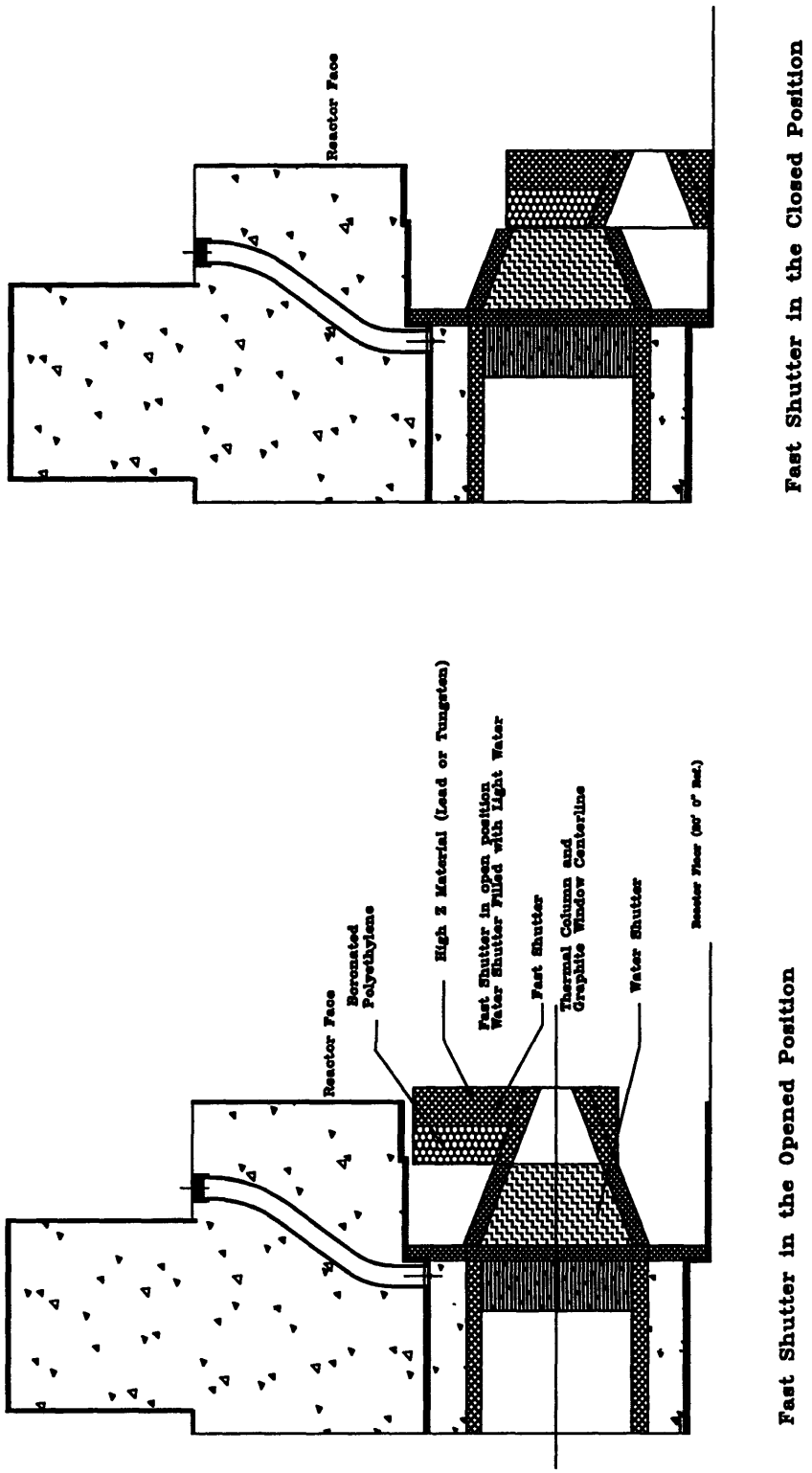

Figure 4.5: Water Shutter and fast shutter arrangement. The fast shutter is shown in the opened and closed positions.

Therefore boron is added to water to reduce the capture gamma rays. The best arrangement of shutters was calculated to be 75 cm thick 1% boronated water, 14 cm thick tungsten and 16 cm thick polyethylene. In this arrangement, the slab thickness is smaller than that shown in the figure 4.3. Hence this arrangement does not require any major modifications to the reactor biological shield and reactor floor.

To open the shutter, the water in the collimator has to be drained and the slab shutter should be moved upward. This slab shutter must reconstitute the collimator when it is in the open position. Since this shutter arrangement meets all the requirements, it was further analyzed with Monte Carlo code MCNP-4A.

2.1.2 MATERIAL SELECTION

It is important to select the right material or combination of materials such that the shutter thickness, cost, and weight can be optimized. These materials should be able to stop fast neutrons and gamma rays. Fast neutrons can be stopped either by first slowing them down and then absorbing the slowed down neutrons or by directly absorbing fast neutrons. The best materials for slowing down fast neutrons of $\approx$ 1 MeV are hydrogenous materials. Materials, which consist of elements like boron, have very high absorption cross-section for thermal neutrons. Therefore, hydrogenous materials plus high thermal neutron absorbing materials are very effective in attenuating fast neutrons. High Z materials are very

effective in attenuating the gamma rays. After careful consideration the following materials were considered for the shutter design.

1. Steel
2. Depleted Uranium
3. Tungsten
4. Lead and Lead Alloy

Steel can be used as shielding material for both neutrons and gamma rays. Steel is commonly used because of its structurally favorable properties, availability, and economy. Common practice is to use iron properties for the shielding analysis. Iron is relatively good for slowing down fast neutrons by inelastic scattering and is a good absorber of thermal neutrons. However, the secondary gamma rays produced by the capture of neutrons are high energy (up to 10 MeV) and these gamma rays are very penetrating. Since the neutron flux is high at the shutter position, it is not acceptable to use iron in the shutter design.

Depleted uranium is an another material used as a neutron-gamma shield. However, it not commonly used even though it is a good gamma ray shield, because it has a potential of fissioning if the neutron flux is high. As mentioned before, the neutron flux at the shutter position is considerable, therefore the use of depleted uranium is not a good choice. It is also expensive and a naturally radioactive α emitter.

Tungsten is primarily used as gamma ray shield, because of its high density (19.3 g/cm^3). When it is exposed to neutrons, secondary captured gamma rays are produced. It can be better utilized for the shutter along with boronated polyethylene because boronated polyethylene can drastically reduce the neutron intensity incident on the tungsten. The disadvantage is that the tungsten is very expensive compared to most of the neutron-gamma shield materials.

Pure lead (11.7 g/cm^3) is primarily used to shield gamma rays. It has a low thermal and fast neutron cross sections. It's shielding effect for neutrons and gamma rays is greatly improved if it is combined with high thermal and fast neutron cross section materials such as boronated polyethylene or boronated light water.

The above material selection process concluded that tungsten and lead along with boron and polyethylene are suitable for the shutter.

2.2 ANALYTICAL CALCULATION

As a first step in the shutter thickness calculations, gamma and neutron spectrums at the patient side of the bismuth photon shield were calculated for the cadmium shutter in the fully close position. This calculation was performed with the use of MCNP-4A. Details about the MCNP-4A calculations are given in section 3. The MCNP-4A computational

results of neutron and gamma spectra at the surface of the bismuth layer are shown in figure 4.6 and 4.7 respectively.

These spectra were calculated for the conditions of 5 MW MITR-II reactor power, eleven fresh MITR-II fuel elements in the fission converter tank, heavy water coolant in the fission converter tank and filter/moderator composed of 68 cm 70% AlF_3/30%Al + 2 cm Ti.

Fast neutron attenuation was calculated by two methods. In the first method, the 8 MeV total neutron removal cross-section was used for the fast neutron attenuation calculation. The commonly used 1 MeV total neutron removal cross section was not used in the fast neutron shielding calculation, because C. Flores[2] and R. Rogus[3] concluded in their studies that it is too high. Furthermore they were able to obtain reasonable results using the 8 MeV cross section data. In the second method, the total neutron removal cross-section as a function of energy was used for the neutron shield calculation. These cross section data were obtained from BNL 235 Neutron Cross Section data book. The following equation was used to calculate the fast neutron attenuation;

$$D = D_{in} \exp[-(\sigma_O n_O a + \sigma_H n_H a + \sigma_F n_F b)]$$

Here σ = Neutron removal cross-section,

D = fast neutron dose rate after the shutter,

Din = fast neutron dose rate before the shutter,

n = atomic density,

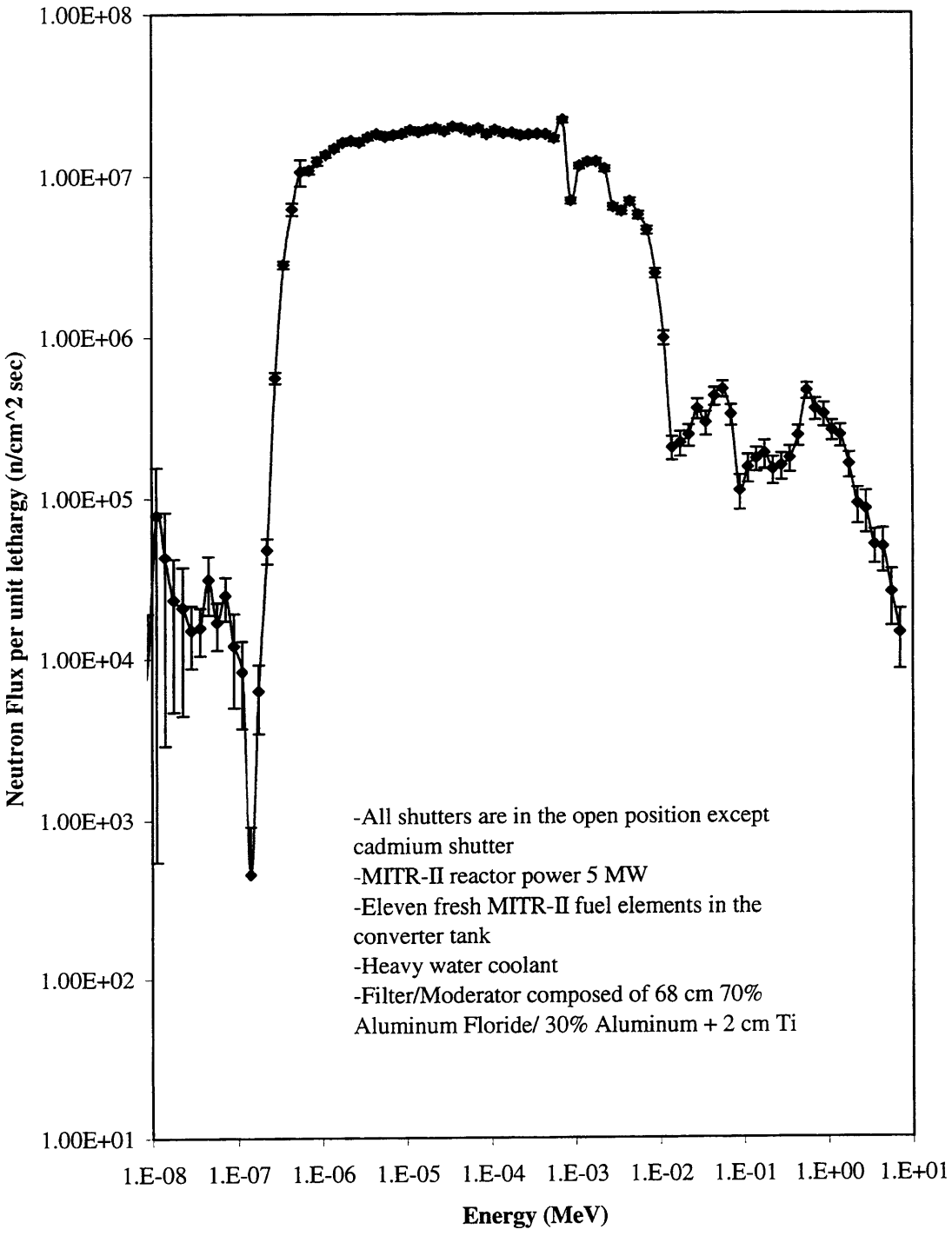

Figure 4.6: Neutron spectrum tallied beyond the photon shield. (All the shutters are in the opened position except the cadmium shutter.

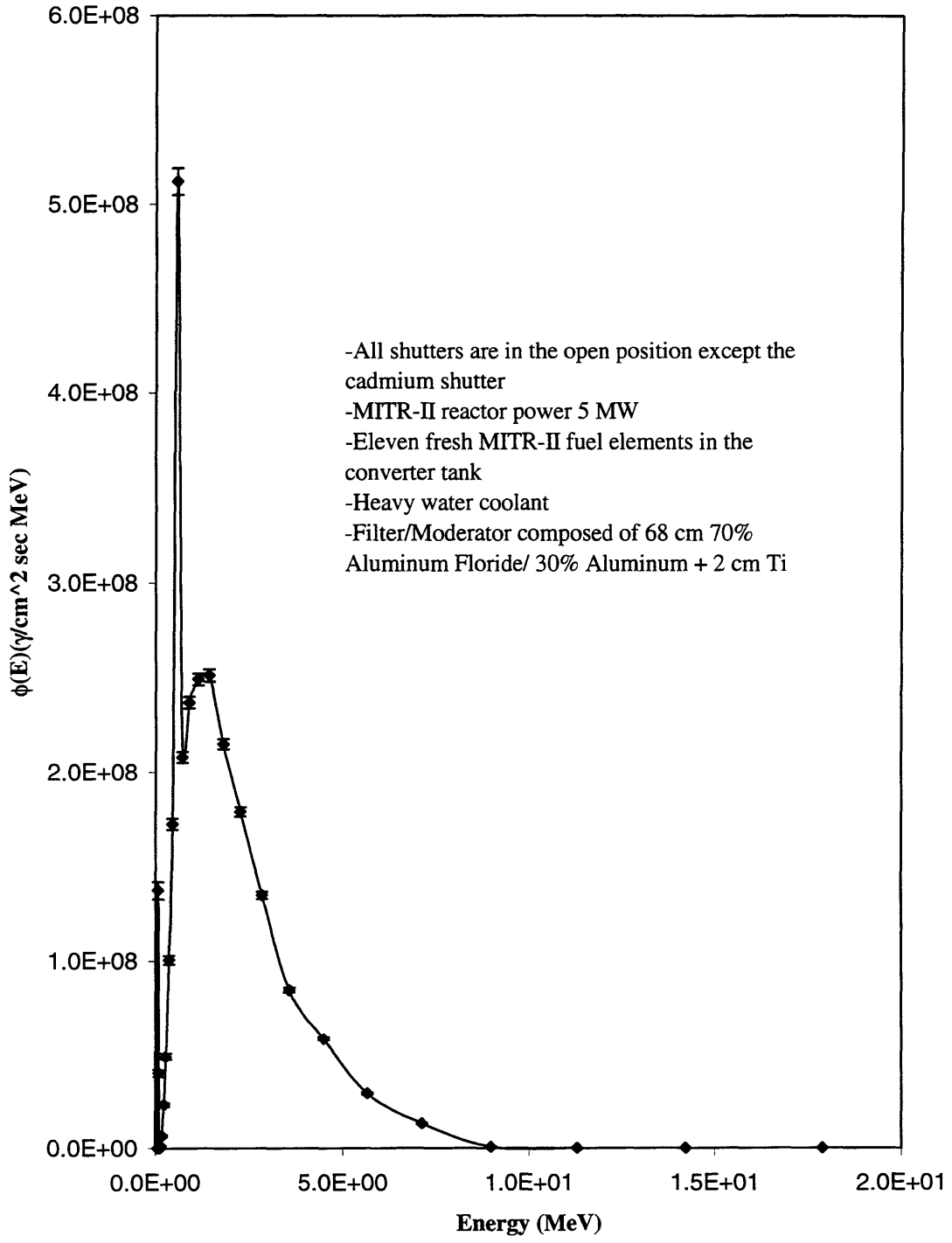

Figure 4.7: Photon spectrum tallied after the photon shield (All the shutters are in the opened position except the cadmium shutter)

a = water shutter thickness, and

b = fast shutter thickness (lead or tungsten)

The subscripts O, H and F are for oxygen, hydrogen and fast shutter material (either lead or tungsten) respectively.

The commonly used 3 MeV gamma ray linear attenuation coefficient was used in the gamma shield calculation. The following equation was used to calculate the gamma attenuation;

$$D_{\gamma} = D_{\gamma,in} B(\mu t, E) \exp(-\mu t)$$

Here μ = gamma attenuation coefficient,

Dγ = gamma dose rate after the shutter,

Dγ,in = gamma dose rate before the shutter,

T = shielding thickness,

B(μt,E) = buildup factor.

The buildup factor was calculated using Capo's formula[5].

Analytically calculated results are shown in the following table. Since the neutron spectrum and total removal cross section as a function of energy were used in method 2, the method 2 result is more reliable than the method 1 result. In all cases, the shutter thickness was calculated such that the total dose rate at the patient position from the neutrons and the gamma rays is 1 mrem/hr with a safety factor of 10 or calculated to be 0.1 mrem/hr. The quality factors given in section three was used here.

Table 4.1: Analytical Calculation Results

	Fast Acting Mechanical Shutter			Water Shutter	Dose Rates at the Patient Position	
Shutter	Tungsten Thickness	Lead Thickness	Boronated Polyethylene Thickness	Boronated Light Water Thickness	Total Neutron Dose rate	Total Gamma Dose rate
Classic Slab Shield Door (Method 1)	0	38 cm	132 cm (no boron)	0	0.1 mrem/hr	0.1 mrem/hr
Classic Slab Shield (Method 2)	0	38 cm	77 cm	0	0.093 mrem/hr	0.1 mrem/hr
Water Plus Fast Shutter	14 cm	0	16 cm	75 cm	0.14 mrem/hr	0.11 mrem/hr

The analytically calculated results were recalculated using MCNP-4A. The MITR-II, fission converter, the collimator, and the shutter MCNP-4A

models are discussed in section 3. The computational methods also discussed in section 3.

3.Computational Method

The primary computational tool used for the shielding calculations was MCNP (Monte Carlo N-Particle); a general purpose, generalized geometry Monte Carlo Radiation transport code. MCNP has the ability to simulate transport of neutrons, photons and electrons. MCNP can transport either independently or coupled neutron/photon/electron mode.

W.S. Kiger[1] initially chose MCNP over the other codes for the neutronic studies of the fission converter beam for the following reasons:

1. "MCNP employs generalized geometry modeling allowing full three dimensional representation of complex structures and it correctly simulate transport effects.
2. The use of point-wise continuous energy cross-sections in MCNP eliminates the need for collapsing data into multi-group cross sections and accurately treats resonance scattering which is essential in neutronic studies.
3. Several different continuous energy cross section evaluations based on ENDF/B-V are included in the code package.

4. The MCNP code has been benchmarked against neutron, photon, and criticality experiments, providing a high degree of confidence in its physics representation"[1].

The same code was also used by S.Sakamoto[4] in his neutronic studies of the fission converter beam. MCNP was the author's choice to simulate the shielding computations because shielding studies are somewhat a continuation of the neutronic studies. Furthermore the MITR-II reactor and a part of the overall fission converter facility were already modeled and benchmarked. Although MCNP provides accurate results for correctly modeled problems, it requires many hours of computer time for each simulation carried out for the shielding computation. The other disadvantage of using MCNP as the computational tool is the statistical uncertainty associated with each tally, which is due to the stochastic nature of the Monte Carlo technique. It is recommended in the MCNP manual that the statistical uncertainty should be less than 10%. If the statistical uncertainty is greater than 10% no conclusions can be reached from the results obtained from the MCNP simulations.

The main objective of this study is to obtain the dose rate at the patient position with shutters closed and outside of the medical room with shutters open. The shutters and the medical room wall thickness were designed such that dose rates are in the range of ≈ 1 mrem/hr at the patient position with beam off and the outside of the medical room walls with beam

on. Furthermore, the dose rates at the patient position were calculated for different combinations of shutters in the open and closed positions.

The simulation steps, which were followed for the shielding computations, are given in figure 4.8. As a first step a criticality calculation of the MITR-II core model alone in neutron only mode is simulated to create a surface source of neutrons at the edge of the graphite reflector. This surface source was created by simulating E.Redmond's[8] MITR-II reactor model. Then the neutrons recorded at the edge of the graphite surface are transported in neutron and photon mode to the patient position and outside the medical room. The neutron and photon fluxes were tallied at the patient position and outside the medical room. Then these fluxes were converted to kerma rates. The quality factors and fluence per unit dose equivalent for neutrons were obtained from 10CFR Part 20 and they are listed in table 4.2.

For gamma rays, the conversion factors from flux to dose equivalent (D) are calculated using the following equation[5]:

$$D = \frac{\phi E \frac{\mu}{\rho} 1.6 * 10^{-6}}{100}$$

Where ϕ = Flux (n/cm^2 sec), E = Energy (MeV), $\frac{\mu}{\rho}$ = Mass attenuation coefficient of gamma rays in air (cm^2/g), and D = Gamma dose rate (rem/s).

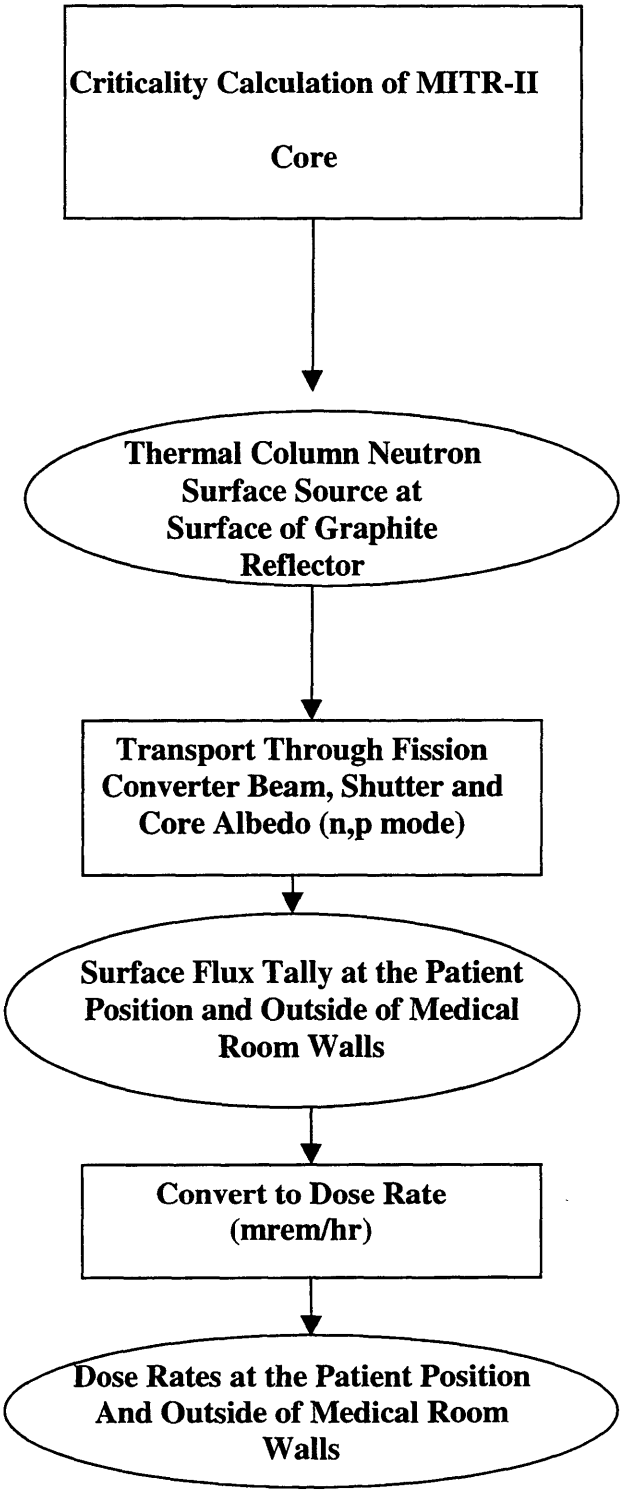

Figure 4.8: Simulation Steps of MCNP Calculations for Shutter and Medical Room Wall Thickness

Table 4.2: Mean Quality Factors and Fluence per Unit Dose Equivalent for Monoenergetic Neutrons[9]

Neutron Energy (MeV)	Quality Factor	Fluence/dose equivalent (neutrons cm^{-2} rem^{-1})
2.5E-8	2	980E6
1E-7	2	980E6
1E-6	2	810E6
1E-5	2	810E6
1E-4	2	840E6
1E-3	2	980E6
1E-2	2.5	1010E6
1E-1	7.5	170E6
5E-1	11	39E6
1	11	27E6
2.5	9	29E6
5	8	23E6
7	7	24E6
10	6.5	24E6
14	7.5	17E6
20	8	16E6

W.S. Kiger[1] and S.Sakamoto[2] utilized the same decoupling which effectively decoples the converter and the MITR-II core models.

Since the converter is driven by the MITR-II core, the MITR-II core and the converter form a coupled system. Even though the MITR-II drives the converter system, the effect on the MITR-II due to the presence of the converter is very weak because the converter and the MITR-II are separated by so much heavy water, graphite, and distance. Since the converter system produces fewer neutrons than that produced in the MITR-II core, the feed back from the converter to the reactor does not significantly change the power distribution in the MITR-II core. However, a method of computation that effectively decouples the converter and the MITR-II core models, increases the speed and the computationally efficiency. The same decoupling method was utilized in the shutter thickness and the medical room wall thickness calculations. Chapter 4 in Ref. 1 has shown that this decoupling methodology retains the accuracy of the coupled model due to the weak feedback from the fission converter.

3.1 Reactor Model

E.Redmond[6] originally modeled the MITR-II in full three dimensions in MCNP. The MITR-II model in MCNP is plotted in figures 4.9, 4.10 and 4.11.

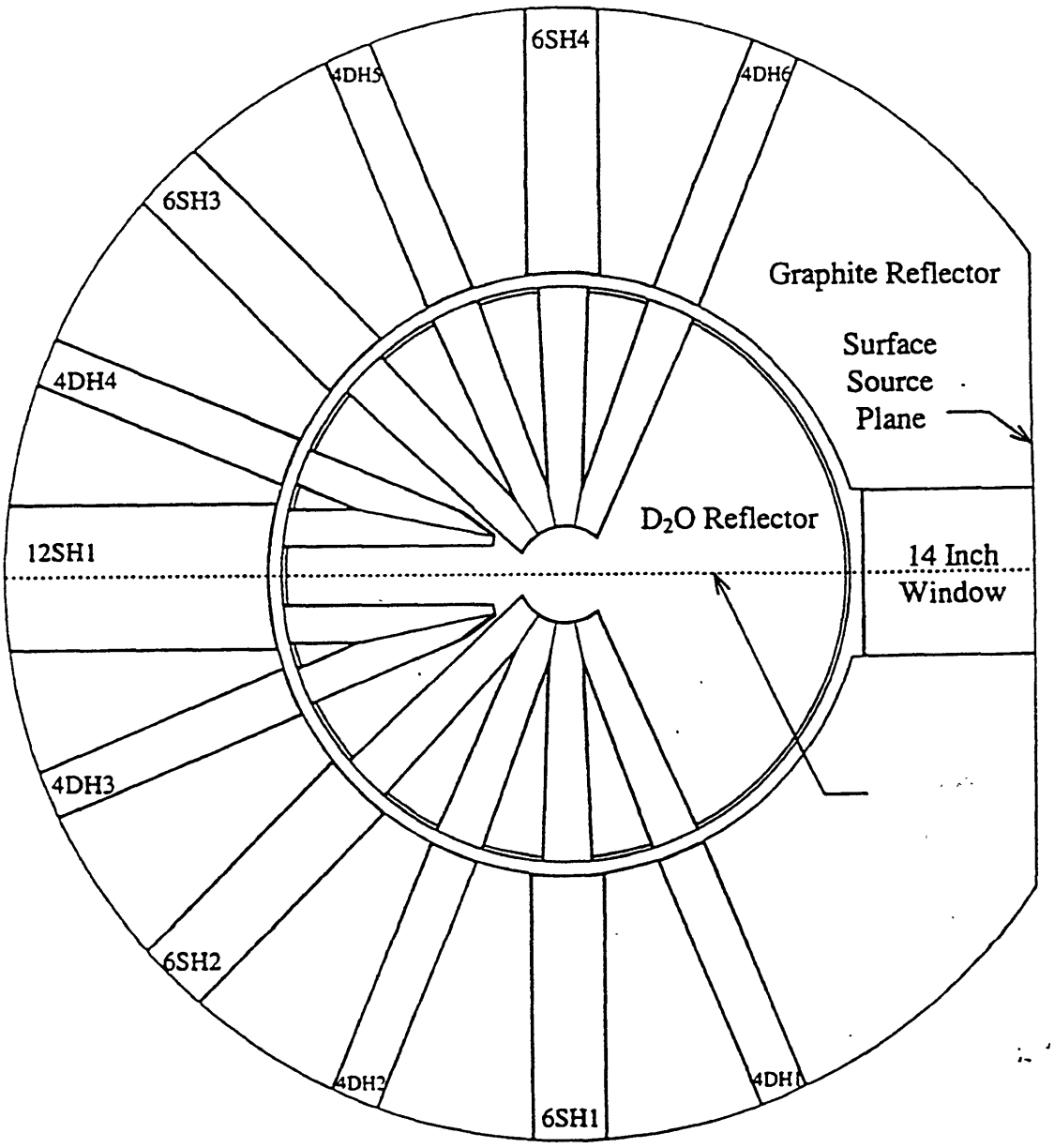

Figure 4.9: Horizontal cross section at the beam tubes' centerline. The vertical cross sectional view through the dashed line is shown in figure 4.11.

(Courtesy of W.S.Kiger)

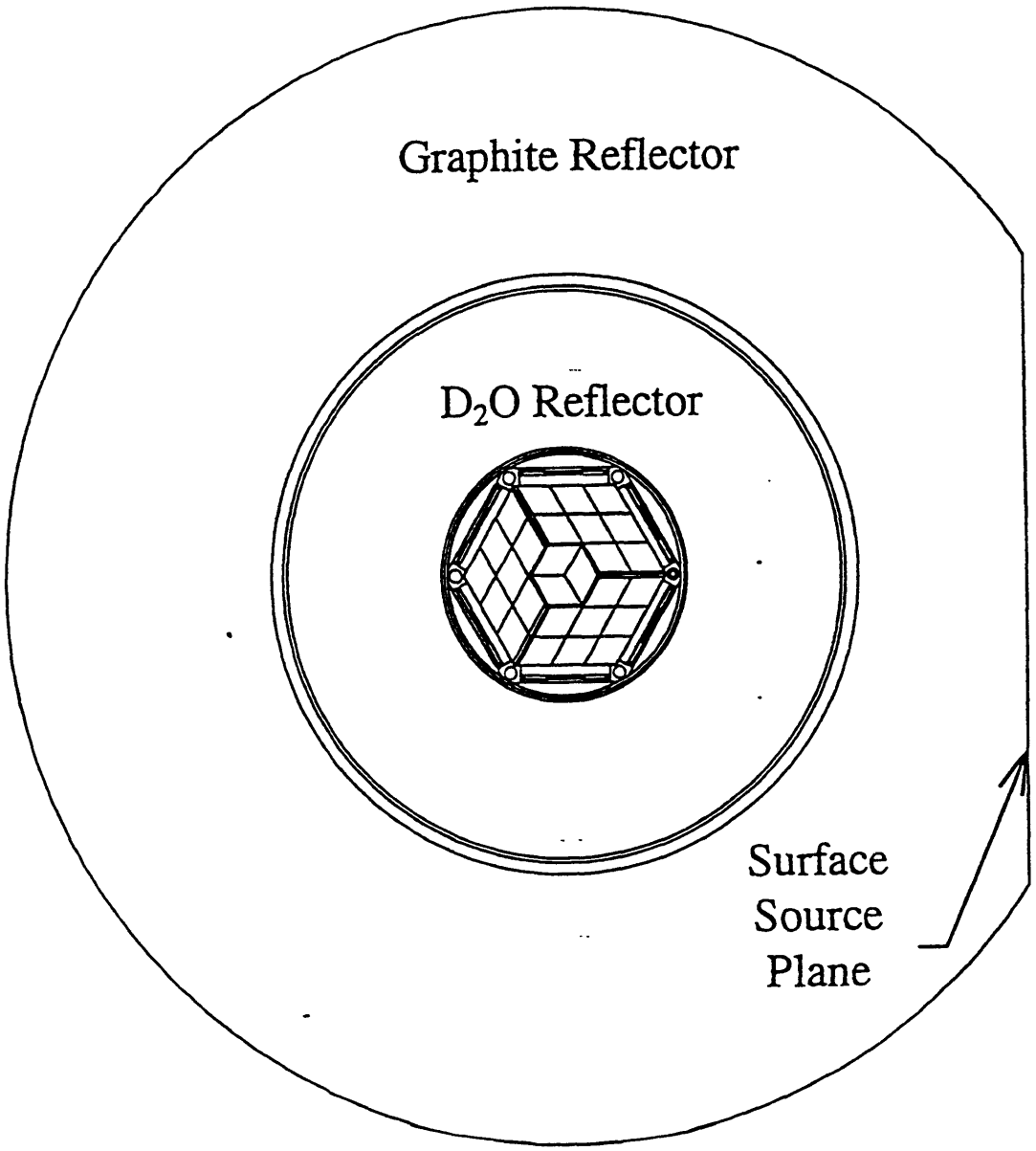

Figure 4.10: Horizontal Cross Section at the Core Centerline

(Courtesy of W.S.Kiger)

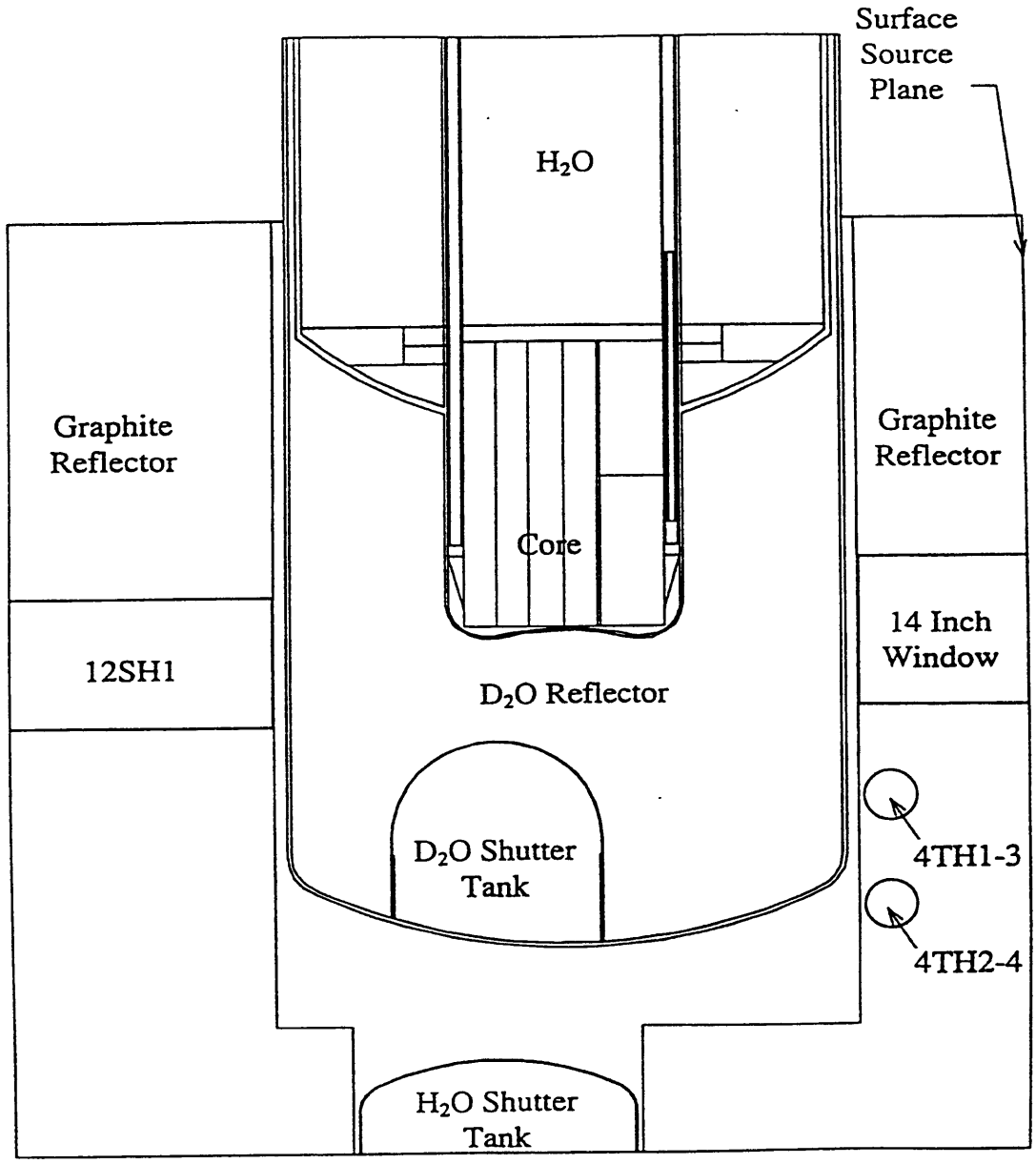

Figure 4.11: Vertical Cross Section Through the center of 12SH1 and the 14 inch Window in the Graphite Reflector as Shown by the dashed line in Figure 4.9 (Courtesy of W.S. Kiger)

Figures 4.9 and 4.10 show the horizontal cross section views at the beam tubes' centerline and at the core centerline respectively. Figure 4.11 shows the vertical cross section view. As is shown in the figures 4.9 and 4.10, the reactor model extends from the core to the graphite reflector in the radial direction. In the vertical direction the model extends above the core 60.96 cm into the light water coolant to the bottom of the current medical room light water shutter. As is obvious from figures 4.9, 4.10 and 4.11, the current medical beam, high density concrete surrounding the reflector, and spent fuel storage ring above the core are not modeled in the reactor model because the effects due to these are negligible. This is further demonstrated by comparing the calculated results and measurements in horizontal throughports 4TH1-3 and 4TH2-3. These comparisons are clearly demonstrated in section 3.1 of Ref. 1.

3.2 Fission Converter Model

Originally W.S. Kiger[1] developed fission converter model for neutronic study of the fission converter beam. S. Sakamoto[2] used the same model with some minor modifications to the model for his parametric studies of the fission converter beam.

For the medical room shielding and the shutter thickness calculations done in this thesis, the original fission converter model of the fission converter tank and the filter/moderator assembly from W.S. Kiger[1] and

S.Sakamoto[2]. The collimator was remodeled and the medical room was added to the fission converter model for the current work. The whole fission converter model used for the shutter thickness and the medical room wall thickness computations is shown in figure 4.12 and 4.13 respectively.

As can be seen in figures 4.12 and 4.13, the sections of the reactor that are not adjacent to the thermal column, including reactor core, were not incorporated in the coupled fission converter/reactor model. The absence of these sections of the reactor model should not affect the dose rate calculated at the patient position and outside of the medical room walls. The reason is that the remaining portions of the reactor model provides an albedo such that the number of neutrons that are killed by entering the missing portion of the model that would have returned to the fission converter is negligibly small. Furthermore, the above approach decreases the computational time drastically because in this method of calculation transport from the core to the edge of the graphite reflector (near the fission converter) is precalculated; using the surface source eliminates the need to simulate this portion of the model in every calculation. In figure 4.12, the water shutter and the fast shutter occupy the collimator region. The empty space of the collimator is filled with light water when the water shutter is in closed position. The fast shutter is made of 1% boronated polyethylene and lead or tungsten.

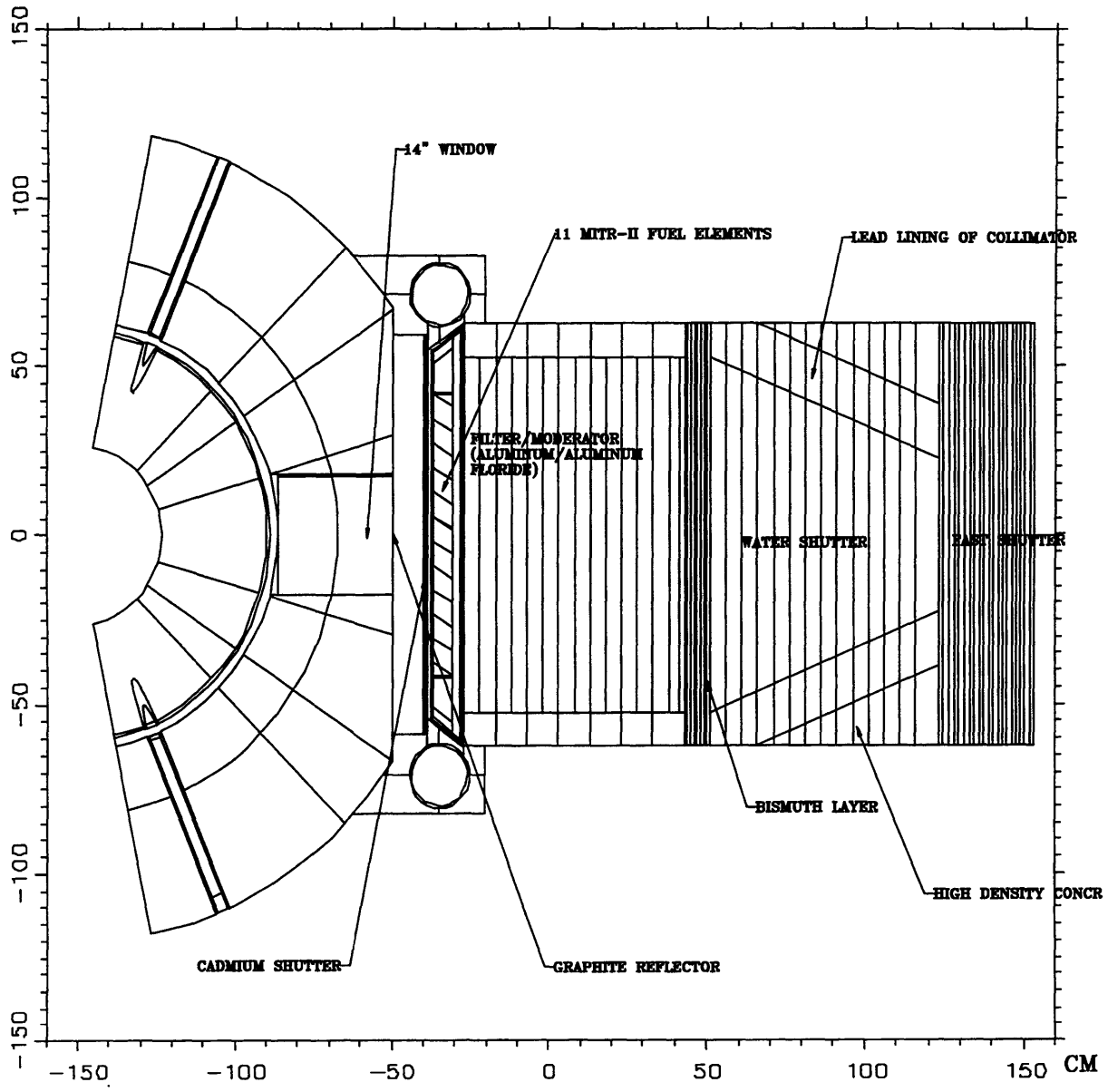

Figure 4.12: Plan view of the MCNP model for the shutter computations, The surfaces used in the model are shown by the lines.

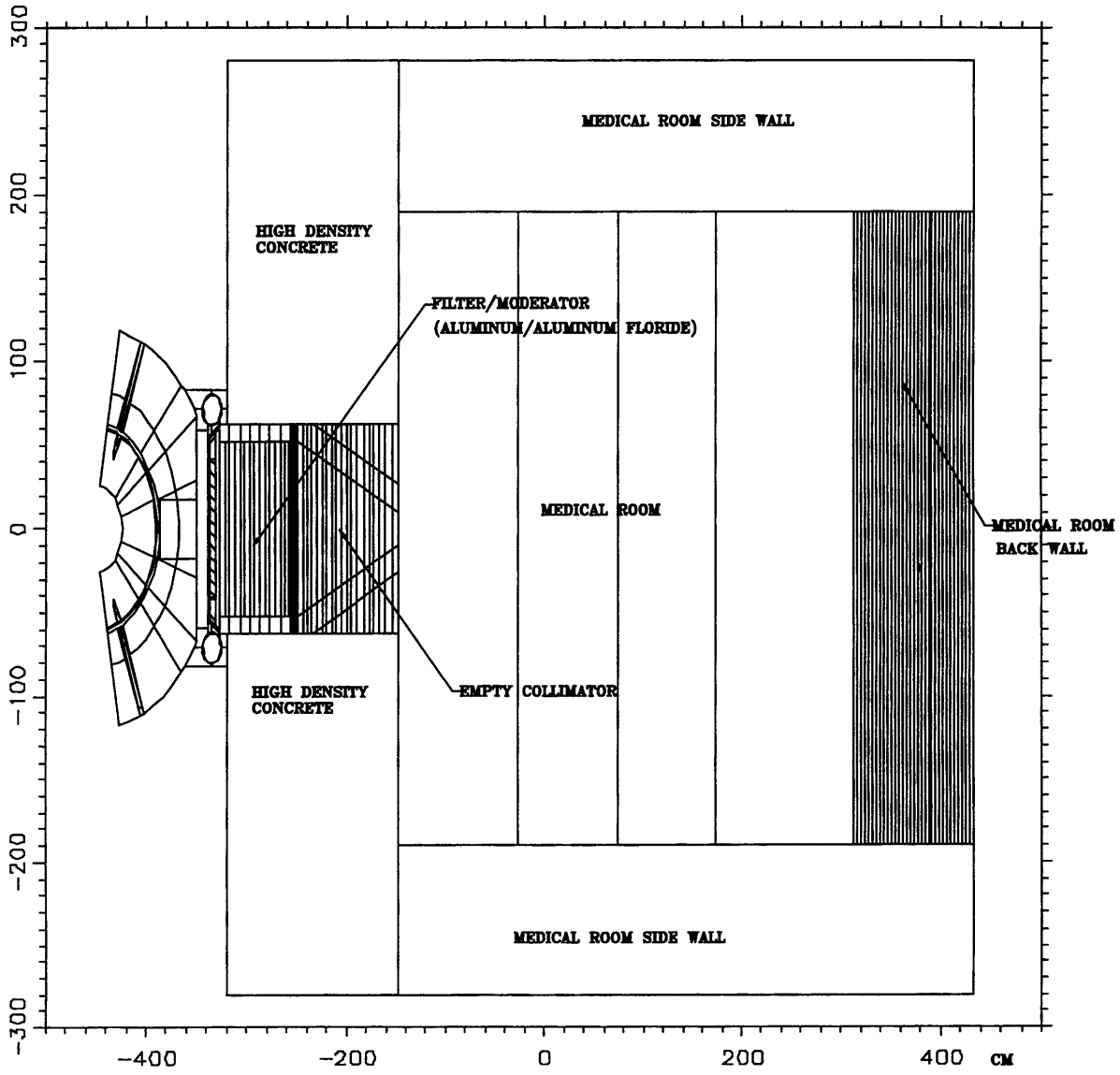

Figure 4.13: Plan view of the MCNP model used for the medical room wall thickness computations. The surfaces used in the model are shown by the lines.

The space around the collimator is filled with high density concrete, which is similar to the reactor biological shield. The collimator lining material is lead. Surface flux at the patient end of the whole fast shutter surface was tallied for neutrons and gamma rays.

The medical room wall material is high density concrete, which was used to build the current hohlraum walls. The high density concrete of the current hohlarum wall material was used to model the medical room walls, because it is a design goal to reuse the existing concrete. After extensive search it was found that the concrete density of hohlraum walls is 230 lbs. per cubic feet. This concrete density information was found in the blue prints for the hohlraum. However, information on the type of concrete is not available. The concrete type information was assumed by comparing the concrete density with commercially available concrete. From the comparison, it was assumed that type of concrete used in the hohlarum is Limonite Swedish I-2a concrete. The ingredients of this concrete are listed in the table 4.3.

Table 4.3: Elemental Composition of Limonite Swedish I-2a Concrete[5] (g of elements/cm^3 of concrete)

Elements	g/cm3 of concrete
^{1}H	0.0219
^{8}O	1.35
^{12}Mg	0.021
^{13}Al	0.0218
^{14}Si	0.0560
^{20}Ca	0.2342
^{22}Ti	0.959
^{25}Mn	0.0302
^{26}Fe	1.0635

3.3 Variance Reduction

Relative error, R, is defined by $C/\sqrt{T}$, where T is the computer time and C is a positive constant. There are two ways of decreasing the relative error: 1) increase the computer run time (run many particles) and 2) decrease the constant value. It is not affordable to increase the computation time; therefore, the favorable option would be to decrease the C value. For this reason MCNP has special variance reduction techniques to decrease the C value.

For some applications of Monte Carlo radiation transport techniques, the natural physical probabilities of events occurring are sufficiently high that variance reduction techniques are not needed to increase the incidence of those events to statistically significant and meaningful levels. For many problems variance reduction is not a way to speed up the problem but it is absolutely necessary to get any answer. The shielding calculation problems, for example, will run too slowly by factors of trillions without adequate variance reduction techniques. In fact, only an infinitesimal portion of the tracks started in the core would reach the patient position without the use of variance reduction techniques for the Monte Carlo model of the fission converter shielding computation. The transport efficiency for a fission neutron born in the fission converter tank to travel to the patient position is about the order of 10^{-12}. If it is assumed that 1000 particles/minute run, it is obvious that on average about 1 track would be scored at the patient position for every 10^{9} minutes of computer time. A few years of computer time is required to score enough tracks at the patient position to have good statistics. It is clearly evident that the fission converter shielding computation requires good variance reduction technique to speed up the computation and also to obtain reasonable results with good statistics.

There are four types of variance reduction techniques available in MCNP. However only two of those four variance reduction techniques were

used for the reactor and the fission converter model. These two variance reduction techniques are briefly described as following:

1. Truncation Methods

   These methods are considered to be the simplest variance reduction methods available. In truncation methods, the computation time is reduced by truncating parts of the phase space, which does not affect the solution. This method is exercised in the coupled fission converter/reactor model where the portions of the reactor that are not adjacent to the thermal column were removed from the model. This allowed speeding up the coupled fission converter/reactor model computations without scarifying the accuracy of the results. The truncation variance reduction technique was also used for the reactor alone model, where part of the reactor structures were avoided in the MCNP model. The reasons are that these structures do not affect the accuracy of results and this truncation increase the computational speed.

2. Population Control Methods

   These methods are very common class of variance reduction techniques where particle splitting and Russian roulette are used to control the number of samples taken in various region of phase space. The available population control methods in MCNP are geometry splitting

and Russian roulette, energy splitting/roulette, weight cutoff and weight windows. In the reactor model and the fission converter model the weight windows were used as the variance reduction technique.

If variance reduction techniques are used correctly, the computational time can be drastically reduced while getting correct answers for the problem. If used incorrectly it can give good statistics with wrong answer. Some variance reduction techniques have general application and they are not usually misused. The use of the weight window technique is more powerful, but it requires more input and good insight about the model. The use of the weight window technique in the reactor model and in the fission converter model will be discussed in the following paragraphs.

Weight windows variance reduction is a space and energy dependent splitting and Russian roulette technique. The user specifies a lower weight bound for space-energy phase space cell in the weight window variance reduction technique. Upper weight bound is a user specified constant multiple of lower weight bound. These weight bounds specify a window of acceptable weights. If the particle weight is higher than the upper bound weight it will split into more particles such that all the split particles' weight are within the acceptable weight window bounds. If the particle weight is below the lower weight bound then Russian roulette is played and the particle's weight is increased to a value which is within the acceptable weight

window bounds or is terminated. However if the particle weight is within the weight window bounds no action is taken.

For the reactor model alone (model used to create the surface source) the weight window variance reduction technique was used. E.Redmond[8] created the weight windows for the reactor model alone. The surface source for the this study was created with the use of E.Redmond's[8] reactor model.

MCNP has a feature of weight window generator, which automatically generates weight windows for a specified tally bin. Although the weight window generator is a useful tool, the user should carefully investigate to decide whether or not the generator provides reasonable results. Most of the time further modification of the generated weight windows increases the computational speed and accuracy.

The weight window variance reduction technique was used for the fission converter shielding computations. The weight windows for the fission converter shielding were first created with the use of weight window generator. For the weight window generator, it is important to provide the initial guess values for the weight windows for the position-energy phase space cells. The weight windows created for the neutronic studies were given as initial values for the weight window generator. The weight window generator uses the initial guesses to estimate the average importance of position-energy phase space cells. There are many ways of modifying the weight windows created by the weight window generator to further improve

the accuracy and speed of the computation. For the fission converter shielding calculation, the weight windows were modified manually; the method used by W.S. Kiger[1].

The statistical uncertainties can be reduced if the number of tracks that reach the tallying position is maximized. The number of tracks that reach the tallying position can be maximized by optimizing the splitting of radiation particles. It is incorrect to split the radiation particles entirely in the location near the source or in a cell. The correct way is that the splitting of the radiation particles should be performed progressively along the path from the source to the tally position. If the splitting of the radiation particles is performed correctly the track density will be constant along the path from the source to the tally position[1].

The adjustment of weight windows is simple because most of surface area of the cells is constant along the beam line. The number of tracks entering and leaving each cell are given in the output file. The ratio of the tracks entering the adjacent cells provides the correction factor for the ratio of the weight window lower bounds. This can be described by the following formula,

$$WW_i' = WW_{i-1}' \left(\frac{WW_i}{WW_{i-1}} \right) \left(\frac{TE_{i+1}}{TE_i} \right)$$

Where WW_i' = adjusted weight window lower bound for cell i

WW_i = prior iteration weight window lower bound for cell i

TE_i = tracks entering cell i

i = cell index, which increases with distance from the source.

A few iterations are required to obtain a reasonable weight windows[1].

The fission converter shielding computation has weight windows for photons and neutrons. The photon weight windows are energy independent. The energy independent weight windows for photons are acceptable because the photon spectrum of the fission converter beam does not vary strongly. The manual optimization of the weight windows works well for the energy independent weight windows because the track information is also energy independent.

The neutron spectrum varies significantly over the energy range; therefore energy independent weight windows are not optimum weight windows for the fission converter neutronic studies. All regions of the neutron spectrum are needed to characterize the beam. However, only the fast neutrons spectrum is of interest in the shielding calculation, because we are mainly interested in the fast neutron dose rate at the patient position and outside the wall. In the fission converter neutronic studies, extensive effort was made to create an energy dependent weight windows to correctly obtain the neutron spectrum at the patient position. Five energy intervals, 0 to 1 eV, 1 to 800 eV, 800 eV to 20 keV, 20keV to 1MeV, and 1MeV to 20 MeV, were chosen for the weight windows in the fission converter neutronic studies The

generation of weight windows for these five energy intervals are explained in the chapter 2 of Ref. 1.

The same weight windows were used in these shielding calculation as initial values. The adjacent cell weight window lower bound was defined for the new cells, which are modeled in the fission converter shielding model. Then the weight windows for the energy interval 4 and 5 (fast neutron energy intervals) was changed using the manual optimization technique used by W.S. Kiger. These procedures were iterated until reasonably optimum weight windows were produced.

3.4 MCNP CALCULATION FOR SHUTTER STUDIES

The statistical uncertainty for each MCNP simulation result is given in bracket beside the result. The statistical uncertainty is reported as one standard deviation.

A MCNP computation was performed to obtain neutron and gamma spectra at the surface of bismuth layer with cadmium shutter closed (see the model shown in figure 4.12). Both neutron and gamma spectra are shown in figures 4.6 and 4.7 respectively. The neutron and gamma dose rates at the surface of the photon shield are 6.9E5 mrem/hr (±3%) and 3.84E6 mrem/hr (±1%) respectively with the cadmium shutter closed. From the bismuth

surface to the patient position (over the 102.1 cm length of the collimator) the fast, epithermal, and thermal fluxes decrease by factors of 4.1, 3.9, and 3.7, respectively. This is shown in figure 5.31 of Ref. 1. Therefore, the total neutron dose rate at the patient position is 2.0E5 mrem/hr when the cadmium shutter is at close position. Since the gamma dose rate will decrease as $\approx \frac{1}{r^2}$ (in the length of collimator), the gamma dose rate at the patient position is about 3E4 mrem/hr. Hence the total dose rate at the patient position is about 203 Rem/hr when the cadmium shutter is in the closed position. The fast neutron dose rate at the patient position is 1.09E4 mrem/hr (3.2%) with cadmium shutter in the closed position. W.S.Kiger[1] (Table 4.6, page 249) calculated the fast neutron dose as 0.13 cGy/min (17%) at the patient position with the cadmium shutter in the closed position. If the fast neutron quality factor is assumed as 12, 0.13 cGy/min dose is equivalent to 0.94E4 mrem/hr (17%) dose rate. Therefore, there is a good agreement between the author's and W.S.Kiger's calculated results.

Another MCNP computation was performed to calculate the dose rate at the patient position for the model shown in the figure 4.12. The shutter thicknesses shown in the figure 4.12 are equal to those that were calculated analytically. The collimator is filled with 1% boronated water and the water thickness along the beam centerline is 72 cm. The fast shutter is modeled as 16 cm thick 1% boronated polyethylene and 14 cm thick tungsten. The neutron and gamma spectra at the patient position are shown in figures 4.14

and 4.15 respectively. The neutron and gamma dose rates at the patient position are 0.02 mrem/hr (10%) and 0.15 mrem/hr (3%) respectively. Another computation was performed in neutron only mode when all shutters are at closed position except the water shutter. The neutron spectrum is shown in figure 4.16. The dose rate at the patient position due to neutron is 17 mrem/hr (9%). The photon dose rate at the patient position for the above condition was not calculated because the photon dose rate is negligible compared to the neutron dose rate.

Since tungsten is very expensive material compared to lead, tungsten was replaced by lead. It is also hard to keep boron as solution in water because it tends to precipitate when the temperature is little higher than room temperature. Another MCNP computation was performed replacing tungsten with lead and boronated water with unboronated water. The neutron and gamma spectra for this simulation are shown in figures 4.17 and 4.18. The neutron and gamma dose rates at the patient position are 0.05 mrem/hr (10 %) and 2 mrem/hr (3.4%) respectively. Then another MCNP simulation was performed with all shutters in the closed position except the water shutter.

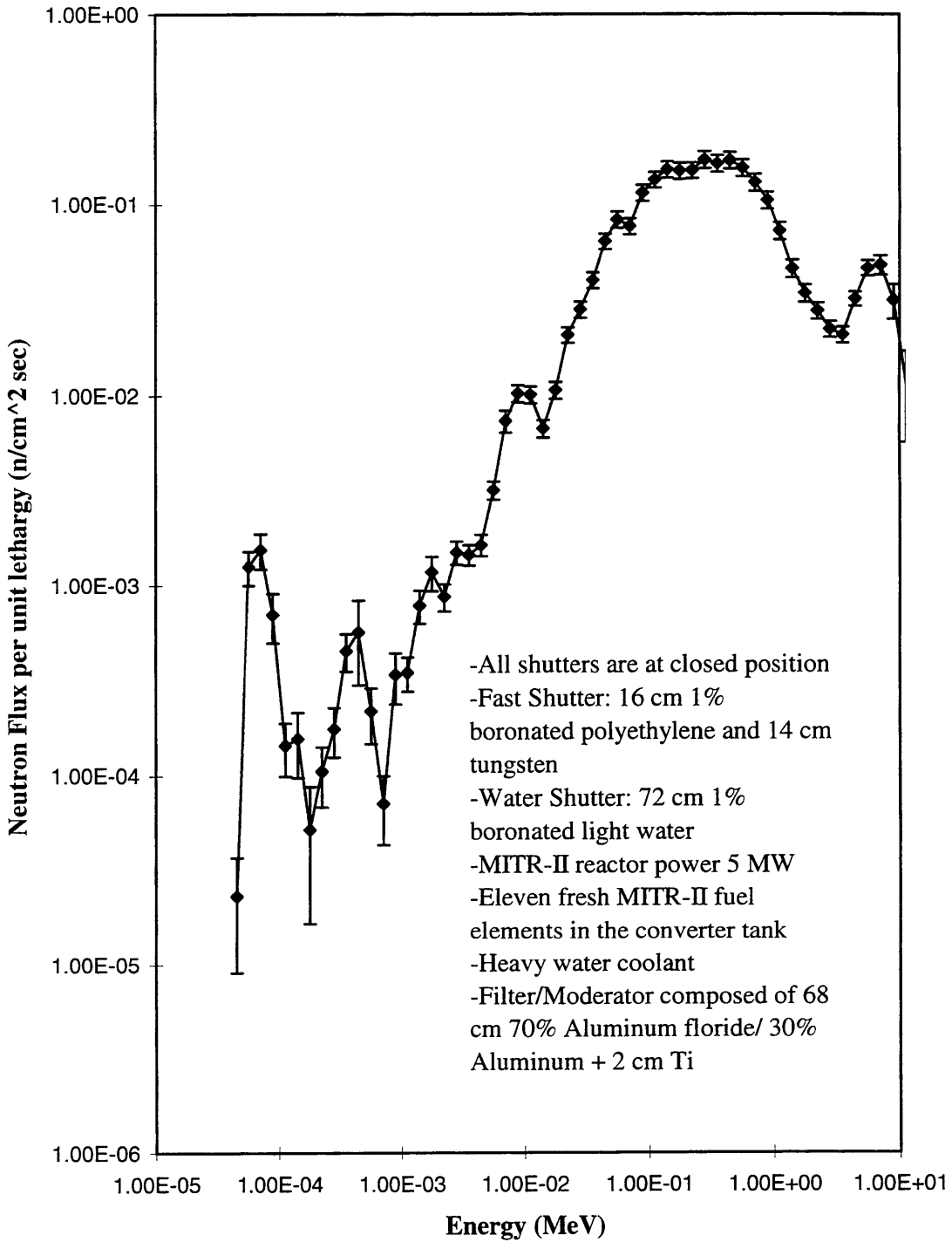

Figure 4.14: Neutron Spectrum at the Patient Position after All Shutters are Closed

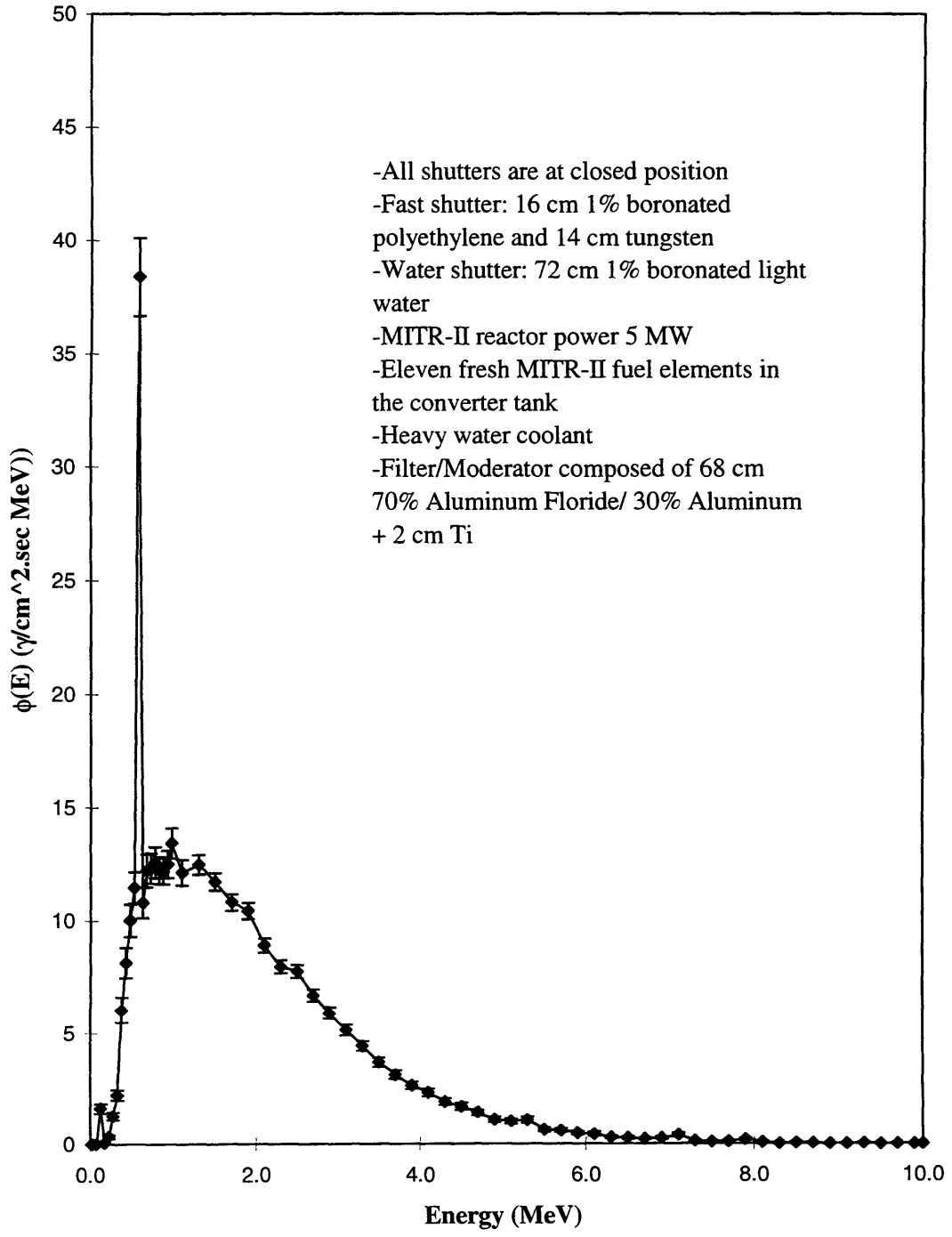

Figure 4.15: Photon Spectrum at the Patient Position after All Shutters are Closed

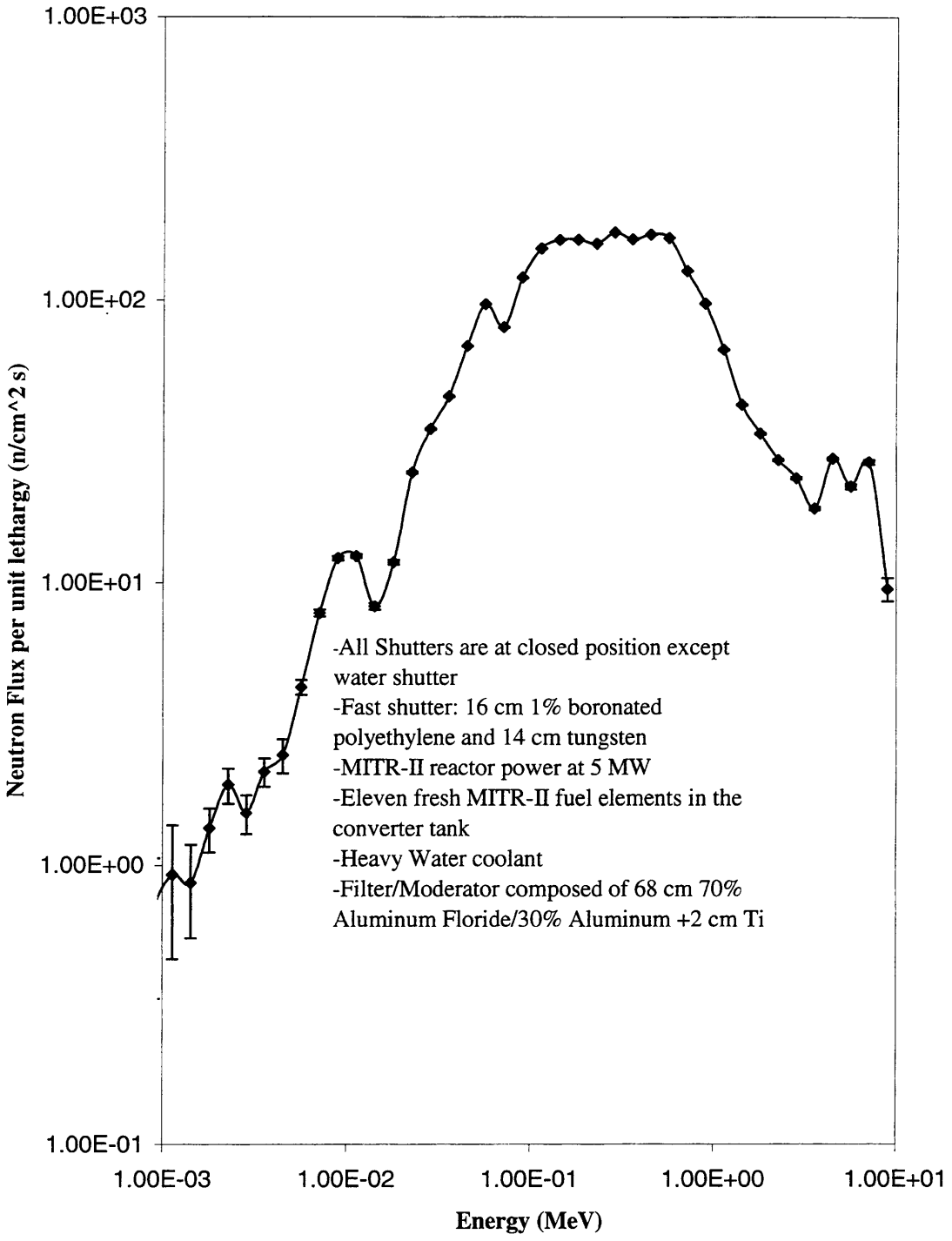

Figure 4.16: Neutron Spectrum at the Patient Position for All Shutters are closed Except Water Shutter

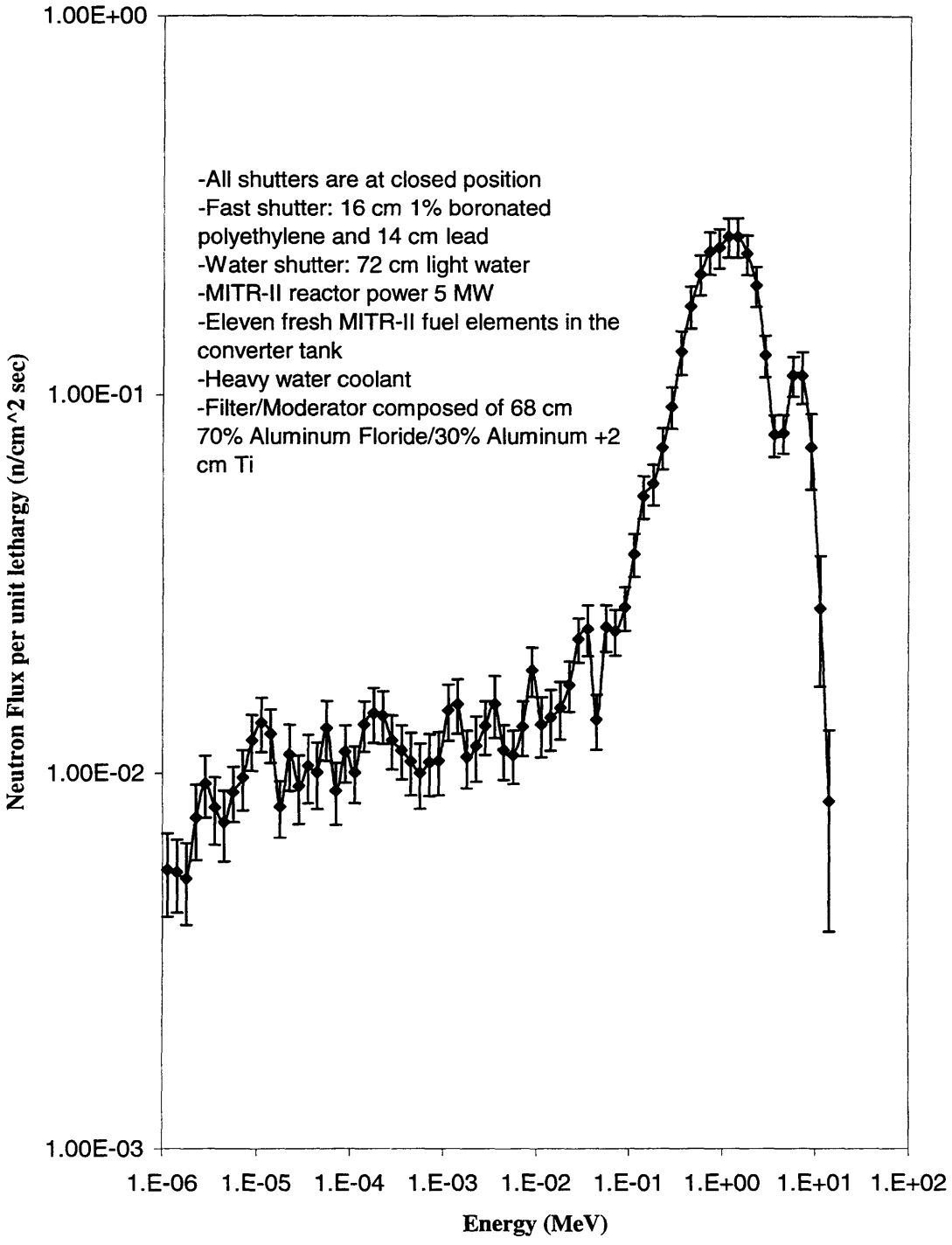

Figure 4.17: Neutron Spectrum at the Patient Position after All Shutters are Closed

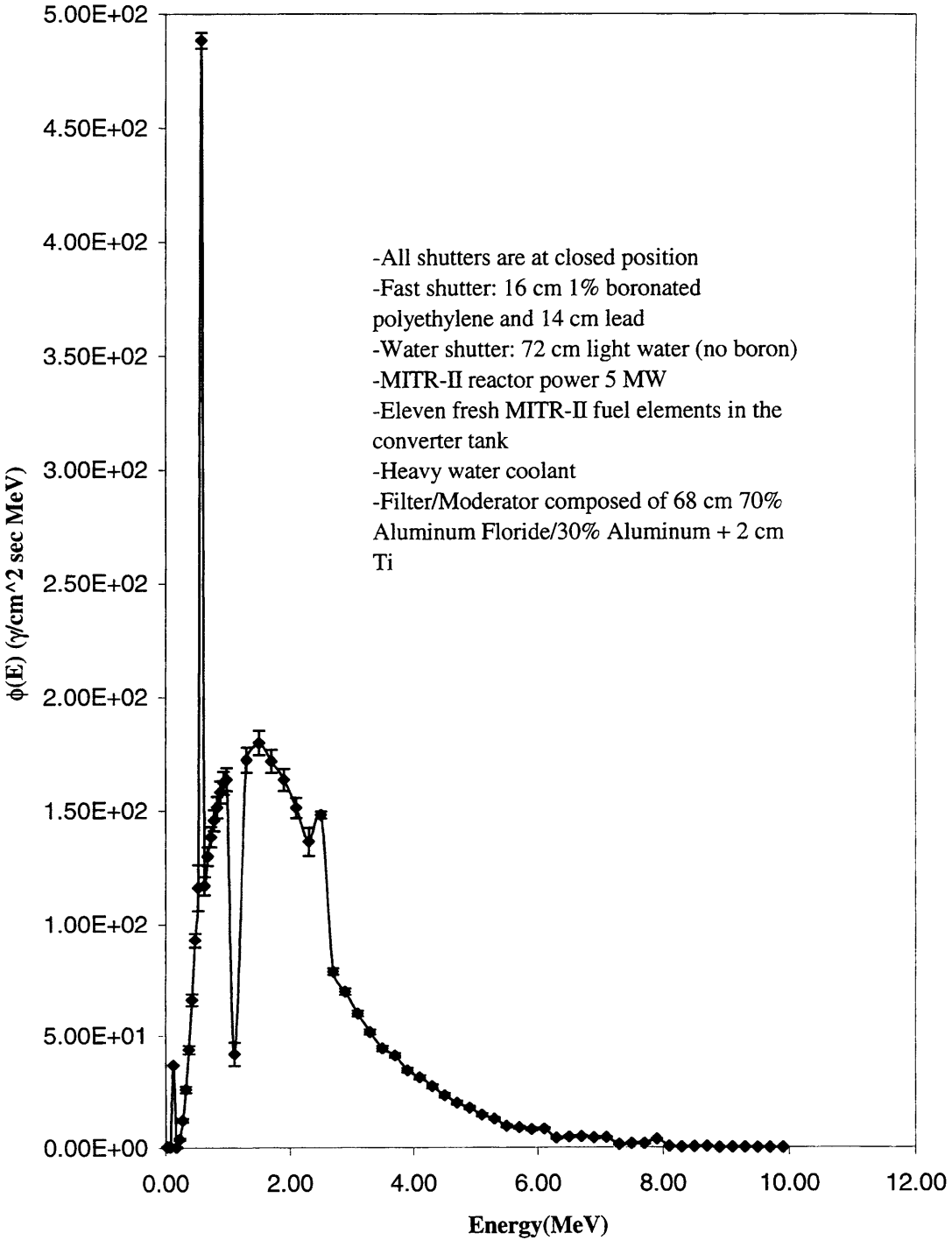

Figure 4.18: Photon Spectrum at the Patient Position after All Shutters are Closed

This run was simulated with neutron only mode and the corresponding neutron spectrum at the patient position is shown in figure 4.19. The dose rate at the patient position due to neutrons is 84 mrem/hr (10%). Again the photon dose rate was not calculated because it is negliable compared to the neutron dose rate.

Water shutter closing time (100 – 120 seconds) is slow compared to the fast shutter closing time (5 – 10 seconds). Therefore, it is preferable to reduce the total dose rate at the patient position when the water shutter is in the open position and all the other shutters are in the closed position. Two more MCNP simulations were performed to determine the total dose rate at the patient position for the following fast shutter thickness:

1. 20 cm thick 1% boronated polyethylene and 20 cm thick lead
2. 25 cm thick 1% boronated polyethylene and 15 cm thick lead.

The MCNP calculation was performed for the above two cases with all shutters in the closed position except the water shutter. The neutron spectrua at the patient position for cases 1 and 2 are given in figures 4.20 and 4.22 respectively. The photon spectra for cases 1 and 2 are given in figures 4.21 and 4.23 respectively. The neutron and gamma dose rates at the patient position for the case 1 are 43 mrem/hr (10%) and

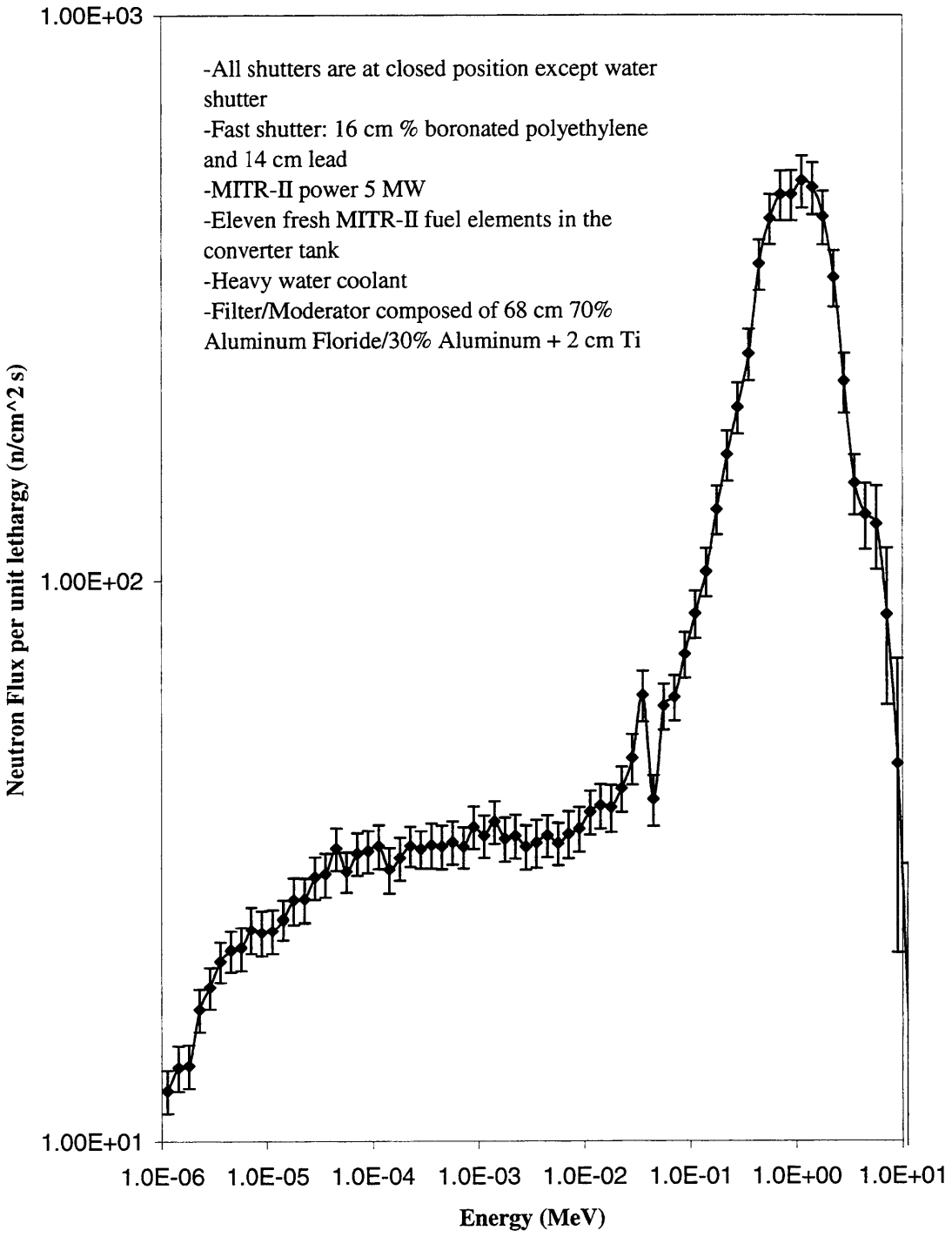

Figure 4.19: Neutron Spectrum at the Patient Position after All Shutters are closed Except Water Shutter

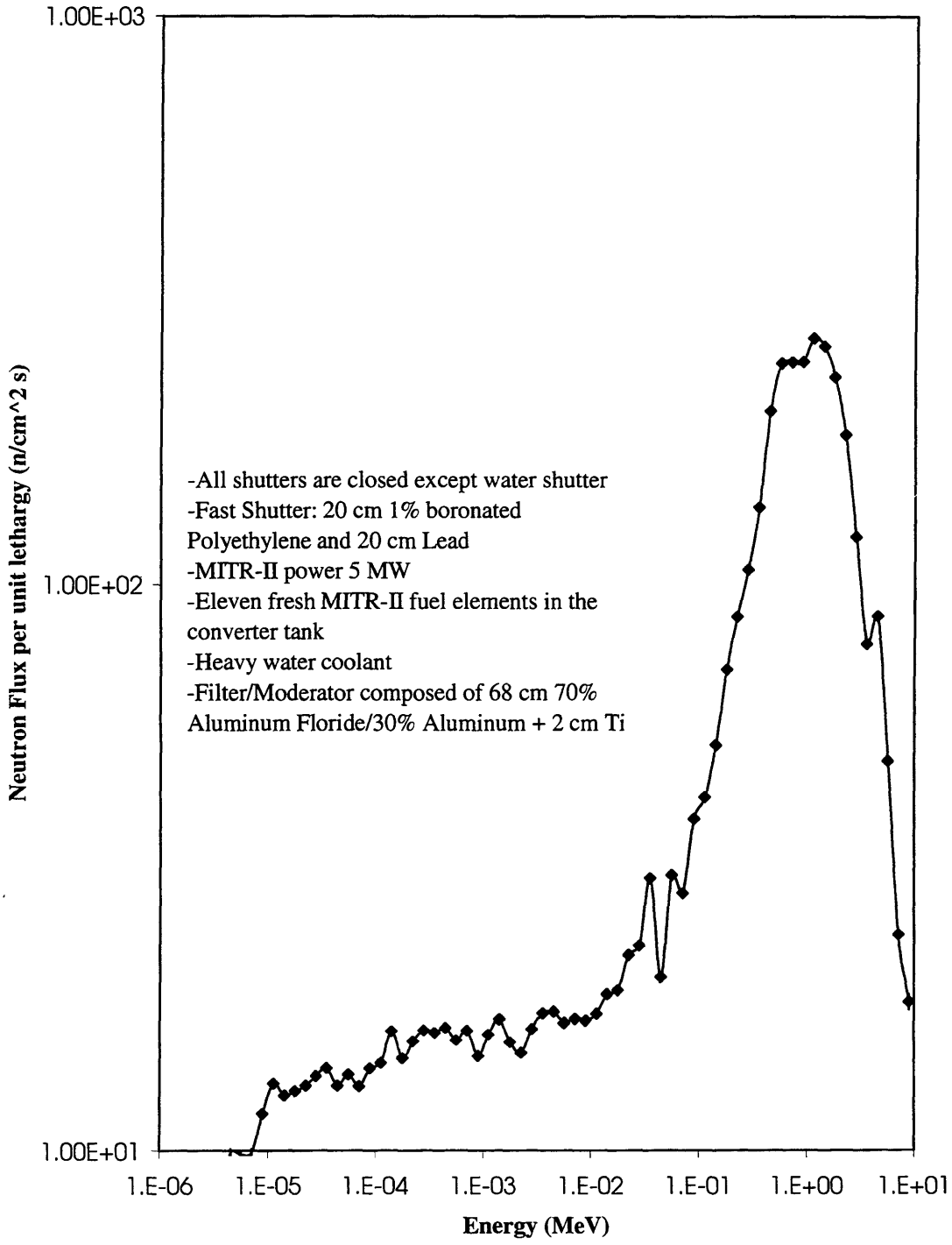

Figure 4.20: Neutron Spectrum at the Patient Position for All Shutters are closed Except Water Shutter

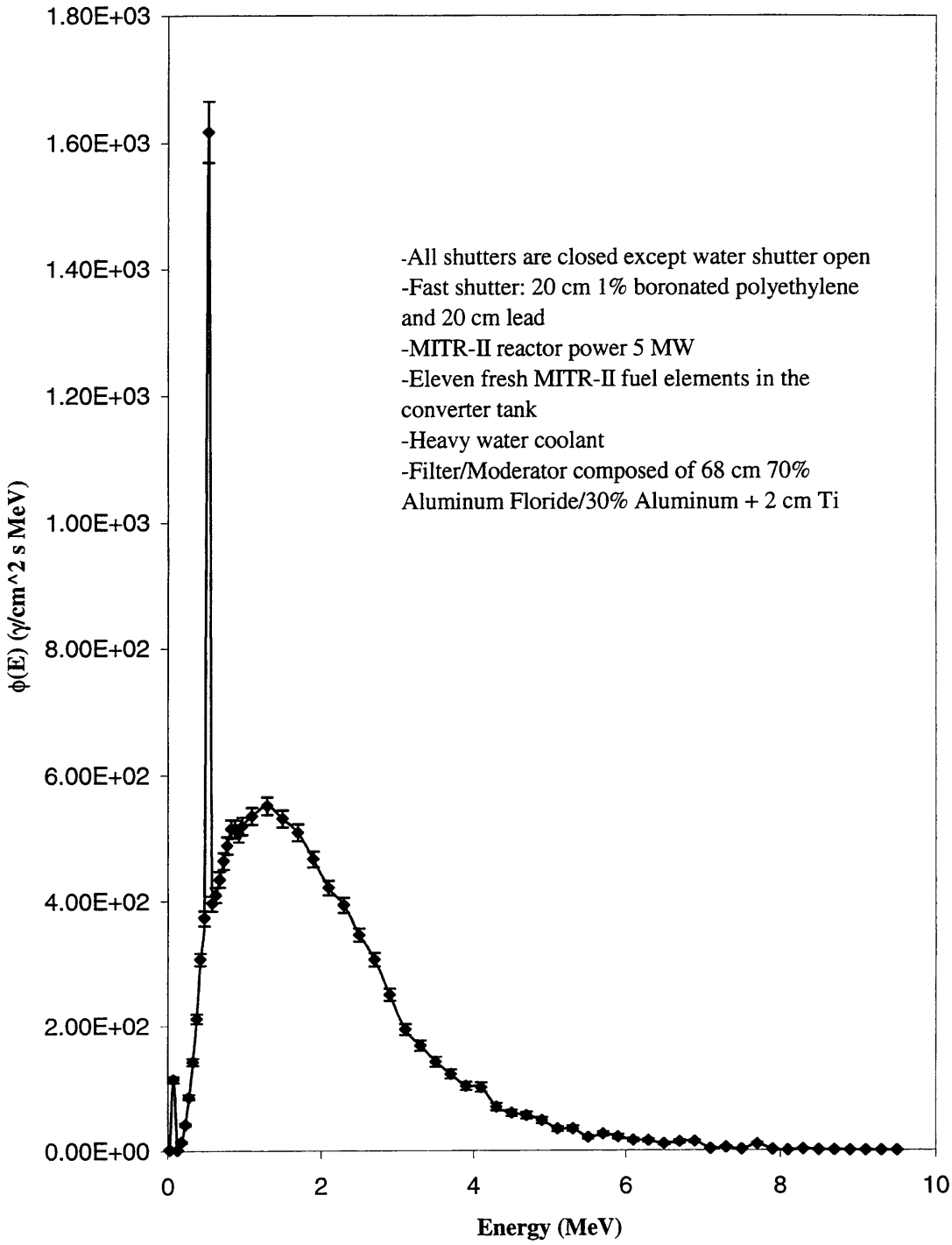

Figure 4.21: Photon Spectrum at the Patient Position for All Shutters are closed Except Water Shutter

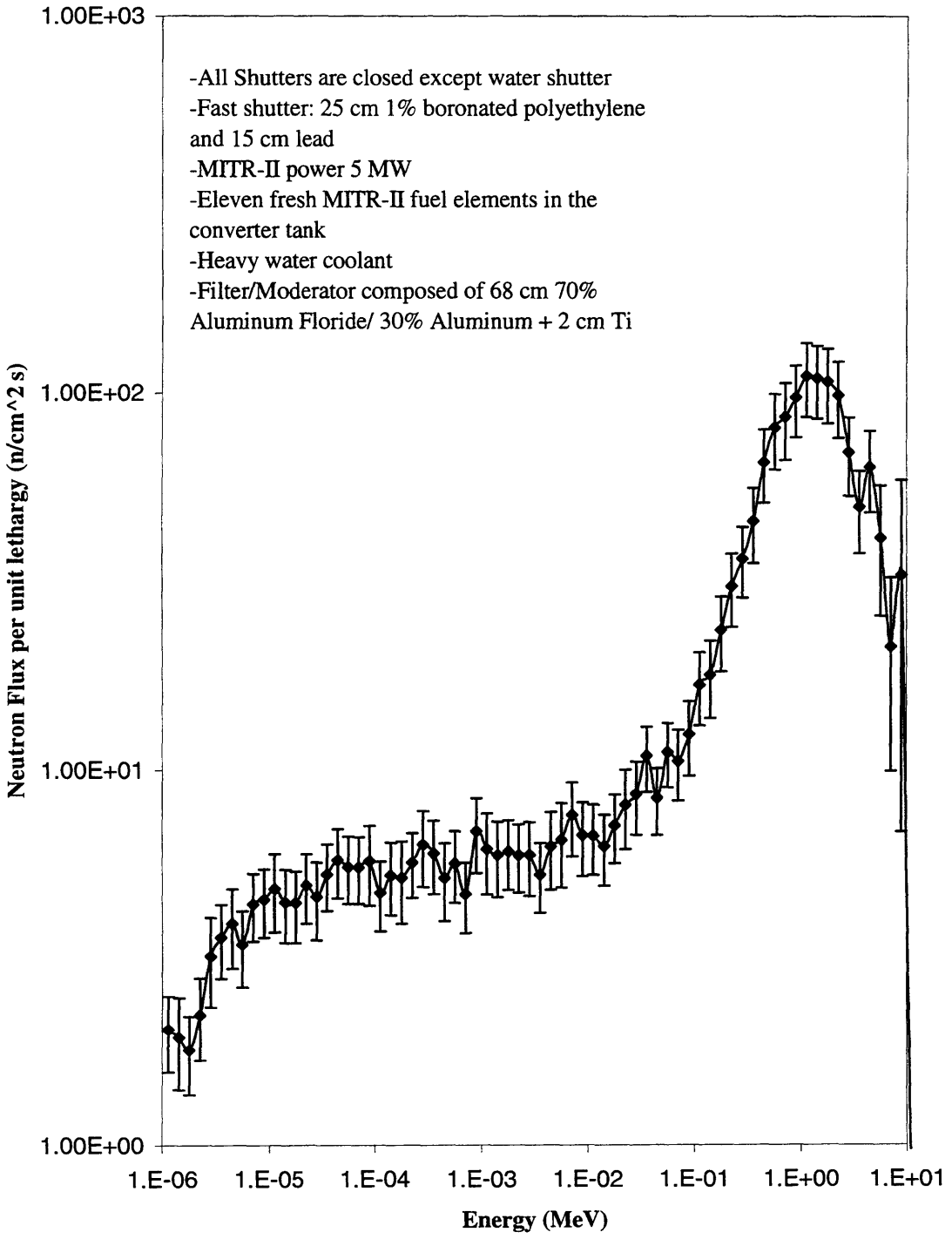

Figure 4.22: Neutron Spectrum at the Patient Position for All Shutters are closed Except Water Shutter

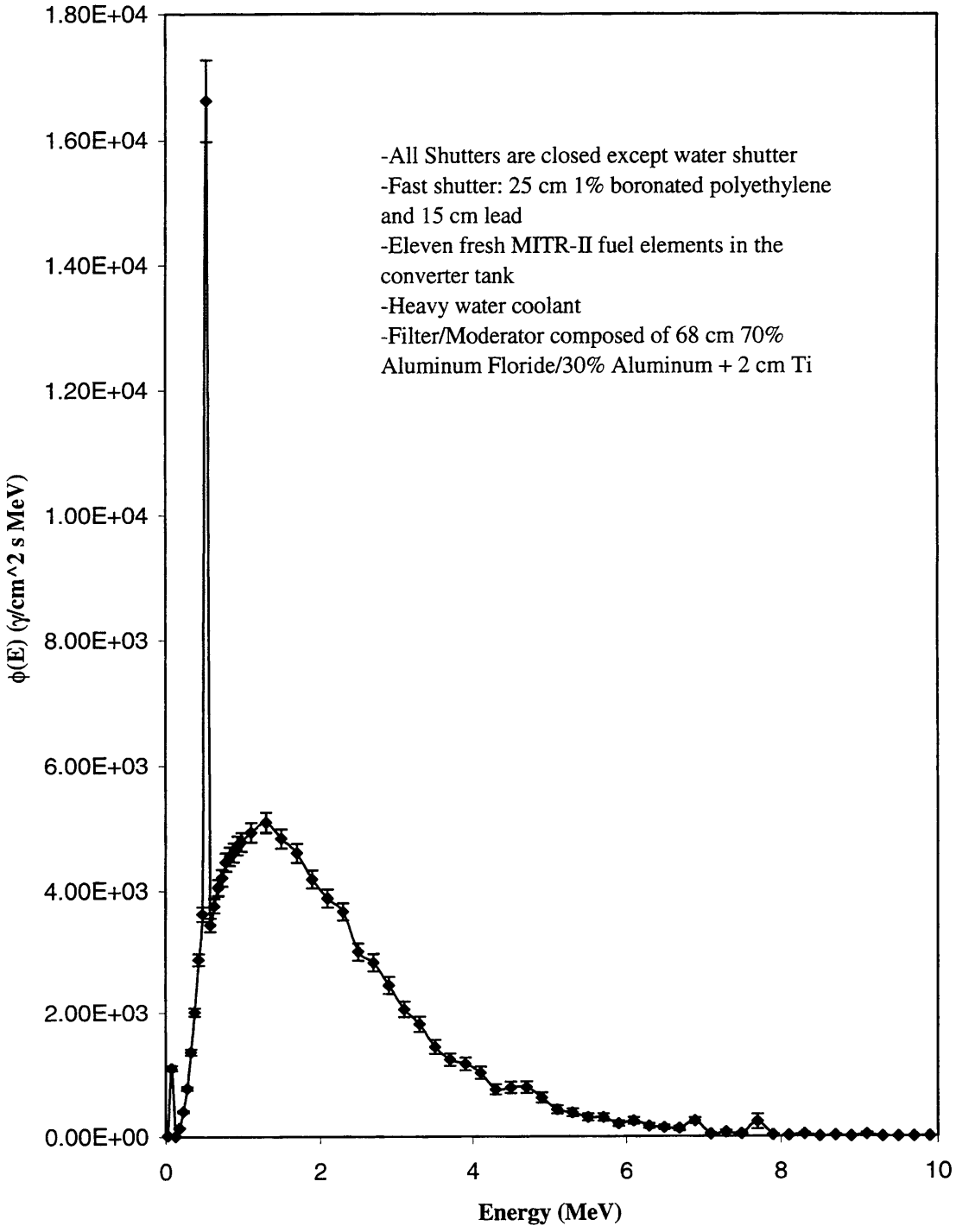

Figure 4.23: Photon Spectrum at the Patient Position for All Shutters are closed Except Water Shutter

6 mrem/hr (2.6%) respectively and for the case 2 neutron and gamma dose rates are 21 (10%) mrem/hr and 63 (6%) mrem/hr respectively.

In all the photon spectra, two peaks(at energies 0.511 MeV and 0.075 MeV) are notably visible. The peak at energy 0.511 MeV is the annihilation peak. The short peak at 0.075 MeV is most likely due to lead or bismuth x-rays.

All the MCNP simulation results are summarized in the following table 4.4. Tungsten with 1 % boronated polyethylene is a good choice for the fast shutter. However, tungsten is very expensive. Hence tungsten is replaced by lead. The optimum shutter thickness is 20 cm 1% boronated polyethylene followed by 20 cm lead. This optimum design gives the lowest dose rate at the patient position when the water shutter is in the opened position. Moreover, the dose rate is below 1 mrem/hr when all shutters are closed.

Table 4.4: Summary of MCNP Results of the Shutter Thickness Computations (statistical uncertainty is reported as one standard deviation)

Water Shutter	Fast Acting Mechanical Shutter				
Water Thickness	Tungsten Thickness	Lead Thickness	1% boronated Polyethylene Thickness	Neutron Dose Rate (Patient Position)	Photon Dose Rate (Patient Position)
72 cm (1% boronated)	14 cm	0	16 cm	0.02 (10%) mrem/hr	0.15 (3%) mrem/hr
72 cm (no boron)	0	14 cm	16 cm	0.05 (10%) mrem/hr	2 (3.4%) mrem/hr
Empty	14 cm	0	16 cm	17 (9%) mrem/hr	Not calculated
Empty	0	14 cm	16 cm	84 (10%) mrem/hr	Not calculated
Empty	0	20 cm	20 cm	43 (10%) mrem/hr	6 (2.6%) mrem/hr
Empty	0	15 cm	25 cm	21 (10%) mrem/hr	63 (6%) mrem/hr

Dose rate as a function of time during shutter opening and closing is given in figure 4.24. Here it is assumed that the fast shutter is made of 20 cm 1 % boronated polyethylene and 20 cm lead and the patient irradiation time is 2 minutes. The cadmium shutter, water shutter and fast shutter opening times are 15 seconds, 100 seconds and 2 seconds respectively. The total dose rate at the patient position with all the shutter in the opened position was calculated by W.S. Kiger[1] (Run ID std473). Figure 4.24 shows each shutter opened and closed one at a time sequentially, but they can be preset to overlap their opening time. Figure 4.24a shows the time sequence for cadmium and fast acting mechanical shutter opening with an expanded time scale. The shutters are assumed to open and close sequentially. The shape of the response curve for closing is similar with inverted slopes.

4.Mechanical Design of Water Shutter

Schematic of water shutter hydraulic system is shown in figure 4.25. Water from a tank on the reactor top flows into the collimator by a gravity head during closing of the water shutter. Since the water shutter is closed by the gravity head, it can be made fail safe if electric power is lost. However, the water shutter closing speed is slower than if a pump is used. It is important to close the water shutter as fast as possible.

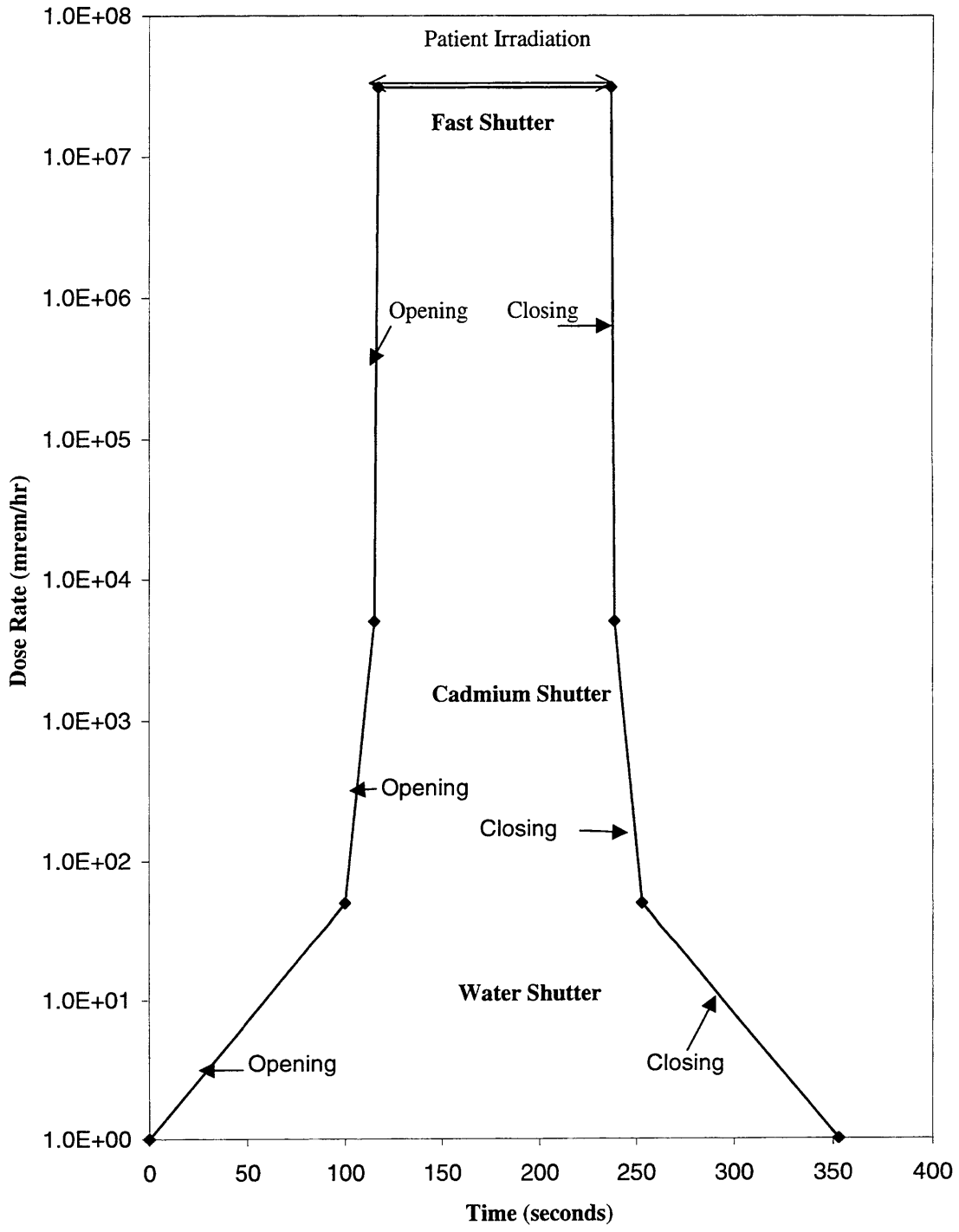

Figure 4.24: Total Dose Rate at the Patient Position as a Function of Time

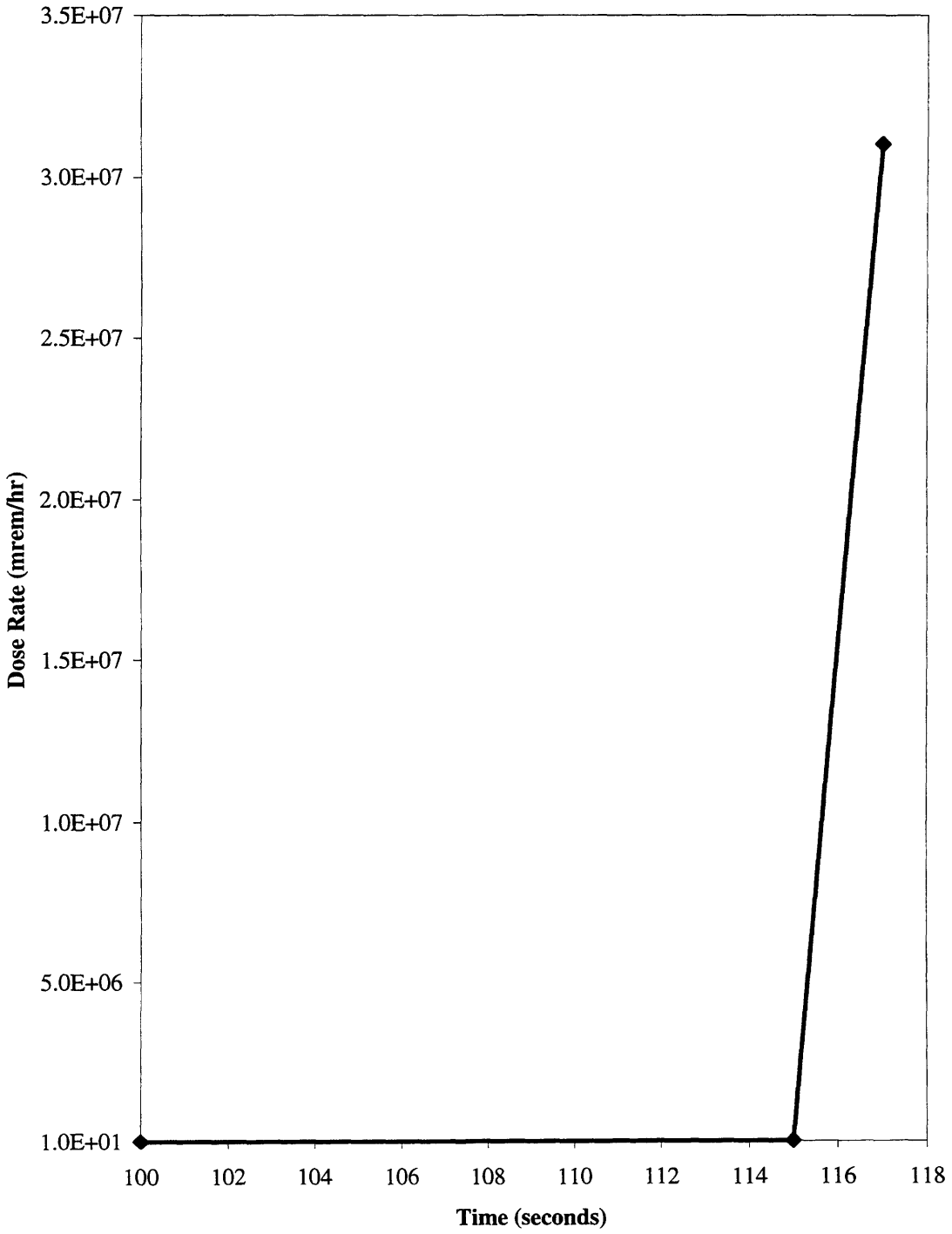

Figure 4.24a: Showing the time sequence for the cadmium and fast shutter opening with an expanded time scale

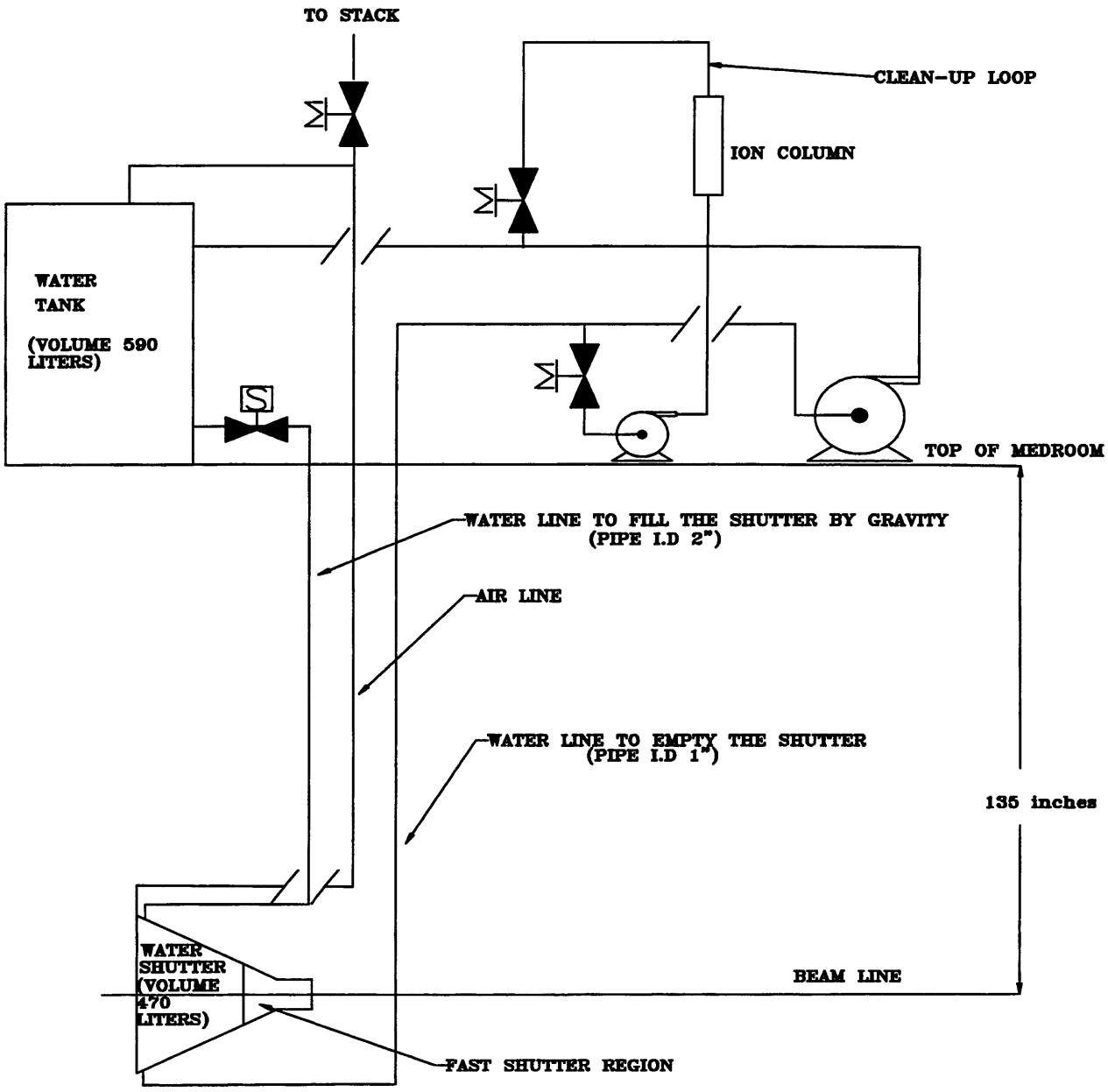

Figure 4.25: Schematic Drawing of Water Shutter Hydraulic System

The water shutter closing time is a function of pipe diameter, i.e. pressure loss in the pipe. The closing time as a function of pipe diameter is shown in the figure 4.26. Diameter of the pipe should be smallest possible, because feeding a larger diameter pipe through the reactor biological shield is difficult. Hence, pipe diameter is chosen as 2 inch I.D such that it is small enough to drill hole through the reactor biological shield and fast enough to fill the collimator shutter. Hence the pipe diameter is 2 inch I.D and the corresponding closing time is 100 seconds. This does not prevent any significant radiation protection problems since the medical staff will not be significantly irradiated even if they enter the medical room while the water shutter is filling.

The water shutter is emptied by pumping the water back to the tank on the reactor top. The water shutter volume is 470 liters and the gravity head is 135 inches of water. The opening time of water shutter is also 100 seconds.

Since it is a closed system, the water is cleaned with the use of the clean up system on the closing loop. The clean up loop is operated when the water shutter is closed (collimator is filled with water). An airline is provided to release air and radioactive argon to the MITR-II stack.

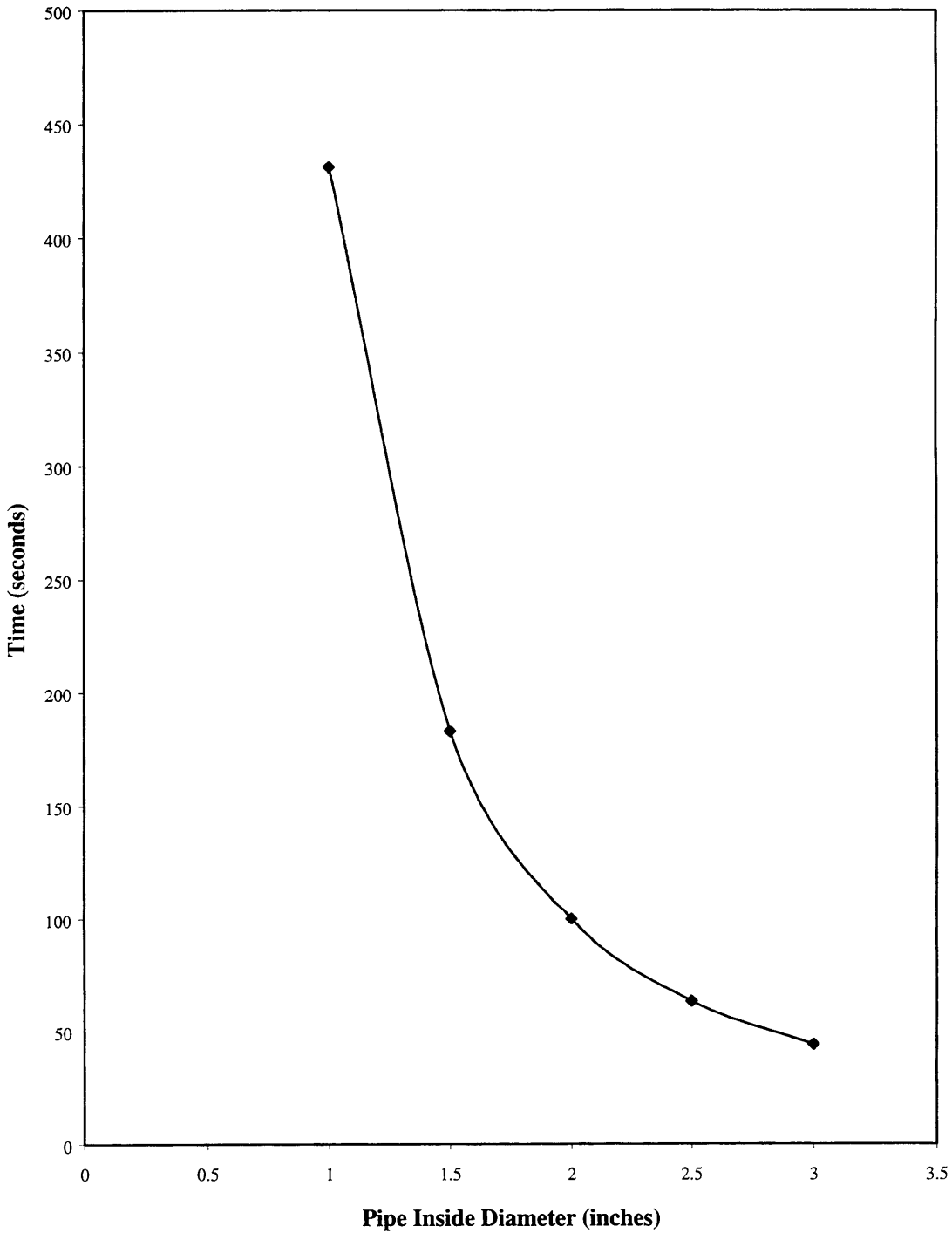

Figure 4.26: Water Shutter Closing Time as a Function of Pipe Inside Diameter

5.Mechanical Design of Fast Shutter

For 40 cm (15.75 inches) shutter thickness, the shutter height (or length) must be equal to the height (51 inches) shown in figure 4.5. If the height is larger than the height shown in figure 4.5, the reactor biological shield should be mined to fully open the shutter. If the shutter height is smaller than the height shown in figure 4.5, the beam can not be fully closed. The shutter width should be larger than the aperture (20 cm X 20 cm)^2 and collimator lining (10 cm)^2. Therefore the shutter width should be larger than 40 cm (15.75inches). The smallest shutter weight is 1,212 kg of lead and 101 kg of polyethylene.

The fast shutter is operated hydraulically. Schematic of the fast shutter hydraulic system is presented in figure 4.27, where arrows show the direction of fluid flow during closing of the fast shutter. A hydraulic pump forces the fluid in the tank through the check valve (v1) to the 4-way valve. Then fluid is forced to the space above the piston and forces the piston to move downward to close the shutter. The fluid in the annulus space (annulus around the piston) is forced through the check valve (v2) and joins the fluid, which flows to the space above the piston. As a result, the fast shutter is closed (pushed downward) by the pressure above the piston and by its weight.

Fluid flow diagram in figure 4.28 shows the opening of the fast shutter. Hydraulic pump forces the fluid to the annulus region through the 4-way valve and the check valve (v2).

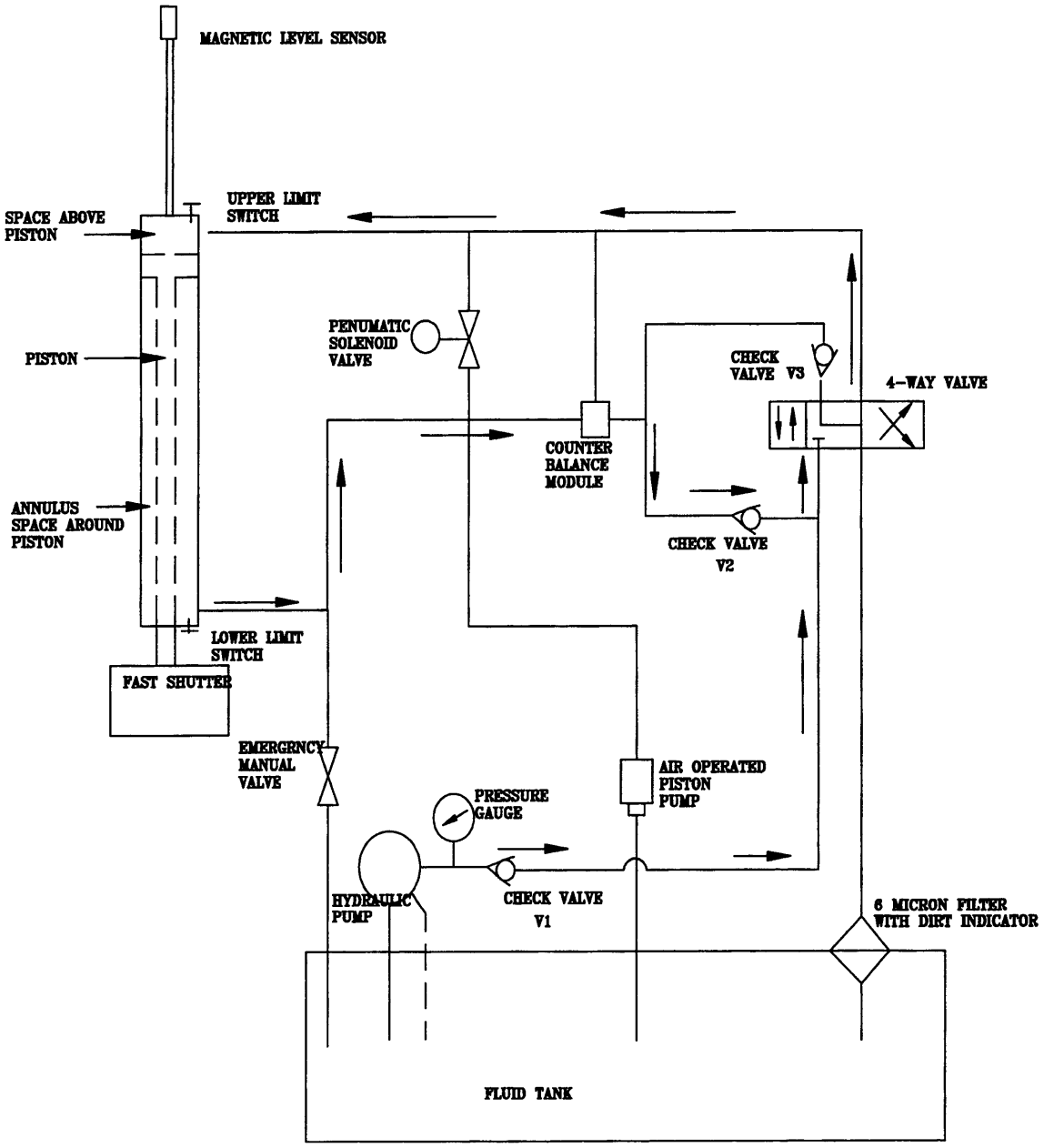

Figure 4.27: Hydraulic Flow Diagram of Fast Shutter Closing

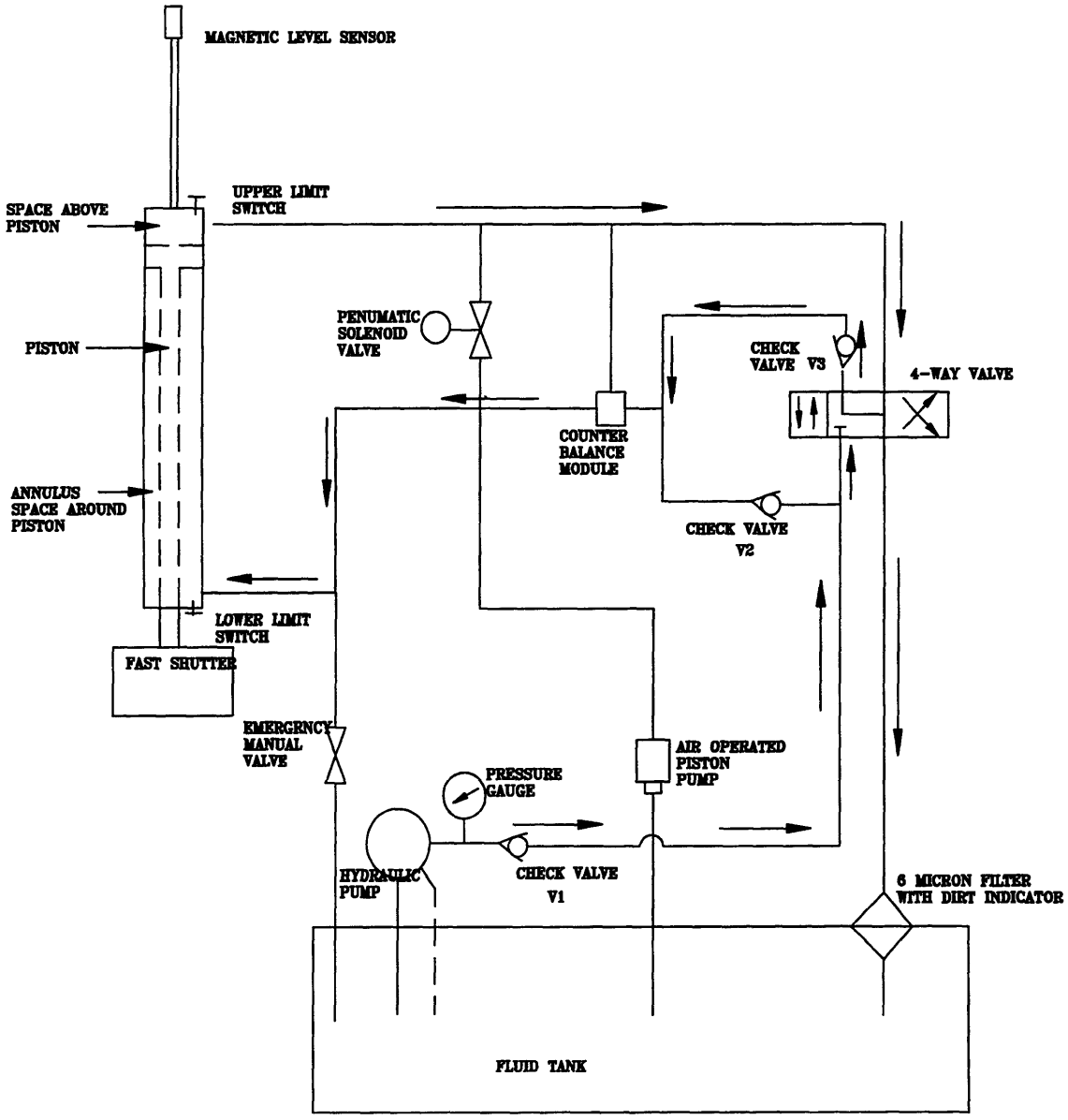

Figure 4.28: Hydraulic Flow Diagram of Fast Shutter Opening

At the same time fluid above the piston space flows into the tank through the 4-way valve and a 6-micron filter. The 6-micron filter filters out particles with a size larger than 6-micron in diameter and keeps the fluid clean. The fast shutter is pushed up by increasing the pressure in the annulus space region. Once the fast shutter is fully opened the hydraulic pump will completely be shut down. An air pump is started and it keeps the shutter in the open position for the preset time. The air pump maintains the pressure by pumping or draining fluid.

Cushions are attached to the top and the bottom of the piston guide pipe and to the top and the bottom of the horizontal piece of the piston. These cushions prevent hard contact between the piston and the piston guide pipe during the closing and opening of the fast shutter. The position of the fast shutter is continually monitored by a magnetic level sensor. The position is continually feed back to control the speed and the deceleration of the fast shutter. The fast shutter starts to decelerate after it has reached 90% of its length of travel (this can be programmed to different values) and comes to a complete stop without banging against the piston guide pipe. There are two sensor switches, upper limit switch and lower limit switch, to indicate the full closure and full opening of the shutter.

During a power failure, fluid in the annulus region flows through the solenoid valve to the upper part of the piston. Since the volume in the annulus region is less than the volume above the piston, the fluid, which

flows from the annulus region to above the piston, is not able to apply the same pressure as it is in normal closing conditions. Hence the fast shutter closes by its weight during the emergency conditions (power failure). The fast shutter hydraulic system has a manually operable emergency valve. The manually operable emergency valve enables one to manually close the fast shutter by opening the valve. When the manually operable valve is opened, the fluid in the annulus region drains into the tank. This manually operable emergency valve is an added safety feature to the fail-safe solenoid valve.

The hydraulic system for the fast shutter will be build by Atlantic Fluid. The Atlantic Fluids Co. provided a similar system for the current Brookhaven National Laboratory's BNCT facility at the Brookhaven Medical Research Reactor.

6.MEDICAL ROOM SHIELDING DESIGN

The purpose of medical room shielding design studies is to calculate wall thickness around the medical room such that the dose rate outside of the medical room wall due to the epithermal beam is about 1 mrem/hr. An access door is designed to access the medical room conveniently.

Anne Le Gal (Exchange Student from Ecole Superieure D'Electronique DE L'Ouest) proposed a preliminary medical room design after performing analytical shielding calculations. This design is shown in figure 4.29. There are two back walls along the beam line. The wall inside the medical room

reduces the incident fluxes of neutron and gamma rays to the access door. As a result, the access door thickness is smaller than the thickness if there was no wall. However, the inside wall reduces the free space in the medical room and makes it harder to bring the patient in and out of the medical room. Hence the inside wall is avoided in the new medical room design, which is shown in figures 4.1 and 4.2. The access door is placed along the side because it can be thinner than if it is placed along the back wall.

The wall thickness for the medical room was calculated using MCNP-4A using similar variance reduction technique as for the beam line shutters. The back wall thickness was calculated for the following conditions;

- All the shutters are open
- MITR-II reactor power 5 MW
- Converter is fueled with 11 fresh MITR-II fuel elements
- Converter coolant is heavy water
- Back wall material is high density Limonite Swedish I-2a concrete

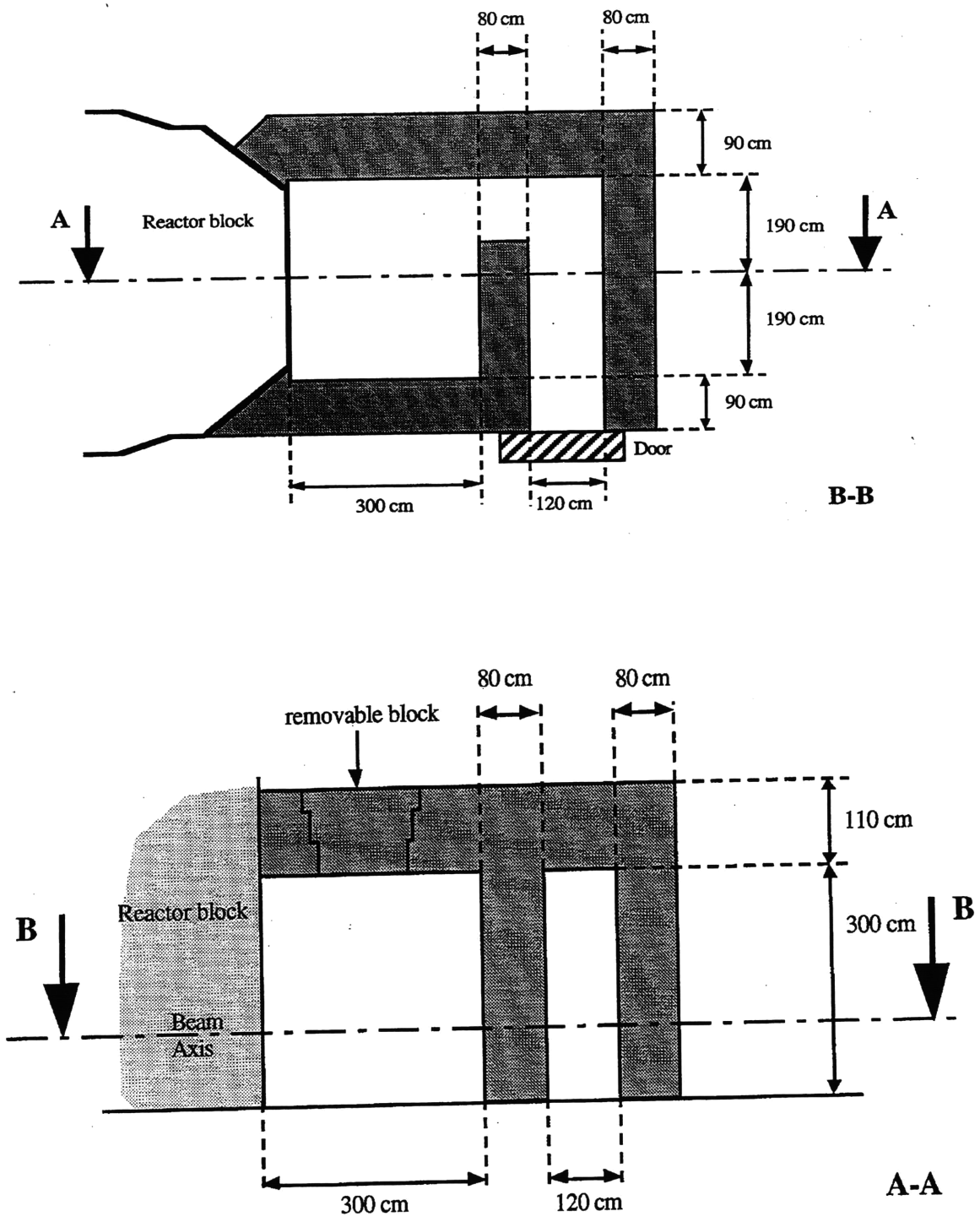

Figure 4.29: Preliminary Medical Room Layout, showing plan and side views (Courtesy of Anne Le Gal)

An MCNP simulation was performed to calculated the dose rate outside the medical room back wall when the back wall thickness is 160 cm. One standard deviation uncertainty is reported in bracket. This 160 cm thick back wall was proposed by Anne Le Gal after her analytical calculations. The MCNP calculated neutron and gamma ray spectra are given in figures 4.30 and 4.31 respectively for 160 cm back wall thickness. These fluxes were tallied outside the medical room back wall. The neutron and gamma dose rates outside the back wall are 5E-5 mrem/hr (4%) and 0.02 mrem/hr (9.2%) respectively when the back wall thickness is 160 cm. Two more MCNP simulations were performed with the back wall thickness of 120 cm and 90 cm. The neutron and gamma spectra for 120 cm thick back wall are given in figures 4.32 and 4.33 respectively. The neutron and gamma dose rates outside the back wall are 0.002 mrem/hr (10 %) and 0.03 mrem/hr (9.1%) respectively for 120 cm thick back wall. The neutron and gamma spectra for 90 cm thick back wall are given in figures 4.34 and 4.35 respectively. The neutron and gamma dose rates outside the back wall are 0.12 mrem/hr (10%) and 0.5 mrem/hr (7%) respectively for a 90 cm thick back wall of heavy concrete density 230 lbs. per cubic feet, Limonite Swedish I-2a. All of the above dose rates were averaged over the entire surface at the outside edge of the medical room back wall. The medical room back wall shielding calculation results are summarized in table 4.5.

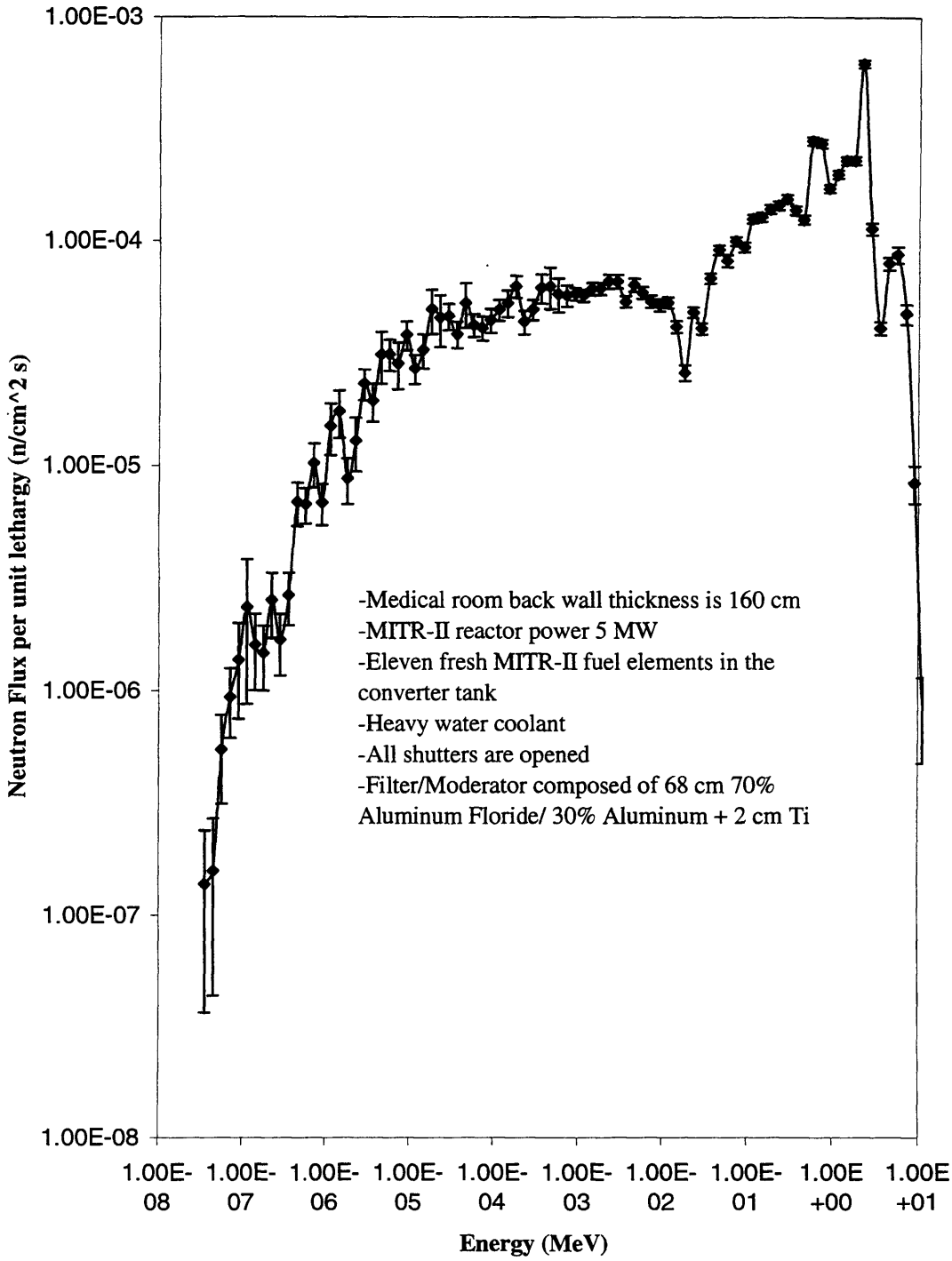

Figure 4.30: Neutron Spectrum Tallied Outside of Medical Room Back Wall (Wall Thickness is 160 cm)

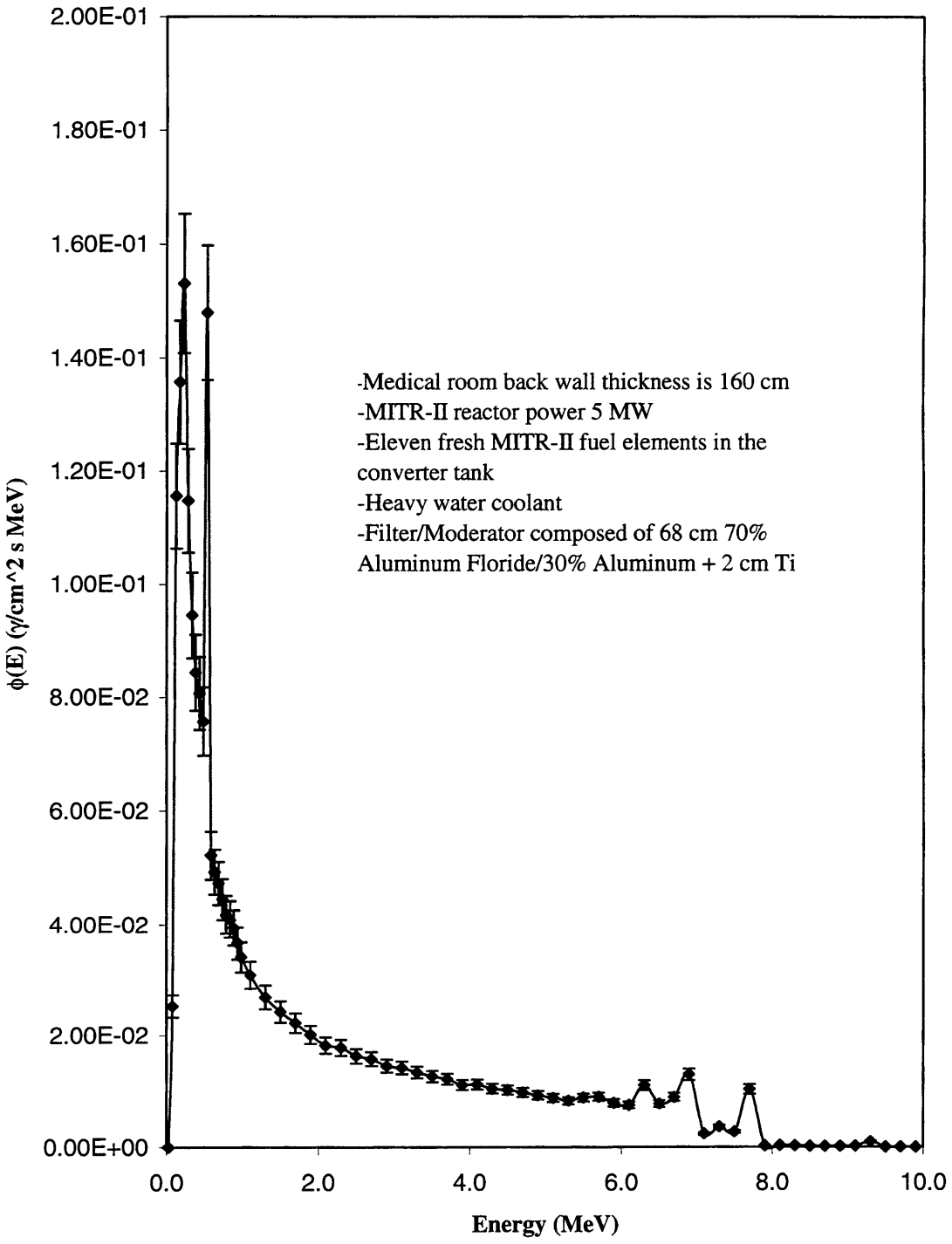

Figure 4.31: Photon Spectrum Tallied Outside of Medical Room Back Wall (Wall Thickness is 160 cm)

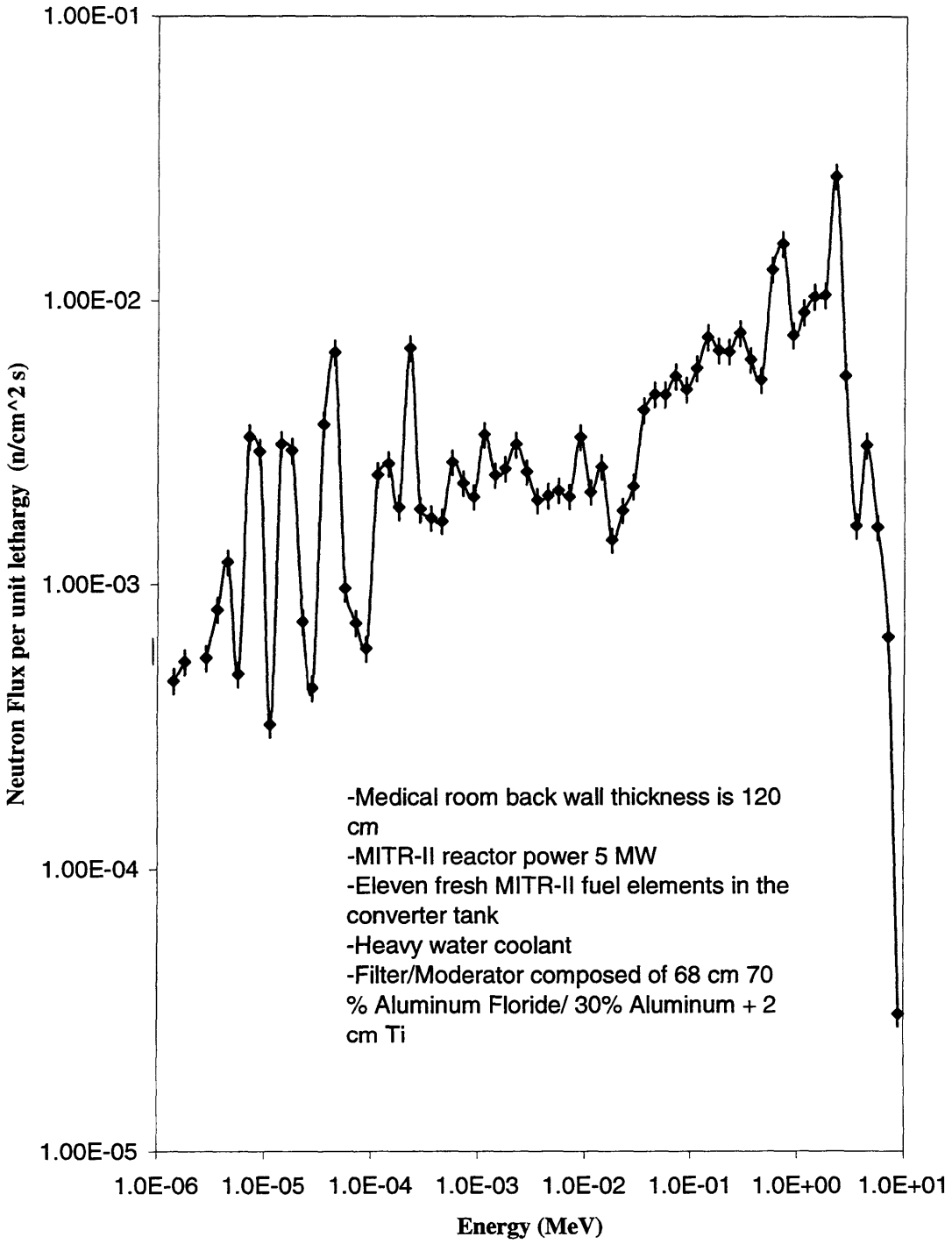

Figure 4.32: Neutron Spectrum Tallied Outside of Medical Room Back Wall (Wall Thickness 120 cm)

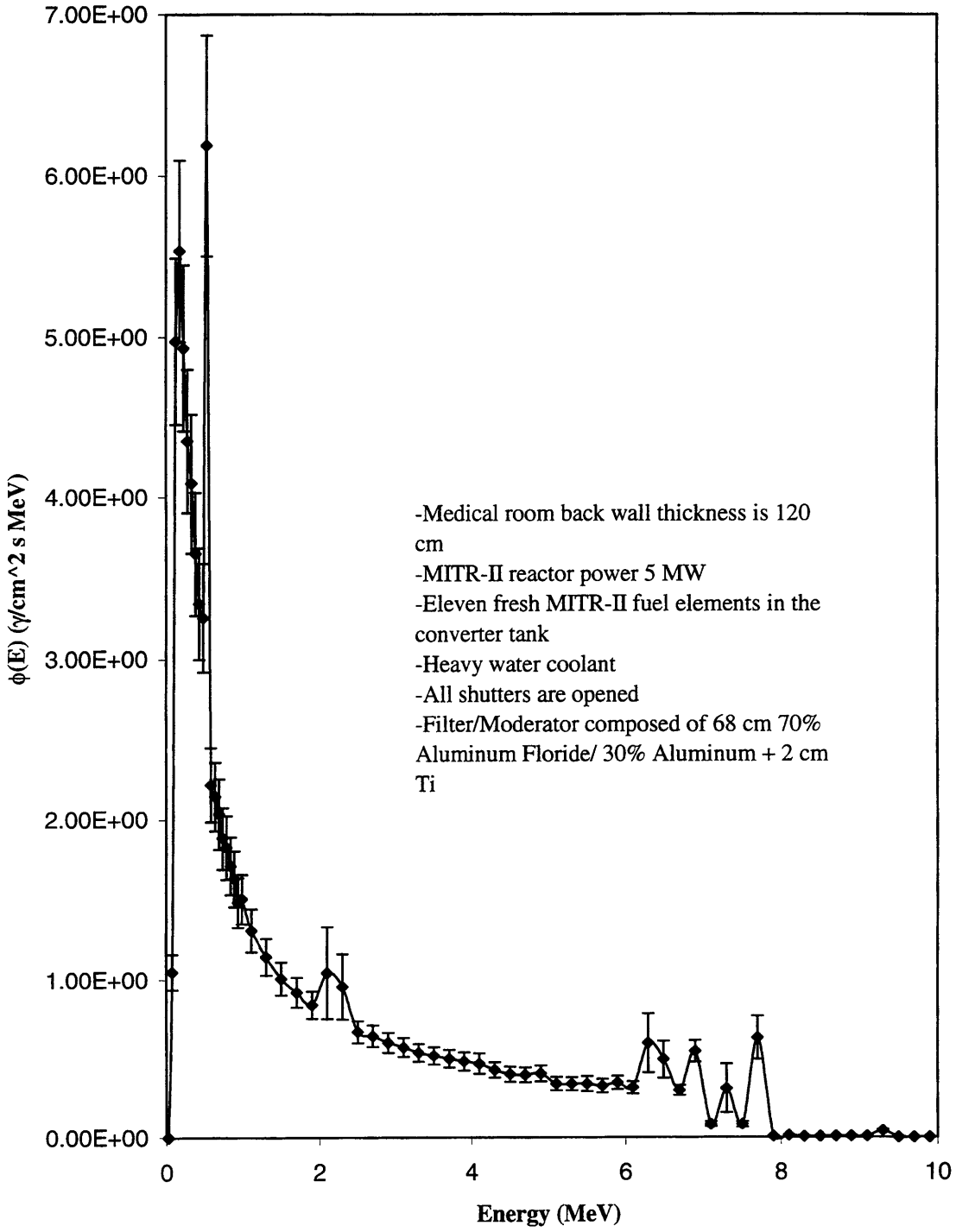

Figure 4.33: Photon Spectrum Tallied Outside of Medical Room Back Wall (Wall Thickness is 120 cm)

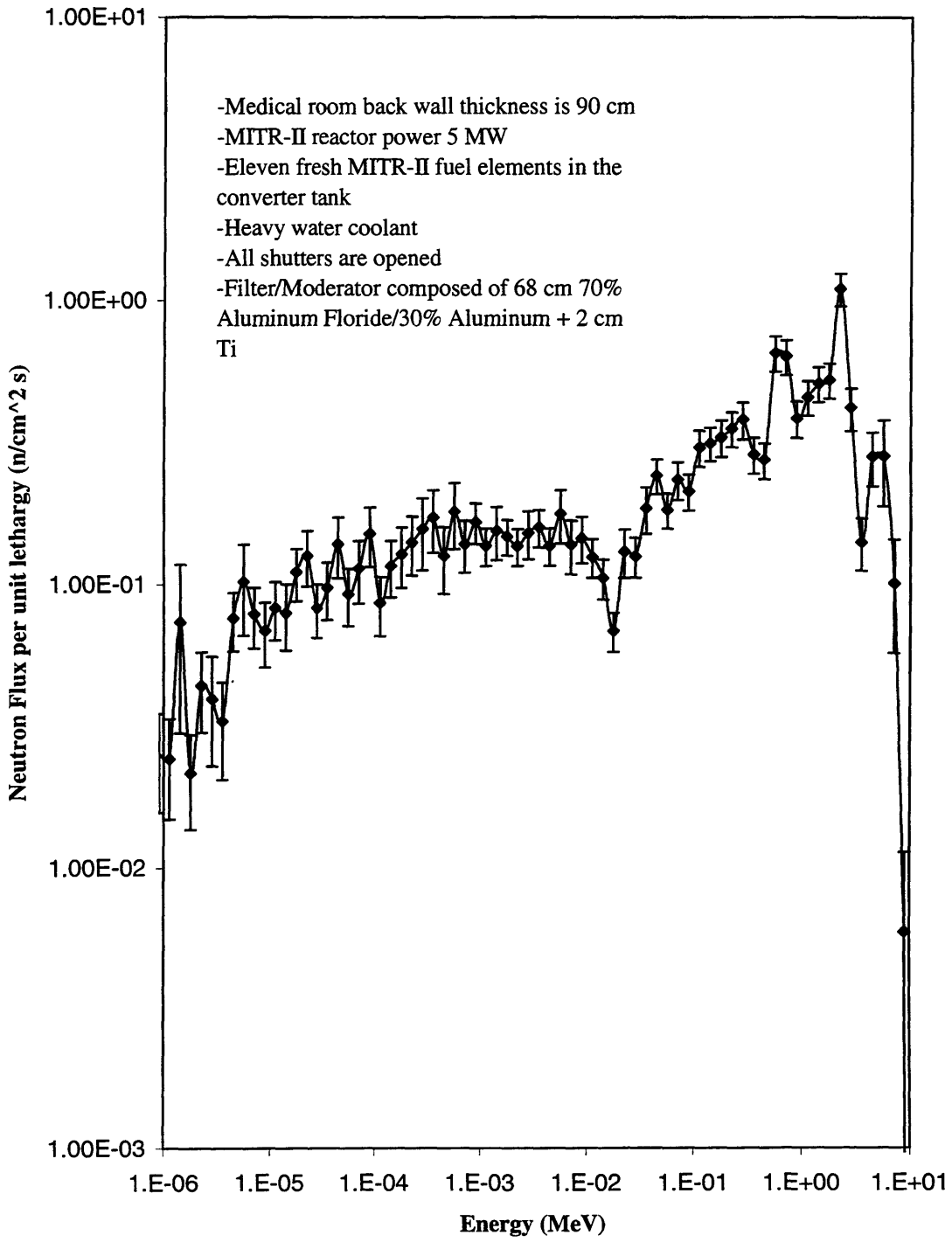

Figure 4.34: Neutron Spectrum Tallied Outside of Medical Room Back Wall (Wall Thickness is 90 cm)

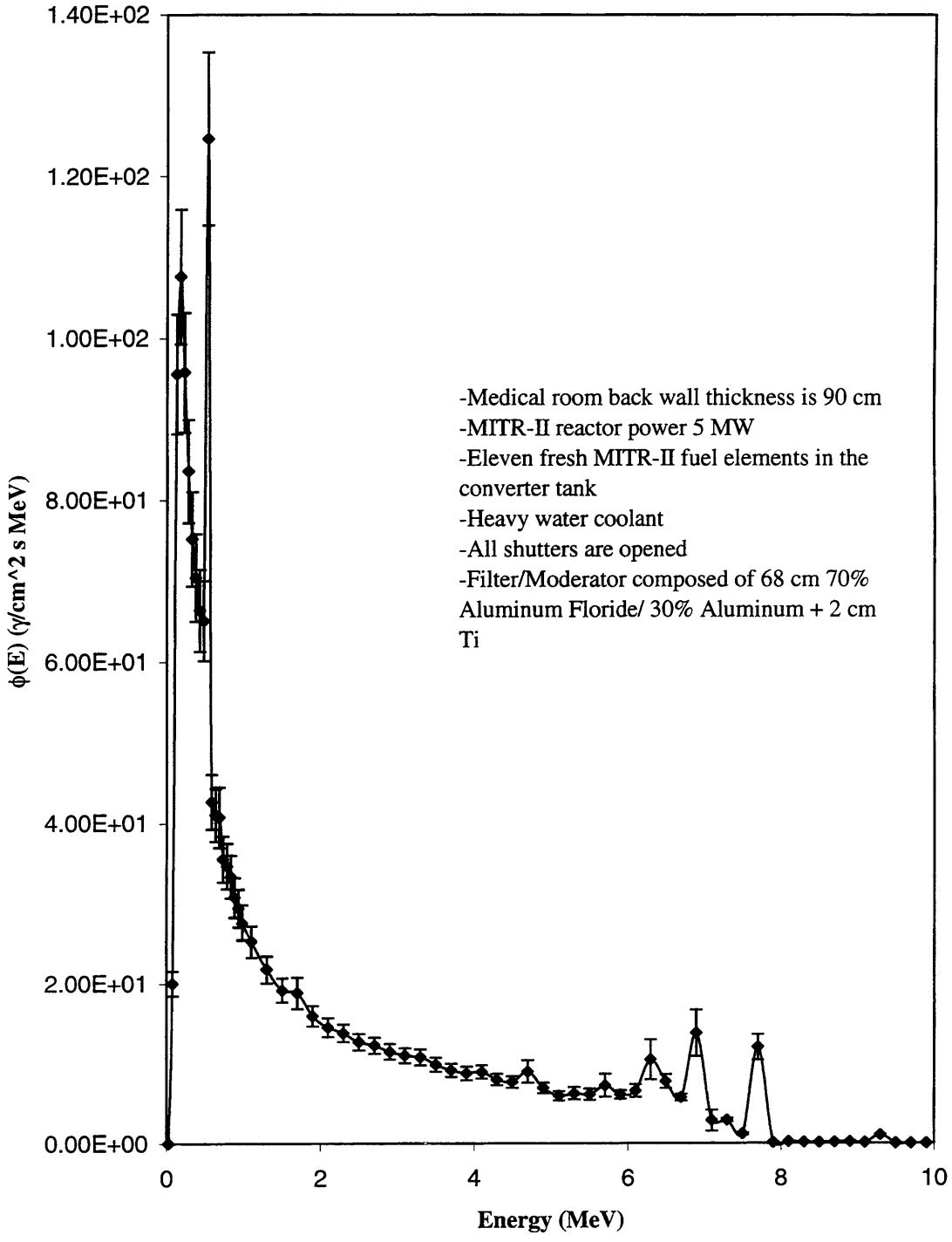

Figure 4.35: Photon Spectrum Tallied Outside of Medical Room Back Wall (Wall Thickness is 90 cm)

Table 4.5: Medical Room Shielding Calculation Results (Statistical uncertainty is reported as one standard deviation)

Medical room backwall thickness	Dose Rates at the outside medical room back wall	
	Neutron dose rate (mrem/hr)	Photon dose rate (mrem/hr)
160 cm	5E-5 (4%)	0.02 (9.2%)
120 cm	0.002 (10%)	0.03 (9.1%)
90 cm	0.12 (10%)	0.5 (7%)

It is evident from above analysis that 90 cm thick medical room back wall is enough to reduce the dose rate to below 1 mrem/hr. M. Ledesman (a masters student) is currently working to optimize the medical room layout and to design a patient setup for the current medical room.

7.References

1. Kiger, W.S., *Neutronic Design of a Fission Converter-Based Epithermal Beam for Boron Neutron Capture Therapy*, Nucl. E. Thesis, Massachusetts Institute of Technology, 1996.
2. Flores, C., *MITR-II Medical Beam Shutter Modification and Engineering Design,* MIT, August 1993.
3. Rogus, R., *Design and Dosimetry of Epithermal Neutron Beams for Clinical Trials of Boron Neutron Capture Therapy at the MITR-II Reactor,* Ph.D. Thesis, Massachusetts Institute of Technology, 1994.
4. Sakamoto, S., *Sensitivity Studies of the Neutronic Design of a Fission Converter-Based Epithermal Beam for Boron Neutron Capture Therapy*, SM Thesis, Massachusetts Institute of Technology, 1997.
5. Blizard, E.P., *Engineering Compendium on Radiation Shielding,* Springer-Verlag New York Inc., Vol. 2, 1977.
6. Redmond, E.L., Yanch, J.C., Harling, O.K., *Monte Carlo Simulation of the Massachusetts Institute of Technology Research Reactor,* Nuclear Technology, Vol. 106, April 1994.

APPENDIX

MathCad Programs Used for Thermal-Hydraulic Analysis

A3.1 Analytical Calculation of Natural Convection Flow Rate and the Temperature Difference across the Fuel Element in the Fission Converter

Define the parameters (all in S.I units)

$cp := 418$

Expansion coefficient

$\beta := 6 \cdot 10^{-4}$

$Q := 300 \cdot 10^{3}$ Heat generation rate

$\rho := 98$

$v := 0.70 \cdot 10^{-6}$

$\Delta h := 145 \cdot 0.025$

$Afu := 131 \cdot 10^{-6}$ Flow cross-sectional area in a fuel channel

$m := 2.5, 2.51 .. 3$ Total mass flow rate through the core. It is varied from 2.5 to 3 by increments of 0.1

$v(m) := \frac{m}{\rho \cdot Afu \cdot 15 \cdot 11}$ Coolant velocity in the fuel channel

1. Pressure drop in the downcomer

$Ap = \frac{9.47 + 2.81}{2} \cdot 5.44 \cdot 0.0254^2$ Downcomer flow cross-sectional area

$Pp = (9.26 + 9.47 + 5.44 + 2.81) \cdot 0.025$ Downcomer perimeter

$Dp = 4 \cdot \frac{Ap}{Pp}$ Downcomer hydraulic diameter

$Lp = 131.62 \cdot 0.025$ Downcomer length

$Vp(m) = \frac{m}{2 \cdot \rho \cdot Ap}$ Coolant velocity in the downcomer

$Rep(m) = \frac{Vp(m) \cdot Dp}{\nu}$

Pressure drop in the transition region is calculated using the same approach as Ref. 3 in Chapter 3.

$FT(m) = \frac{Rep(m) - 210}{7900}$

$fp(m) = (1 - FT(m)) \cdot \frac{91.5}{Rep(m)} + FT(m) \cdot 0.316 \cdot Rep(m)^{(-0.25)}$

$\Delta Pp(m) = \frac{1}{2} \cdot \rho \cdot Vp(m)^2 \cdot \left(fp(m) \cdot \frac{Lp}{Dp} + 3.58 \right)$

2. Pressure drop in the fuel element

$Dfu = 2.24 \cdot 10^{-3}$ Fuel element hydraulic diameter

$Lfu = 0.66675$ Length of a fuel element

$Refu(m) = \frac{v(m) \cdot Dfu}{\nu}$ Flow is assumed to be laminar. This assumption is checked later in the analysis.

$ffu(m) = \frac{91.5}{Refu(m)}$

$\Delta Pfu(m) = \frac{1}{2} \cdot \rho \cdot v(m)^2 \cdot ffu(m) \cdot \frac{Lfu}{Dfu}$

3. Pressure loss due to contraction (from the lower plenum to fuel)

$Alpl = (49.37 \cdot 0.0254 + 40.22 \cdot 0.0254) \cdot 0.5 \cdot (5.44 \cdot 0.0254)$ Cross-sectional area of the lower plenum

$$Kc := 0.5 \cdot \left[1 - \left(\frac{Afu}{Alpl} \right)^2 \right]$$

Kc = 0.5

$$\Delta Pc(m) := \frac{Kc \cdot v(m)^2 \cdot \rho}{2}$$

4. Pressure drop due to expansion (from pipe to plenum)

$$Aupl := Alpl$$

$$vupl(m) := \frac{m}{\rho \cdot 2 \cdot Aupl}$$

$$ke := \left(1 - \frac{Afu}{Aupl} \right)^2$$

ke = 0.998

$$\Delta Pe(m) := \frac{ke \cdot vupl(m)^2 \cdot \rho}{2}$$

4. Form Pressure Loss

k1 := 0. entrance from a plenum to fuel (sharp edge entrance), taken from Nuclear Systems I, page 358

k2 := 1. pipe exit to a plenum (any pipe exit), taken from Nuclear Systems I, page 358

$$\Delta Pform(m) := \frac{(k1 + k2) \cdot \rho \cdot v(m)^2}{2}$$

$\Delta Pt(m) := \Delta Pp(m) + \Delta Pfu(m) + \Delta Pc(m) + \Delta Pform(m) + \Delta Pe(m)$ Total pressure loss in the system

5. Buoyancy Pressure Head

$$R(v) := \frac{\Delta Pt(m) \cdot \rho \cdot 2}{m}$$ Derivation of these equations are in Nuclear Systems II page 77.

g := 9.8

$$mc(m) := \left(\frac{2 \cdot \beta \cdot Q \cdot g \cdot \Delta h \cdot \rho^2}{cp \cdot R(m)} \right)^{\frac{1}{2}}$$

$$\Delta T(m) := \frac{Q}{cp \cdot mc(m)}$$

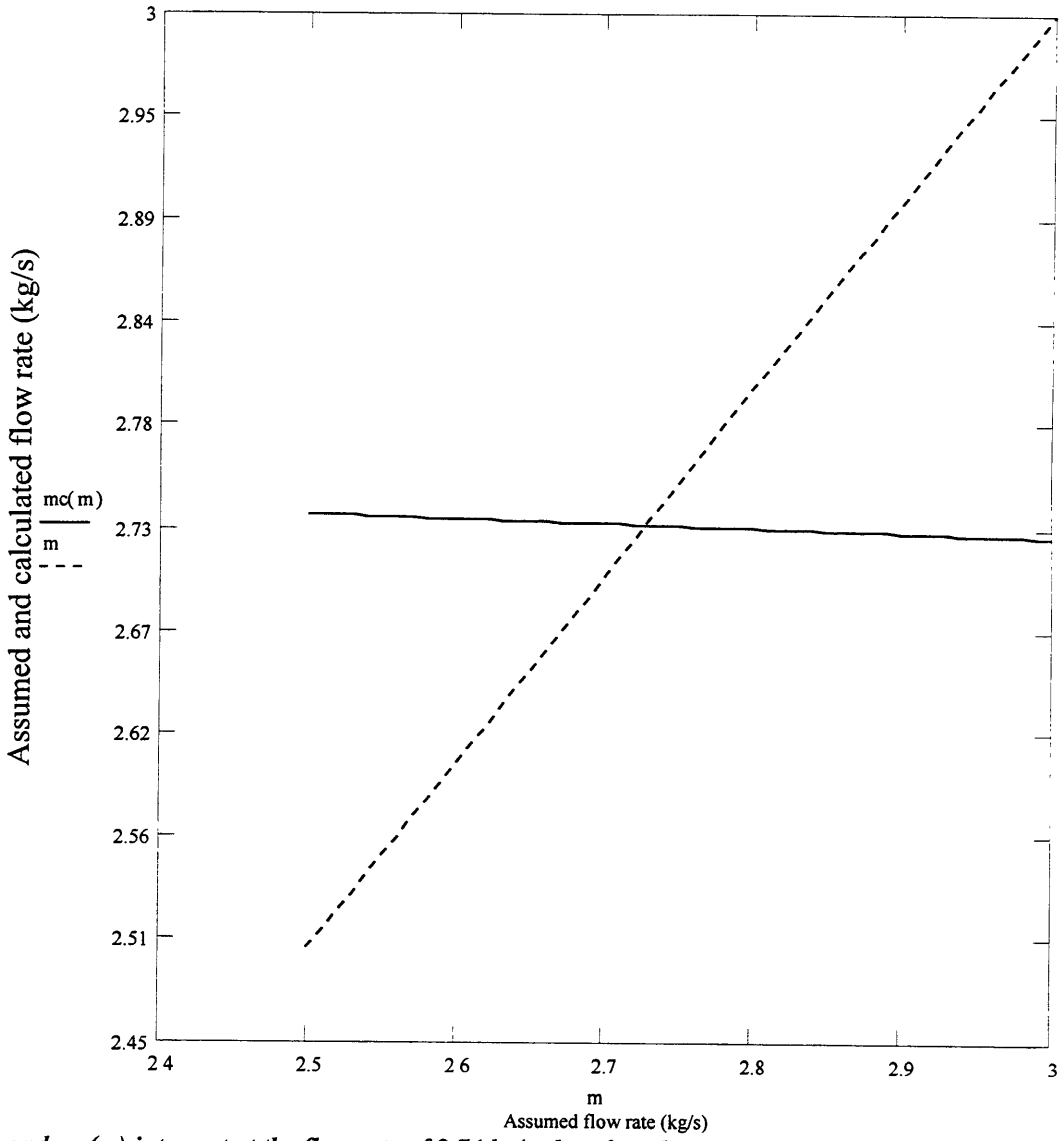

m and mc(m) intersect at the flow rate of 2.74 kg/s, therefore the natural convection flow rate will be 2.74 kg/s. **ΔT across the fuel is 26.3 ^{0}C**

Here the total pressure drop (ΔPt(m)) and the pressure drops in the downcomer (ΔPp(m)) and the core (ΔPfu(m)) are shown.

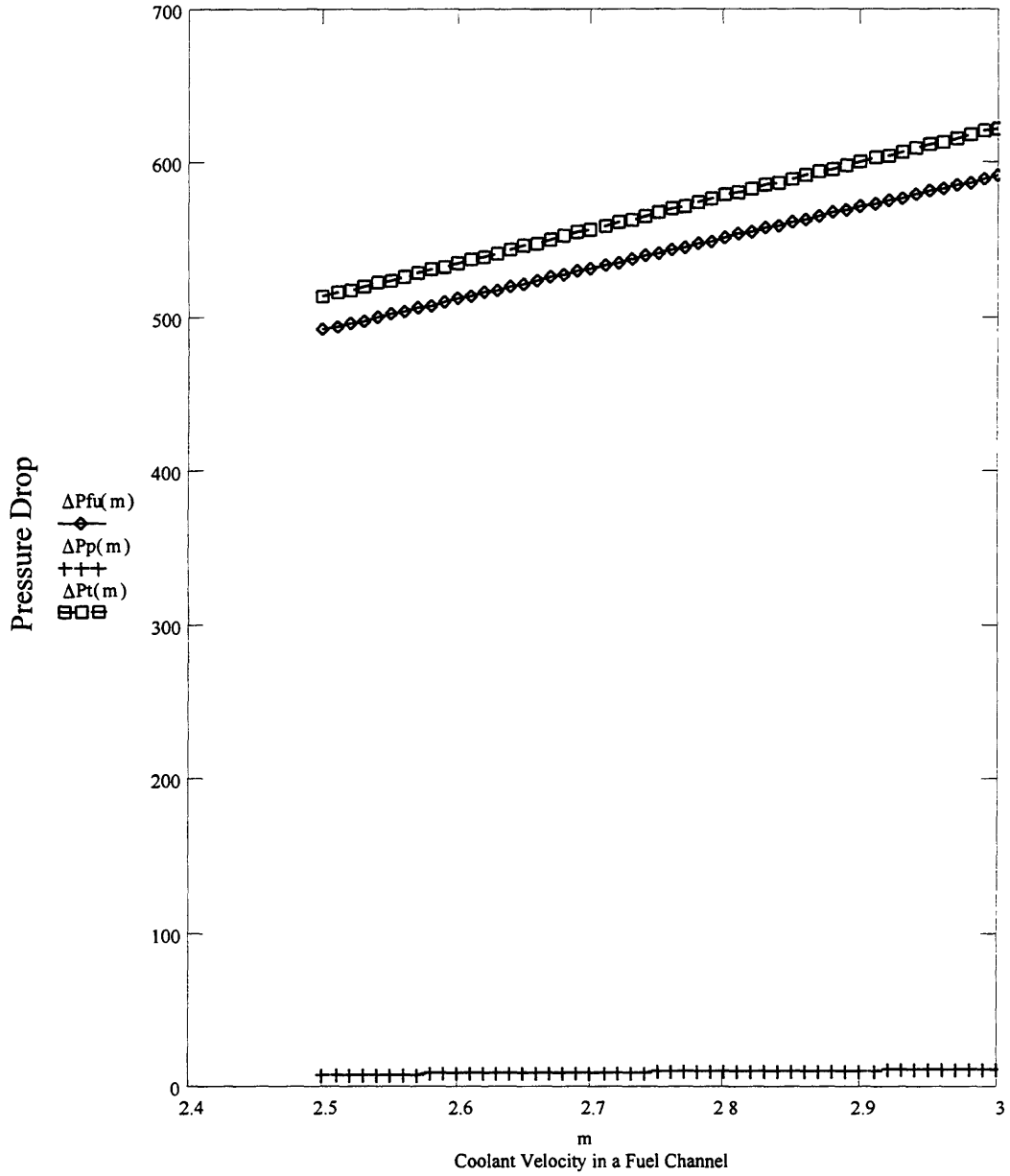

As it is obvious from the above figure, the pressure loss in the core is much higher than the pressure drop in the downcomer.

A3.2 Forced Convection With Bypass Channel Analysis

Optimizing the bypass channel width

$L_{bypass} = 2.59$ bypass channel height in meters

$L_{fuel} = 0.66$ fuel element height in meters

$\rho = 98$ density at 53 ^0C

$\nu = 0.467 \cdot 10^{-6}$ viscosity at 53 ^0C

$P_{total} = 30$ total core power in kW

$c_p = 4.$ specific heat capacity

$P_{hot} = 3$ hot channel power

$T_{hot} = 8$ hot channel exit temperature in ^0C

$m_{total} = 4.$ total inlet flow rate in kg/s

$$m_{hot}(T_{hot}) = \frac{P_{hot}}{c_p \cdot (T_{hot} - 40)}$$ flow rate through hot channel in kg/s

$m_{core}(T_{hot}) = 11 \cdot m_{hot}(T_{hot})$ total flow rate through the core in kg/s

$m_{bypass}(T_{hot}) = m_{total} - m_{core}(T_{hot})$ total by pass channel flow rate in kg/s

$A_{fuel} = 15.131 \cdot 10^{-6}$ flow cross sectional area for a single fuel element in m^2

$$v_{fuel}(T_{hot}) = \frac{m_{hot}(T_{hot})}{\rho \cdot A_{fuel}}$$ velocity in the fuel in m/s

$D_{fuel} = 2.24 \cdot 10^{-3}$ hydraulic diameter of the MITR-II fuel element

$$Re_{fuel}(T_{hot}) = \frac{v_{fuel}(T_{hot}) \cdot D_{fuel}}{\nu}$$

$$f_{fuel}(T_{hot}) = \frac{91.5}{Re_{fuel}(T_{hot})}$$

$$\Delta P_{fuel}(T_{hot}) = \frac{1}{2} \cdot f_{fuel}(T_{hot}) \cdot \rho \cdot v_{fuel}(T_{hot})^2 \cdot \frac{L_{fuel}}{D_{fuel}}$$

Pressure loss in the core

$$A_{lower\_plenum} = 41 \cdot 0.02544 \cdot 0.025$$

$$K_{c\_fuel} = 0.5 \cdot \left[1 - \left[\frac{\frac{A_{fuel}}{15}}{A_{lower\_plenum}} \right] \right]^2$$

$$\Delta P_{c\_fuel}(T_{hot}) = \frac{K_{c\_fuel} \cdot v_{fuel}(T_{hot})^2 \cdot \rho}{2}$$

Pressure drop due to expansion (from fuel to upper plenum)

$$A_{upper\_plenum} = A_{lower\_plenum}$$

$$v_{upper\_plenum}(T_{hot}) = \frac{m_{core}(T_{hot})}{A_{upper\_plenum} \cdot \rho}$$

$$K_{e\_fuel} = \left[1 - \frac{\frac{A_{fuel}}{15}}{A_{upper\_plenum}} \right]^2$$

$$\Delta P_{e\_fuel}(T_{hot}) = \frac{K_{e\_fuel} \cdot v_{upper\_plenum}(T_{hot})^2 \cdot \rho}{2}$$

$$\Delta P_{total\_fuel}(T_{hot}) = \Delta P_{fuel}(T_{hot}) + \Delta P_{c\_fuel}(T_{hot}) + \Delta P_{e\_fuel}(T_{hot}) + \frac{1.5 \cdot \rho \cdot v_{fuel}(T_{hot})^2}{2}$$

Pressure loss calculation in the bypass channel as a function of bypass channel width W.

$$A_{bypass}(W) = 4 \cdot 0.0254 W$$

$$\rho_{bypass} = 99$$

$$v_{bypass} = 0.659 \cdot 10^{-6}$$

$$\mu_{bypass} = \rho_{bypass} \cdot v_{bypass}$$

$$v_{bypass}(T_{hot}, W) = \frac{m_{bypass}(T_{hot})}{2 \cdot 4 \cdot 0.0254 W \cdot \rho_{bypass}}$$

$$D_{bypass}(W) = \frac{4 \cdot 4 \cdot 0.0254 W}{2 \cdot (4 \cdot 0.0254 + W)}$$

$$L_{ud\_bypass}(W) = 40 \cdot D_{bypass}(W)$$

$$\Delta P_{ud\_bypass}(T_{hot}, W) = 8 \cdot \mu_{bypass} \cdot v_{bypass}(T_{hot}, W) \cdot \frac{L_{ud\_bypass}(W)}{\left(\frac{D_{bypass}(W)}{2}\right)^2} + \frac{1}{2} \cdot 2.45 \cdot \rho_{bypass} \cdot v_{bypass}(T_{hot}, W)$$

$$Re_{bypass}(T_{hot}, W) = \frac{v_{bypass}(T_{hot}, W) \cdot D_{bypass}(W)}{v_{bypass}}$$

$$f_{bypass}(T_{hot}, W) = \frac{0.316}{Re_{bypass}(T_{hot}, W)^{0.25}}$$

$$\Delta P_{bypass}(T_{hot}, W) = \left(\frac{1}{2} \cdot f_{bypass}(T_{hot}, W) \cdot \rho \cdot v_{bypass}(T_{hot}, W)^2 \cdot \frac{L_{bypass}}{D_{bypass}(W)}\right)$$

Pressure loss due to contraction (from lower plenum to bypass channel)

$$A_{lower\_plenum} = 41 \cdot 0.02544 \cdot 0.025$$

$$K_{c\_bypass}(W) = 0.5 \cdot \left[1 - \left(\frac{A_{bypass}(W)}{A_{lower\_plenum}}\right)^2\right]$$

$$\Delta P_{c\_bypass}(T_{hot}, W) = \frac{K_{c\_bypass}(W) \cdot v_{bypass}(T_{hot}, W)^2 \cdot \rho_{bypass}}{2}$$

Pressure drop due to expansion (from bypass to upper plenum)

$$A_{upper\_plenum} = A_{lower\_plenum}$$

$$v_{upper\_plenum}(T_{hot}) = \frac{m_{bypass}(T_{hot})}{A_{upper\_plenum} \cdot \rho_{bypass}}$$

$$K_{e\_bypass}(W) = \left(1 - \frac{A_{bypass}(W)}{A_{upper\_plenum}}\right)^2$$

$$\Delta P_{e\_bypass}(T_{hot}, W) = \frac{K_{e\_bypass}(W) \cdot v_{upper\_plenum}(T_{hot})^2 \cdot \rho_{bypass}}{2}$$

$$\Delta P_{bypass\_form}(T_{hot}, W) = \frac{1.5 \cdot \rho_{bypass} \cdot v_{bypass}(T_{hot}, W)^2}{2}$$

$$\Delta P_{total\_bypass}(T_{hot}, W) = \Delta P_{bypass}(T_{hot}, W) + \Delta P_{c\_bypass}(T_{hot}, W) + \Delta P_{e\_bypass}(T_{hot}, W) + \Delta P_{bypass\_for}$$

$$\Delta P(T_{hot}, W) = \Delta P_{total\_fuel}(T_{hot}) - \Delta P_{total\_bypass}(T_{hot}, W) - \Delta P_{ud\_bypass}(T_{hot}, W)$$

$W = 0.00$

$$\frac{root(\Delta P(T_{hot}, W), W)}{0.0254} = 1.478$$

A3.3 Calculation of Coolant Exit Temperature as a Function of Inlet Primary Flow Rate for Different Bypass Channel Widths

$L_{bypass} := 2.59$ bypass channel height in meters

$L_{fuel} := 0.66$ fuel element height in meters

$\rho := 98$ density at 53 ^0C

$\nu := 0.467 \cdot 10^{-6}$ viscosity at 53 ^0C

$P_{total} := 30$ total core power in kW

$c_p := 4.$ specific heat capacity

$P_{hot} := 3$ hot channel power

$\beta := 4.52 \cdot 10^{-4}$

$m_t := 4, 4.5 .. 6.$ total primary flow rate

$m_{core}(m_t, X) := X \cdot m_t$ total flow rate through core

$m_{bypass}(m_t, X) := m_t \cdot (1 - X)$ total by pass channel flow rate in kg/s

$A_{fuel} := 15.131 \cdot 10^{-6}$ flow cross sectional area for a single fuel element in m^2

$$m_{hot}(m_t, X) := \frac{m_{core}(m_t, X)}{11}$$ flow rate through hot channel

$$v_{fuel}(m_t, X) := \frac{m_{hot}(m_t, X)}{\rho \cdot A_{fuel}}$$ velocity in the fuel in m/s

$D_{fuel} := 2.24 \cdot 10^{-3}$ hydraulic diameter of the MITR-II fuel element

$$Re_{fuel}(m_t, X) := \frac{v_{fuel}(m_t, X) \cdot D_{fuel}}{\nu}$$

$$f_{fuel}(m_t, X) := \frac{91.5}{Re_{fuel}(m_t, X)}$$

$$\Delta P_{fuel}(m_t, X) := \frac{1}{2} \cdot f_{fuel}(m_t, X) \cdot \rho \cdot v_{fuel}(m_t, X)^2 \cdot \frac{L_{fuel}}{D_{fuel}}$$

Pressure loss in the core

$$A_{lower\_plenum} := 41 \cdot 0.02544 \cdot 0.025$$

$$K_{c\_fuel} := 0.5 \cdot \left[1 - \left[\frac{\frac{A_{fuel}}{15}}{A_{lower\_plenum}} \right] \right]^2$$

$$\Delta P_{c\_fuel}(m_t, X) := \frac{K_{c\_fuel} \cdot v_{fuel}(m_t, X)^2 \cdot \rho}{2}$$

Pressure drop due to expansion (from fuel to upper plenum)

$$A_{upper\_plenum} := A_{lower\_plenum}$$

$$v_{upper\_plenum}(m_t, X) := \frac{m_{core}(m_t, X)}{A_{upper\_plenum} \cdot \rho}$$

$$K_{e\_fuel} := \left[1 - \frac{\frac{A_{fuel}}{15}}{A_{upper\_plenum}} \right]^2$$

$$\Delta P_{e\_fuel}(m_t, X) := \frac{K_{e\_fuel} \cdot v_{upper\_plenum}(m_t, X)^2 \cdot \rho}{2}$$

$$\Delta P_{total\_fuel}(m_t, X) := \Delta P_{fuel}(m_t, X) + \Delta P_{c\_fuel}(m_t, X) + \Delta P_{e\_fuel}(m_t, X)$$

Pressure loss calculation in the bypass channel as a function of bypass channel width W.

$$W := 0.75 \cdot 0.025$$

$$A_{bypass} := 4 \cdot 0.0254 W$$

$$\rho_{bypass} := 99$$

$$v_{bypass} := 0.659 \cdot 10^{-6}$$

$$\mu_{bypass} := \rho_{bypass} \cdot v_{bypass}$$

$$v_{bypass}(m_t, X) = \frac{m_{bypass}(m_t, X)}{2 \cdot A_{bypass} \cdot \rho_{bypass}}$$

$$D_{bypass} = \frac{4 \cdot 4 \cdot 0.0254 W}{2 \cdot (4 \cdot 0.0254 + W)}$$

$$L_{ud\_bypass} = 40 \cdot D_{bypass}$$

Developing flow length

$$\Delta P_{ud\_bypass}(m_t, X) = 8 \cdot \mu_{bypass} \cdot v_{bypass}(m_t, X) \cdot \frac{L_{ud\_bypass}}{\left(\frac{D_{bypass}}{2}\right)^2} + \frac{1}{2} \cdot 2.45 \cdot \rho_{bypass} \cdot v_{bypass}(m_t, X)^2$$

Pressure drop in the developing region

$$Re_{bypass}(m_t, X) = \frac{v_{bypass}(m_t, X) \cdot D_{bypass}}{v_{bypass}}$$

$$f_{bypass}(m_t, X) = \frac{0.316}{Re_{bypass}(m_t, X)^{0.25}}$$

$$\Delta P_{bypass}(m_t, X) = \left(\frac{1}{2} \cdot f_{bypass}(m_t, X) \cdot \rho \cdot v_{bypass}(m_t, X)^2 \cdot \frac{L_{bypass} - L_{ud\_bypass}}{D_{bypass}}\right)$$

Pressure loss due to contraction (from lower plenum to bypass channel)

$$A_{lower\_plenum} = 41 \cdot 0.02544 \cdot 0.025$$

$$K_{c\_bypass} = 0.5 \cdot \left[1 - \left(\frac{A_{bypass}}{A_{lower\_plenum}}\right)^2\right]$$

$$\Delta P_{c\_bypass}(m_t, X) = \frac{K_{c\_bypass} \cdot v_{bypass}(m_t, X)^2 \cdot \rho_{bypass}}{2}$$

Pressure drop due to expansion (from bypass to upper plenum)

$$A_{upper\_plenum} = A_{lower\_plenum}$$

$$v_{upper\_plenum}(m_t, X) = \frac{m_{bypass}(m_t, X)}{A_{upper\_plenum} \cdot \rho_{bypass}}$$

$$K_{e\_bypass} := \left(1 - \frac{A_{bypass}}{A_{upper\_plenum}}\right)^2$$

$$\Delta P_{e\_bypass}(m_t, X) := \frac{K_{e\_bypass} \cdot v_{upper\_plenum}(m_t, X)^2 \cdot \rho_{bypass}}{2}$$

$$\Delta P_{bypass\_form}(m_t, X) := \frac{1.5 \cdot \rho_{bypass} \cdot v_{bypass}(m_t, X)^2}{2}$$

$$\Delta P_{total\_bypass}(m_t, X) := \Delta P_{bypass}(m_t, X) + \Delta P_{c\_bypass}(m_t, X) + \Delta P_{e\_bypass}(m_t, X) + \Delta P_{bypass\_form}(m_t, X)$$

$$\Delta P(m_t, X) := \Delta P_{total\_fuel}(m_t, X) - \Delta P_{total\_bypass}(m_t, X) - \Delta P_{ud\_bypass}(m_t, X)$$

$X := 0.0$

$$S(m_t) := root(\Delta P(m_t, X), X)$$

$root(\Delta P(m_t, X), X)$

0.662
0.677
0.689
0.7
0.71
0.719

$$T_{hot}(m_t) := \frac{P_{hot}}{\left(\frac{m_t \cdot S(m_t)}{11}\right) \cdot c_p} + 4$$

$T_{hot}(m_t)$

74.625
70.11
66.599
63.795
61.507
59.606

A3.4 Calculation of Natural Convection Flow Rate for the Forced Convection with Bypass Channel Design during Loss of Flow Accident

1. Initial Condition of Loss of Flow Transient

This Mathcad program is used to calculated the natural convection flow rate for different bypass channel widths.

Define parameters (all parameter values are given in S.I units)

$c_p := 4.1$ Heat capacity of light water

$\beta := 6 \cdot 10^{-4}$ Volumetric expansion coefficient of light water

$P := 30$ Total power

$P_{hot} := 3$ Hot channel power

$\rho := 99$ Density of light water at 40 ^{0}C

$\nu := 0.659 \cdot 10^{-6}$ Dynamic viscosity of light water at 40 ^{0}C

$\Delta h := 2$ Elevation from top of fuel element to top of bypass channel

$m_t := 0.1, 0.15 .. 3$ Total flow rate through 11 fuel elements and it ranges from 0.5 to 3

1. Pressure drop along the bypass channel

$W := 0.75 \cdot 0.025$ Bypass channel width

$A_{bypass} := 5.44 \cdot 0.0254 \cdot W$ Bypass channel flow cross sectional area

$D_{bypass} := \frac{4 \cdot A_{bypass}}{2 \cdot (5.44 \cdot 0.0254 + W)}$ Bypass channel hydraulic diameter

$L_{bypass} := 2.66$ Bypass channel height

$v_{bypass}(m_t) := \frac{m_t}{2 \cdot \rho \cdot A_{bypass}}$ Coolant velocity in each bypass channel

$Re_{bypass}(m_t) := \frac{v_{bypass}(m_t) \cdot D_{bypass}}{\nu}$ Reynolds number in bypass channel

$$f_{bypass}(m_t) := \text{if}\left(Re_{bypass}(m_t) \le 2100, \frac{91.5}{Re_{bypass}(m_t)}, \frac{0.3161.09}{Re_{bypass}(m_t)^{0\,25}}\right)$$ -Friction coefficient

$$\Delta P_{bypass}(m_t) := \frac{1}{2}\cdot\rho\cdot v_{bypass}(m_t)^2\cdot\left(\frac{L_{bypass}}{D_{bypass}}\cdot f_{bypass}(m_t) + 3.58\right)$$ Total pressure loss in the

bypass channel (includes entrance and exit losses)

2. Pressure drop in the hot channel

$T_{sat} := 10$ Saturation temperature at the core elevation

$T_{inlet} := 6$ Inlet temperature to the core

$A_{fuel} := 15.131\cdot 10^{-6}$ MITR-II fuel element flow cross sectional area

$D_{fuel} := 2.24\cdot 10^{-3}$ MITR-II fuel element hydraulic diameter

$L_{fuel} := 0.66$ Fuel element height

$q := \frac{P_{hot}}{L_{fuel}}$ Assuming equal flow rate through each fuel element, the hot element flow rate is calculated.

$$m_{hot}(m_t) := \frac{m_t}{11}$$

$$L_b(m_t) := \text{if}\left[\frac{m_{hot}(m_t)\cdot c_p\cdot(T_{sat} - T_{inlet})}{q} \ge L_{fuel}, L_{fuel}, \frac{m_{hot}(m_t)\cdot c_p\cdot(T_{sat} - T_{inlet})}{q}\right]$$ Boiling

length

$h_{fg} := 2691 - 41.$

$$x(m_t) := \text{if}\left[\frac{q\cdot(L_{fuel} - L_b(m_t))}{m_{hot}(m_t)\cdot h_{fg}} \ge 1.0, 1.0, \frac{q\cdot(L_{fuel} - L_b(m_t))}{m_{hot}(m_t)\cdot h_{fg}}\right]$$

$$x_{exit}(m_t) := \text{if}(x(m_t) \le 0.0, 0.0, x(m_t))$$ Hot channel exit quality

$$L_1(m_t) := \text{if}\left(x_{exit}(m_t) < 1, L_{fuel} - L_b(m_t), \frac{m_{hot}(m_t)\cdot h_{fg}}{q}\right)$$

$$L_{TP}(m_t) := \text{if}(L_b(m_t) \ge L_{fuel}, 0, L_1(m_t))$$ Two-phase length

$$L_{g\_SP}(m_t) := \text{if}(L_{TP}(m_t) \le 0, 0, L_{fuel} - L_{TP}(m_t) - L_b(m_t))$$ Vapor phase length

$\rho_l = 95$ Density of light water at 106 ^{0}C

$\rho_g = 0.82$ Density of light water vapor at 106 ^{0}C

$\nu_l = 0.282 \cdot 10^{-6}$ Dynamic viscosity of light water at 106 ^{0}C

Dynamic viscosity if light water vapor

$\nu_g = 15.1 \cdot 10^{-6}$

$$v_{SP}(m_t) = \frac{m_{hot}(m_t)}{\rho_l \cdot A_{fuel}}$$

SP,TP and g_SP subscripts are for single phase liquid two phase and single phase vapor respectively.

$$Re_{SP}(m_t) = \frac{v_{SP}(m_t) \cdot D_{fuel}}{\nu_l}$$

$$f_{SP}(m_t) = if\left(Re_{SP}(m_t) \le 2100, \frac{91.5}{Re_{SP}(m_t)}, \frac{0.316}{Re_{SP}(m_t)^{0.25}}\right)$$

$$\Delta P_{SP}(m_t) = \frac{1}{2} \cdot f_{SP}(m_t) \cdot \rho_l \cdot v_{SP}(m_t)^2 \cdot \frac{L_b(m_t)}{D_{fuel}}$$

$$G(m_t) = \frac{m_{hot}(m_t)}{A_{fuel}}$$ Mass flux

$$X_o(m_t) = x_{exit}(m_t) \cdot \left(\frac{\rho_l - \rho_g}{\rho_g}\right)$$

$$\Delta P_{TP}(m_t) = \frac{f_{SP}(m_t)}{2} \cdot L_{TP}(m_t) \cdot \frac{G(m_t)^2}{D_{fuel}} \cdot \frac{1}{\rho_l} \cdot \left(1 + \frac{X_o(m_t)}{2}\right) + \frac{G(m_t)^2 \cdot X_o(m_t)}{\rho_l}$$

$$\Delta P_{acc}(m_t) = \frac{G(m_t)^2 \cdot X_o(m_t)}{\rho_l}$$

$$v_{g\_SP}(m_t) = \frac{m_{hot}(m_t)}{\rho_g \cdot A_{fuel}}$$

$$Re_{g\_SP}(m_t) = \frac{v_{g\_SP}(m_t) \cdot D_{fuel}}{\nu_g}$$

$$f_{g\_SP}(m_t) := \text{if}\left(Re_{g\_SP}(m_t) \le 2100, \frac{91.5}{Re_{g\_SP}(m_t)}, \frac{0.3161.09}{Re_{g\_SP}(m_t)^{0.25}}\right)$$

$$\Delta P_{g\_SP}(m_t) := \frac{1}{2} \cdot f_{g\_SP}(m_t) \cdot \rho_g \cdot v_{g\_SP}(m_t)^2 \cdot \frac{L_{g\_SP}(m_t)}{D_{fuel}}$$

3. Buoyancy pressure

$\Delta P_{buoyancy\_upper\_plenum} := 0$ Buoyancy pressure above the top of fuel element

$h_{fg} := 2691 - 461.$

$$c(m_t) := \frac{\rho_g \cdot \rho_l \cdot 9.81 \cdot m_{hot}(m_t) \cdot h_{fg}}{q \cdot (\rho_l - \rho_g)}$$

$$\Delta T(m_t) := \frac{P_{hot}}{m_{hot}(m_t) \cdot c_p}$$

$$\Delta P_{SP\_buoyancy}(m_t) := \frac{\rho \cdot \beta \cdot 9.81 \cdot m_{hot}(m_t) \cdot c_p \cdot \Delta T(m_t)^2}{q \cdot 2}$$

$$\Delta P_{TP\_buoyancy}(m_t) := \left[\frac{\rho \cdot \beta \cdot 9.81 \cdot m_{hot}(m_t) \cdot c_p \cdot (T_{sat} - T_{inlet})^2}{q \cdot 2} - c(m_t) \cdot \ln\left[\frac{\rho_g + (\rho_l - \rho_g) \cdot x_{exit}(m_t)}{\rho_g}\right]\right] + L_{TP}(m_t) \cdot$$

$$\Delta P_{g\_buoyancy}(m_t) := L_{g\_SP}(m_t) \cdot 9.81 \cdot (\rho_l - \rho_g)$$

$$\Delta P_{fuel\_buoyancy}(m_t) := \text{if}\left[\Delta T(m_t) \le (T_{sat} - T_{inlet}), \Delta P_{SP\_buoyancy}(m_t), \Delta P_{TP\_buoyancy}(m_t) + \Delta P_{g\_buoyancy}(\right.$$

$$\Delta P_{total}(m_t) := \Delta P_{bypass}(m_t) + \Delta P_{SP}(m_t) + \Delta P_{TP}(m_t) + \Delta P_{g\_SP}(m_t)$$

$$\Delta P_{buoyancy}(m_t) := \Delta P_{buoyancy\_upper\_plenum} + \Delta P_{fuel\_buoyancy}(m_t)$$

A3.5 Calculation of Natural Convection Flow Rate for the Forced Convection with Bypass Channel Design during Loss of Flow Accident

2. Hydrodynamic Steady State Condition (t=t)

This Mathcad program is used to calculated the natural convection flow rate for

different bypass channel widths.

Define parameters (all parameter values are given in S.I units)

$c_p = 4.1$ Heat capacity of light water

$\beta = 4.536 \cdot 10^{-4}$ Volumetric expansion coefficient of light water

$P = 30$ Total power

$P_{hot} = 3$ Hot channel power

$\rho = 95$ Density of light water at 106 ^{0}C

$\nu = 0.282 \cdot 10^{-6}$ Dynamic viscosity of light water at 106 ^{0}C

$\Delta h = 2$ Elevation from top of fuel element to top of bypass channel

$m_t = 0.5, .55 .. 1$ Total flow rate through 11 fuel elements and it ranges from 0.5 to 10

1. Pressure drop along the bypass channel

$W = 1.0 \cdot 0.025$ Bypass channel width

$A_{bypass} = 4 \cdot 0.0254 W$ Bypass channel flow cross sectional area

$$D_{bypass} = \frac{4 \cdot A_{bypass}}{2 \cdot (4 \cdot 0.0254 + W)}$$ Bypass channel hydraulic diameter

$L_{bypass} = 2.66$ Bypass channel height

$$v_{bypass}(m_t) = \frac{m_t}{2 \cdot \rho \cdot A_{bypass}}$$ Coolant velocity in each bypass channel

$Re_{bypass}(m_t) := \frac{v_{bypass}(m_t) \cdot D_{bypass}}{\nu}$ Reynolds number in bypass channel

$f_{bypass}(m_t) := if\left(Re_{bypass}(m_t) \le 2100, \frac{91.5}{Re_{bypass}(m_t)}, \frac{0.316 1.09}{Re_{bypass}(m_t)^{0.25}}\right)$ -Friction coefficient

$\Delta P_{bypass}(m_t) := \frac{1}{2} \cdot \rho \cdot v_{bypass}(m_t)^2 \cdot \left(\frac{L_{bypass}}{D_{bypass}} \cdot f_{bypass}(m_t) + 3.58\right)$ Total pressure loss in the bypass channel (includes entrance and exit losses)

2. Pressure drop in the hot channel

$T_{sat} := 10$ Saturation temperature at the core elevation

$T_{inlet} := 10$ Inlet temperature to the core

$A_{fuel} := 15 \cdot 131 \cdot 10^{-6}$ MITR-II fuel element flow cross sectional area

$D_{fuel} := 2.24 \cdot 10^{-3}$ MITR-II fuel element hydraulic diameter

$L_{fuel} := 0.66$ Fuel element height

$q := \frac{P_{hot}}{L_{fuel}}$ Assuming equal flow rate through each fuel element, the hot element flow rate is calculated.

$m_{hot}(m_t) := \frac{m_t}{11}$

$L_b(m_t) := \frac{m_{hot}(m_t) \cdot c_p \cdot (T_{sat} - T_{inlet})}{q}$ Boiling length

$x_{exit}(m_t) := if\left[L_b(m_t) \ge L_{fuel}, 0.0, \frac{q \cdot (L_{fuel} - L_b(m_t))}{m_{hot}(m_t) \cdot (2691 - 461.3)}\right]$ Hot channel exit quality

$\rho_l := 95$ Density of light water at 106 ^{0}C

$\rho_g := 0.82$ Density of light water vapor at 106 ^{0}C

$\nu_l := 0.282 \cdot 10^{-6}$ Dynamic viscosity of light water at 106 ^{0}C

$v_{SP}(m_t) := \frac{m_{hot}(m_t)}{\rho_l \cdot A_{fuel}}$ SP and TP subscripts are for single phase and two phase respectively.

$$Re_{SP}(m_t) := \frac{v_{SP}(m_t)\cdot D_{fuel}}{v_l}$$

$$f_{SP}(m_t) := if\left(Re_{SP}(m_t) \le 2100, \frac{91.5}{Re_{SP}(m_t)}, \frac{0.3161.09}{Re_{SP}(m_t)^{0.25}}\right)$$

$$\Delta P_{SP}(m_t) := if\left(L_b(m_t) \ge L_{fuel}, \frac{1}{2}\cdot f_{SP}(m_t)\cdot \rho_l \cdot v_{SP}(m_t)^2 \cdot \frac{L_{fuel}}{D_{fuel}}, \frac{1}{2}\cdot f_{SP}(m_t)\cdot \rho_l \cdot v_{SP}(m_t)^2 \cdot \frac{L_b(m_t)}{D_{fuel}}\right)$$

$$L_{TP}(m_t) := if(x_{exit}(m_t) > 0.0, L_{fuel} - L_b(m_t), 0.0)$$ Height of fuel channel in two phase

$$G(m_t) := \frac{m_{hot}(m_t)}{A_{fuel}}$$ Mass flux

$$X_o(m_t) := x_{exit}(m_t)\cdot\left(\frac{\rho_l - \rho_g}{\rho_g}\right)$$

$$\Delta P_{TP}(m_t) := \frac{f_{SP}(m_t)}{2}\cdot L_{TP}(m_t)\cdot \frac{G(m_t)^2}{D_{fuel}}\cdot \frac{1}{\rho_l}\cdot\left(1 + \frac{X_o(m_t)}{2}\right) + \frac{G(m_t)^2 \cdot X_o(m_t)}{\rho_l}$$

3. Buoyancy pressure

$$V := 0.359 + 0.226 + 0.13$$

$$v_{bubble} := 0.2$$

$$t := \frac{3}{v_{bubble}}$$

$$h_f := 461.$$

$$h_g := 269$$

$$h_{fg} := h_g - h_f$$

$$M := (0.359 + 0.226 + 0.135)\cdot \rho_l$$

$$x_{upper\_plenum} := \frac{P\cdot t}{M\cdot h_{fg}}$$

$$x_{upper\_plenum} = 2.68\cdot 10^{-3}$$

$$\rho_{TP} = \frac{\rho_l \cdot \rho_g}{x_{upper\_plenum} \cdot \rho_l + \left(1 - x_{upper\_plenum}\right) \cdot \rho_g}$$

$$\Delta P_{buoyancy\_upper\_plenum} = \Delta h \cdot 9.81 \cdot \left(\rho_l - \rho_{TP}\right)$$

$$h_{fg} = 2691 - 461.$$

$$c\left(m_t\right) = \frac{\rho_g \cdot \rho_l \cdot 9.81 \cdot m_{hot}\left(m_t\right) \cdot h_{fg}}{q \cdot \left(\rho_l - \rho_g\right)}$$

$$\Delta T\left(m_t\right) = \frac{P_{hot}}{m_{hot}\left(m_t\right) \cdot c_p}$$

$$\Delta P_{SP\_buoyancy}\left(m_t\right) = \frac{\rho \cdot \beta \cdot 9.81 \cdot m_{hot}\left(m_t\right) \cdot c_p \cdot \Delta T\left(m_t\right)^2}{q \cdot 2}$$

$$\Delta P_{TP\_buoyancy}\left(m_t\right) = \left[\frac{\rho \cdot \beta \cdot 9.81 \cdot m_{hot}\left(m_t\right) \cdot c_p \cdot \left(T_{sat} - T_{inlet}\right)^2}{q \cdot 2} - c\left(m_t\right) \cdot \ln\left[\frac{\rho_g + \left(\rho_l - \rho_g\right) \cdot x_{exit}\left(m_t\right)}{\rho_g}\right]\right] + L_{TP}\left(1\right.$$

$$\Delta P_{fuel\_buoyancy}\left(m_t\right) = \text{if}\left[\Delta T\left(m_t\right) \le \left(T_{sat} - T_{inlet}\right), \Delta P_{SP\_buoyancy}\left(m_t\right), \Delta P_{TP\_buoyancy}\left(m_t\right)\right]$$

$$\Delta P_{total}\left(m_t\right) = \Delta P_{bypass}\left(m_t\right) + \Delta P_{SP}\left(m_t\right) + \Delta P_{TP}\left(m_t\right)$$

$$\Delta P_{buoyancy}\left(m_t\right) = \Delta P_{buoyancy\_upper\_plenum} + \Delta P_{fuel\_buoyancy}\left(m_t\right)$$

Appendix B

Here the assumption of constant concrete surface temperature (150°C) in the loss of coolant analysis is checked for its validity. The maximum heat flux on the concrete surface is 0.28 kW/m^2 during the loss of coolant accident. This occurs when the fuel clad temperature is at its maximum value of 450°C (about 3000 seconds after the loss of coolant). Let us evaluate the temperature at the surface of the concrete assuming the constant heat flux (q'') has been suddenly applied to a semi-infinite plane. The surface temperature rise can be calculated using the following equation:

$$T(t) = \sqrt{\frac{4t}{\pi}} \frac{q''}{(k\rho C_p)^{1/2}}$$

The definitions of the symbols and the values used for the analysis follow.

T = temperature of the concrete surface (°C)

t = time (3000 seconds)

k = heat conductivity of concrete (0.014 kW/m °C)

C_p = heat capacity of concrete (0.88 kJ/kg °C)

ρ = density (3700 kg/m^3)

Normal concrete k and C_p values were used for the concrete surface temperature rise calculation because k and C_p values for the reactor biological shield concrete were not available. Since the reactor biological shield concrete has a large amount of steel, k and C_p values for the reactor biological shield concrete should be larger than those for normal concrete. Hence, the temperature rise calculated using the normal concrete k and C_p values is a conservative value. The reactor biological concrete density value was available from reactor construction records and was used for the temperature rise calculation.

The temperature of the concrete surface will rise 7°C at 3000 seconds if the constant heat flux is taken to equal the maximum value, that is the heat flux associated with the maximum fuel temperature. The 7°C increase in the concrete surface temperature is well

below the 300°C rise in fuel temperature and, hence, the heat transfer rate by radiation from the fuel assembly around the time of peak fuel clad temperature is not affected by a small variation in the surface temperature of the concrete. Consequently, the assumption of constant surface temperature is valid.